

# SELFORGANIZATION IN NONEQUILIBRIUM SYSTEMS



Society of Physical Chemists of Serbia  
Belgrade, 2004

# SELFORGANIZATION IN NONEQUILIBRIUM SYSTEMS

## *Papers*

*from the International Conference  
in Nonlinear Sciences*

Organized by:  
Society of Physical Chemists of Serbia



In cooperation with:

Institute of Catalysis, Bulgarian Academy of Sciences,  
Sofia, Bulgaria



Boreskov Institute of Catalysis,  
Siberian Branch of the Russian Academy of Sciences,  
Novosibirsk, Russian Federation



September 24-25, 2004,  
Belgrade

ISBN 86-82475-15-4  
Title: Selforganization in Nonequilibrium Systems (Papers)  
Published by: Society of Physical Chemists of Serbia, Studentski trg  
12-16, P.O.Box 137, 11001 Belgrade, Yugoslavia  
For publisher: Ankica Antić-Jovanović, president of the Society of  
Physical Chemists of Serbia  
Editor: Slobodan Anić, Željko Čupić and Ljiljana Kolar-Anić  
Printed by: VMD Printing Comp. – Belgrade  
100 Copies; Number of Pages – xii +226; Format B5;  
Printing finished in September 2004.  
Text and Layout: Aleksandar Nikolić

*100 – copy printing*

The Conference is held under the auspices of the  
Ministry of Science and Environmental Protection of Republic of Serbia

## **Organizing Committee**

*Chairman:* Slobodan Anić (SCG)

*Vice-chairman:* L. Petrov (BG), Ž. Čupić (SCG)

*Members:*

B. Adnađević (SCG), T. Grozdić (SCG), N. Ostrovski (SCG), V. Vukojević (SCG)

## **International Scientific Committee**

*Chairman:* Ljiljana Kolar-Anić (SCG)

*Vice-chairman:* M. Koleva (BG), S. Milošević (SCG)

*Members:*

P. Alen (UK), V.I. Elokhin (RUS), V. Gáspár (H), P. Graae Sørensen (DK), Z. Noszticzius (H), Č. Radenović (SCG), A.R. Tančić (SCG), G. Schmitz (B), S.K. Scott (UK), P. Ševčík (SK)

## **Executive Committee**

*Chairman:* Željko Čupić (SCG)

*Vice-chairman:* T. Grozdić (SCG), D. Stanisavljev (SCG)

*Members:*

N. Begović (SCG), M. Beljanski (SCG), S.N. Blagojević (SCG), Đ. Cvijović (SCG), M. Daković (SCG), D. Lončarević (SCG), N. Pejić (SCG), N. Potkonjak (SCG)

## **SPONSORS**

Ministry of Science and Environmental Protection of Republic of Serbia

The Faculty of Physical Chemistry, University of Belgrade

Institute for Chemistry, Technology and Metalurgy, Belgrade

Institute of General and Physical Chemistry, Belgrade

MOL, Belgrade

Hemofarm Group, Vršac

Gradski zavod za zaštitu zdravlja, Belgrade

Organisation for the Prohibition of Chemical Weapons, Hague

## Contents

Preface

### PAPERS OF THE INVITED LECTURES

---

P.M. Allen	3
<b>Self-Organisation: From Physics to Social Systems</b>	
G. R. Armstrong, V. Gáspár, S.K. Scott, A.F. Taylor	20
<b>Chemical Wave Propagation in Inhomogeneous Media</b>	
V. Gáspár, I. Z. Kiss, Z. Kazsu	28
<b>Effect Of Double-Layer Capacitance on the Stability of Electrochemical Oscillators</b>	
V.I. Elokhin	35
<b>Variety of Spatiotemporal Patterns Revealed by Monte-Carlo Simulation of the Oscillatory Behavior in CO Oxidation Reaction over Platinum Metals. Comparison with Experiment.</b>	
M. K. Koleva, L.A. Petrov	41
<b><math>1/f</math> Noise: A Criterion for a Long-Term Stable Evolution of the Open Catalytic Systems</b>	
Z. Noszticzius, M. Wittmann, K. Pelle, G. Taba	49
<b>Models of the Classical B-Z Reaction and the Role of Oxalic Acid</b>	
G. Schmitz	58
<b>Modelling the Bray-Liebhafsky Reaction</b>	
S.I. Kuchanov	66
<b>Nonlinear Problems of Quantitative Theory of Free-Radical Copolymerization</b>	
<b>PAPERS OF THE ORAL PRESENTATIONS</b>	
<hr/>	
I. Gudelj, R. E. Beardmore	77
<b>Mutation – Induced Chaos in Evolving Parasitoid Populations</b>	
M. Suchá, P. Vaňková, H. Ševčíková	81
<b><i>Dictyostelium discoideum</i>: A Biological System for Investigation of Nonlinear Phenomena</b>	
Ž. Čupić, S. Anić	85
<b>Stoichiometric Approach to The Modeling of the Terrorism</b>	
A. L. Kawczyński	89
<b>Model of Reaction-Diffusion System as Generator of Old Hebrew Alphabet</b>	
T. Trávníčková, I. Schreiber, M. Kubiček	92
<b>Complex Patterns and Chaos in a Model of Catalytic Cross-Flow Reactor</b>	
A.M. Spasić, M.P. Lazarević, M.M. Mitrović, D.N. Krstić	97
<b>Electron Transfer at Rigid and Deformable Interfaces: Electroviscoelasticity</b>	

N.V. Peskov, M.M. Slinko, S.A.C. Carabineiro, B.E. Nieuwenhuys	101
<b>Mathematical Modeling of Rate Oscillations in <math>N_2O+CO</math> Reaction Over Ir(110)</b>	
E.S. Kurkina, N.L. Semendyaeva	109
<b>Spatiotemporal Phenomena in the <math>NO+CO</math> Reaction Over Pt(100): Simulation Results</b>	
N.I. Koltsov, E.S. Patmar	112
<b>Sistematization of Reaction Mechanisms with Multiplicity Stationary States on the Changing Activity of the Catalyst</b>	
Lj. Kolar-Anić, T. Grozdić, V. Vukojević, G. Schmitz, S. Anić	115
<b>Simulations of Complex Oscillations Based on a Model of the Bray-Liebhaftsky Reaction</b>	
N. Pejić, Lj. Kolar-Anić, V. Vukojević, M. Milošević	119
<b>Determination of Ascorbic Acid in Pure and Pharmaceutical Dosage Form by Using Pulse Perturbation Technique</b>	
M. B. Plavšić	122
<b>Conformational Scaling and Selforganization of Enzymes</b>	
D. Stoiljković, B. Pilić, R. Radičević, I. Bakočević, S. Jovanović, D. Panić, Lj. Korugić-Karasz	126
<b>Polymerization of Organized Monomers</b>	
M. Lazman	130
<b>Application of Polynomial Elimination in Chemical Kinetics</b>	
T. Turányi, I. Gy. Zsély, J. Zádor	134
<b>Selforganization in High Temperature Reaction Kinetic Systems</b>	
B. Nowakowski, A.L. Kawczyński	138
<b>Master Equation Simulations of Bistable and Excitable Dynamics in a Model of Thermochemical System</b>	
<b>PAPERS OF THE POSTER PRESENTATIONS</b>	
<hr/>	
P. Vaňková, M. Suchá, H. Ševčíková	145
<b>Investigation of the Controlled Initiation of cAMP Waves in a Slime Mold Dictyostelium Discoideum</b>	
Č. Radenović, M. Beljanski, A. Ergelj, G.V. Maksimov	149
<b>Induction of Oscillatory Transmembrane Transport by Ammonium Ion</b>	
S. Jelić, Ž. Čupić, Lj. Kolar-Anić	152
<b>Modelling of the Hypothalamic-Pituitary-Adrenal System Activity</b>	
S. Malkov, M. Živković, M. Beljanski, S. Zarić	156
<b>Correlation of Secondary Structure Types with Nearby Amino Acids</b>	
E. P. Zemskov, K. Kassner	159
<b>Analytic Solutions for Traveling Waves in a 3-Component Reaction-Diffusion Model</b>	

T. Godula, H. Ševčíková	162
<b>The Mathematical Study of Spontaneous Excitations in Spatially 1D and 2D Media</b>	
I. Lagzi, F. Izsák	166
<b>Models of Precipitation Pattern Formation in an Electric Field</b>	
D. R. Stanisavljev, A. R. Đorđević, V. D. Likar-Smiljanić	170
<b>Influence of Microwave Heating on the Bray-Liebhafsky Reaction Dynamics</b>	
Lj. S. Rožić, S. Petrović, Ž. Čupić, T. B. Novaković, D. M. Jovanović	174
<b>The Fractal Dimensions of Activated Alumina Samples Obtained in the Reactor for Pneumatic Transport</b>	
S. Blagojević, S. Anić	178
<b>Examination of the Temperature Variations on Belousov-Zhabotinsky Oscillatory Reaction</b>	
S. Blagojević, N. Pejić	182
<b>New Details About the Influence of Acidity and Temperature on the Belousov-Zhabotinsky Reaction</b>	
S. Blagojević	186
<b>Temperature Dependence of the Rate Constant of the Overall Belousov-Zhabotinsky Oscillatory Reaction</b>	
R. Cervellati, S.D. Furrow	190
<b>Perturbations on the Oscillations of the Briggs-Rauscher Reaction by Free-Radical Scavengers: An Overview</b>	
N. Pejić, M. Milošević, V. Vukojević	194
<b>Optimization of Pulse Perturbation Technique for Quantitative Determination of Paracetamol in Pharmaceuticals</b>	
M. Leda, A.L. Kawczyński	198
<b>Wave Trains in Two-Variable Chemical Model of Bistable Reaction-Diffusion System</b>	
S.N. Blagojević, M. Ilić	202
<b>Prediction of Properties In Microemulsion: Molecular Theory</b>	
S. N. Blagojević, N. Potkonjak	205
<b>Prediction of Properties in Microemulsion: The Lattice Fluid Self-Consistent Field Theory</b>	
S. N. Blagojević	208
<b>Prediction of Properties in Microemulsion: Statistical Mechanics of Microemulsion</b>	
O. Pešek, L. Schreiberová, I. Schreiber	211
<b>HPTCu Reaction System in Two Mass-Coupled Reaction Cells</b>	
N. Begović, Z. Marković	215
<b>Activation Energies of Hydrogen Peroxide Decomposition in the Presence of Oxyiodine Species</b>	

## PREFACE

The International Conference Selforganization in Nonequilibrium Systems is the first one from the Nonlinear Sciences in our country. The following topics in theoretical and applied aspects of Nonlinear Sciences are included: Dynamics of Nonlinear Processes, Oscillations and Chaos, Modeling of Selforganization Phenomena, Stability analysis, Stochastic Analysis, Transport Phenomena and Traveling Waves, Perturbations of Nonlinear Systems, – all in physics, chemistry, physical chemistry, biochemistry, ecology and social sciences.

In the total of 44 Papers there are 8 Invited Lectures, and also 16 Contributed Talks and 20 Poster Presentations, both peer-reviewed.

We are grateful to the Ministry of Science and Environmental Protection of the Republic of Serbia, and to all other sponsors for their help. The editors extend their gratitude to the members of the International Scientific Committee and the colleagues who reviewed the supplied contributions. Thanks are also due to the colleagues who took part in the organization of the Symposium and in the preparation of the Book.

It was pleasure to work on this book.

September 2004

Editors

## **Papers of the Invited Lectures**



# SELF-ORGANISATION: FROM PHYSICS TO SOCIAL SYSTEMS

P.M. Allen

*Complex Systems Management Centre,  
Cranfield University, Bedford, MK43 0AL, England*

## Introduction

Ideas that emerged in the natural sciences concerning initially self-organisation and pattern formation (Nicolis and Prigogine, 1977; Haken, 1977; Prigogine, 1981 and Prigogine and Stengers, 1987), provide us with a new basis for understanding both ecological and social systems as the results of evolutionary processes. In this paper we shall focus on the fundamental issue that means that our models and understanding of the world are necessarily incomplete once we move beyond the interaction of simple molecules. We shall explore the essence of “being” and “becoming”, and try to show that these are not just attractive phrases that publishers can put on popular science books to increase sales. It is a real issue and we shall try to show how becoming and being differ and what is the underlying explanation of this. In the first part we shall move from chemistry to ecology and demonstrate these ideas. Then in the next section we shall look at the application of these ideas to human systems and eventually to the issues of policy and decision making that concern us all.

We shall also attempt to explain why a real, natural system is more than the sum of its parts, and the importance of emergent properties and attributes.

## Dissipative Structures - Models of Complexity

As is well known today, in systems with some degree of strong coupling between its elements, when a critical level of thermodynamic disequilibrium is reached then many amazing and surprising things can happen. One of the earliest and most studied cases was the "Brusselator", because of the intensive study it has received by the group at Brussels.

It consists of a simple, fixed, non-linear reaction mechanism,



where A and B feed the reaction, D and E are produced by it, and X and Y are intermediates. Let us suppose further that X is red in colour, and Y is blue. The kinetic equations for this reaction scheme are very simple to write, and we assume that the products of reaction E and D are removed to avoid the occurrence of a back reaction:

$$\begin{aligned}\frac{dx}{dt} &= A - BX + X^2Y - X \\ \frac{dy}{dt} &= BX - X^2Y\end{aligned}\tag{2}$$

As is well documented, under conditions of chemical disequilibrium All sorts of moving or stationary patterns can emerge. For example, if we stir the reaction, then at a certain critical reaction rate, instead of the system being uniform (a homogeneous mixture of red and blue, of  $X$  and  $Y$ ) it suddenly begins to oscillate steadily from all red to all blue and back, in a perfectly rhythmic manner. Even if perturbed momentarily, it will return to this particular, stable beat. The random, incoherent movements and reactions of the molecules is abruptly transformed into disciplined, coherent, co-ordinated behaviour worthy of a good choir! In a system that is not stirred all sorts of spatial and spatio-temporal structures can appear spontaneously: from simple left/right inhomogeneities, to expanding spiral waves of various well defined dimensions, to moving or stationary bands of red and blue - a whole bundle of different possibilities.

This process of self-organisation is a remarkable phenomenon that strikes at the heart of some of our deepest preconceptions concerning physical systems. For example, if we take a particular spatial structure, then at the interface of "red" and "blue" there will clearly be fluxes of  $X$  and  $Y$  caused by the concentration gradients. Our normal reaction would be to say that they are "explained" by the "forces" that must exist between the zones. But in fact these forces themselves are generated by the spatial structure of which the interface is a part, and which in turn reflects the fluxes that are occurring in the system. If, for example, the coefficient of diffusion were modified, or the temperature, then the spatial structure itself would change or perhaps even disappear. In this sense, the "cause" of this particular structure is the precise values of the fluxes, which in their turn, according to our simple preconceptions, result from this structure. Clearly, the circularity of the apparent "causation" is showing up some weakness in our way of thinking about things.

In reality, a "dissipative structure" is an entity that has as mutually dependent facets the flows and spatial structures that characterize it. Interference with one will modify both through a cascade of feedback processes. We see that we have a system that has created its own "boxes" and "arrows". Furthermore, we see that the "Modeler's Nightmare", i.e., the fact that complex systems evolve structurally (new boxes, new arrows) is quite clearly part of the behaviour of a dissipative structure. A particular type of behaviour, homogeneous temporal oscillation, moving parallel bands, etc. can spontaneously change to a qualitatively different one. If we had been rash enough to model the system on the basis of its particular macro-behaviour at the earlier time, then suddenly our model would fail to describe what was occurring.

Also, we come upon the dilemma that faces any ecologist trying to understand the system before him. We can "track" the energy flow in the Brusselator, or make balance equations (accountancy) for particular materials (carbon, nitrogen etc.); but these always *only indicate or reflect* the structure that had appeared in the system, and do not explain it, nor predict when some new structure may emerge. The "explanation" behind a par-

ticular "structure/flow" pattern lies in the history of instabilities it has traversed, and especially in the stability or instability of the structure at the moment we are observing it.

What is new, and important, is that different solution branches can emerge which are qualitatively different from each other. We have, therefore, a *non-conservation* of symmetry, and hence of the number and nature of the "qualities" which characterize the system. In one stride we have moved from the relative banality of simple arithmetic to the quantitative modelling of morphogenetic processes whereby structure and function emerge, where the qualitative differences of the living world appear, and in which we find creation instead of conservation.

Evolution represents a dialogue between the real, rich micro-detail of the system, and the simpler deterministic average behaviour that we have considered to be adequate to represent it.

### **Evolving Ecologies Evolving**

Can we extend the ideas and modelling methods from chemical kinetics – the population dynamics of reacting molecules – to ecologies? What differences would exist between chemical kinetics and population dynamics of real populations? If so, then can the lessons of self-organisation be transferred to ecologies, and from there to social systems. Let us consider this by taking the following example. Consider an ecosystem, and let us attempt to model it using population dynamics. We can establish the different species that exist there, and then find out how many of each population there are. We can also, by sampling, find out which population eats which other population and calibrate the multiple plant/herbivore and predator/prey interactions. Now, once this is established, we can put the whole system of equations on a computer, and run it forward. What happens is shown in figure (1).

This is an astonishing result. It means that although the model was calibrated on what was happening at time  $t = 0$  it diverged from reality as time moved forward. The real ecosystem stayed complex, and indeed continued to adapt and change with its real environment. But this shows us that the mechanical representation of reality differs critically from that reality.

What is missing? This can be discovered if we examine carefully the assumptions that we made in formulating our population dynamics. Although it worked for chemistry – it didn't work for ecology.

What happened is that the loops interactions of a real ecosystem form parallel food chains, with cross connections and complications of course, but essentially with each level feeding on the lower one, some of these dying and others being eaten by the level above. The whole system of food chains loops back through death and micro-organisms that recycle all the carbon and minerals. When we run the population dynamics with the fixed birth, death capture and escape rates that we have found on average in the real system (in analogy with chemical reaction rates), then the food chain with the highest performance simply eliminates all the others. In other words, selection between metabolic chains operates and this selects for the highest performing chain. However, reality does not. Therefore we need to understand what is missing between the dynamic model and the original real system.

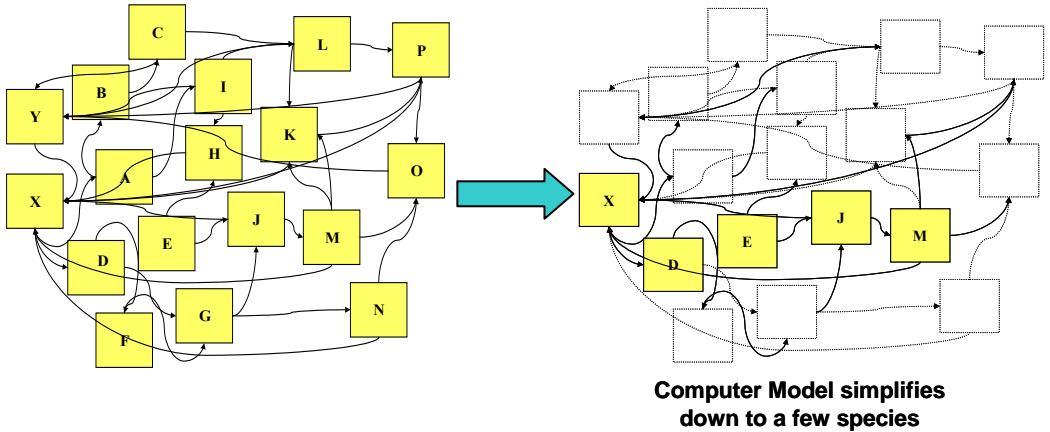


**Figure 1.** A calibrated ecosystem represented by the population dynamics of its constituent species collapses when run forward in time.

The key answer is that what is missing is the internal diversity of the populations. In chemistry, one molecule is very like another, and the only difference is their spatial location. Dissipative structures can create spatio-temporal patterns because of this. But populations of organisms differ in an infinite number of ways. Firstly in location, but also in age, size, strength, speed, colour etc. and so this means that whenever a population, X, is being decreased by the action of some particular predator or environmental change, then the individuals that are most vulnerable will be the ones that “go” first. Because of this the parameter representing the average death rate will actually change its value as the distribution within the population X increases the average “resistance”. In other words, the whole system of populations has built in through the internal diversities of its populations, a multiple set of self-regulatory processes that will automatically strengthen the weak, and weaken the strong. In the same way that reaction diffusion systems in chemistry can create patterns in space and time, so in this more complex system, the dynamics will create patterns in the different dimensions of diversity that the populations inhabit. But neither we, nor the populations concerned, need to know what these dimensions are. It just happens as a result of evolutionary dynamics.

In this case it becomes key to understand the sequence of assumptions that take us from reality to a mechanical representation of that reality. This leads us to the general view that is shown in figure (2). This sets out the kind of models that result from a particular set of assumptions.

This succession of models arises from making successive, simplifying assumptions, and therefore models on the right are increasingly easy to understand and picture, but increasingly far from reality. **They also are shorn of their capacity to evolve – their real underlying exploratory, error-making processes.** The operation of a mechanical system may be easy to understand but that simplicity has assumed away the more complex sources of its ability to adapt and change. They become more like “descriptions” of the system at a particular moment, but do not contain the magic ingredient of micro-diversity that will really allow the system to undergo structural

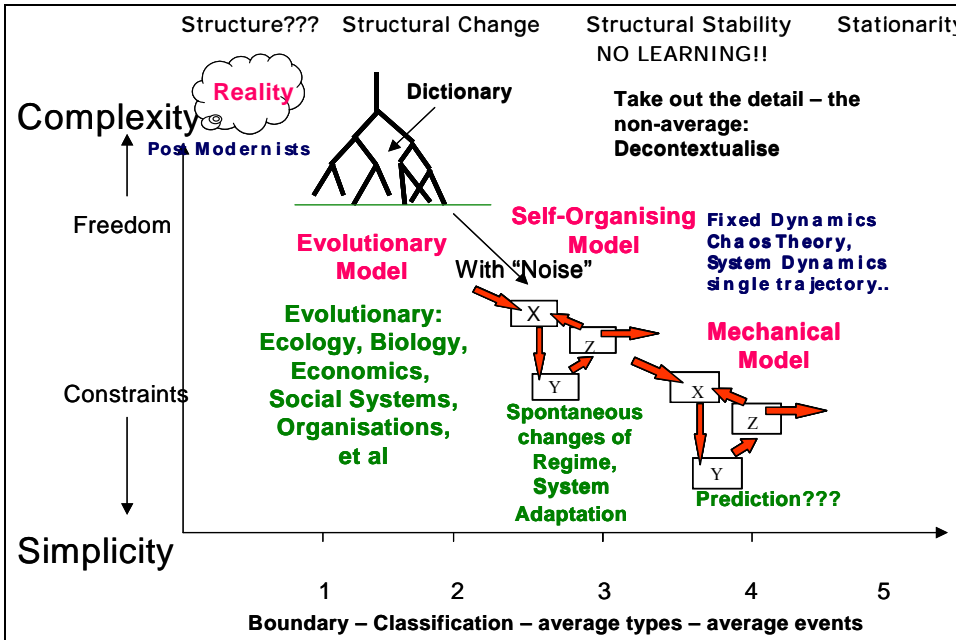


**Figure 2.** This shows the results of successive simplifying assumptions that take us from a complex evolving system to its mechanical representation.

change and create a new, qualitatively different system, with some new variables and some emergent performance. The ability to adapt and change is still present in the “evolutionary” model that only makes assumptions 1 and 2, but not those of average type and average behaviours. This therefore tells us that the evolutionary capacity is generated by the behaviours that are averaged by assumptions 3 and 4 – average types and average events – and therefore that organisations or individuals that can adapt and transform themselves, do so as a result of the generation of micro-diversity and the interactions with micro-contextualities. This tells us the difference between a reality that is “becoming” and our simplified understanding of this that is merely “being” (Prigogine 1981).

All of this is fairly irrelevant for the chemistry of simple molecules, because a population does not have internal diversity, and so there is nothing for evolution to work on. However, as soon as we reach organic molecules, with complex polymers, and different ways of folding, then we see that these same ideas apply and an evolutionary process becomes possible that makes the real system more than its mechanical representation.

### The Importance of Micro-Diversity

Let us now consider the workings of this “micro-diversity” and see how it both drives evolution – and is also selected for by evolution. If consider the simplest possible equation for a population of organisms, it is the logistic equation.

$$\frac{dx}{dt} = bx\left(1 - \frac{x}{N}\right) - mx \quad (1)$$

Now let us consider the effect in such a simple of “error making” at the level of reproduction of  $x$ . This would potentially produce different types of  $x$ , with different characteristics, and different parameters of birth and death.

Let us consider a 1-dimensional “population character space” of different possible behaviours for the population  $x$ . If we consider that initially we have a single “pure” population type then it will sit on one particular behaviour,  $i$ . However, if there are any “errors” or “explorations” made in the reproduction of this behaviour, this will correspond to diffusion outwards in that space.

$$\frac{dx_i}{dt} = \{(b_i * x_i * f + .5 * b_{i+1} * x_{i+1} (1-f) + .5 * b_{i-1} * x_{i-1} (1-f)) * (1 - \frac{x_i}{N}) - m * x_i$$

So,  $(1-f)x_i$  flow from behaviour  $i$  to  $i+1$  and  $i-1$ , while

- $.5*(1-f)v x_{i+1}$  and
- $.5*(1-f)v x_{i-1}$

flow in from the neighbouring behaviours, where  $v$  represents the fraction of explorations that are simply non-viable. Figure (3) shows us what happens.

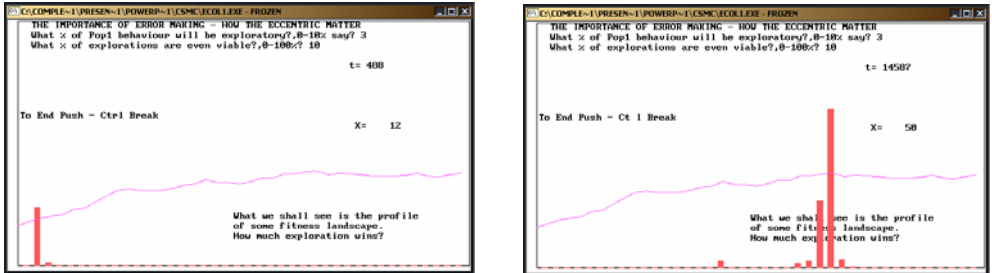


**Figure 3.** In a space of possible behaviours random modifications will lead the population to “climb” the hill.

This experiment tells us that evolutionary progress – hill climbing - occurs as a result of processes that generate a “diffusion” in character space. Ignorance and error making are very robust sources of such exploration, but clearly random changes in the design of any complicated entity will mean that most experiments are simply non-viable, and only half of those that remain are “better”. This effectively tells us that there is an “opportunity cost” to behavioural exploration, and that there will be some “best” amount of “exploration” in a given situation, at which the pay-offs found, minus the opportunity cost is a maximum.

In a model with two competing populations with different degree of error making, we find that initially the “explorer” (error-maker) climbs the hill faster and leaves the other behind, but later, when there is nothing left to discover, the exploiter (non-error-maker) wins. Our model reveals to us a strategic reality – when we are in a new domain, and there is a lot to learn – then learning/exploration pays off. However,

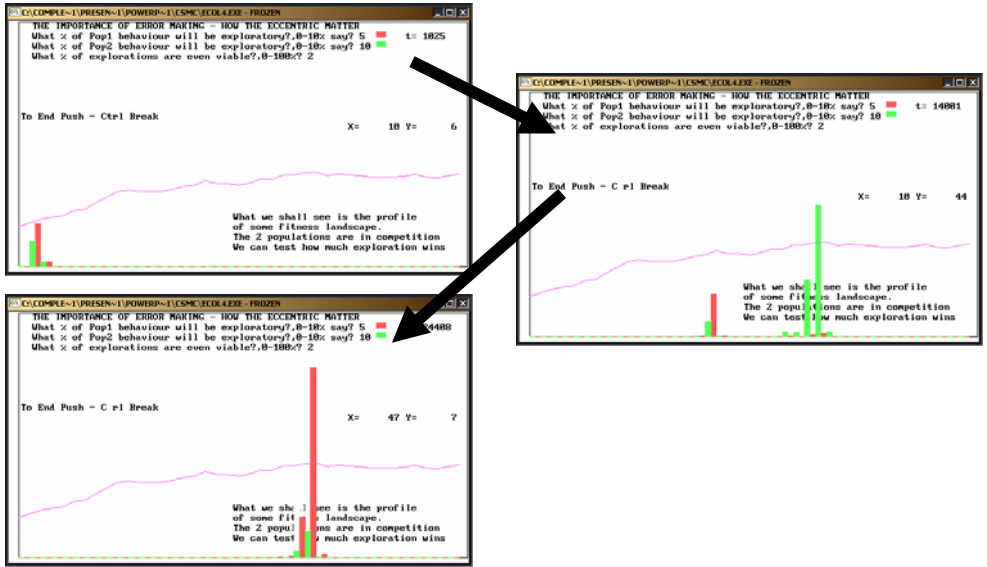


**Figure 4.** If we have two populations that have different rates of “exploration” then we find that the relative success changes from early exploration to late exploitation.

when we are in a mature system that has already been thoroughly explored there is no point wasting effort on further exploration. Of course, we can only know there are opportunities or not by actually engaging in exploration, but clearly, unless there is some structural change, the value of exploration falls with sector maturity, and this will lead exploration behaviour to switch to exploitation.

In other words, the presence of populations with different levels of exploration and exploitation (error-making and accuracy) will automatically lead to evolution selecting whichever is most appropriate. So, evolution will be driven by the amount of diversity generation to which it leads. Evolution selects for an appropriate capacity to evolve.

Another important point made here is that it shows us how the micro-diversity that is constantly generated at a **low level** in a system, leads to the evolution of structure, organisation and diversity, characterised by the development through a “life cycle” of any new domain – exploring and rapidly expanding in a new domain and gradually filling and saturating as a mature stage is reached.

## Modelling Human Systems

These ideas can now be transferred to human systems. Behaviours, practices, routines and technologies are invented, learned and transmitted over time between successive actors and firms, so that evolutionary processes arise in exactly the same way.

### 5.1 A Fisheries Example

In this example we refer to a detailed model that was developed of Canadian Atlantic fisheries (Allen and McGlade, 1987). This is a spatial model that generates the movement of fishermen, based on the information they have concerning fish abundances,

and the "expected revenue" that could be obtained from fishing a particular zone. This information comes from the fishing activity of other boats, and therefore there is a tendency for the pattern of fishing to structure spatially because high catches result in a concentration of effort and, in consequence, high catches in that zone. Areas where fishing boats are absent send no information about potential catch and revenue. This provides a spatial positive feedback mechanism that structures fishing patterns.

The model describes how boats are attracted to zones in which they know high catches and catch rates are occurring, but of course, they only know this if there is communication between the boats in  $i$  and in  $j$ . This will depend on the "information exchange" matrix, which will express whether there is cooperation, spying or indifference within and between fleets. However, in deciding which zone to go to, fishermen take into account the distances involved to go there, and to return to port and the cost of fuel.

In addition to these effects, however, our equation takes another very important factor into account. This factor  $R$  expresses how "rationally", how "homogeneously" or with what probability a particular skipper will respond to the information he is receiving. For example, if  $R$  is small, then whatever the "real" attraction of a zone  $i$ , the probability of going to any zone is roughly the same. In other words, "information" is largely disregarded, and movement is "random". We have called this type of skipper a *stochast*. Alternatively if  $R$  is large, then it means that even the smallest difference in the attraction of several zones will result in every skipper of that fleet going, with probability 1, to the most attractive zone. In other words, such deciders put complete faith in the information they have, and do not "risk" moving outside of what they *know*. These "ultra rationalists" we have called *Cartesians*. The movement of the boats around the system is generated by the difference at a given time between the number of boats that would like to be in the each zone, compared to the number that actually are there. As the boats congregate in particular locations of high catch, so they fish out the fish population that originally attracted them. They must then move on the next zone that attracts them, and in this way there is a continuing dynamic evolution of fish populations and of the pattern of fishing effort.

This is a remarkable result. The higher the value of  $R$ , the better the fleet optimizes its use of information and in the short-term increases profits. But, this does not necessarily succeed in the long term. After leaving the port and locating a first fish aggregate, they "lock on" to this zone and stay fishing there for too long, because it is the only information available. These **Cartesians are not "risk-takers"** and will not go out to zones with no information, and hence they get "locked in" to the existing pattern of fishing. The **Stochasts** ( $R=.5$ ), providing that they are not totally random ( $R < .1$ ) succeed in both **discovering** new zones with fish stocks, and also in exploiting those that they have already located.

This paradoxical situation results from the fact that in order to fish effectively, two distinct phases that must be accomplished. First the fish must be "discovered". This requires spatial diversity and risk taking by those willing to go into the "unknown" and explore, whatever present knowledge is. The second phase, however, requires that when a concentration of fish have been discovered, then the fleet will move

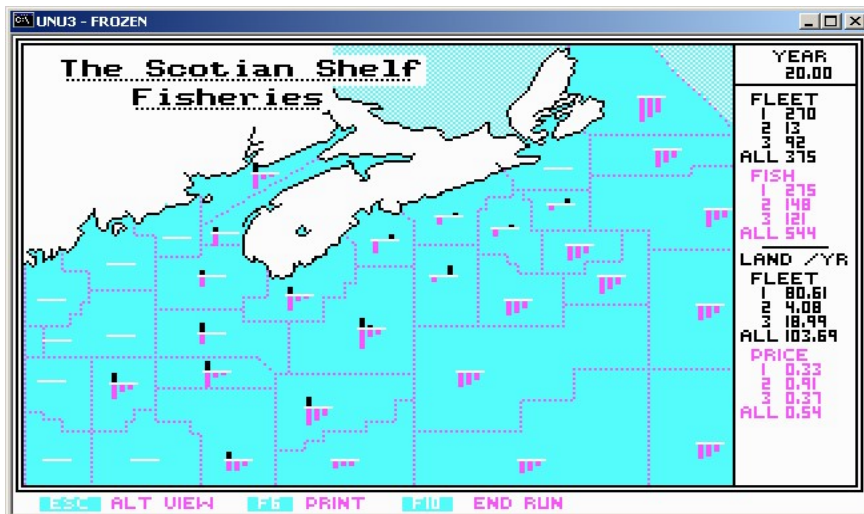


**Figure 5.** After 20 years with fleet 1 defeats 2 by having less rationality.  $R = .5$  for fleet 1 and  $R = 3$  for fleet 2.

in massively to exploit this, the most profitable location. These two facets are both necessary, but call on different qualities.

The simulation system can be used to explore which behavioural strategies work for different fleets and examine how the pattern of fishing results from a process of spatial self-organization, which needs to “fit” the patterns of fish stocks, and of their decline under fishing, and recovery when fishing pressure relaxes. Let us briefly summarize the pattern of behaviours that could evolve in a fishery as the result of experimentation among fishermen.

- Fleets find a moderate behaviour with rationality between .5 and 1
- Cartesians try to use the information generated by Stochasts, by following them, and by listening in to their communications.
- Stochasts attempt to conceal their knowledge, by communicating in code, by sailing out at night, and by providing misleading information.
- Stochasts and Cartesians combine to form a cooperative venture with Stochasts as “scouts” and Cartesians as “exploiters”. Profits are shared.
- Different combinations a stochoast/Cartesian behaviour compete.
- In this cooperative situation, there is always a short term advantage to a participant who will cheat.
- different strategies of specialization are adopted. E.g. Deep-sea or inshore fishing, or specialization by species.
- a fleet may adopt “variable” rationality, adapting its search effort according to the circumstances.
- in all circumstances, the rapidity of response to profit and loss turns out to be advantageous, and so the instability of the whole system increases over time.

The real point of these results is that they show us that there is no such thing as an Optimal Strategy. As soon as any particular strategy becomes dominant in the system, then it will always be vulnerable to the invasion of some other strategy. More importantly for this paper, we see that it is the capacity of fleets to generate new knowledge and forget old that allows them to continue fishing into the future. So, once again we see that in order to create a learning capacity to respond to the fishermen exhausting their immediate environment of fish, we need to relax their rationalities and make them wander and explore in order to make new discoveries. What is interesting is that instead of our “rationality” making us superior to nature and its unintentional ways, we see that we need to turn off our rationality, our clever economic calculations and our directed, intentional behaviour in order to continue fishing and find ways of returning to behaviour that is simpler.

### *Emergent Market Structure*

The ideas developed in the sections above have been applied to a variety of systems, but here will be applied to the structuring of economic markets, as competition creates ecologies of firms producing goods in different market niches. The fundamental process can be explored initially using a simple model in which we consider the possible growth/decline of several firms that are attempting to produce and sell goods on the same market. The potential customers of course will see the different products according to their particular desires and needs, and in the simple case examined here, we shall simply consider that customers are differentiated by their revenue, and therefore have different sensitivities to price.

The structure of each firm that is modelled is as shown in Figure (6). Inputs and labour are necessary for production, and the cost of these, added to the fixed and start-up costs, produce goods that are sold by sales staff who must “interact” with potential customers in order to turn them into actual customers. The potential market for a product is related to its qualities and price, and although in this simple case we have assumed that customers all like the same qualities, they have a different response to the price charged. The price charged is made up of the cost of production (variable cost) to which is added a mark-up. The mark-up needs to be such that it will turn out to cover the fixed and start-up costs as well as the sales staff wages. Depending on the quality and price, therefore, there are different sized potential markets coming from the different customer segments.

When customers buy a product, they cease to be potential customers for a time that is related to the lifetime of the product. For high quality goods this may be longer than for low quality, but of course, many goods are bought in order to follow fashion and style rather than through absolute necessity. Indeed, different strategies would be required depending on whether or not this is the case, and so this is one of the many explorations that can be made with the model.

The model calculates the relative attractivity of a product (of given quality and price) for a customer of a given type (poor, medium or rich). This results in a calculation of the “potential market” for each firm at each moment, and the sales staff must interact with these potential customers in order to turn them into customers. When a

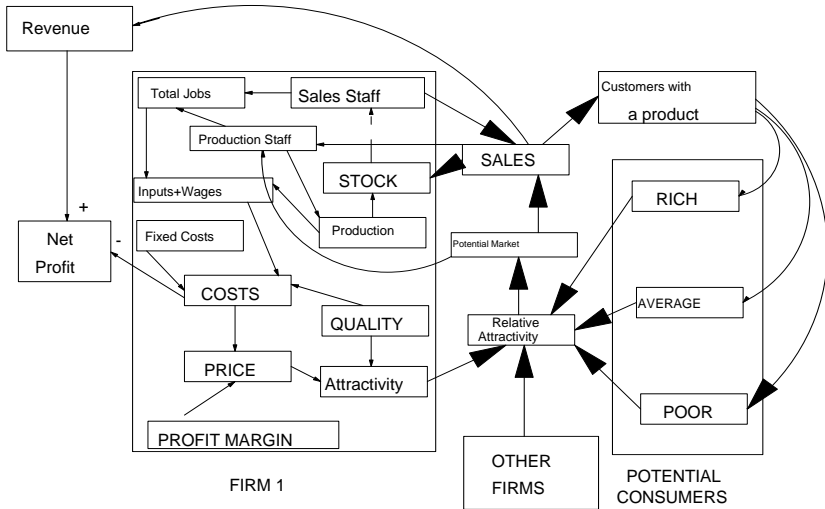


**Figure 6.** The Evolutionary Market Model structure.

sale is made, then the potential customer becomes a customer and disappears from the market for a time that depends on the product lifetime.

A very important issue that arises in the modelling concerns the rationality of the manager of the firm in electing to adopt whatever strategy is chosen. In traditional economic theories firms are supposed to act, or to have acted, in such a way as to obtain maximum profit. But, here, we can see that if we used the profit as the driving force for increased production, then the system could not start. **Every new action must start with an investment.** That is with a negative profit. So, if firms do start production, and increase it, then this cannot be modelled by linking the increase in production to the profit at that time. Instead, we might say that it is driven by the **expected profit** over some future time. But how does a manager form his expectations? Probably a model of the kind that is being described here is way beyond what is usually used, and in any case, there is a paradox. In order to build this model, in order perhaps for managers to formulate their expectations, the model requires a representation of manager's expectations. But this is only a paradox if we believe that the model is about **prediction**. Really, it is about exploration, the exploration of how we think a market works, and so it is a part of a learning process, which may indeed lead participants to behave differently from the way that was supposed initially. Such an outcome would already be a triumph.

Despite this paradox, and the difficulty in knowing what is going to happen beforehand, firms do start up, production is increased, and economic sectors are populated with firms, so, even though there is this logical problem. Obviously it does not worry participants in reality. Since bankruptcies obviously also occur, then we can be sure that the expectations that drive the investment process are not necessarily related to the real outcomes. In our model therefore we simply have assumed that managers

want to expand to capture their potential markets, but are forced to cut production if sales fall. So, they can make a loss for some time, providing that it is within their credit limit, but they much prefer to make a profit, and so attempt to increase sales, and to match production to this.

The picture that emerges from this study of a dynamically, self-organizing market sector model is that of the emergence of product niches. It is the economies and diseconomies of production and distribution that will determine the number, size and scale of these niches, and they will depend on the initial history of the market sector in question as a "lock-in" evolves. However, as new technology appears, or as the rest of society evolves, new attributes can come into play for the products. However, the effect and importance of these may be different when viewed by the producers as opposed to consumers.

We can use our model to explore the effect of different learning strategies of firms.

- a. Death and Replacement.** In this we assume that firms do not adapt their price and quality strategies but pursue them to success or bankruptcy. Following bankruptcy, however, we re-launch the firms into the system with a new, randomly chosen strategy. This either survives or fails in its turn. A typical long-term simulation is shown in figure (7). This shows the 2-D space of mark up (%) and quality (Q), and the positions of the various firms.

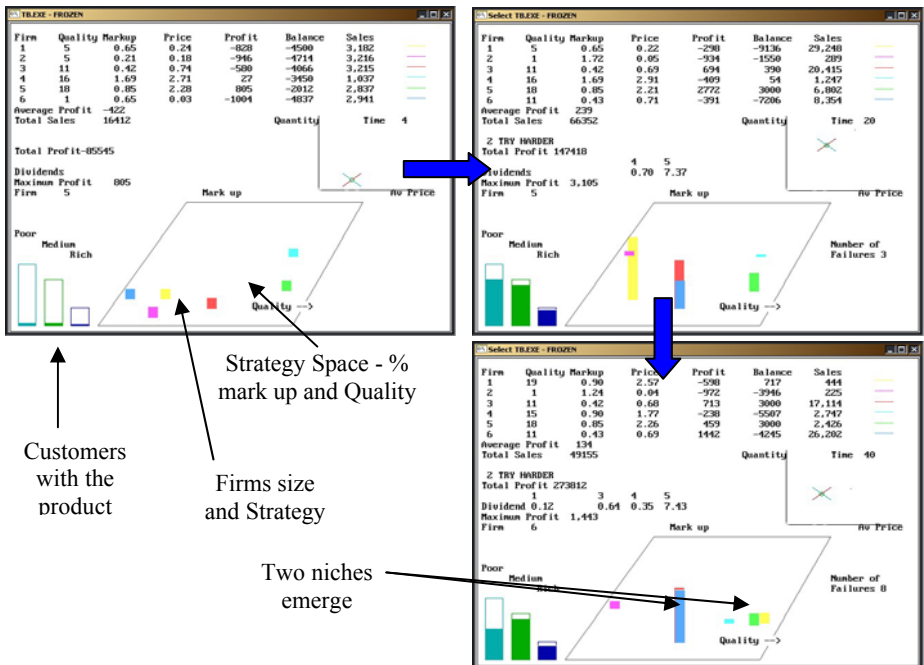


**Figure 7.** A typical evolutionary run where gradually the “Darwinian” process discovers two fairly stable niches – around  $Q=11$ ,  $\% = 40$  and  $Q = 18$ ,  $\% = 85$ .

- b. Hill-climbing.** In the next version, firm 1 uses the “hill-climbing” method described in section 3 of the paper. Micro-diversity experiments allow learning.

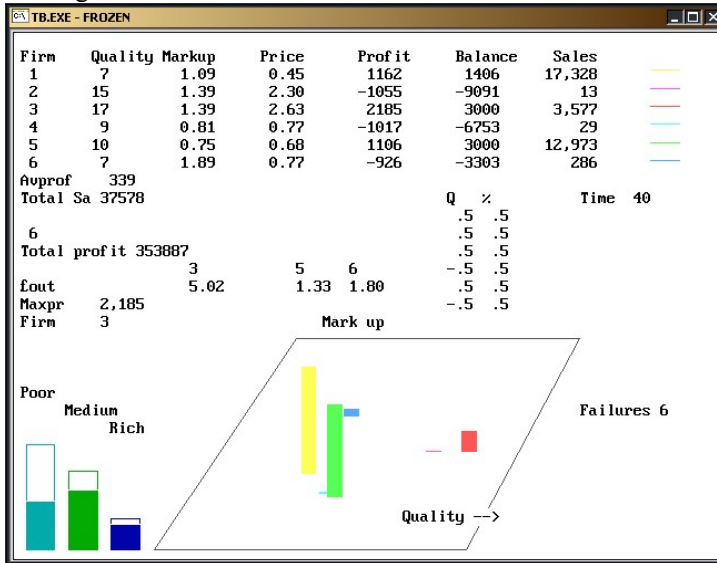


**Figure 8.** Here firm 1 tests the “profit gradient” and moves Q and % accordingly up-hill. It does much better, making a profit and paying a dividend to investors.

- c. All Hill-Climb.** However, if we allow all the firms to “hill-climb”, then their mutual interaction reduces the advantage of learning.
- d. Imitation** – Another strategy is for a firm to monitor the market carefully and for it to adapt its production as rapidly as possible to copy whichever firm is currently making most profit.
- e. All Imitation** - We can also consider the impact on the system when all the firms imitate whoever is winning. All the firms move to the same place in strategy space, and in so doing increase the degree of competition that they each feel. As a result, there are more bankruptcies (9) than in any of the other simulations. What might have seen a “risk averse” strategy turns out to be the opposite! To imitate in a market of imitators is highly risky.
- f. Diverse learning Strategies** - In section 5.1 concerning the emergence of different strategies among fleets of fishing boats it was shown that what mattered was that an ecology of strategies emerged. Once again diverse strategies are best. The market ecology/niches emerge fastest.

In some ways, for public policy what matters is the level of customer satisfaction, and the level of overall profit for the sector. In our accounting for overall costs we need to include that of bankruptcy since every time that it occurs in our model, the social system, other firms etc. lose 10,000 units. In the real world the costs can be more devastating still to those involved and could even lead to a serious limitation on the willingness of actors to innovate.

We can examine the question as to the overall outcomes for the “industry” of different strategies. In order to look at this, we have calculated the overall profits of the whole market, and we have included the costs of bankruptcies, in which often, a loser takes trade away from others in an attempt to keep going, but eventually crashes with debts. In the figure (9) we show the over all outcome for four different learning strategies. They are:

- Darwinian (random strategies, no learning)
- Old Strategy (If profit less than half average, reduce %)
- Hill-Climbing
- 3-6 hill-climbers, 1-3 imitators

However, here we have also performed four different runs for different sequences of random numbers, implying simply a different sequence of chance events.

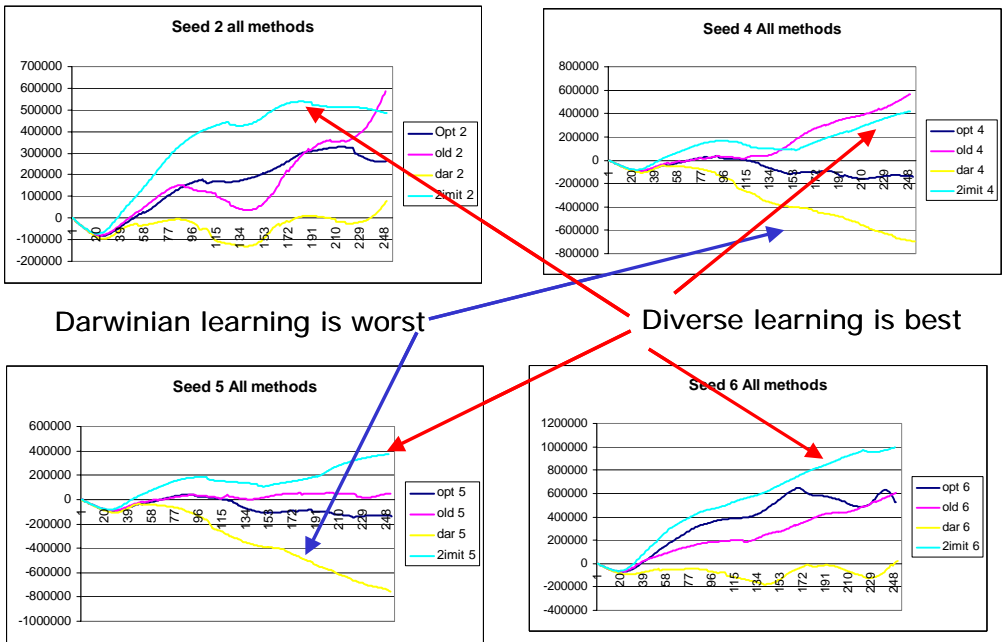


**Figure 9.** Mixed learning strategies work best. However, luck (the random sequence) can lead to very different market outcomes from highly profitable to only marginally so. The invisible hand seems to be highly capricious – one might doubt its existence.

**Conclusions**

There are several important points about these results. They show us that for a system of co-evolving agents with underlying micro-diversity and idiosyncrasy, then we **automatically** obtain the emergence of structural attractors such as figure (9). A structural attractor is the temporary emergence of a particular dynamical system of limited dimensions, from a much larger space of possible dynamical systems and di-

mensions. These are complex systems of interdependent behaviours whose attributes are on the whole synergetic. They have better performance than any single, pure homogeneous behaviour, but are less diverse than if all “possible” behaviours were present. In other words, they show how an evolved entity will not have “all possible characteristics” but will have some that fit together synergetically, and allow it to succeed in the context that it inhabits. The structural attractor (or complex system) that emerges results from the particular history of search and accident that has occurred and is characteristic of the particular patterns positive and negative interactions of the components that comprise it. In other words, a structural attractor is the emergence of a set of interacting factors that have mutually supportive, complementary attributes.

What are the implications of these structural attractors:

- ◆ self-organisation in chemistry and physics is limited by the lack of micro-diversity of the underlying components. Once we reach polymers and organic compounds however, this situation changes and evolution becomes a reality.
- ◆ The search carried out by the “error-making” diffusion in character space leads to the emergence of diverse structures and organisation expressing overall synergy
- ◆ the whole process leads to the evolution of a complex, a “community” of agents whose activities, whatever they are, have effects that feed back positively on themselves and the others present. It is an emergent “team” or “community” in which positive interactions are greater than the negative ones.
- ◆ a successful and sustainable evolutionary system will clearly be one in which there is freedom and encouragement for the exploratory search process in behaviour space. Sustainability in other words results from the existence at multiple levels of a capacity to explore and change. This process leads to a highly co-operative system, where the competition per individual is low, but where loops of positive feedback and synergy are high. In other words, the free evolution of the different populations, each seeking its own growth, leads to a system that is more co-operative than competitive. The vision of a modern, free market economy leading to, and requiring a cut-throat society where selfish competitiveness dominates, is shown to be a false view of evolution, but probably reflects a convenient one for the powerful.

The most important point really is the generality of the model presented above. Clearly, this situation characterizes almost any group of humans: families, companies, communities etc., but only if the exploratory learning is permitted will the evolutionary emergence of structural attractors be possible.

The structural evolution of complex systems is as shown in figure (9) how explorations and perturbations lead to attempts to suggest modifications, and these lead sometimes to new “concepts” and structural attractors that have emergent properties. The history of any particular product sector can then be seen as an evolutionary tree, with new types emerging and old types disappearing. But in fact, the evolution of “products” is merely an aspect of the larger system of organisations and of consumer lifestyles that also follow a similar, linked pattern of multiple co-evolution.

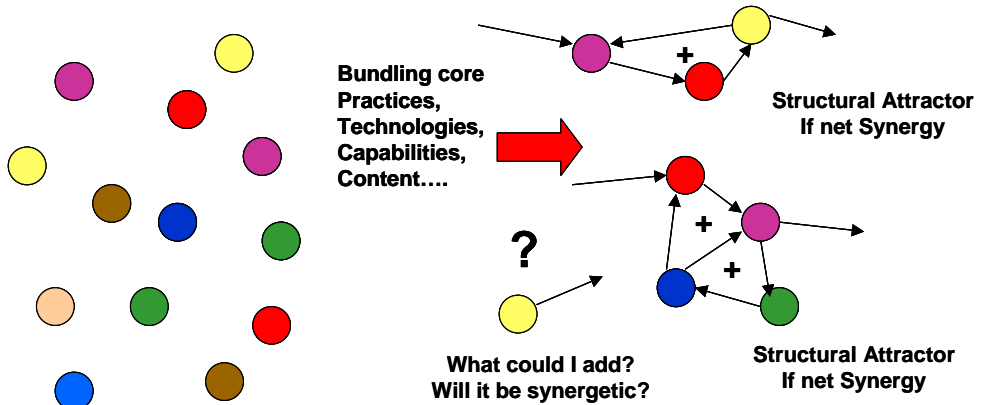


**Figure 9.** On the left we have “dictionary” of possible core concepts, practices or ideas. These are “bundled” on the right and if the different elements have synergy then the structure is successful.

Throughout the economy, and indeed the social, cultural system of interacting elements and structures we see a generic picture at multiple temporal and spatial scales in which uncertainty about the future **allows** actions that are exploratory and divergent, which are then either amplified or suppressed by the way that this modifies the interaction with their environment. Essentially, this fulfils the early vision of dissipative structures (Nicolis and Prigogine, 1977; Prigogine and Stengers, 1987), in that their existence and amplification depend on “learning” how to access energy and matter in their environment. Can they form a self-reinforcing loop of mutual advantage in which entities and actors in the environment wish to supply the resources required for the growth and maintenance of the system in question. In this way, structures emerge as multi-scalar entities of co-operative, self-reinforcing processes.

What we see is a theoretical framework that encompasses both the evolutionary and the resource-based theory of the firm. And, not only of the firm, but also of the social and economic system as a whole. It is the complex systems dialogue between explorations of possible futures at one level, and the unpredictable effects of this both at the level below and the level above. There is a dialogue between the “trade-offs” or “non-linearities” affected inside and outside the particular level of exploration. But it is also true that all levels are exploring. Unless there is an imposition of rigid homogeneity up and down the levels of the system, there will necessarily be behavioural explorations due to internal diversity. In this way, multi-level systems are precisely the structures that can “shield” the lower levels from instantaneous selection, and allow an exploratory drift to occur, that can generate enough diversity to eventually DISCOVER a new behaviour that will grow. Without the multiple levels, selection would act instantly, and there would be no chance to build up significant deviations from the previous behaviour.

This paper sketches out an integrated theory of biological, economic and social evolution. It suggests how the diversity that characterizes an evolved structure is created by the action of lower level error making processes that generate micro-diversity. Furthermore, evolution itself selects for systems that can evolve and adapt structures –

that is ones that allow internal error-making explorations. This is as true for our organisations and social structures and for the artefacts that we create. Products themselves exist as embodiments of attributes that are synergetic (internally coherent) clusters, and different product markets emerge naturally as a result of inherent conflicts between attributes. For example, a palmtop computer cannot have a really easy to use keyboard (under existing design concepts) and so notebooks and laptops exist in a different market to palmtops. Similarly, toasters and telephones also occupy separate markets because answering a call on a toaster/telephone can set your hair on fire. So, again it is the “complementarities and conflicts” of possible attributes that structures the space of possible product or service markets.

If we return to the fundamental level of why a mathematical model will always be a model of being and not one of becoming, we see that the fundamental assumption is that of an underlying Markov Process. But, what we see is that although all the information can be present in a model concerning the mechanisms we know, there will always be mechanisms that we don’t know about that are on-going! In the ecological case of section 2 the fact is that we do not know which dimensions of micro-diversity really matter for the system, nor do we know how memories within organisms will affect their behaviour. This means that fundamentally our simplification turns a living, evolving reality into a dynamic description that does not contain the “future” of the real system, but only the simpler future of its reduced description. We can see why some mathematical models can be successful at predicting behaviour in physical systems, but not in predicting evolution in complex biological and social ones.

## Acknowledgement

This work was supported by the ESRC NEXSUS Priority Network.

## References

- [1] P.M Allen, “Evolution, Population Dynamics and Stability”, Proc Nat Acad Sci, USA, 1976, 73(3), 665.
- [2] P.M. Allen, "Evolution: Persistent Ignorance from Continual Learning", in "Nonlinear Dynamics & Evolutionary Economics", Oxford University Press, 1993, Chapter III, 8, 101.
- [3] P.M. Allen, "Evolutionary Complex Systems: Models of Technology Change", in "Chaos and Economic Theory", Eds L.Leydesdorff and P.van den Besselaar, Pinter, London, 1994.
- [4] P.M. Allen, Knowledge, Ignorance and the Evolution of Complex Systems, in *Frontiers of Evolutionary Economics: Competition, Self-Organisation and Innovation Policy*, Eds J. Foster and S. Metcalfe, Edward Elgar, Cheltenham, UK, 2001.
- [5] P.M. Allen, A Complex Systems Approach to Learning, *Adaptive Networks*, International Journal of Innovation Management, June 2001, 5(2), 149.
- [6] Haken H., *Synergetics*, Springer Verlag, Berlin, 1977.
- [7] G. Nicolis, I. Prigogine, *Self-organization in non-equilibrium systems*, Wiley Interscience, New York, NY1977.
- [8] I. Prigogine, *From being to becoming*, W.H. Freeman, New York, 1981.
- [9] I. Prigogine, I. Stengers, *Order out of Chaos*, Bantam Books, New York, 1987.

## CHEMICAL WAVE PROPAGATION IN INHOMOGENEOUS MEDIA

G. R. Armstrong<sup>1</sup>, V. Gáspár<sup>2</sup>, S.K. Scott<sup>1</sup>, A.F. Taylor<sup>1</sup>

<sup>1</sup>*School of Chemistry, University of Leeds, Leeds LS2 9JT, UK*

<sup>2</sup>*Department of Chemistry, University of Debrecen, 4010 Debrecen, Hungary*

### Abstract

Experimental and computational studies are reported of reaction-diffusion waves in the Belousov-Zhabotinsky system with an immobilised catalyst printed on a membrane. Inhomogeneous media are created by printing domains with pre-determined “gaps” in which no catalyst is present. The propagation of single waves or of wave trains across either a single gap or a series of gaps is determined for excitable systems. This provides a chemical model of wave propagation in the simplest inhomogeneous biological systems but may throw light on features relevant in AV node block in cardiac arrhythmia or in the action of local anaesthetics. Experimental results show complete wave propagation for small gaps, complete wave block for large gaps, and an intermittent response between these extremes with  $n$  waves transmitted for every  $m$  incident waves ( $n < m$ ) analogous to the Wenckebach rhythms observed in heart tissue. These observations are confirmed through computed solutions using an Oregonator model for the BZ reaction.

### Introduction

The propagation of waves in excitable or active media is of vital importance in living systems and has, consequently, been an area of considerable research [1]. Biological systems are necessarily complex and typically extensively heterogeneous in nature. Chemical systems, by contrast, provide an attractive medium in which to study generic features of such waves: chemical systems are more easily controlled and waves typically evolve on convenient length and time scales that can be monitored directly by optical imaging. On the length-scales involved, effectively homogeneous domains can be created – with then inhomogeneity introduced in a step-by-step manner under the control of the experimenter. Furthermore, the corresponding reaction-diffusion equations can be written in a rigorous manner allowing experimental phenomena to be tested by numerical computation.

One area in which observations of wave activity in chemical media has contributed to enhanced understanding of biological systems concerns the arrhythmia that develop in unhealthy heart tissue – potentially leading to diseased states such as ventricular fibrillation and sudden cardiac death [2]. Various potential causes of the break-up of normal waves of cardiac muscle contraction which may then lead to the creation of “re-entrant structures” or scroll waves representing abnormal organisation of cardiac activity have been identified. One particular area of interest involves the communication of the initial wave across the atria to the ventricles involving transmission of the activity through the AV node region to the Purkinje fibres. In a classic experiment, Jalife and Moe [3] used excised canine Purkinje fibres which were threaded through

three chambers in which the fibre is perfused with different solutions rendering it spontaneously oscillatory in one region, inactive to wave propagation in the second and excitable in the third. This “sucrose gap” preparation was taken as an *in vitro* model for an ectopic (abnormal) pacemaker system coupled to a region of depressed conductivity.

In this paper, we report on an even more simplified version of this classic experiment involving an “inexcitable” or “inactive” gap within an excitable or active domain based on the well-known Belousov-Zhabotinsky system. Results are expected to be generic and therefore of relevance to AV node transmission and also to other biological manifestations of (essentially) 1D wave propagation such as those in the ureter [4,5].

## Experimental

The experimental system comprises a polysulfone membrane printed with the redox catalyst in the form of bathoferroin [6]. The printing is carried out via an ink-jet printer loaded with 0.025 M bathoferroin solution, using a standard computer drawing package to design the desired domain geometry (typically a long, thin rectangle of homogeneous colour density with one or more “gaps”). The membrane is then mounted on an agar gel (1.5%) which has been bathed in a solution of the remaining BZ reagents. Typical reagent concentrations are: malonic acid 0.17 M, bromate ion 0.30 M, sulfuric acid 0.25 M yielding an excitable system.

The reaction domain is illuminated from below and imaged from above with a video-camera linked to a PC-based data-capture and image-processing system. (For full experimental details see [7].) Waves are initiated using a silver wire and either single waves or a succession of waves forming a wave train of selected wavelength governed by the periodic initiation frequency is obtained.

## Results

Figure 1(a) shows successive image of a pseudo-one dimensional strip of printed catalyst with a single gap approximately half-way along the domain. An oxidation wave enters at one end in the 14<sup>th</sup> image and propagates along the strip. In the 20<sup>th</sup> image it reaches the gap. After a slight delay, the an excitation is initiated on the other side of the gap and the “signal” propagates successfully into the second region. (The approximate position of the wave in each image is shown in the space-time plot beneath the main figure – this reveals the phase delay at the gap more clearly.) This is characteristic of a system with a narrow gap. For domains with significantly wider gaps there is no propagation of the excitation across the gap and the “signal” fails – corresponding to a “wave-blocked” state.

These results suggest the existence of a “critical gap width”. However, investigation of gap widths slightly larger than for figure 1(a) shows a different response, as indicated in figure 1(b) In this case the system is subjected to a series of waves in the form of a wave train of a particular wavelength. The first wave is able to propagate across the gap and excite the second region. The second wave, however, does not lead to excitation or propagation across the gap. This arises as the first wave has experienced a delay at the gap and the second wave arises before the domain has fully

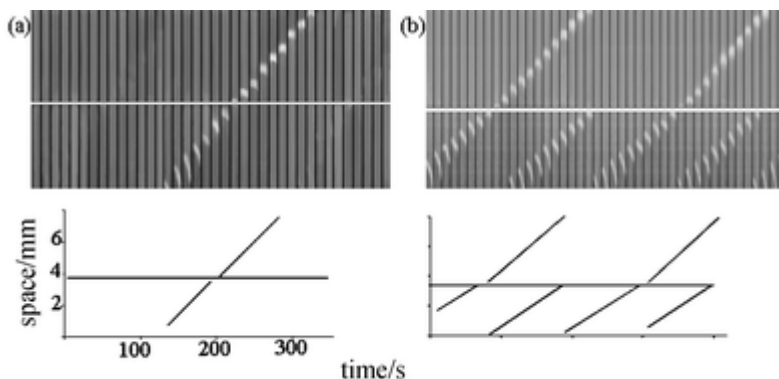


**Figure 1.** Experimental space-time plots showing successive images of a wave propagating along a quasi-1D domain with a single gap. In (a) gap width  $W = 0.10$  mm and the signal is transmitted across the gap after some phase delay (see lower image). In (b)  $W = 0.12$  mm and the wave train has a period  $T_p = 100$  s: only every second wave is transmitted across the gap, yielding a firing number  $f_n = 0.5$ . Note the increase in velocity of the successful wave as it emerges across the gap (seen most clearly in the lower image).

recovered – the autocatalyst diffusing across the gap encounters a raised concentration of the inhibitor bromide ion and cannot excite the system. The third wave approaches and, as the domain on the far side of the gap now has had longer to recover, this excitation is able to enable wave propagation. This alternation between transmission and failure continues so that one wave is transmitted for every two waves that enter the domain and there has been a “frequency transformation” across the gap. The space-time plot also indicates that after crossing the gap, successful waves show an increase in velocity as they are entering a region in which the previous wave did not progress and therefore did not produce an enhanced concentration of the inhibitor bromide ion species.

As the gap width (or the reagent concentrations) are varied, so different numbers of transmitted waves compared to failing waves are encountered. This can be quantified in terms of a “firing number”  $f_n = \text{no. of waves transmitted} / \text{no. of incident waves}$ . The firing number is a decreasing function of the gap width, with  $f_n = 1$  for sufficiently small gaps (complete propagation) and  $f_n = 0$  for sufficiently large gaps (complete failure). The variation of the firing number with gap width forms a “Devil’s staircase” as shown in figure 2. The variation of the firing number with gap width varies with the period of the wave train –  $f_n$  decreases as the period decreases as does the critical gap width  $W_{cr}$  (the width at which  $f_n$  falls to zero).

For a system with two (identical) gaps in which each gap is less than the critical gap width, successful propagation depends also on the spacing  $S$  between the gaps. The variation of the domain firing number  $f_r$ , defined as the fraction of waves propagating through the whole system (i.e. over both gaps) with  $S$  for two-gap systems with various gap widths is shown in figure 3.

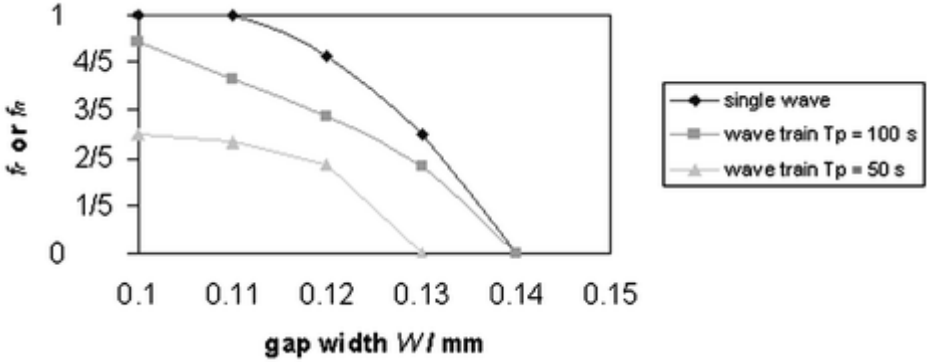


**Figure 2.** The experimentally-determined variation of the firing number  $f_n$  with gap width  $W$  for single waves and for wave trains of two different periods for a system with a single gap.

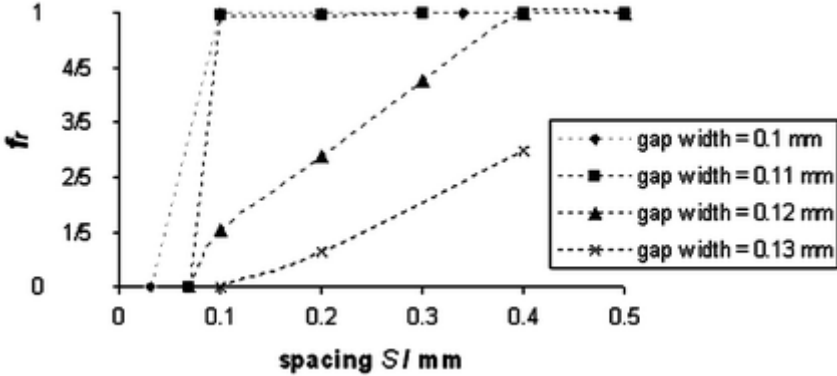


**Figure 3.** The variation of the domain firing number  $f_r$  with the spacing  $S$  between gaps of various widths  $W$  as determined experimentally for a two-gap systems.

Similar experiments with systems of many gaps can be performed and the firing number determined as a function of gap number: see [7] for details.

In terms of modelling AV node block, this mimics the situation in which not all excitations of the atria lead to contractions of the ventricles and to the phenomena of Wenckebach cycles [8]. Similar “resonance effects” have been reported for the BZ system previously by Toth et al. [9] who followed the propagation of waves from one domain to another along narrow tubes in order to establish the existence of a critical initiation radius, and by Suzuki et al. [10] for propagation across gaps in membrane-localised systems.

### Numerical Modelling

The basic dynamics of the BZ system can be adequately modelled using the two-variable Oregonator model [11] which can be written for our system in the following dimensionless reaction-diffusion form [12]

$$(1) \quad \frac{\partial u}{\partial t} = \frac{\partial^2 u}{\partial x^2} + \varepsilon^{-1} \left\{ u(1-u) - fv \frac{(u-q)}{(u+q)} \right\}, \quad \frac{dv}{dt} = u - v$$

where  $u$  and  $v$  are the dimensionless concentrations of the autocatalytic species  $\text{HBrO}_2$  and the oxidised form of the redox catalyst (the “recovery” variable) respectively. These equations describe wave evolution within active domains.

To model gaps of inactive medium within the domain, the redox catalyst is taken to be absent and the only chemistry occurring is the disproportionation of the autocatalyst, so the system is governed by the simpler equations

$$(2) \quad \frac{\partial u}{\partial t} = \frac{\partial^2 u}{\partial x^2} + \varepsilon^{-1} u^2$$

Equations (1,2) were integrated numerically using the package XPPAUT [13]. Waves were initiated by setting  $u$  periodically to some value  $u_{\max}$  over the first five grid points.

The computed wave solutions show the same generic responses as the experiments described in the previous section. A typical space-time plot showing a 2:3 resonance pattern is shown in figure 4.

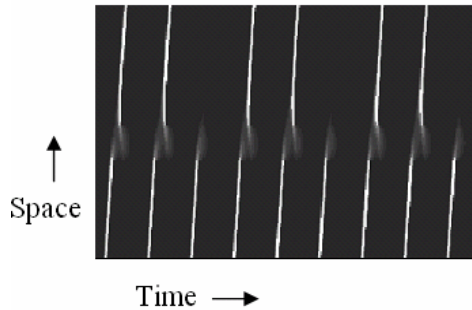


**Figure 4.** Computed space-time plot for a single gap system with  $W = 0.108$  mm and a wave train of period  $T_p = 35.3$  s computed with  $f = 3$  and  $\varepsilon = 0.054$ .

The firing number can be determined as a function of both the gap width and the period of the wave train. Using estimates of the rate coefficients from [12] and typical initial reactant concentrations from our experiments, these can be converted into dimensional quantities. The resulting variation of  $f_n$  across the  $W$ - $T_p$  parameter plane is shown in figure 5 for two different values of the stoichiometric factor  $f$  in equation (1), namely  $f = 2.4$  and  $f = 3$  (the latter being less excitable).

For systems with two gaps, and for which the gap width is less than the critical width for a single gap, the ability of a wave to propagate through the whole system depends additionally on the spacing between the gaps. This spacing represents a part of the domain in which the wave which has become attenuated as it has passed the first gap can “recover” in amplitude before encountering the second gap. Again, we observe resonance effects in both experiment and computation. Figure 6 shows the variation of the firing number with the spacing  $S$  between two gaps for a variety of gap widths  $W$ .

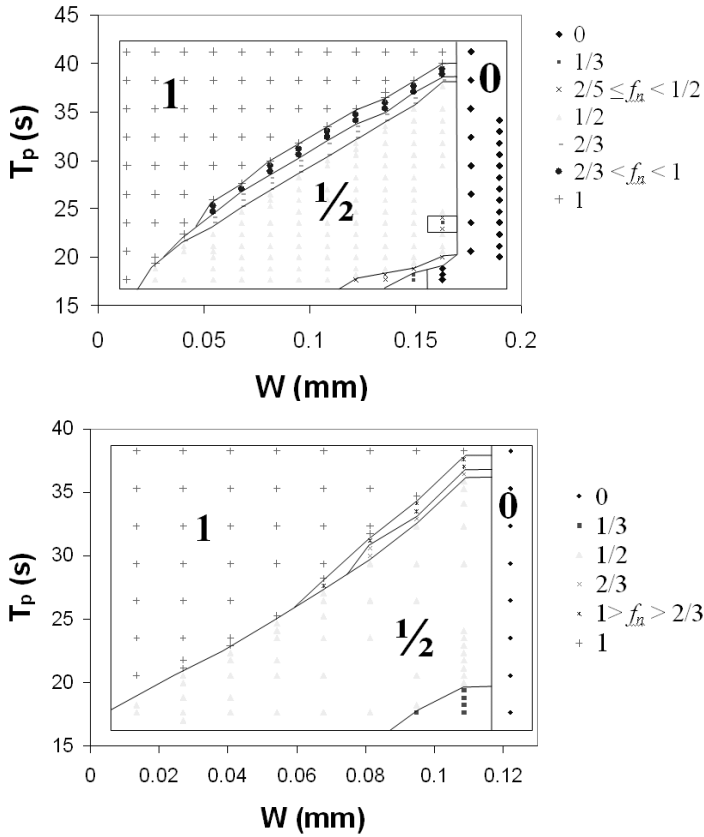


**Figure 5.** The variation of the firing number  $f_n$  with gap width and wave train period for a system with a single gap as determined numerically from equations (1,2).

In general, the larger the gap width, the larger the spacing required to allow the wave to propagate. Resonance, and hence frequency transformation, may occur at either gap and in some cases (typically where resonance effects arise at the first gap) the fraction of waves propagating across the whole system may decrease as the spacing between the gaps increases.

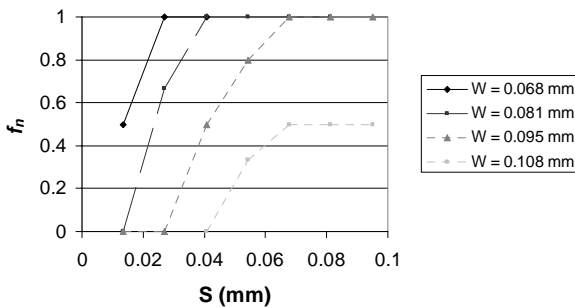


**Figure 6.** The variation of the firing number  $f_n$  with the spacing  $S$  between two gaps for a two-gap system for various gap widths as determined numerically from equations (1,2).

Finally, we have investigated systems with large numbers of gaps. In both experiment and in numerical computations, we find that for a given set of experimental conditions (as expressed in terms of the parameter values), there is some maximum number of gaps across which the wave can propagate.

## Conclusions

The results described above indicate that excitable chemical systems can serve as models for generic phenomena in such systems and so help contribute to the understanding of, for example, important biological systems. In this study we have demonstrated effects such as wave block, a critical wave gap and “resonance effects” in single and multiple gap systems. These have been observed experimentally and confirmed qualitatively (and semi-quantitatively) numerically based on a simple Oregonator-model representation. In earlier numerical work on systems with single gaps, Siewewiesiuk and Gorecki [14,15] have proposed that the existence of a critical gap width and of resonance responses could form the basis of a “chemical electronics”, and several key components such as logic gates and memories have been demonstrated by printing appropriate domains of catalyst on membranes of different types [6, 9, 16-18]. With systems containing many gaps, the spacing between the gaps becomes an important parameter. In general, the larger the spacing, the more the wave can recover between gaps and hence the higher the probability of complete propagation. In some circumstances, however, there appears to be a more complex response and this may be (numerical evidence) of the unexpected phenomenon predicted by Yang et al. [19] on the basis of an analysis of the bistable wave equation.

## Acknowledgements

We thank the University of Leeds for a studentship for GRA and we acknowledge the following for financial support: the Nuffield Foundation (grant NUF-NAL02 AFT), EPSRC (grant GR/509753/01 AFT), ESF Scientific Programme *REACTOR* and OTKA (grant T038071, VG).

## References

- [1] L Glass and M C Mackey, *From Clocks to Chaos: The Rhythms of Life*, Princeton University Press, 1988.
- [2] J Jalife, *Annu. Rev. Physiol.*, 2000, 62, 25.
- [3] J Jalife and G K Moe, *Circ. Res.*, 1976, 39, 801.
- [4] R M Weiss, M L Wagner and B F Hoffman, *Invest. Urol.*, 1968, 5, 462.
- [5] C L Prosser, C E Smith and C E Melton, *Am. J. Physiol.*, 1955, 181, 651.
- [6] O Steinbock, P Kettunen and K Showalter, *Science*, 1995, 269, 1857.
- [7] A F Taylor, G R Armstrong, N Goodchild and S K Scott, *Phys. Chem. Chem. Phys.*, 2003, 5, 3928.
- [8] K F Wenckebach, *Arrhythmia of the heart: a physiological and clinical study*. Green, Edinburgh, 1904.
- [9] A Toth, V Gáspár and K Showalter, *J. Phys. Chem.*, 1994, 98, 522.
- [10] K Suzuki, T Yoshinobu and H Iwasaki, *J. Phys. Chem. A*, 2000, 104, 5154.
- [11] R J Field and R M Noyes, *J. Am Chem. Soc.*, 1974, 96, 2001.
- [12] J J Tyson and P C Fife, *J. Chem. Phys.*, 1980, 73, 2224.
- [13] B Ermentrout, <http://www.math.pitt.edu/~bard/xpp/xpp.html>

- [14] J Siewiesiuk and J Gorecki, *Phys. Chem. Chem. Phys.*, 2002, 4, 1326.
- [15] J Siewiesiuk and J Gorecki, *J. Phys. Chem. A*, 2002, 106, 4068.
- [16] K Suzuki, T Yoshinobu and H Iwasaki, *J. Phys. Chem. A*, 2000, 104, 5154.
- [17] K Agladze, R R Aliev, T Yamaguchi and K Yoshikawa, *J. Phys. Chem.*, 1996, 100, 13895.
- [18] I N Motoike, K Yoshikawa, Y Iguchi and S Nakata, *Phys. Rev. E*, 2001, 6303, 36220
- [19] J Yang, S Kalliadasis, J H Merkin and S K Scott, *SIAM J. Appl. Math.*, 2003, 62, 485.

## EFFECT OF DOUBLE-LAYER CAPACITANCE ON THE STABILITY OF ELECTROCHEMICAL OSCILLATORS

V. Gáspár<sup>1</sup>, I. Z. Kiss<sup>2</sup>, Z. Kazsu<sup>1</sup>

<sup>1</sup>*Inst. Physical Chemistry, University of Debrecen, Debrecen, Hungary,* <sup>2</sup>*Dept. Chemical Engineering, University of Virginia, Charlottesville, VA, USA*

### Abstract

A new method for the classification of electrochemical oscillators is proposed. It is based on changing the specific capacitance  $C_d$  of the double-layer via a special feedback procedure. Effect of such changes is numerically tested on prototype models for N-NDR and S-NDR oscillators.

### Introduction

Dynamics of oscillating electrochemical systems depends not only on the surface concentration of electrochemically active species but also on the potential drop  $\phi_{DL}$  (V) across the double-layer. Considering the nonessential or essential role of double-layer potential, the electrochemical oscillators are classified, respectively, as *i*) truly potentiostatic or *ii*) NDR-type oscillators. Here, NDR stands for the Negative Differential Resistance of the cell observed at  $R_\Omega = 0$  series resistance. NDR-type oscillators are further grouped into N- and S-type systems where S and N refer to the characteristic shape of the polarization curve. In N- and S-type systems the electrode potential acts, respectively, as an essential positive or negative feedback variable. There also exist systems of hidden negative resistance of the N-type (HN-NDR). These systems oscillate under galvanostatic conditions, while N-NDR systems show bistability only [1].

In recent years, an operational procedure – based on studying the dynamics as a function of the cell resistance – has been proposed to identify the type of an electrochemical oscillator [2]. However, changing the resistance of the cell is not always an easy task. Chemically, it can be achieved by changing electrolyte composition that might affect kinetic parameters; electronically, the solution resistance can be varied by IR compensation.

In this paper, we propose a new method for the classification of electrochemical oscillators. It is based on changing the specific capacitance  $C_d$  of the double-layer via a special feedback procedure. The effect of such changes will be numerically studied on prototype models for N-NDR and S-NDR oscillators.

### Method

In electrochemical systems, the specific double layer capacitance  $C_d$  defines the time-scale for the variation of  $\phi_{DL}$  as shown by the following equation:

$$C_d \frac{d\phi_{DL}}{dt} = -i_F(c, \theta, \phi_{DL}, \dots) + \frac{V - \phi_{DL}}{AR_\Omega}, \quad (1)$$

where  $i_F$  is the Faraday current density,  $c$  is the concentration of some electroactive species,  $\theta$  is the surface coverage,  $V$  is the applied circuit potential,  $A$  is the surface area of the electrode, and  $R_\Omega$  is the cell resistance. That is, by changing the value of  $C_d$ , the fast or slow character of dynamical variable  $\phi_{DL}$  can be modified. Therefore, current oscillations could be easily suppressed or induced.

Value of  $C_d$  can be changed chemically by covering the electrode, for example, with a poly-aniline-film acting as a pseudo-capacitance [3]. Our proposed new method, which is a modified (recursive) version of the so called derivative control, is more effective and better controllable since the pseudo-capacitance is set and varied electronically. Let us change the circuit potential according to the following equation:

$$V = V_o + \alpha \frac{dV}{dt} - \alpha R_\Omega \frac{di}{dt} = V_o + \frac{d\phi_{DL}}{dt}, \quad (2)$$

where  $\alpha$  is the control parameter. Substituting eq (2) into eq (1) results in a new dynamical equation for the cell under recursive control:

$$\left( C_d - \frac{\alpha}{AR_\Omega} \right) \frac{d\phi_{DL}}{dt} = -i_F(c, \theta, \phi_{DL} \dots) + \frac{V_o - \phi_{DL}}{AR_\Omega}, \quad (3)$$

It is easy to see that the new term  $C_d' = -\alpha/AR_\Omega$  on the left-hand side of eq (3) acts on the system as we have created a pseudo-capacitance. The effect of changing the special double-layer capacitance will be numerically studied on the model of the following electrochemical systems:

- A) Cu electro-dissolution (N-NDR type oscillator)
- B) Zn electro-deposition (S-NDR type oscillator)

## Results and discussion

### A) The effect $C_d$ on N-NDR oscillators.

The Koper-Gaspard dimensionless model [4] was used to simulate Cu dissolution in phosphoric acid solution:

$$C_d \frac{de}{dt} = \frac{V - e}{R} - 120k(e)u, \quad (4a)$$

$$\frac{du}{dt} = -1.25d^{1/2}k(e)u + 2d(w - u), \quad (4b)$$

$$\frac{dw}{dt} = 1.6d(2 - 3w + u), \quad (4c)$$

where  $V$  is the applied circuit potential,  $e$  the double-layer potential,  $R$  is the series resistance,  $d$  is the rotation rate,  $u$  and  $w$  are the dimensionless concentrations of some

electroactive species, respectively, in the surface and diffusion layers,  $k(e)$  is the potential dependent rate constant defined as:

$$k(e) = 2.5\theta^2 + 0.01 \exp[0.5(e - 30)], \quad (5)$$

where  $\theta$  is related to the potential dependent surface coverage by the electroactive species:

$$\theta = \begin{cases} 1 & \text{for } e \leq 35 \\ \exp[-0.5(e - 35)^2] & \text{for } e > 35 \end{cases} \quad (6)$$

The experimentally measurable quantity, the current, is obtained as  $i = (V - e)/R$ . Dynamics of model eqs 1-6 have been studied in detail by Koper and Gaspard [4]. For an appropriate range of parameters, the model simulates the experimentally observed dynamical behavior of Cu dissolution in phosphoric acid. In this study, we set  $R = 0.02$  and  $d = 0.11913$ , and the dynamical features are explored (see Figures 1-3) by systematically varying the circuit potential  $V$  and the specific double-layer capacitance  $C_d$ .

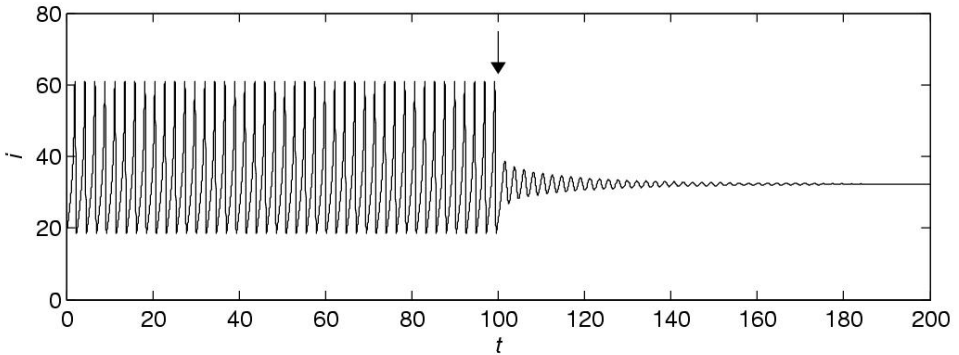


**Figure 1.** Current oscillations at  $V = 36.72$  are suppressed by increasing the double-layer capacitance  $C_d$  from 1 to 2.5 at  $t = 100$  (shown by the arrow).

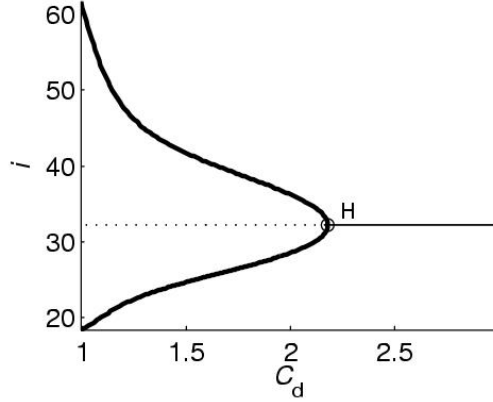


**Figure 2.** One parameter bifurcation diagram showing the minima and maxima of current oscillations as a function of the double-layer capacitance  $C_d$  at  $V = 36.72$ . Oscillations disappear by a supercritical Hopf-bifurcation (H).

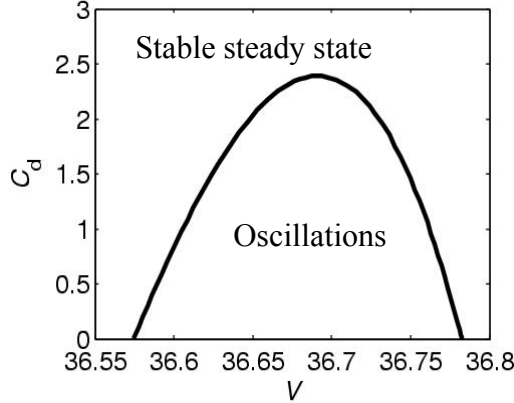


**Figure 3.** Phase diagram of the N-NDR model system (eqs. 4). Solid line is the locus of Hopf bifurcations.

*B) The effect  $C_d$  on S-NDR oscillators.*

The Lee-Jorné model [5] has been applied to simulate Zn electro-deposition. The originally two-variable model describing the coverage by the adsorbed H and  $Zn^+$  ( $\theta_1$  and  $\theta_2$ , respectively) has been extended to incorporate the IR drop through the electrolyte and an external resistance. The dimensional equations are as follows:

$$C_d \frac{de}{dt} = \frac{V - e}{R} - j_F(e, \theta_1, \theta_2) \quad (7a)$$

$$\Gamma_1 \frac{d\theta_1}{dt} = A_1(1 - \theta_1 - \theta_2) - A_2\theta_1 - A_4\theta_1\theta_2 - A_6\theta_1 \quad (7b)$$

$$\Gamma_2 \frac{d\theta_2}{dt} = A_3\theta_2(1-\theta_1-\theta_2) - A_3'\theta_2^2 - A_4\theta_1\theta_2 - A_5\theta_2 + A_6\theta_1 \quad (7c)$$

where  $e$  and  $V$  are, respectively, the double-layer and circuit potentials (V),  $R$  is resistivity ( $\Omega\text{cm}^2$ ),  $\Gamma_1$  and  $\Gamma_2$  are the surface concentrations of  $\text{H}_{\text{ad}}$  and  $\text{Zn}_{\text{ad}}^+$ , and  $A_k$  are kinetic parameters. The current density  $j_F$  is defined by the following equation:

$$j_F(e, \theta_1, \theta_2)/F = -A_1(1-\theta_1-\theta_2) - A_2\theta_1 - A_3\theta_2(1-\theta_1-\theta_2) + A_3'\theta_2^2 - A_5\theta_2 \quad (7d)$$

where  $F$  is the Faradaic constant. The kinetic parameters were optimized by Lee and Jorné as follows:

$$\begin{aligned} A_1 &= 5.53 \times 10^{-7} \exp(-19.3 \text{ V}) \text{ mol/cm}^2 \text{ s}, \\ A_2 &= 3 \times 10^{-9} \exp(-29.3 \text{ V}) \text{ mol/cm}^2 \text{ s}, \\ A_3 &= 2.45 \times 10^{-5} \exp(-33.8 \text{ V}) \text{ mol/cm}^2 \text{ s}, \\ A_3' &= 7.5 \times 10^{-5} \exp(4.8 \text{ V}) \text{ mol/cm}^2 \text{ s}, \\ A_4 &= 1 \times 10^{-6} \text{ mol/cm}^2 \text{ s}, \\ A_5 &= 5.4 \times 10^{-8} \exp(-38.6 \text{ V}) \text{ mol/cm}^2 \text{ s}, \\ A_6 &= 1 \times 10^{-9} \text{ mol/cm}^2 \text{ s}. \end{aligned}$$

$\Gamma_1$  and  $\Gamma_2$  were approximated by Epelboin et al. from impedance data [6, 7]:

$$\begin{aligned} \Gamma_1 &= 1.36 \times 10^{-7} \text{ mol/cm}^2, \\ \Gamma_2 &= 9.067 \times 10^{-11} \text{ mol/cm}^2. \end{aligned}$$

In this study, we set  $R = 2 \Omega \text{ cm}^2$ , and the dynamical features are explored (see Figures 4-6) by systematically varying the circuit potential  $V$  and the specific double-layer capacitance  $C_d$ . The current density is calculated as  $j = (V - e)/R$ .

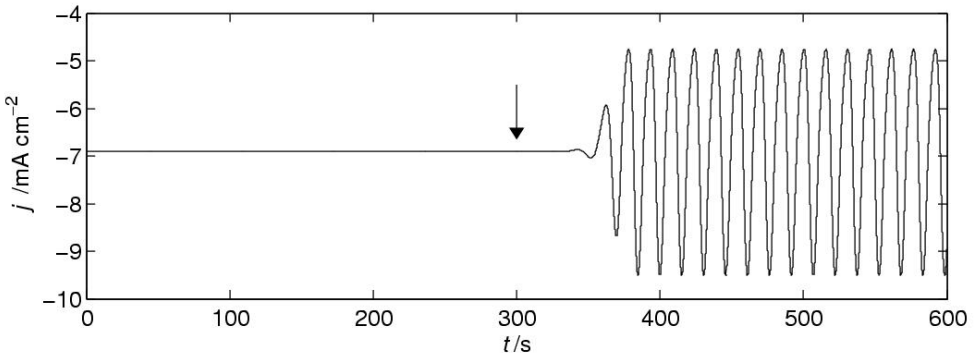


**Figure 4.** Current oscillations at  $V = -55 \text{ mV}$  are induced by increasing the specific double-layer capacitance  $C_d$  from  $2.5 \mu\text{F cm}^{-2}$  to  $2.5 \text{ F cm}^{-2}$  at  $t = 300 \text{ s}$ .

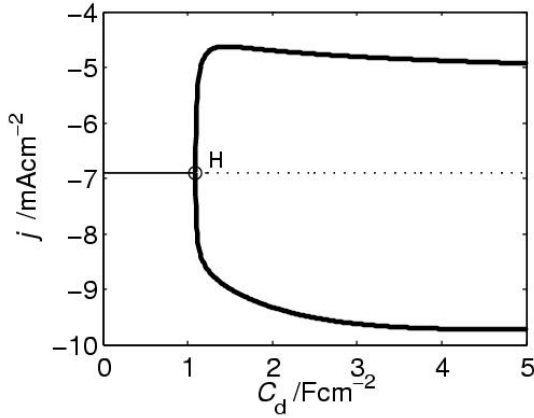


**Figure 5.** Bifurcation diagram showing the minima and maxima of current oscillations as a function of the double-layer capacitance  $C_d$  at  $V = -55$  mV. Oscillations appear by a Hopf-bifurcation (H).

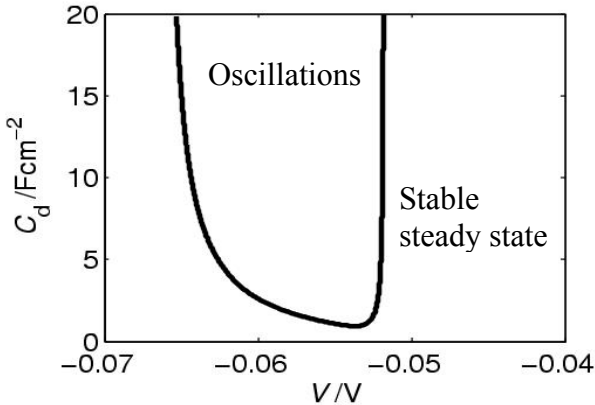


**Figure 6.** Phase diagram of the S-NDR model system (eqs. 7). Solid line is the locus of Hopf bifurcations.

## Conclusions

As shown by the calculated time series data, bifurcation diagrams and phase diagrams, the effect of double-layer capacitance on the stability of electrochemical oscillators can be summarised as follows:

- N-NDR oscillators are stable at large  $C_d$  values,
- S-NDR oscillators are stable at small  $C_d$  values.

The proposed feedback method is based on being able to experimentally vary the time-scale of an essential variable in a dynamical system. Experiments in good accordance with the presented numerical results are in progress, and results will be reported elsewhere. We also plan to extend our investigation to HN-NDR systems as well.

### **Acknowledgement**

We acknowledge OTKA (Grant T038071) for financial support.

### **References**

- [1] K. Krischer, Principles of temporal and spatial pattern formation in electrochemical systems, In *Modern Aspects of Electrochemistry*; B. E. Conway, O. M. Bockris, R. E. White, Eds.; Kluwer Academic/Plenum Press: New York, 1999, 32, 1.
- [2] P. Strasser, M. Eiswirth, M. T. M. Koper, *J. Electroanal. Chem.*, 1999, 478, 50.
- [3] G. Inzelt, V. Kertész, *Electrochim. Acta*, 1997, 42, 229.
- [4] M. T. M. Koper, P. Gaspard, *J. Chem. Phys.*, 1992, 96, 7797.
- [5] M. G. Lee, J. Jorne, *J. Electrochem. Soc.*, 1992, 139, 2841.
- [6] I. Epelboin, M. Ksouri, E. Lejay, R. Wiart, *Electrochim. Acta*, 1975, 20, 603.
- [7] I. Epelboin, M. Ksouri, R. Wiart, *J. Electrochem. Soc.*, 1975, 122, 1206.

## VARIETY OF SPATIOTEMPORAL PATTERNS REVEALED BY MONTE-CARLO SIMULATION OF THE OSCILLATORY BEHAVIOR IN CO OXIDATION REACTION OVER PLATINUM METALS. COMPARISON WITH EXPERIMENT.

V.I. Elokhin

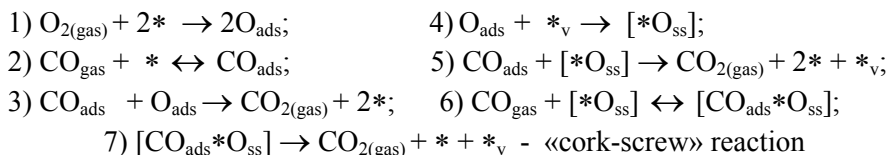
*Boreskov Institute of Catalysis SB RAS,  
Prosp. Akad. Lavrentieva, 5, 630090, Novosibirsk, Russia*

The complex dynamic behavior in oxidation reaction over platinum metals (bistability, oscillations, surface autowaves, etc.) can be directed by the structure of the reaction mechanism, specifically by the laws of physicochemical processes in the «reaction medium - catalyst» system. The most popular factors used to interpret the critical effects are the following [1]: i) phase transformations on the catalyst surface, including the formation and decomposition of surface and subsurface oxides during the reaction (e.g., Pd(110)), ii) structural phase transitions of the surface and its reconstruction due to the influence of the reaction media (e.g., Pt(100)).

In our opinion, the imitation (or statistical) simulation based on the Monte-Carlo technique is the most efficient tool for describing the spatio-temporal dynamics of the behaviour of adsorbates on the real catalytic surface, whose structure can change during the reaction. Recently the statistical lattice models for imitating the oscillatory and autowave dynamics in the adsorbed layer during CO oxidation over Pd(110) [2] and Pt(100) [3] single crystals, differing by the structural properties of catalytic surfaces, has been studied.

The aim of this contribution is to study the influence of surface diffusion intensity on the shapes of surface concentration waves obtained in simulations. Let us restrict our consideration by CO oxidation reaction over Pd(110) (similar results has been obtained by simulation of CO+O<sub>2</sub>/Pt(100) [3]).

Detailed mechanism of this reaction has been established by means of FEM, TPR and XPS studies [4]:



Let us briefly describe the algorithms used in simulations. The model catalyst surface was represented by the square lattice N×N (N = 400 – 1600) with periodic boundary conditions. States of the lattice cells are determined according to the rules prescribed by the detailed reaction mechanisms used in the cases under study. So-called Monte Carlo step (MCS) consisting from N×N elementary actions was used as a time unit. During the MCS each cell is tested on the average once. By elementary action it is meant a trial to change a state of the randomly chosen centre in such a man-

ner, as it will with the substances taking part in the elementary processes (steps) constitute the detailed reaction mechanism. The probability of the particular process  $w_i$  is determined by a ratio between the rate coefficients, therewith the rate coefficients for the adsorption processes are multiplied by the relevant partial pressures. The values of the rate coefficients of the elementary processes used in simulations could be found in [2,3]. During the MCS after each of  $N \times N$  trial to carry out one of the elementary action the inner cycle of  $\text{CO}_{\text{ads}}$  diffusion has been arranged (usually  $M = 50-100$  attempts of diffusion). The diffusion is necessary for the spatio-temporal processes synchronization occurring on the different regions of the model surface. The reaction rate and surface coverages were calculated after each MCS as a number of  $\text{CO}_2$  molecules formed (or the number of cells in the corresponding state) divided by the total number of the lattice cells  $N^2$ .

In both cases [2,3] the synchronous oscillations of the reaction rate and surface coverages are exhibited within the range of the suggested model parameters under the conditions very close to the experimental observations – e.g., Fig 1. These oscillations are accompanied by the autowave behaviour of surface phases and adsorbate coverages, Fig. 2. One can see from the Figs. 1 and 2 that the oscillations are quite regular, and the shape of oxygen waves is of prominent cellular pattern of change: the initiation of oxygen fronts propagation proceeds simultaneously at different local regions of the model surface, and the  $\text{O}_{\text{ads}}$  and  $\text{CO}_{\text{ads}}$  coverages alternate during the period of oscillations. The intensity of  $\text{CO}_2$  formation in the  $\text{CO}_{\text{ads}}$  layer is low, inside oxygen island it is intermediate and the highest intensity of  $\text{CO}_2$  formation is related to a narrow zone between the moving  $\text{O}_{\text{ads}}$  island and surrounding  $\text{CO}_{\text{ads}}$  layer - «reaction zone», characterised by the elevated concentration of the free active centres [2]. The presence of the narrow reaction zone was found experimentally by means of the field ion probe-hole microscopy technique with 5 Å resolution [5]. The important role of the diffusion rate and of the lattice size on the synchronisation and stabilisation of surface oscillations has been demonstrated. Particularly, in the case of Pt(100), the decrease of the diffusion intensity (parameter  $M$ ) from 100 to 30 leads to the irregular oscillations and to the turbulent patterns on the model surface – in this case the mobile islands of  $\text{O}_{\text{ads}}$  shaped as cellular waves, spiral fragments, etc., are formed [3]. Similar spatiotemporal behavior was experimentally observed in  $\text{CO} + \text{O}_2 / \text{Pt}(100)$  using the EMSI technique [6].

Let us study the influence of diffusion intensity  $M$  on the shape of the surface waves in the case shown in the Fig. 2. Decrease of  $M$  up to value  $M = 50$  doesn't change significantly the oscillatory and wave dynamics, but decreasing  $M$  to value  $M = 20$  drastically changes both the shape of oscillations and the spatiotemporal behaviour of simulated surface waves. Period and amplitude of oscillations decrease

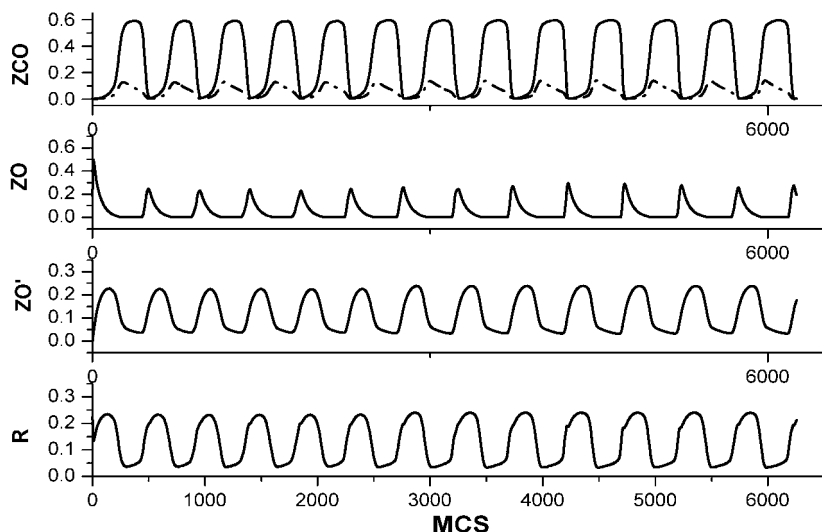


**Figure 1.** Dynamics of changes in the surface coverages  $\text{CO}_{\text{ads}}$  (solid line)  $[\text{CO}_{\text{ads}} * \text{O}_{\text{ss}}]$  (dash-dotted line) (a),  $[\text{*O}_{\text{ss}}]$  (b),  $\text{O}_{\text{ads}}$  (c),  $R$  (d) - for CO oxidation over Pd(110).  $N = 1000$ ,  $M = 100$ . The values of the rate constants of steps ( $\text{s}^{-1}$ ) (see scheme):  $k_1=1$ ,  $k_2=1$ ,  $k_{-2}=0.2$ ,  $k_3=\text{inf}$ ,  $k_4=0.03$ ,  $k_5=0.01$ ,  $k_6=1$ ,  $k_{-6}=0.5$ ,  $k_7=0.02$ . The partial pressures of reagents (CO and  $\text{O}_2$ ) are included in the rate constants of adsorption ( $k_1$ ,  $k_2$ ,  $k_6$ ).

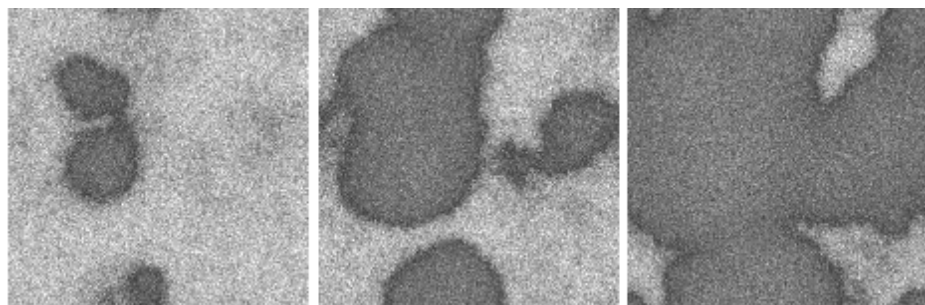


**Figure 2.** The distribution of different adsorbates over the surface at the moment when the coverage change on the Pd(110) surface. Dark grey regions indicate the propagating oxygen islands, light grey regions –  $\text{CO}_{\text{ads}}$  layer. The lattice size  $N = 1000$ , diffusion intensity parameter  $M = 100$ .

considerably, the dynamic behaviour of reaction rate and surface coverages demonstrate the intermittence (oscillatory regime I). During these oscillations oxygen ( $\text{O}_{\text{ads}}$ ) is always present on the surface (as opposed to the case of Figs. 1 and 2) in the form of turbulent spatiotemporal structures (Fig. 3a). It is seen from Fig. 3a that the whole surface is divided in several islands oscillating with the same

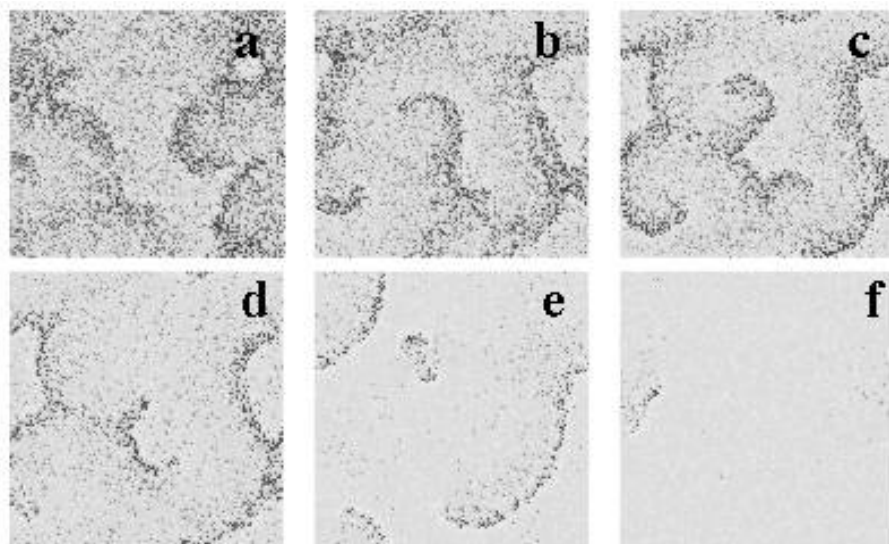


**Figure 3.** Typical snapshots of the adsorbate distribution over the surface ( $N = 1000$ ) at step-by step reducing of  $k_1$  in the case of restricted diffusion intensity of  $\text{CO}_{\text{ads}}$  ( $M=20$ ). The designations of adsorbate are the same as for Fig. 2. The values of partial pressure of oxygen (i.e.,  $k_1$ ) are the following: 1 (a), 0.9 (b), 0.85 (c), 0.8 (d), 0.73 (e), and 0.71 (f).

period but with a phase shift relative to each other, therefore the reaction rate and coverage's time dependencies demonstrate the intermittence peculiarities. Here it can observe on the surface the spatio-temporal pattern of complicated turbulent shape. The colliding oxygen islands form the spiral-like patterns. The nature of the appearing of spiral-like patterns could be explained using the results obtained in [7]. Here we studied the oscillations in the  $\text{CO} + \text{O}_2/\text{Pd}(110)$  over the few nanocrystals of Pd initially independent of each others, i.e., the  $\text{CO}_{\text{ads}}$  diffusion between the different parts of the surface was prohibited. After the removing boundaries for the  $\text{CO}_{\text{ads}}$  diffusion the colliding oxygen waves generate the stable spiral wave. The main conclusion of [7] was that namely the phase shift between colliding local oscillators could lead to the spiral patterns formation. Step-by step decrease of oxygen partial pressure (remember, that the values for  $\text{O}_2$  and  $\text{CO}$  adsorption coefficients,  $k_1$ ,  $k_2$ , and  $k_6$ , can be treated as product of the impingement rate ( $k_i \times P_i$ ) and of the sticking coefficient ( $S_i$ )) leads to the gradual thinning of oxygen travelling waves (Fig. 3b-e). At low values of  $k_1$  (Fig. 3d-f) the long and thin oxygen stripe (or worm-like) patterns are formed on the simulated surface, and the clear tendency of turbulent patterns to combine into spirals disappeared at  $k_1 < 0.8$ . The amplitude of oscillations diminished with decreasing of  $k_1$ . At last, at  $k_1 = 0.71$ , the oxygen stripe wave vanish slowly from the surface and the system transform to the low reactive state (the surface is predominantly covered by  $\text{CO}_{\text{ads}}$ ).

The reverse increasing of  $k_1$  leads to hysteresis in oscillatory behaviour. The os-

cillation appears only at  $k_1 = 0.85$  via very fast “surface explosion” (Fig. 4a-h). It

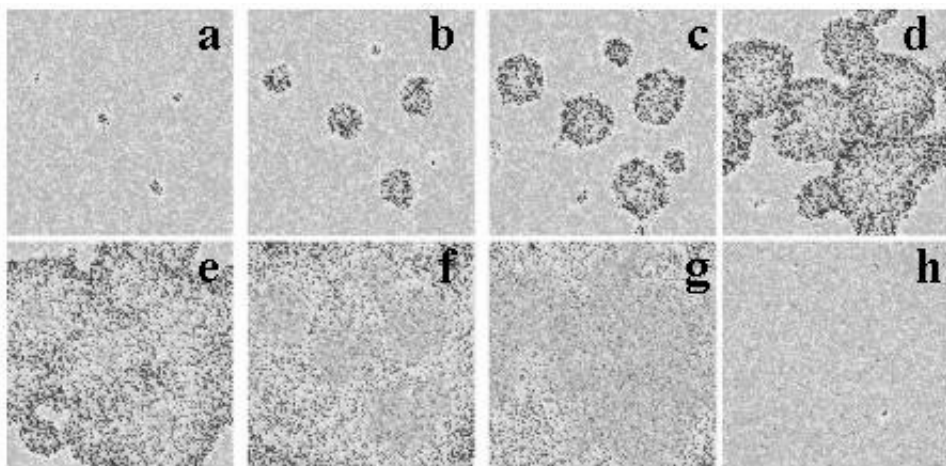


**Figure 4.** The snapshots illustrating the rise of oscillations at inverse step-by-step increasing of  $k_1$ ,  $k_1 = 0.85$ . The difference between the frames is 5 MC steps.

is surprising that the characteristics of oscillations differ drastically from those observed at gradual decreasing of  $k_1$  at the same value of  $k_1 = 0.85$ . Now the amplitude of oscillations (coverage's and reaction rate) is larger than in regime I, and instead of turbulent spiral-like pattern (Fig. 3c) we observe the alternately change of  $O_{\text{ads}}$  and  $CO_{\text{ads}}$  layers via growing cellular oxygen islands (Fig. 4) similar to the case with large diffusion intensity (Fig. 2). The interval of existence of this regime (regime 2) is quite large:  $0.98 > k_1 > 0.83$ . At low bound of this interval (i.e.,  $k_1 = 0.83$ ) the ring structures of growing oxygen islands had been observed (Fig. 5) – during the oxygen island propagation CO have time to adsorb into its centre. In this case the period of oscillations increased significantly.

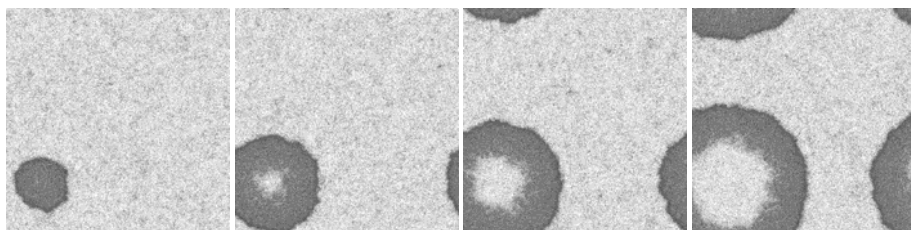


**Figure 5.** The snapshots illustrating the propagation of ring-like islands of oxygen at  $k_1 = 0.83$ . The difference between the frames is 50-80 MC steps.

Only at  $k_1 = 1$  occurs the transformation from the regime 2 to the regime 1 – we observe again the turbulent patterns over the surface (Fig. 3a). Thus, the hysteresis in oscillatory behaviour has been found by kinetic Monte-Carlo modelling of CO oxidation reaction over Pd(110). Two different oscillatory regimes (Fig. 6) could exist at one and the same parameters of the reaction (e.g., oxygen partial pressure). The pa-

rameters of oscillations (amplitude, period and the shape of spatiotemporal patterns on the surface) depend on the kinetic prehistory of the system.

Thus, the possibility for the appearance of the cellular and turbulent patterns, spiral and stripe waves on the surface in the cases under study has been shown. The results obtained make possible to interpret the surface processes on the atomic scale.

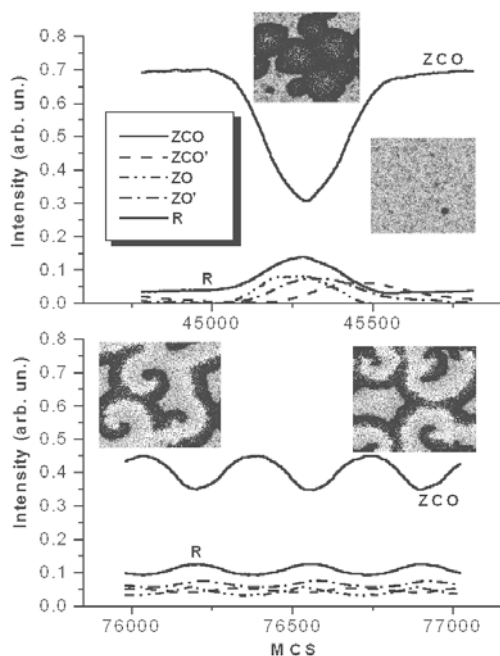


**Figure 6.** The characteristics of two different oscillatory regimes at  $k_1 = 0.85$ . At the bottom of Figure – characteristics of the regime I: period of oscillations  $\sim 250$  MCS, turbulent spiral-like patterns on the surface. On the top of Figure – characteristics of the regime II: period of oscillations  $\sim 1000$  MCS, the alternately change of  $O_{\text{ads}}$  and  $CO_{\text{ads}}$  layers via growing cellular oxygen islands.

## Acknowledgement

This work was supported by Russian Fund for Basic Research (RFBR Grant # 02-03-32568) and by NWO Grant # 047.015.002.

## References

- [1] G. Ertl. *Surface Sci.*, 1994, **299/300**, 742, and references therein.
- [2] E.I. Latkin, V.I. Elokhin, A.V. Matveev, V.V. Gorodetskii. *J. Molec. Catal. A, Chem.*, 2000, **158**, 161.
- [3] E.I. Latkin, V.I. Elokhin, V.V. Gorodetskii. *J. Molec. Catal. A, Chem.*, 2001, **166**, 23.
- [4] V.V. Gorodetskii, A.V. Matveev, A.V. Kalinkin, B.E. Niewenhuys. *Chem. for Sustain. Dev.*, 2003, **11**, 67.
- [5] V.V. Gorodetskii, W. Drachsel. *Appl. Catal. A: General*, 1999, **188**, 267.
- [6] J. Lauterbach, G. Bonilla, T.D. Fletcher. *Chem. Eng. Sci.*, 1999, **54**, 4501.
- [7] E.I. Latkin, V.I. Elokhin, V.V. Gorodetskii. *Chem. Engng. Jour.*, 2003, **91**, 123.

# $1/f$ NOISE: A CRITERION FOR A LONG-TERM STABLE EVOLUTION OF THE OPEN CATALYTIC SYSTEMS

M. K. Koleva, L.A. Petrov

*Institute of Catalysis, BAS, 1113 Sofia, Bulgaria*

## Abstract

A general necessary condition providing a long-term stable evolution of any natural system is - the fluctuations that the system exerts should be bounded so that the system permanently stays within its thresholds of stability. The relation between the boundedness of the fluctuations and the presence at the power spectra of a continuous band that fits the shape  $1/f^{\alpha(f)}$  makes the observation of such band criterion for a stable long-term evolution.  $\alpha(f) \rightarrow 1$  at  $f \rightarrow \frac{1}{T}$  ( $T$  is the length of the time series and  $\alpha(f)$  monotonically increases at  $f$  increasing. A mechanism that sustains the fluctuations bounded at open catalytic systems is presented.

## Introduction

One of the most challenging tasks of the catalytic reactions study is the issue about their long-term stability. Usually it is associated with the particular changes of the catalyst properties happened in the course of time. The major goal of the present paper is to verify that, when presented, certain characteristics of the temporal behavior of each catalytic reaction serve as a simple criterion for a stable long-term evolution. Next the case when the catalyst properties remain unchanged in the course of the time is considered.

Our study starts with revealing the properties of the temporal variations of the catalyst bed temperature recorded at the oxidation of *HCOOH* over supported *Pd* catalyst [1] at large range of the feed concentrations and in broad temperature interval. Though the amplitude of the most of the variations does not exceed 7% of the average, there are occasional variations as large as 50% of the average. The permanent presence of irregular variations poses the question about their origin and the relation to the stability of the system. Two of 80 recorded time series are presented at Fig.1 and Fig.2.

The most powerful tool for revealing the properties of irregular time series is the study of their power spectra. There is a straightforward relation between the power spectra and the stability of the system: the variance of the variation sequence equals the integrated over the frequency range power spectrum.

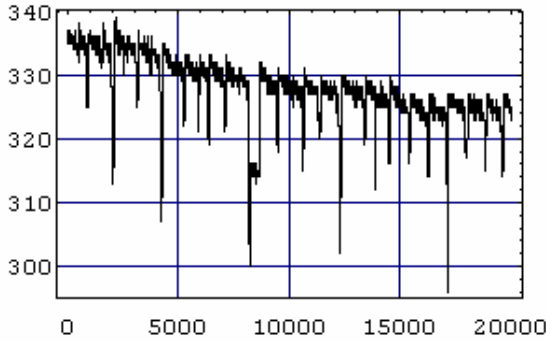


**Figure 1** A time series in relative units of the catalyst bed temperature variation (K) in the course of time (sec) at the oxidation of HCOOH

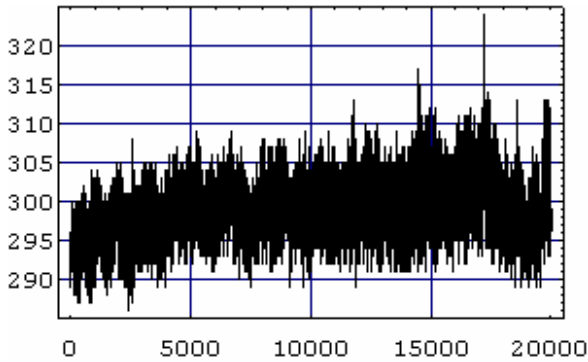


**Figure 2** A time series in relative units of the catalyst bed temperature variation (K) in the course of time (sec) at the oxidation of HCOOH

In our case the power spectra of all 80 time series exhibit a persistent presence of a continuous band of the shape  $1/f^{\alpha(f)}$  where  $\alpha(f) \rightarrow 1$  at  $f \rightarrow \frac{1}{T}$  ( $T$  is the length of the time series) and  $\alpha(f)$  monotonically increase at  $f$  increasing. The power spectra of the time series presented at Fig.1,2 are presented at Fig.3 and Fig.4 correspondingly. The gradual deviations of the power from  $\alpha = 1$  become visible at higher frequencies.

The persistent presence of a continuous band whose infrared edge uniformly fits the shape  $1/f$  is associated with the widespread yet enigmatic phenomenon called  $1/f$  noise.

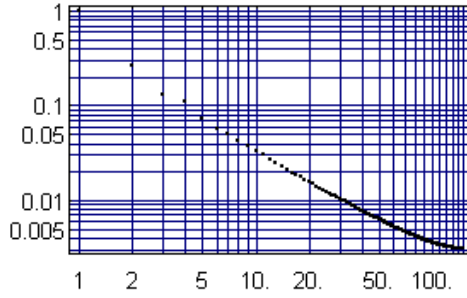


**Figure 3** The power spectrum in relative units of the time series presented in Fig.1

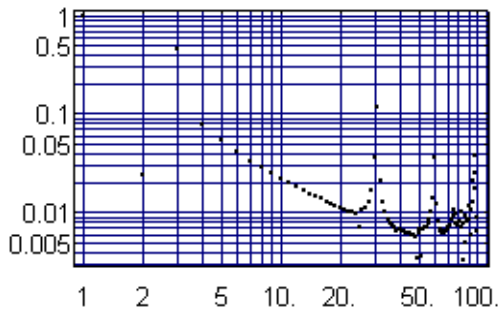


**Figure 4** The power spectrum in relative units of the time series presented in Fig.2

### $1/f$ Noise

The major characteristic of the  $1/f$  noise is that the infrared edge of a power spectrum uniformly fits the shape  $1/f$ . The fit does not depend on: (I) the incremental statistics, i.e. the details of the variation succession in a time series; (ii) the length of the time series; (iii) the nature of the system. The phenomenon is observed in a large variety of systems: quasar pulsations, meteorology, financial time series, music and speech etc.

One of its greatest controversies is how it is related to the long-term stability of a system: on the one hand the shape  $1/f$  of the power spectra makes the variance of the time series infinite. In turn, the infinite variance makes most probable fluctuations large enough to carry the system beyond the thresholds of stability. Therefore, any system would blow up or get extinct in a finite time interval. However, it does not happen. Moreover, it is established that the  $1/f$  behavior is spanned over several dozens of order. Thus, it is rather to be associated with a long-term stability.

The revealing of the controversy is achieved by the use of the precise shape of the entire power spectrum, namely the shape  $1/f^{\alpha(f)}$  mentioned in the Introduction

$(\alpha(f) \rightarrow 1$  at  $f \rightarrow \frac{1}{T}$  ( $T$  is the length of the time series) and  $\alpha(f)$  monotonically increases at  $f$  increasing. It has been proven [2] that this shape makes the variance finite. It has been verified that the shape  $1/f^{\alpha(f)}$  is generic for the power spectrum of any bounded irregular sequence (BIS) regardless to the details of the incremental statistics. However, the boundedness of the fluctuations is straightforwardly related to the issue of stability. It implies that a system stays stable until the exerted fluctuations are bounded so that not to exceed the thresholds of stability. Thus, being a hallmark of the boundedness, the presence in a power spectrum of a continuous band that fits the shape  $1/f^{\alpha(f)}$  serves as a criterion for a long-term stability of the system.

Another controversy arises from the superimposing of the continuous band to a discrete one shown in Fig.4. The discrete band has the typical properties of a limit cycle. Thus, it originates from a system of ordinary differential equations. Then, it is to be expected that the macroscopic evolution of our catalytic reaction is given by a system of ordinary differential equations (ODE) set on the reaction mechanism. However, the solution of neither system of ODE can comprise both a discrete and continuous band at the same time.

The mathematical analysis of the problem of the presence in the power spectra of a continuous band and its coexistence with a discrete one suggests that a successful solution is brought about by permanent, persistent at every parameter choice, bounded variations of the adsorption and/or reaction rates.

Recently one of us has put forth a mechanism [4] that couples certain type of local fluctuations that occur at every surface at each parameter choice. Its distinctive property is that it produces variations of the adsorption and reaction rates with the desired properties. The importance of this mechanism is revealed in its universality: it is insensitive to the details of the reaction mechanism and the surface properties. Furthermore, the local fluctuations that it couples are inevitable for the surface reactions exposed to a steady flow of the reactants.

### **Diffusion-Induced Noise**

The task of this section is to elucidate the inevitability and ubiquity of the presence of certain type local fluctuations. Their driving mechanism has been recently introduced [2,3] and has been called diffusion-induced noise. It is presented for the adsorption, since it is a step prerequisite of any surface reaction at each parameter choice. The mechanism is based on the interplay between: (I) the lack of correlation between moments and points of the gas phase species trapping at the surface; (ii) the generic property of any adlayer that no more than one species can be adsorbed at a single active site. That interplay causes fundamental changes of the properties of the overall probability for adsorption. Given is a species trapped in a vacant site. Its further relaxation to the ground state can be interrupted by an adspecies that arrives at the same site and most probably occupies it. Thus the adspecies violates the further trapped species relaxation at that site, since no more than one species can be adsorbed

at a single site. The trapped species can complete the adsorption if and only if after migration it finds another vacant site. The impact of the adspecies intervention to the trapped species probability for adsorption is twofold: first, it cannot be considered as a perturbation, since it changes the adsorption potential qualitatively, namely from attractive it becomes repulsive. That is why, that type of interaction has been called diffusion-induced non-perturbative interaction. Second, the lack of coherence between the trapping moment and the moment of adspecies arrival makes the probability for adsorption multi-valued function: each selection corresponds to a certain level of relaxation at which a diffusion-induced non-perturbative interaction happens. Therefore, the adspecies mobility brings about fundamental duality of the probability for adsorption (and of the adsorption rate correspondingly): though each selection can be computed at microlevel, the establishing of a given selection is a stochastic process since it is a random choice of a single selection among all available.

Evidently, the driving mechanism is insensitive to the details of the adsorption Hamiltonian, the adspecies spatio-temporal configuration, the details of the reaction mechanism and the parameter choice. This broad insensitivity provides its inevitability and ubiquity.

Since the diffusion-induced non-perturbative interactions are local events, the non-correlated mobility of the adspecies produces a lack of correlation between the established selections at any distance and at any instant. As a result, the produced adlayer would be always spatially non-homogeneous even in the academic case of identical adsorption and mobility properties of all types of adspecies. Outlining, the non-correlated diffusion-induced non-perturbative interactions always make the adsorption rates that come from different adsorption sites non-identical that immediately yields spatial non-homogeneity. Furthermore, the induced non-homogeneity would be permanently sustained by the lack of coherence between the trapping moments and the adspecies mobility. In turn, the adlayer configuration would vary in uncontrolled way which in a short time would cause either the reaction termination or the system breakdown. Thus, a stable long-term evolution is available if and only if there is a mechanism that suppresses the induced non-homogeneity. A mechanism that removes the induced non-homogeneity through a feedback that couples the local fluctuations has been introduced in [4].

The outcome of the synchronization is that at any instant the global adsorption rate is always identical to the individual adsorption rate that comes from certain local configuration. It is verified that the feedback always selects that individual adsorption rate which currently is in the most favourable local configuration: such that the difference in the state of that species and its immediate neighbours is the smallest. This, in turn makes the global rate a multi-valued function at each value of the control parameters. The stochastic behavior appears from the permanent random choice among selections because only one selection takes place at every instant. Therefore the macroscopic kinetic equations read:

$$\frac{d\vec{X}}{dt} = \vec{\alpha}\hat{A}_{\text{det}}(\vec{X}) - \vec{\beta}\hat{R}_{\text{det}}(\vec{X}) + \vec{\alpha}\hat{\mu}_{\text{at}}(\vec{X}) - \vec{\beta}\hat{\mu}_{\text{ri}}(\vec{X}) \quad (1)$$

where  $\hat{A}_{av}(\vec{X})$  and  $\hat{R}_{av}(\vec{X})$  are the mean values of the adsorption and reaction rates at given parameter choice  $\vec{\alpha}$  and  $\vec{\beta}$ ;  $\hat{\mu}_{ai}(\vec{X}) = \hat{A}(\vec{X}) - \hat{A}_{av}(\vec{X})$  and  $\hat{\mu}_{ri}(\vec{X}) = \hat{R}(\vec{X}) - \hat{R}_{av}(\vec{X})$ ;  $\hat{A}(\vec{X})$  and  $\hat{R}(\vec{X})$  are the adsorption and reaction rates. It should be stressed that at any instant each component of  $\hat{A}(\vec{X})$  and  $\hat{R}(\vec{X})$  is a selection randomly chosen among all available. Then, in the course of the time  $\hat{\mu}_{ai}(\vec{X})$  and  $\hat{\mu}_{ri}(\vec{X})$  appear as successive terms of corresponding zero-mean bounded irregular sequence (BIS). The subscript  $i$  serves to stress that only one selection, randomly chosen among all available, takes place at a given instant.  $\hat{\mu}_{ai}(\vec{X})$  and  $\hat{\mu}_{ri}(\vec{X})$  has a Markovian property in the sense that the probability for occurrence of a given selection does not depend on the probability for the appearance of any selection at the previous instant.

A representative property of the eqs.(1), figured out in [2], is that at each parameter choice the power spectrum of its solution  $\vec{X}(t)$  comprises additively two parts. The first one is the power spectrum of  $\vec{X}_{det}$  settled by the following equations:

$$\frac{d\vec{X}_{det}}{dt} = \vec{\alpha}\hat{A}_{det}(\vec{X}_{det}) - \vec{\beta}\hat{R}_{det}(\vec{X}_{det}) \quad (2)$$

The second part is the power spectrum of the zero-mean BIS resolved by the variations of  $(\vec{X}(t) - \vec{X}_{det})$ . Next in [2] it has been proven that the power spectrum of any zero-mean BIS is a continuous band that fits the shape  $1/f^{\alpha(f)}$ , where  $\alpha(f) \rightarrow 1$  at  $f \rightarrow 1/T$  ( $T$  is the length of the sequence) and  $\alpha(f)$  monotonically increases to  $p > 2$  at  $f \rightarrow \infty$ . This shape is insensitive to the details of the incremental statistics. In our case, this implies that the shape  $1/f^{\alpha(f)}$  is robust to the particularities of the adsorption and reaction mechanism involved in  $\hat{\mu}_{ai}(\vec{X})$  and  $\hat{\mu}_{ri}(\vec{X})$ . So, a continuous band of the shape  $1/f^{\alpha(f)}$  exhibits a persistent presence at each parameter choice.

To outline, the separation of the power spectrum into two parts is robust to the particularities of r.h.s. of eqs.(1). Thus, in particular, it is robust to the details of the reaction mechanism.

## Large-Scaled Fluctuations in the Course of Time

So far, the evolution of the catalytic reactions is described by systems of ordinary or partial differential equations of the type of eqs.(2). They define the bifurcation diagram. As a result, the temporal evolution should be steady and the dynamical regime would remain unchanged in the course of time. However, the interplay between the determinism of eqs. (2) and the fluctuations in eqs.(1) causes permanent deviations

from any dynamical regime prescribed by eqs.(2). Formally, any difference  $(\vec{X}(t) - \vec{X}_{\text{det}})$  can effectively be presented as the solution of eq.(2) at “shifted” control parameters. The latter immediately causes change either of the characteristics of the dynamical regime or it even induces change of the type of the dynamical regime. It is obvious that any induced bifurcation needs a fluctuation of certain size. Thus, the problem about the frequency for occurrence of a fluctuation of a given size becomes crucial for the induced bifurcations. Recently we have found out explicitly the frequencies of appearance of a fluctuation of a given size and duration [5]. More precisely, we have found out the relations size  $\leftrightarrow$  duration and frequency of appearance  $\leftrightarrow$  size. It turns out that the boundedness makes each fluctuation to be loaded in an embedding interval so that no other fluctuation appears in that interval. Thus the successive fluctuations are well separated one from another.

Another prominent result of our considerations [5] is that the fluctuations could be separated into two major classes: reaction-sensitive and universal. The relation size  $\leftrightarrow$  duration of the former ones depends on the reaction mechanism. On the contrary, all the features of the universal fluctuations are insensitive to the details of the reaction mechanism and the catalyst properties.

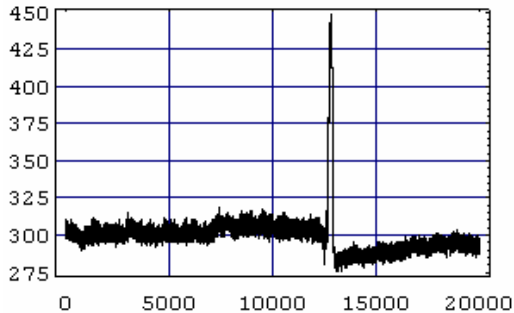


**Figure 5** The second part of the time series presented in Fig.2

Next, an example that the large fluctuations indeed induce an effective “shift” of the control parameters is presented. One of our time series is divided into 2 equal parts: the first one is presented at Fig.2 and the second one at Fig. 5. The latter comprises a fluctuation as large as 50% of the average. Its power spectrum is presented at Fig.6.

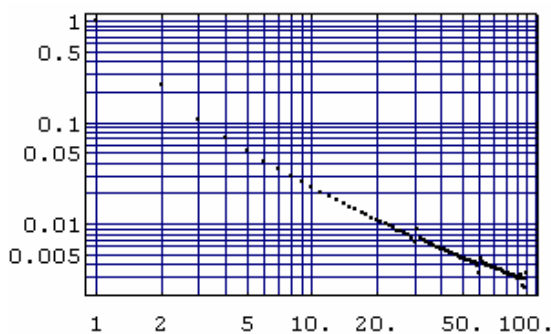


**Figure 6** The power spectrum in relative units of the time series presented in Fig.5

The comparison between the power spectra at Fig.4 and Fig.6 reveals the typical property of a limit cycle: strong sensitivity of the amplitude to the control parameter values while the period remains robust to them. The amplitude of the limit cycle at Fig.6 is 10 times less than that in Fig.4. Thus, indeed, the presence of a large fluctuation effectively “shifts” the control parameters.

## Conclusions

The relation between the boundedness of the fluctuations and the presence at the power spectra of a continuous band that fits the shape  $1/f^{\alpha(f)}$  makes the observation of such band criterion for a stable long-term evolution. The ubiquity of the fluctuations produced by the diffusion-induced noise makes this criterion available for all the surface reactions.

Another problem posed by the fluctuations produced by the diffusion-induced noise is that they can change the dynamical regime in the course of time even when the control parameters and the catalyst properties remain steady. This gives rise to the question about the most appropriate feedback in order to control the temporal behavior of the industrial catalytic reactions.

## References

- [1] M. K. Koleva, A. E. Elyias and L. A. Petrov, Proceedings of NATO ASI Science Series C, Metal-Ligand Interactions in Chemistry, Physics and Biology, Eds. N. Russo and D.R. Salahub, Kluwver, 2000, 546, 353.
- [2] M. K. Koleva and V. C. Covachev, *Fluct. Noise Lett.*, 2001, 1, R131.
- [3] M. K. Koleva, *Bulg. Chem. Ind.*, 1998, 69, 119.
- [4] M. K. Koleva, <http://arXiv.org/cond-mat/0212357>.
- [5] M. K. Koleva and L. A. Petrov, <http://arXiv.org/cond-mat0309272>.

## MODELS OF THE CLASSICAL B-Z REACTION AND THE ROLE OF OXALIC ACID

Z. Noszticzius, M. Wittmann, K. Pelle, G. Taba

*Center for Complex and Nonlinear Systems and the Department of Chemical Physics,  
Budapest University of Technology and Economics, H-1521 Budapest, Hungary*

### Abstract

Since the discovery of the classical Belousov-Zhabotinsky (BZ) reaction (substrate: malonic acid, catalyst: cerium) the mechanism of this oscillatory reaction is the subject of intense research. Here we review the suggested mechanisms including the latest developments which point to the role of an intermediate, namely oxalic acid.

The first detailed mechanism, the Field-Kőrös-Noyes (FKN) theory (1972) and the Oregonator model (1974) was based on a negative feedback loop via bromide ion but neglected another negative feedback loop via organic free radicals. Discovery of this second feedback loop in 1989 led to the Radicalator model proposed by Försterling and co-workers.

The next model by Györgyi, Turányi and Field (GTF 1990) included many reactions of the organic free radicals but in the absence of an appropriate analytical technique many of the reaction routes were hypothetical. In the following decade many new reaction routes and intermediates were discovered with the aid of high performance liquid chromatography (HPLC). Among others it was realized that organic free radicals do not disproportionate as it was assumed originally by FKN and GTF but they recombine. For example the reaction products of two malonyl radicals are not malonic and tartronic acids but ethane-tetracarboxylic acid (ETA) and malonyl malonate (MAMA).

The new Marburg-Budapest-Missoula (MBM) model suggested in 2001 included both negative feedback loops (bromous acid - bromide ion Oregonator type and bromine dioxide - organic free radicals Radicalator type feedback) and also the radical - radical recombination reactions. Simulation of experiments with the MBM model gave a good qualitative agreement but various open problems still remained. One of these was the role of oxalic acid, an intermediate found by HPLC both in the induction period and in the oscillatory regime of the classical BZ reaction.

Here we present perturbation experiments of the classical BZ reaction where the perturbant is oxalic acid. The experiments show that the oxalic acid intermediate plays an important role in the mechanism of the classical BZ reaction, a role which was not taken into account in the previous model calculations. To discover this role we suggest mechanistic investigations on a more simple BZ oscillator with oxalic acid as the only substrate.

### Introduction

The classical Belousov[1]-Zhabotinsky[2] (BZ) reaction, the cerium ion catalysed oxidation and bromination of malonic acid by acidic bromate, is the most studied chemical oscillator and a prime example for both temporal and spatial nonlinear

phenomena in chemistry [3-6]. In spite of that, due to the complexity of the so-called organic reaction subset, there are still important processes, which are not known or at least not well understood. The best way to understand the nature of these problems is if we regard the various mechanisms suggested for this oscillatory reaction.

### **Three early mechanisms of the BZ reaction**

#### *The FKN mechanism and bromide controlled oscillations*

The basic mechanism of the BZ reaction was elucidated in 1972 by Field, Kőrös and Noyes [7] (FKN). According to the FKN theory oscillations are due to an interplay of a positive and a delayed negative feedback loop. The positive feedback is the autocatalytic bromous acid and bromine dioxide production in the course of the oxidation of  $Ce^{3+}$  to  $Ce^{4+}$  by acidic bromate. The first step in the negative feedback is the bromide ion generation by  $Ce^{4+}$  in a reaction with bromomalonic acid. Bromide ion then reacts rapidly with bromous acid which is an autocatalytic intermediate. This way bromide ion controls switches between an oxidized and a reduced state. When the bromide level is high the system stays in the reduced state and the  $Ce^{4+}$  concentration is gradually decreasing. In this reduced state the bromide concentration is also decreasing as it reacts with bromate in the acidic medium. (Hypobromous acid and bromine produced in the latter reaction brominate malonic acid.) The reduced state becomes unstable when  $[Br^-]$  falls below a critical value allowing the autocatalytic reaction to take over. In the resulting new oxidized state the  $Ce^{4+}$  concentration and the intensity of bromide ion generation grows rapidly up to a point when the autocatalytic reaction is extinguished. Then  $[Br^-]$  jumps to a high level again and the cycle resumes. The FKN mechanism is thus referred to as bromide controlled. The mechanism was generally accepted and its simplified version, the Oregonator [8] was applied successfully to model oscillations and other nonlinear phenomena in the BZ reaction. Actually, the system of the inorganic reactions (the "inorganic subset") - after a revision of its rate constants [9-11] - is still used basically in the same form as it was suggested by FKN. Changes were necessary in the organic subset, however, because it turned out that organic free radicals (like malonyl radicals for example) play a more important role than it was originally suspected.

#### *The Radicalator and non-bromide controlled oscillations*

Bromide ion plays the role of a control intermediate because it reacts rapidly with the autocatalytic intermediate  $HBrO_2$ . Beside bromous acid bromine dioxide radical is also a part of the autocatalytic cycle consequently any intermediate reacting with  $BrO_2$  can also act as a control intermediate. It was Brusa et al. [12] who suggested first that malonyl radicals could replace bromide if they were able to react either with bromous acid or bromine dioxide. In 1989 Försterling and Noszticzius<sup>13</sup> reported that malonyl radicals react with bromine dioxide at a diffusion controlled rate. Thus an additional negative feedback loop was discovered in the BZ reaction. Initially it was not clear whether this second feedback alone is also able to control the oscillations. This possibility was demonstrated soon by Försterling et al. [14] who found non-bromide controlled oscillations in the so-called Rác system [15]. They also suggested a new mechanistic model, the Radicalator, in which malonyl radical

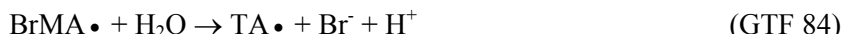
plays the role of the control intermediate. The same model was applied successfully to explain certain stirring effects of the BZ reaction [16].

#### *The Györgyi-Turányi-Field (GTF) mechanism*

The next important development in the theory of the BZ reaction was the mechanism proposed by Györgyi, Turányi and Field [17,18] in 1990 and 1993. The GTF mechanism aimed to incorporate all the experimental information available at that time. It contains 26 variable species and 80 elementary reactions. GTF assumed that organic free radicals, when they react with each other, disproportionate rather than recombine. (As they wrote they continued this assumption of the FKN mechanism “reluctantly” because no direct experimental evidence was available at that time.) For example malonyl radicals disproportionate according to reaction 41 in their scheme:



Here MA and TA stand for malonic and tartronic (hydroxymalonic) acids and  $\text{MA}\bullet$  denotes a malonyl radical. In their second paper [18] GTF added the hydrolysis reaction of  $\text{BrMA}\bullet$  (bromomalonyl radical) to their scheme:



as an additional bromide source. (It is a prerequisite to obtain enough bromide for an effective negative feedback for oscillations. Not enough bromide is a usual problem of the various models.) Another new source of bromide ions in the GTF mechanism is the reduction of bromomalonic acid by carboxyl radicals:



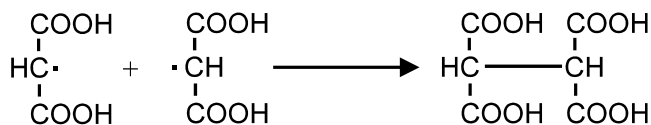
Finally we mention a serious problem of the GTF mechanism: while it reproduces  $\text{Ce}^{4+}$  oscillations with high fidelity if the initial substrate is malonic acid the model fails to oscillate with pure bromomalonic acid as initial substrate in a parameter range where oscillations with such a substrate are observed experimentally.

### **Identification of Organic Intermediates with HPLC Measurements and the MBM Mechanism**

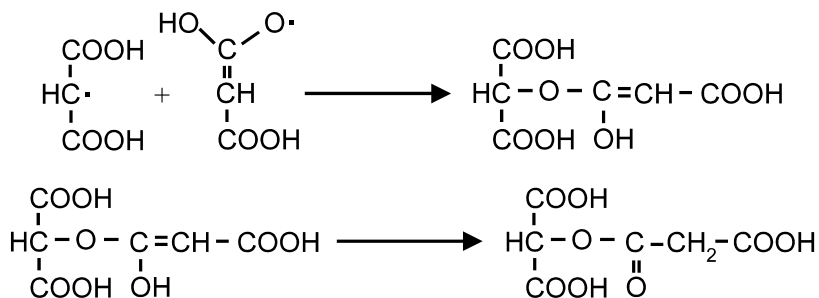
In the times when the FKN mechanism was proposed modern analytical techniques (like NMR and HPLC) were not widely available thus it was not possible to test the presence of the hypothetical organic intermediates experimentally. This situation was changed fundamentally in the last decade and, in 1994, a systematic program was initiated in Marburg applying mostly HPLC to identify various organic products and intermediates of the BZ reaction [19-23].

#### *HPLC of the organic subsystems*

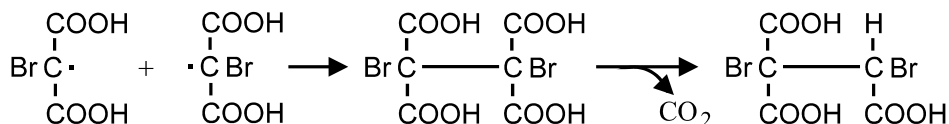
The research was started with HPLC studies on the products of the  $\text{Ce}^{4+}$  - malonic acid and the  $\text{Ce}^{4+}$  - bromomalonic acid reactions. These organic subsystem studies have shown that the primary organic radicals do not disproportionate but recombine. In the case of malonic acid radicals the recombination products are ethanetetra-carboxylic acid (ETA) [19]:


**ETA**

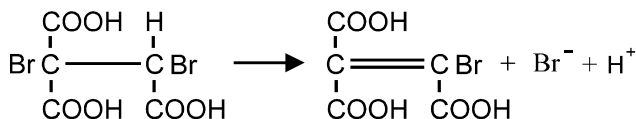
and malonyl malonate (MAMA) [20]:


**MAMA**

because the malonic acid radical is capable of mesomerism [24]. When bromomalonyl radicals react with each other the final product is bromoethenetricarboxylic acid (BrEETRA) [21]. The first step is again a recombination of two alkyl bromomalonyl radicals then the produced dibromo ETA decarboxylates:



and loses a HBr to form the final product BrEETRA:


**BrEETRA**

It is also important to mention here that no tartronic acid was found in the  $\text{Ce}^{4+}$  - bromomalonic acid reaction thus GTF 84, the proposed hydrolysis of bromomalonyl radicals, cannot play a role in the mechanism.

#### *HPLC of complete BZ systems in the induction period*

The next step was to study the reaction products of a complete BZ system but first only in its induction period [23]. The induction period was chosen for two reasons:

i) Complications due to reactions of organic substrates other than malonic acid were hoped to be less serious in this period especially when a higher than normal initial malonic acid concentration is applied.

ii) In the induction period the BZ system is in its oxidized state and this period lasts much longer than the oxidized state of a single oscillation. In the oxidized state the autocatalytic reaction is “switched on” establishing a relatively high  $\text{BrO}_2$  level. As it is known [13]  $\text{BrO}_2$  radicals react with malonyl radicals in a fast, diffusion controlled way, thus the already studied self-recombination routes leading to ETA and MAMA are suppressed.

In the experiment, to enhance concentrations of intermediates appearing in the  $\text{BrO}_2$  radical - malonyl radical reaction, higher than normal initial catalyst concentration was applied ( $[\text{Ce}^{4+}]_0 = 5 \times 10^{-3} \text{ M}$ ). The presence of oxalic acid was proven combining HPLC with various tests. Beside oxalic acid another new intermediate, ethenetetracarboxylic acid (EETA) was also identified.

#### *HPLC analysis during oscillations and the MBM mechanism [25]*

HPLC analysis of cerium and ferriin catalysed batch BZ systems were performed in their oscillatory regime [25]. Batch reactor experiments were chosen because accumulation of certain intermediates can be monitored this way. As oxygen has a dramatic effect on the BZ reaction [26] due to its fast reaction with the organic free radicals<sup>27,28</sup> all experiments were carried out in a nitrogen atmosphere. Higher than normal catalyst concentration ( $5 \times 10^{-3} \text{ M}$ ) was applied to produce elevated intermediate concentrations and to accelerate consumption of the organic substrate. This way the oscillatory regime and consequently the length of the experiment was shortened.

HPLC analysis revealed important differences between the cerium and ferriin catalysed systems. No recombination products of malonyl radicals were found in the ferriin systems showing that a direct reaction between ferriin and malonic acid does not occur or it is negligible. In spite of that ferriin catalysed oscillations start immediately without any induction period even if the substrate is pure malonic acid. This is not the case in cerium systems. Also the ferriin catalysed system contains much more oxalic and mesoxalic acid than the cerium catalysed one.

After collecting all the available experimental data for the  $\text{Ce}^{4+}$  catalysed system, we performed calculations with a revised and updated GTF model which is referred to as Marburg-Budapest-Missoula (MBM) model.

#### *Model calculations with the MBM mechanism [25]*

Due to the differences between the cerium and ferriin systems the MBM model was applied to the cerium catalysed BZ oscillators exclusively.

At low catalyst concentrations there was a good agreement between the model and experiments regarding only the  $\text{Ce}^{4+}$  oscillations. In a next step calculated concentration-time diagrams were compared with the experimental ones for various components measured with HPLC in a BZ system with a higher  $\text{Ce}^{4+}$  concentration. In this case a qualitative agreement was found for many components but serious disagree-

ments were also detected. For example the model seriously overestimates tartronic acid and underestimates BrEETRA.

Another important question which remained open is the role of oxalic acid. Oxalic acid is a product of the autocatalytic regime. Most probably it is produced from mesoxalic acid. Mesoxalic acid is a decomposition product of malonyl bromite. Malonyl bromite is produced when malonyl and bromine dioxide radicals recombine in the autocatalytic regime.

### The effect of oxalic acid on the classical BZ reaction

A main question is whether oxalic acid has a significant impact on the dynamics or not. Looking for an answer we perturbed the BZ reaction by adding some oxalic acid to it. As in a recent paper [29] we studied the effect of methanol on the BZ reaction it was reasonable to compare the effect of the two perturbants and to perform perturbation experiments with the same BZ system but applying oxalic acid instead of methanol. (BZ systems are rather sensitive to methanol perturbations. This is because that perturbant reacts with acidic bromate in a direct reaction to yield bromous acid which is the autocatalytic intermediate of the BZ reaction.) Our results are shown in Figure 1.

The result suggested that oxalic acid can be an even more effective perturbant than methanol and most probably its direct reaction with acidic bromate is also faster than that of the other perturbant. Unlike methanol, however, oxalic acid in a BZ system can participate in other significant reactions as well. Thus if we want to understand the role of oxalic acid in the classical BZ reaction it is a prerequisite to know all of its significant reactions in a BZ system. To this end, however, the best possible test ground is not the classical BZ system with all the complex organic chemistry of malonic acid but the more simple BZ oscillator with oxalic acid substrate.

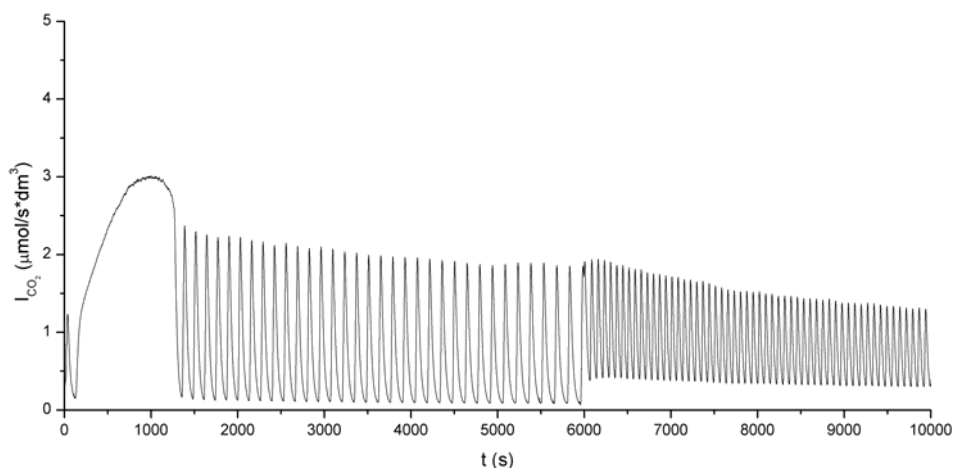


**Figure 1.** Perturbation of a BZ system with oxalic acid at  $t = 6000$  s.  $\text{CO}_2$  evolution rate.  $[\text{MA}] = 10$  mM,  $[\text{BrO}_3^-] = 30$  mM,  $[\text{Ce}^{4+}] = 0,4$  mM,  $[\text{H}_2\text{SO}_4] = 1$  M,  $[\text{OA}] = \sim 1$  mM

## Previous research with the oxalic acid oscillators

### *Experimental studies*

The BZ reaction of oxalic acid is well known [30,31], it was discovered [30] already in 1979. Oscillations with this substrate can be observed when a stream of inert gas (like  $N_2$  or  $H_2$ ) is bubbled through the reaction mixture. The role of this inert gas stream is to remove the dissolved  $Br_2$  produced in the reaction. This way semi-batch experiments (applying a batch reactor with product removal) were performed where the flow rate of the inert gas stream played the role of a dynamical parameter [32]. Gáspár and Galambosi [33] performed CSTR experiments without any gas stream: in that case it was the liquid flow of the CSTR which removed the produced bromine. Another possibility for bromine removal is to apply a second substrate beside oxalic acid like acetone, which can be brominated [34]. Such mixed substrate systems can exhibit various interesting dynamical phenomena already in a batch reactor and were studied by many authors, see e.g. Refs. 35-36.

### *Model calculations*

In spite of the relative simplicity of the oxalic acid substrate system there are only few model calculations in the literature [33, 37-40]. The first attempt was made by Bódiss and Field [37] who suggested that the system is a so-called bromine hydrolysis controlled (BHC) oscillator. According to that model the source of bromide ions is the hydrolysis of bromine. The idea of bromine hydrolysis control was also applied in Field and Boyd (FB) [38] in the simulation of the oxalic acid - acetone mixed substrate oscillator. All models were reviewed critically by Ševčík and Hlaváčová [39] who also suggested a new model with an optimum combination of the above reactions and rate constants [40]. However, it was a general conclusion of these studies that while all the various models were able to oscillate in certain parameter ranges all of them had difficulties in explaining some of the experiments.

## Conclusion: reasons to reinvestigate the oxalic acid oscillator

Beside the above mentioned difficulties of the various models there are other reasons which support that it is worthwhile to reinvestigate the BZ system with oxalic acid substrate by performing new experiments and model calculations. The following arguments can be mentioned:

- i) Some of the earlier model calculations [33,37,38] were made with an old set of rate constants, which were later revised by Field and Försterling [11]. There were some further changes since then (see e.g. the MBM mechanism [25]). Nowadays, however, most of the reactions and the rate constants of the inorganic subset of the BZ reaction are well established and these data can be applied in the modelling of the oxalic acid oscillator, too.
- ii) Most of these rate constants, however, were measured in 1 M sulphuric acid and at 20 °C while previous experiments with the oxalic acid oscillator were performed mainly in 1.5 M sulphuric acid and at laboratory temperature (around 25 °C). Thus it seems reasonable to repeat the oxalic acid experiments in 1 M sulphuric acid and at 20 °C before comparing the experimental observations with model calculations.

- iii) The mechanism of this simple BZ oscillator contains only two organic reactants, namely oxalic acid and carboxyl radical but the information available about the rate constants of their reactions with the bromine species is limited.

## Acknowledgement

The authors thank H. D. Försterling, R. J. Field, M. L. Turco Liveri, R. Lombardo, L. Hegedűs, J. Bódiss, A. Horváth and H. Farkas for helpful discussions. This work was partially supported by OTKA T-042708 and M-045272 grants and the ESF Program: "Re-actor".

## References

- [1] B. P. Belousov, in *Sbornik Referatov po Radiatsionnoi Meditsine*, Medgiz, Moscow 1958, 145.
- [2] A. M. Zhabotinsky, *Biofizika*, 1964, 9, 306.
- [3] *Oscillations and Traveling Waves in Chemical Systems*, eds. R. J. Field and M. Burger, Wiley, New York, 1985.
- [4] P. Gray and S. Scott, *Chemical Oscillations and Instabilities. Nonlinear Chemical Kinetics*. Clarendon, Oxford, 1994.
- [5] *Chemical Waves and Patterns*, eds. R. Kapral and K. Showalter, Kluwer, Dordrecht, 1995.
- [6] I. R. Epstein and J. A. Pojman, *An Introduction to Nonlinear Chemical Dynamics*. Oxford University Press, New York, 1998.
- [7] R. J. Field, E. Körös and R. M. Noyes, *J. Am. Chem. Soc.*, 1972, 94, 8649.
- [8] R. J. Field and R. M. Noyes, *J. Chem. Phys.*, 1974, 60, 1877.
- [9] Z. Noszticzius, E. Noszticzius and Z. A. Schelly, *J. Phys. Chem.*, 1983, 87, 510.
- [10] F. Ariese and Zs. Ungvárai-Nagy, *J. Phys. Chem.*, 1986, 90, 1.
- [11] R. J. Field and H. D. Försterling, *J. Phys. Chem.*, 1986, 90, 5400.
- [12] M. A. Brusa, L. J. Perissinotti and A. J. Colussi, *J. Phys. Chem.*, 1985, 89, 1572.
- [13] H. D. Försterling and Z. Noszticzius, *J. Phys. Chem.*, 1989, 93, 2740.
- [14] H. D. Försterling, Sz. Murányi and Z. Noszticzius, *J. Phys. Chem.*, 1990, 94, 2915.
- [15] K. Rácz, PhD Theses, Lorand Eötvös University, Budapest, 1984.
- [16] Z. Noszticzius, Zs. Bodnár, L. Garamszegi and M. Wittmann, *J. Phys. Chem.*, 1991, 95, 6575.
- [17] L. Györgyi, T. Turányi and R. J. Field, *J. Phys. Chem.*, 1990, 94, 7162.
- [18] L. Györgyi, T. Turányi and R. J. Field, *J. Phys. Chem.*, 1993, 97, 1931.
- [19] Y. Gao, H. D. Försterling, Z. Noszticzius and B. Meyer, *J. Phys. Chem.*, 1994, 98, 8377.
- [20] A. Sirimungkala, H. D. Försterling and Z. Noszticzius, *J. Phys. Chem.*, 1996, 100, 3051.
- [21] J. Oslovovitch, H. D. Försterling, M. Wittmann and Z. Noszticzius, *J. Phys. Chem.*, 1998, 102, 922.
- [22] I. Szalai, H. D. Försterling and Z. Noszticzius, *J. Phys. Chem.*, 1998, 102, 3118.
- [23] L. Hegedűs, H. D. Försterling, E. Kókai, K. Pelle, G. Taba, M. Wittmann and Z. Noszticzius, *Phys. Chem. Chem. Phys.*, 2000, 2, 4023.
- [24] W. F. Wang, M. N. Schuchmann, H. P. Schuchmann and C. von Sonntag, *Chemistry*, 2001, 7, 791.
- [25] L. Hegedűs, M. Wittmann, Z. Noszticzius, S. Yan, A. Sirimungkala, H. D. Försterling and R. J. Field, *Faraday Discussions*, 2001, 120, 21.
- [26] P. Ruoff and R. M. Noyes, *J. Phys. Chem.*, 1989, 93, 7394.
- [27] B. Neumann and S. C. Müller *J. Am. Chem. Soc.*, 1995, 117, 6372.
- [28] L. Hegedűs, H. D. Försterling, M. Wittmann and Z. Noszticzius, *J. Phys. Chem. A*, 2000, 104, 9914.

- [29] K. Pelle, M. Wittmann, Z. Noszticzius, R. Lombardo, C. Sbriziolo and M. L. Turco Liveri, *J. Phys. Chem. A*, 2003, 107, 2039.
- [30] Z. Noszticzius, J. Bódiss, *J. Am. Chem. Soc.*, 1979, 101, 3177.
- [31] P. Ševčík, L. Adamčíková, *Coll. Czech. Chem. Comm.*, 1982, 47, 891.
- [32] Z. Noszticzius, P. Stirling and M. Wittmann, *J. Phys. Chem.*, 1985, 89, 4914.
- [33] V. Gáspár and P. Galambosi, *J. Phys. Chem.*, 1986, 90, 2222.
- [34] Z. Noszticzius, *Magyar Kémiai Folyóirat*, 1979, 85, 330.
- [35] M. Wittmann, P. Stirling and J. Bódiss, *J. Chem. Phys. Lett.*, 1987, 141/3, 241.
- [36] M. C. Guedes and R. B. Faria, *J. Phys. Chem. A*, 1998, 102, 1973.
- [37] Chapter 2, p. 71. Fig. 2.3 in Ref 3.
- [38] R. J. Field and P. M. Boyd, *J. Phys. Chem.*, 1985, 89, 3707.
- [39] P. Ševčík and J. Hlaváčová, *Chem. Papers*, 1990, 44, 451.
- [40] J. Hlaváčová and P. Ševčík, *Chem. Phys. Lett.*, 1991, 182, 588.

## MODELLING THE BRAY-LIEBHAFSKY REACTION

G. Schmitz

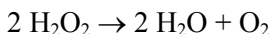
*Faculté des Sciences Appliquées, Université Libre de Bruxelles,  
CP165/63, Av.F.Roosevelt 50, 1050 Bruxelles, Belgium*

### Abstract

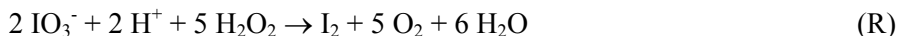
The oxidation of iodine by hydrogen peroxide is a part of the Bray-Liebhafsky oscillating reaction. In this work, we compare the experimental kinetics of this oxidation at 25 °C with the predictions of the model we have proposed to explain the oscillations. Several rate constants are obtained from independent kinetics and thermodynamics studies. With these constraints, the simplified form of our model is insufficient to explain quantitatively all the experimental results. We show that with the additional reaction  $2 \text{IO}_2\text{H} \rightleftharpoons \text{IOH} + \text{IO}_3^- + \text{H}^+$  the agreement becomes excellent.

### The Oxidation of Iodine by Hydrogen Peroxide

The Bray-Liebhafsky (BL) reaction [1-5] is the decomposition of hydrogen peroxide catalysed by iodate and iodine in acidic solutions. The global reaction



is the result of the reduction (R) of iodate to iodine and the oxidation (O) of iodine to iodate.



These reactions are complex and their mechanisms involve several intermediates, especially iodide and hypoiodous acid. The kinetics of reaction (R) is closely related to the kinetics of the Dushman reaction [6]



We have studied the kinetics of reaction (O) previously [7] and summarize here its main features. The first surprising observation is the need of some iodate, a reaction product, to start reaction (O). After it has started, iodate has usually no effect on the rate. The second surprising observation is its rate decreasing when the concentration of the reactant  $\text{H}_2\text{O}_2$  increases. Fig.1 shows examples of results obtained using the experimental technique described previously [7]. Under the conditions of experiment (a), the rate of reaction seems to be proportional to  $[\text{I}_2]$ . However, if we increase the concentration of hydrogen peroxide it appears that there is no simple rate law. Experiment (b) was performed under the same conditions as experiment (a) except a much larger hydrogen peroxide concentration. The rate is smaller and the iodine concentration does not tend to zero at the end of the experiments. At still higher hydrogen peroxide concentrations it is impossible to observe the reaction (O). The effect of the acidity is neither simple. Experiment (c) shows that when the acidity decreases the initial rate decreases. It shows also that at low acidities, as at high hydrogen peroxide concentrations, the iodine concentration does not tend to zero. At still lower acidities, reaction (O) is preceded by an induction period or never starts.

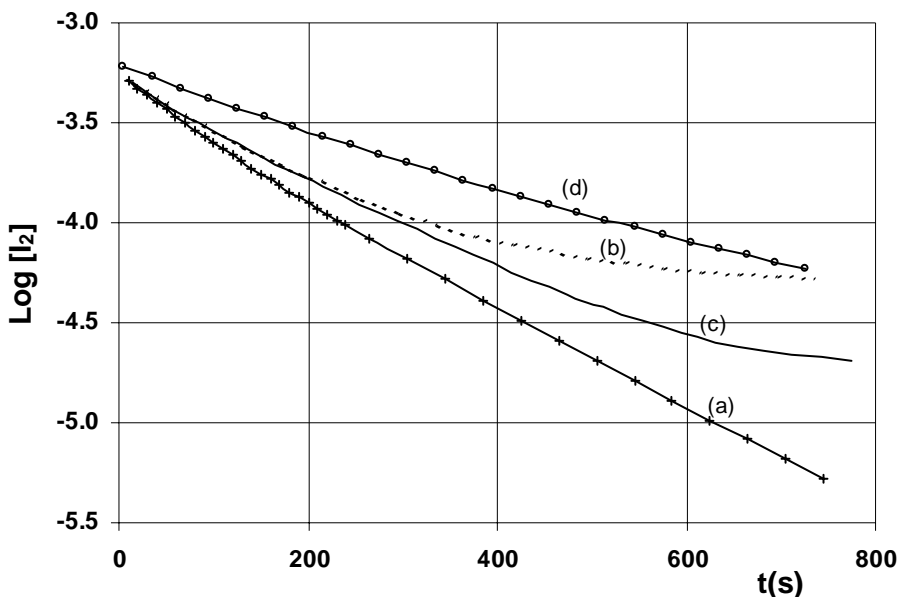


**Figure 1.** Log  $[I_2]$  vs. time at 25°C;  $[I_2]_0 = 6 \times 10^{-4}$  M;  $[NaIO_3] = 0.01$  M;  $[H_2O_2] = 0.01$  M (a, c, d), 0.20 M (b);  $[HClO_4] = 0.10$  M (a, b), 0.02 M (c), 0.40 M (d).

Experiment (d) shows that the rate decreases also when the acidity increases. However, at high acidities, the rate remains proportional to  $[I_2]$  and the iodine concentration tends to zero. The rate passes through a maximum under the conditions of experiment (a) and decreases at lower or higher acidities but with different shapes of the curves log  $[I_2]$  vs. time.

### Mechanism

The general form of the model we have proposed [3] to explain the BL oscillations includes the reactions of iodine and its compounds constituting the mechanism of the Dushman reaction or its reverse reaction, the disproportionation of I(+1) [8], and the reactions of hydrogen peroxide with all these iodine compounds. The rate constants of many reactions of this general model are unknown and trying to adjust them empirically to experimental data would be a useless job, and by no mean a proof of the model. Thus, we have adopted a different approach. We start with a simplified form of the model and add other reactions only when they are necessary and experimentally justified. This simplified model includes reactions (M1-M5) in Table I. These reactions are not elementary but reactions (M1) to (M4) have simple rate laws with orders equal to their stoichiometric coefficients. The detail mechanism of reaction (M5) has been discussed recently [8]. We must add to these reactions at least two reactions of hydrogen peroxide reactions, one where its acts as a reductant and one where it acts as an oxidant. The reduction (M6) is well known [9, 10]. The simplified form of our model rests on the observation that it is sufficient to add the oxidation (M7) to explain the main features of the BL reaction. Other reactions were considered previously and are ne-

glected in this work. The oxidation of iodide by oxygen, reaction M8, was added to explain qualitatively that oxygen could sometimes modify the oscillations [11]. Its mechanism is unknown and involves probably radicalar species. This is a disturbing phenomenon, not related with the origin of the oscillations. The reduction of iodate by hydrogen peroxide, reaction (M9), was studied by Liebhafsky [12]. We suspect that its rate constant is overestimated because reaction (M1) takes place simultaneously and increases the observed rate. The oxidation of iodous acid by hydrogen peroxide,  $\text{IO}_2\text{H} + \text{H}_2\text{O}_2 \rightarrow \text{IO}_3^- + \text{H}^+ + \text{H}_2\text{O}$ , has been proposed previously [4] because it improves the simulations of the oscillations at 50 °C but we have observed that it is detrimental to the simulation of reaction (O) kinetics. The effect of disproportionation (M10) is the subject of this work.

**Table I.** Mechanism and rate constants.

Reactions	$k_+^{\circ (a)}$	$k_-^{\circ (a)}$	
$\text{IO}_3^- + \Gamma + 2 \text{H}^+ \rightleftharpoons \text{I}_2\text{O}_2 + \text{H}_2\text{O}$	M1 and M2 replaced with A		M1
$\text{I}_2\text{O}_2 + \text{H}_2\text{O} \rightleftharpoons \text{IOH} + \text{IO}_2\text{H}$	$k_{\text{A}}^{\circ} = 4.5 \times 10^3$	$k_{\text{-A}}^{\circ} = 240$	M2
$\text{IO}_2\text{H} + \Gamma + \text{H}^+ \rightleftharpoons \text{I}_2\text{O} + \text{H}_2\text{O}$	$2.1 \times 10^{10}$	$2.1 \times 10^{-2}$	M3
$\text{I}_2\text{O} + \text{H}_2\text{O} \rightleftharpoons 2 \text{IOH}$	100	$1.2 \times 10^5$	M4
$\text{IOH} + \Gamma + \text{H}^+ \rightleftharpoons \text{I}_2 + \text{H}_2\text{O}$	$2.3 \times 10^9$	$1.2 \times 10^{-3}$	M5 <sup>(b)</sup>
$\text{IOH} + \text{H}_2\text{O}_2 \rightarrow \Gamma + \text{H}^+ + \text{O}_2 + \text{H}_2\text{O}$	1.0		M6
$\text{I}_2\text{O} + \text{H}_2\text{O}_2 \rightarrow \text{IOH} + \text{IO}_2\text{H}$	$k_7/k_4 = 400$		M7
$\text{I}^- + \text{H}^+ + \frac{1}{2} \text{O}_2 \rightarrow \text{IOH}$	neglected		M8
$\text{IO}_3^- + \text{H}^+ + \text{H}_2\text{O}_2 \rightarrow \text{IO}_2\text{H} + \text{O}_2 + \text{H}_2\text{O}$	neglected		M9
$2 \text{IO}_2\text{H} \rightleftharpoons \text{IOH} + \text{IO}_3^- + \text{H}^+$	$3.0 \times 10^4$	neglected	M10

<sup>(a)</sup> The superscript  $^{\circ}$  means values extrapolated at zero ionic strength. The units are  $\text{mol.l}^{-1}$  and s.

<sup>(b)</sup> In acidic solutions  $r_5 = k_5(\text{IOH})(\Gamma) - k_{-5}(\text{I}_2)/(\text{H}^+)$  [8]

In this section, we show how our model can qualitatively explain the experimental results. Numerical simulations will be presented in section IV. The rate of reaction (R) is the rate of iodine species reduction by hydrogen peroxide. Following the simplified model it is the rate of reaction (M6). The rate of reaction (O) is the rate of iodine species oxidation by hydrogen peroxide. Following the simplified model it is the rate of reaction (M7). When we observe only the catalytic decomposition of hydrogen peroxide, these two rates are equal. We call this state the *catalytic steady state* and note the corresponding iodine concentration  $[\text{I}_2]_{\text{ss}}$ . This state can be stable or unstable. When it is stable the system moves towards it. When it is unstable, the rates of the reactions (O) and (R) cannot become equal and we get a succession of periods R and O. During the periods R the rate of the reaction (R) is larger than the rate of reaction (O) and the concentration of iodine increases. During the periods O the rate of the reaction (O) is larger than the rate of reaction (R) and the concentration of iodine decreases. We get the oscillatory decomposition of hydrogen peroxide. Fig.2 shows the shape of the trajectories predicted by the model, projected on the phase plane  $[\text{IOH}]$ -

$[I_2]$ . When the catalytic steady state is stable the system follows the branch R or O until it is reached. If the iodine concentration is less than  $[I_2]_{ss}$  we get a period R, if it is higher than  $[I_2]_{ss}$  we get a period O. When the catalytic steady state is unstable, the system follows a limit cycle around it. Starting with no iodine, the system follows the branch R until point  $T_1$  is reached. Then the system jumps on the branch O and the iodine concentration decreases. When it reaches point  $T_2$  the system jumps on branch R and this completes the cycle. If the initial concentration of iodine is larger than  $[I_2]$  at point  $T_1$ , the evolution is the same but starts with a period O.

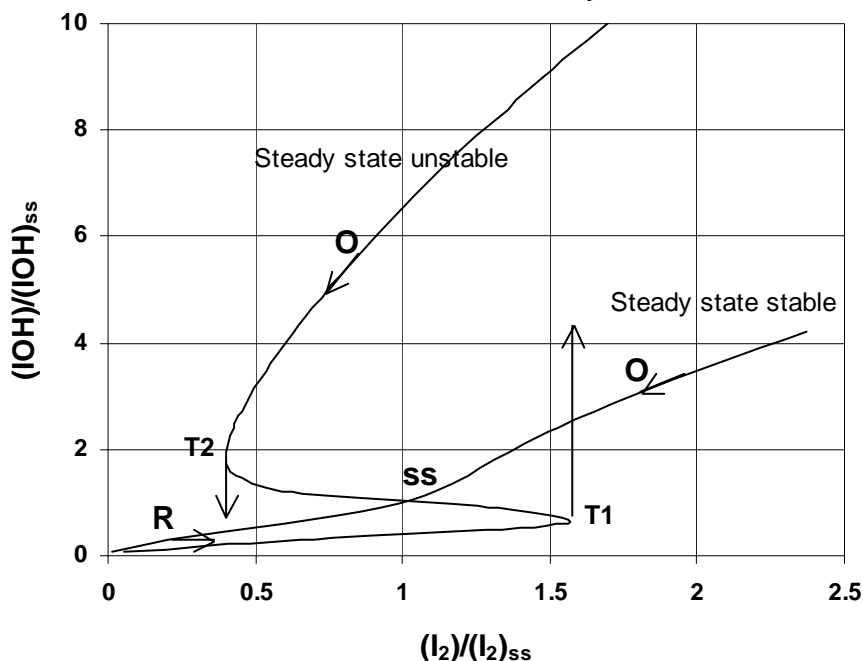


**Figure 2.** Shape of the trajectories projected on the phase plane  $[IOH]$ - $[I_2]$ .

During these evolutions, the measured rate  $d[I_2]/dt$  is not equal to the rate of reaction (R) or reaction (O) but is equal to the difference between them. Noting  $r_i$  the rate of reaction  $M_i$ , our model gives  $d[I_2]/dt = (r_6 - r_7)/5$ . At the catalytic steady state  $r_6 = r_7$  and  $d[I_2]/dt = 0$ . If we move away from the catalytic steady state, the absolute value of  $d[I_2]/dt$  increases. If  $[I_2] < [I_2]_{ss}$  it is positive giving a period R, if  $[I_2] > [I_2]_{ss}$  it is negative giving a period O. We can now explain the above results obtained with a given initial concentration of iodine  $[I_2]_0 \sim 6 \times 10^{-4}$ . The concentration  $[I_2]_{ss}$  depends on the experimental conditions. It increases when  $[IO_3^-]$  decreases, when  $[H_2O_2]$  increases and when  $[H^+]$  decreases. If  $[IO_3^-]$  is too low,  $[I_2]_{ss}$  is higher than  $[I_2]_0$  and we get a period R. This explains why we must add the product iodate to start the reaction O. If  $[H_2O_2]$  increases from 0.01 M to 0.20 M (experiments a and b),  $[I_2]_{ss}$  increases. The difference  $[I_2]_0 - [I_2]_{ss}$  decreases and this explains why the rate decreases. At too high hydrogen peroxide concentrations  $[I_2]_{ss}$  is higher than  $[I_2]_0$  and this explains why we cannot get a period O. The effect of a  $[H^+]$  decrease is explained in a similar way. The

effect of a  $[H^+]$  increase needs a different explanation. Under the conditions of experiment (d),  $[I_2]_{ss}$  is very low. The rate is smaller than for experiment (a) because the rate of iodine hydrolysis  $r_{-5}$  is inversely proportional to  $[H^+]$ . Under the conditions of experiment (a), reaction (M5) is nearly at equilibrium but this is no longer true under the conditions of experiment (d). At high acidities the hydrolysis of iodine tends to become the rate-determining step of the reaction (O).

## Studies of Iodine and Iodine Compounds Reactions

In order to validate our model we have looked for independent information about individual rate constants. Such information about the steps (M1)-(M4) is given by kinetic studies of iodine and iodine compounds reactions without hydrogen peroxide. In systems where (M1) and (M2) are the only reactions of  $I_2O_2$ , we can use the steady state approximation and replace them with reaction (A) = (M1) + (M2).



$$k_A = k_1 k_2 / (k_{-1} + k_2) \quad k_{-A} = k_{-1} k_{-2} / (k_{-1} + k_2)$$

The value of  $k_A$  is the observed value of the rate constant of the Dushman reaction at low iodide concentrations ( $[I^-] < 10^{-7}$  mol/l). We have obtained [13]  $k_A = 1\,250 \text{ mol}^{-3} \cdot \text{l}^3 \cdot \text{s}^{-1}$  at  $25^\circ\text{C}$  and 0.2 M ionic strength. At this ionic strength the activity coefficient  $\gamma$  is about 0.75 giving  $k_A^\circ = k_A / \gamma^4 = 4.0 \times 10^3$  in good agreement with Liebhaftsky value [14]  $k_A^\circ = 4.7 \times 10^3$ . For the reverse reaction Furrow [10] has obtained  $k_{-A} \sim 240 \text{ mol}^{-1} \cdot \text{l} \cdot \text{s}^{-1}$ , in rather good agreement with the results of Noszticzius [15]. In systems where (M3) and (M4) are the only reactions of  $I_2O$  we can use the steady state approximation and replace them with (B) = (M3) + (M4).



$$k_B = k_3 k_4 / (k_{-3} + k_4) \quad k_{-B} = k_{-3} k_{-4} / (k_{-3} + k_4)$$

The value of  $k_B$  is the observed value of the rate constant of IOH disproportionation. Our value at  $25^\circ\text{C}$  [8] is in perfect agreement with Furrow's value [10],  $k_B = 25 \text{ mol}^{-1} \cdot \text{l} \cdot \text{s}^{-1}$ .

These experimental values can be correlated with the value of  $k_B$  using criteria of internal consistency of reactions mechanisms [16]. Following the principle of detailed balancing, when a reaction is at equilibrium the rate of every reaction in one direction must be equal to its rate in the opposite direction. On the other hand, thermodynamics gives an expression relating the concentrations and the equilibrium constant  $K$ . In general, this thermodynamic expression give no information about the kinetics and the relation  $k_f/k_r = K$  between the rate constants in the forward and reverse directions,  $k_f$  and  $k_r$ , is not necessarily true for complex reactions. However, when the rate expression in one direction is known, the equivalence between the kinetic and thermodynamic expressions of the equilibrium dictates the rate in the opposite direction. We know that  $r_{+A} = k_A (IO_3^-)(I^-)(H^+)^2$ . At equilibrium  $K_A = (IO_2H)(IOH)/(IO_3^-)(I^-)(H^+)^2$  and  $r_{+A} = r_{-A}$ . Then  $r_{-A}$  must be equal to  $k_{-A} (IO_2H)(IOH)$  with  $k_A/k_{-A} = K_A$ . For reaction (B), we know that  $r_{-B} = k_{-B} (IOH)^2$ . Then  $r_{+B}$  must be equal to  $k_B (IO_2H)(I^-)(H^+)$  with  $k_B/k_{-B} = K_B$ . The equilibrium constants of reactions (D) and (M5) are well known,  $K_D^\circ = 1.0 \times 10^{47}$  [17, 18] and  $1/K_5^\circ = 5.3 \times 10^{-13}$  [8] at  $25^\circ\text{C}$ . The superscript  $^\circ$  means values extrapo-

lated at zero ionic strength. As  $(A) + (B) + 3(M5) = (D)$ , we get an important relation between the rate constants:

$$k^{\circ}_A k^{\circ}_B / k^{\circ}_{-A} k^{\circ}_{-B} = K^{\circ}_A K^{\circ}_B = K^{\circ}_D / (K^{\circ}_5)^3 = 1.5 \times 10^{10}$$

The above values give  $K^{\circ}_A = 18$ ,  $K^{\circ}_B = 8.3 \times 10^8$  and  $k^{\circ}_B = 25 \times 8.3 \times 10^8 = 2.1 \times 10^{10} \text{ mol}^{-2} \cdot \text{l}^2 \cdot \text{s}^{-1}$ . This value is close to the value accepted to simulate numerically the kinetics of different systems involving reaction (B) [19, 20].

## Numerical Simulations

In our kinetic study of reaction (O), we have expressed the measured rates using the parameter  $k_{\text{exp}}$ , function of all the concentrations including  $[I_2]$ .

$$k_{\text{exp}} = (-d[I_2]/dt)/[I_2]$$

Fig.3 shows some others experimental results. We have seen that our model can explain qualitatively that the rate decreases when  $[H_2O_2]$  increases. Here we propose a quantitative description. As we will add no other reactions of  $I_2O_2$ , we replace reactions (M1) and (M2) with reaction (A) and use the above rate constants  $k_A$  and  $k_{-A}$ . During the disproportionation of IOH the rate determining step is  $(-M3)$  [8] giving  $k_4 \gg k_{-3}$ . This inequality is also supported by the very high value of  $k^{\circ}_B$  giving  $k^{\circ}_3 = 2.1 \times 10^{10} (1 + k_{-3}/k_4)$ . Even if (M3) is not an elementary reaction, the value of  $k^{\circ}_3$  cannot be much larger than a diffusion controlled rate constant and  $(1 + k_{-3}/k_4)$  cannot be much larger than one. Thus,  $k^{\circ}_3 = 2.1 \times 10^{10}$ . Furrow [10] has obtained  $k_6 = 3 \pm 2 \text{ mol}^{-1} \cdot \text{l} \cdot \text{s}^{-1}$ . The results of the simulations are improved taking its lowest value  $k_6 = 1$ . For the simplified model (M1)-(M7), it remains four unknown rate constants  $k_{-3}$ ,  $k_4$ ,  $k_{-4}$  and  $k_7$  with a relation between them,  $k_{-3}k_{-4}/k_4 = k_{-B} = 25$ .

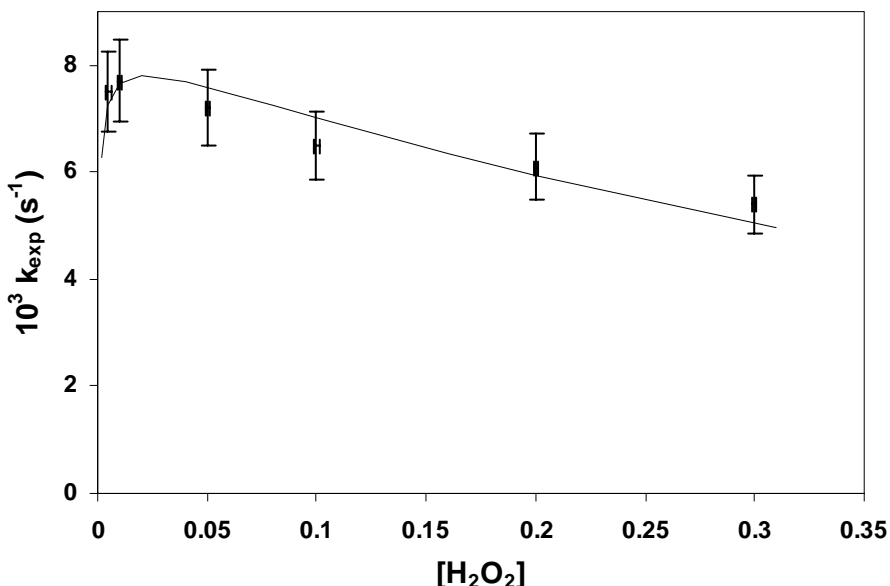


**Figure 3.** Values of  $k_{\text{exp}}$  at 25°C if  $[KIO_3] = 0.012$ ,  $[HClO_4] = 0.10$ ,  $[I_2] = 4 \times 10^{-4} \text{ M}$ ; Experimental results ( $\pm$ ) and values calculated with the rate constants in Table 1 ( $\text{—}$ ).

The value of  $k_3$  has no effect on the numerical simulations as long as it is much smaller than  $k_4$ . Finally, a sensitivity analysis shows that the calculated values of  $k_{\text{exp}}$  depend on the ratio  $k_7/k_4$  but not on their individual values and we are left with only two adjustable parameters  $k_4$  and  $k_7/k_4$ .

We have tried to reproduce the experimental values of  $k_{\text{exp}}$  using the simplified model but have found that, with the above rate constants, the calculated value of  $[\text{IO}_2\text{H}]$  becomes always larger than  $10^{-4} \text{ mol.l}^{-1}$ , the same order of magnitude as  $[\text{I}_2]$ . As a consequence, the reaction begins with an induction period not observed under the conditions of Fig.3. We have thus considered different ways to decrease  $[\text{IO}_2\text{H}]$ . We cannot suppose that the experimental value  $k_A = 240$  is too low because if we increase  $k_A$  the above thermodynamic relation shows that we have also to increase  $k^{\circ}_3$ . A significant lowering of  $[\text{IO}_2\text{H}]$  implies  $k^{\circ}_3$  values much too large for a diffusion controlled reaction. Thus, we must add to reactions (M1)-(M7) a reaction of iodosic acid producing iodate. The most obvious possibility is the reaction  $\text{IO}_2\text{H} + \text{H}_2\text{O}_2 \rightarrow \text{IO}_3^- + \text{H}^+ + \text{H}_2\text{O}$ . However, its effect increases with  $[\text{H}_2\text{O}_2]$  in such a way that if we choose a rate constant giving correct calculated values when  $[\text{H}_2\text{O}_2] = 0.01 \text{ M}$ , it becomes impossible to simulate the results at much higher hydrogen peroxide concentrations. Then, we have found that we can perfectly reproduce the experimental results adding reaction (M10). The results presented in Fig.3 were obtained adjusting only three parameters,  $k_4$ ,  $k_7/k_4$  and  $k_{10}$ . The used values of the rate constants are given in table I but, in the limit of the experimental uncertainties, equally good fits could be obtained with different values and the change of one can be offset by the change of another.

## Conclusion

Our model of the BL reaction gives an explanation of the complicated kinetic of the iodine oxidation by hydrogen peroxide. A quantitative agreement could be obtained keeping only reactions (M1)-(M7) but with a value of  $k_A$  much higher than measured independently. The criterion of internal consistency of reaction mechanisms also sets bounds to the values of the rate constants. Therefore, we must add to the model another reaction of iodate formation from iodosic acid. The reaction  $\text{IO}_2\text{H} + \text{H}_2\text{O}_2 \rightarrow \text{IO}_3^- + \text{H}^+ + \text{H}_2\text{O}$  does not allow to simulate the experimental results but the additional reaction  $2 \text{IO}_2\text{H} \rightleftharpoons \text{IOH} + \text{IO}_3^- + \text{H}^+$  gives excellent results. Other explanations exist and works are in progress to decide between them. We must keep in mind that a mechanism can never be proved. It becomes only more and more likely as the number of facts supporting it increases.

## References

- [1] (a) W.C.Bray, J.Am.Chem.Soc., 1921, 43, 1262. (b) W.C.Bray and H.A.Liebhaufsky, J.Am.Chem.Soc., 1931, 53, 38.
- [2] S.D.Furrow in Oscillations and Travelling Waves in Chemical Systems, ed. R.J.Field and M.Burger, Wiley-Interscience, New York, 1985, p.171-192.
- [3] G.Schmitz, J.chim.phys. 1987, 84, 957.
- [4] Lj.Kolar-Anic and G.Schmitz, J.Chem.Soc., Faraday Trans., 1992, 88, 2343.

- 
- [5] Lj.Kolar-Anic, Z.Cupic, S.Anic and G.Schmitz, *J.Chem.Soc., Faraday Trans.*, 1997, 93, 2147.
- [6] G.Schmitz, *Phys.Chem.Chem.Phys.*, 1999, 1, 1909.
- [7] G.Schmitz, *Phys.Chem.Chem.Phys.*, 2001, 3, 4741.
- [8] G.Schmitz, *Int.J.Chem.Kinet.*, 2004, in press.
- [9] H.A.Liebhafsky and A.Mohammad, *J.Am.Chem.Soc.*, 1933, 55, 3977.
- [10] S.Furrow, *J.Phys.Chem.*, 1987, 91, 2129.
- [11] G.Schmitz, *Phys.Chem.Chem.Phys.*, 1999, 1, 4605.
- [12] H.A.Liebhafsky, *J.Am.Chem.Soc.*, 1931, 53, 896.
- [13] G.Schmitz, *Phys.Chem.Chem.Phys.*, 2000, 2, 4041.
- [14] R.Furuichi and H.A.Liebhafsky, *Bull.Chem.Soc.Japan*, 1975, 48, 745.
- [15] Z.Noszticzius, E. Noszticzius and Z.A.Schelly, *J.Phys.Chem.*, 1983, 87, 510.
- [16] G.Schmitz, *J.Chem.Phys.*, 2000, 112, 10714.
- [17] R.D.Spitz and H.A.Liebhafsky, *J.Electrochem.Soc.*, 1975, 122, 363.
- [18] D.A.Palmer, R.W.Ramette and R.E.Mesmer, *J.Sol.Chem.*, 1984, 13, 685.
- [19] P. De Kepper and I.R.Epstein, *J.Am.Chem.Soc.*, 1982, 104, 49.
- [20] R.H.Simoyi, M.Manyonda, J.Masere, M.Mtambo, I.Ncube, H.Patel, I.R.Epstein and K.Kustin, *J.Phys.Chem.*, 1991, 95, 770.

# NONLINEAR PROBLEMS OF QUANTITATIVE THEORY OF FREE-RADICAL COPOLYMERIZATION

S.I. Kuchanov

*Keldysh Institute of Applied Mathematics Russian Academy of Sciences  
Miusskaya Square, 4, 125047 Moscow, Russia*

## Introduction

Polymerization processes occupy the leading position in modern chemical technology, that stipulates the necessity of a comprehensive treatment of these processes on the molecular level. In this respect of considerable promise is the copolymerization of  $m$  types of monomers. Varying their initial stoichiometry and the process mode it is possible to govern physico-chemical and mechanical properties of a copolymer formed by mere change of its molecular characteristics. Special role is performed here by the multicomponent ( $m \geq 3$ ) copolymers possessing unique potentialities in imparting a material prepared on their basis a variety of properties inherent to the individual components. However, an empirical search for optimal conditions of obtaining of a polymer material with desired service properties by direct exhaustion of variants calls for an extensive routine experimental work which dramatically increases with the number of types of monomers involved. So, for overcoming the above difficulties it is critically important to elaborate approaches based on the mathematical modeling that enable one to predict theoretically some properties of multicomponent copolymers. The efficiency of such approaches for the prediction of the transparency and the thermostability of a number of particular terpolymers ( $m = 3$ ) is conclusively shown [1,2].

A considerable progress made in this field is largely due to two reasons. The first is the simplicity and the reliability of the mathematical models of the copolymerization, the values of the parameters of which have been experimentally found for an abundance of particular copolymerization processes [3,4]. The second reason is the fruitful engagement for the analysis of these nonlinear models of the methods of the theory of the dynamical systems [1,5-8]. The presentation reviews briefly the results achieved in this area, discussing both mathematical aspects of the problem and some applications of the theoretical results to the description of real polymer systems.

## Formulation of the Problem and Mathematical Model

In order to conduct a copolymerization of monomers  $M_1, \dots, M_i, \dots, M_m$  to their mixture an initiator is introduced. Its molecules decompose to form primary radicals capable upon reacting with monomers to initiate their subsequent addition. The succession of such acts results in the propagation of a polymer chain which bears resemblance to threading of beads (monomers) on string when making a necklace (copolymer macromolecule). The two growing macroradicals deactivate under chemical interaction of their reactive centers, that stops these chains' propagation.

During the formation of each macromolecule the monomers' concentration in a reaction system remains virtually unchanged. This permits one first to calculate all

statistical characteristics of a copolymer at a given monomer mixture composition  $\mathbf{x} = (x_1, \dots, x_i, \dots, x_m)$  and then to average these “instantaneous” characteristics taking into account the evolution of  $\mathbf{x}$  in the course of the process [1]. Such a two-stage calculation procedure (when the statistical and dynamical problems of free-radical copolymerization are solved successively) is dictated by the specific nature of this process and does not depend on the kinetic model chosen. The latter specifies just the analytic expression for the dependence of the “instantaneous” statistical characteristics on  $\mathbf{x}$  and the kinetic parameters.

Such dependencies are well known for the Mayo-Lewis model [1] where the reactivity of polymer radical  $R_i$  is controlled by type  $i = 1, \dots, m$  of its terminal unit exclusively. It is characterized by  $m - 1$  kinetic parameters  $r_{ij} = k_{ii} / k_{ij}$  ( $j \neq i$ ) each equal to the ratio of the rate constants of the addition of the “similar”  $M_i$  and “different”  $M_j$  monomers. A complete set of such parameters for an  $m$ -component system consists of  $m(m - 1)$  reactivity ratios  $r_{ij}$ , each being determined in a standard way from the experiment on binary copolymerization of monomers  $M_i$  and  $M_j$ . The values of these parameters are tabulated for many hundreds of monomeric pairs [3], that enables one to carry out mathematical modeling of an immense number of multicomponent systems involving these pairs escaping additional routine experimental investigations.

The state of a reaction system at every instant of copolymerization, when the value of overall conversion of monomers is equal to  $p$ , is characterized by vector  $\mathbf{x}(p)$  of the monomer mixture composition. The  $i$ -th component  $x_i$  of this vector equals the molar fraction of monomer  $M_i$  in a mixture. The copolymer formed at this instant is described by vector of the instantaneous composition  $\mathbf{X}(p)$  whose component  $X_i$  is the molar fraction of monomeric units  $\bar{M}_i$  in all macromolecules.

The evolution with conversion of  $m$ -component monomer mixture composition  $\mathbf{x}(p)$  is depicted according to the condition  $x_1 + \dots + x_m = 1$  by a trajectory inside some bounded region of  $(m - 1)$ -dimensional space which is referred to as  $m$ -simplex. Under copolymerization of  $m = 2, 3$  and 4 monomers the phase space will be, respectively, an interval of a unit length, equilateral triangle and regular tetrahedron. In the analogous simplex the change of vector  $\mathbf{X}$  occurs whose evolution unambiguously characterizes the distribution  $\langle f_w(\zeta) \rangle$  of macromolecules for their composition  $\zeta$ . Vector  $\zeta$  has components  $(\zeta_1, \dots, \zeta_i, \dots, \zeta_m)$  equal to molar fractions of monomeric units of all types in a macromolecule chosen at random. Evidently, this vector being averaged over the ensemble of macromolecules formed under fixed conversion  $p'$  yields vector  $\mathbf{X}(p')$ . To find the composition of the copolymer present in a reaction system at given value  $p$  the vector  $\mathbf{X}(p')$  should be averaged over all conversions  $p'$  preceding  $p$

$$\langle X_i \rangle = \frac{1}{p} \int_0^p X_i(p') dp' \quad (i = 1, \dots, m) \quad (1)$$

An analogous averaging should be also performed when calculating elements  $\lambda_{ij}$  of the covariance matrix of the composition distribution

$$\lambda_{ij} = \frac{1}{p} \int_0^p [X_i(p') - \langle X_i \rangle][X_j(p') - \langle X_j \rangle] dp' \quad (2)$$

through which the heat of the mixing of a copolymer melt is expressed in a simple manner [9]. Hence the application of the method of mathematical modeling opens up fresh opportunities for the prediction of the thermodynamic behavior of the copolymerization products.

Under experimental examination of the composition inhomogeneity by the Liquid Gel-Chromatography technique they normally use a set of  $m$  one-dimensional distributions for each component [1,5,6]

$$\langle f_W(\zeta_i) \rangle = \frac{1}{p} \sum_{p'} \left| \frac{dX_i}{dp} \right|_{X_i=\zeta_i}^{-1} \quad (i=1, \dots, m) \quad (3)$$

where the summation is over all those values of conversion  $p'$  at which  $X_i$  has fixed value  $\zeta_i$ .

The copolymerization dynamics is described by the set of equations [1,5-7]

$$\frac{dx_i}{d\tau} = x_i - \pi_i(\mathbf{x}), \quad x_i(0) = x_i^0, \quad (i=1, \dots, m) \quad p = 1 - \exp(-\tau) \quad (4)$$

where every component  $\pi_i(\mathbf{x})$  of the composition vector  $\boldsymbol{\pi}(\mathbf{x})$  is the ratio of the uniform polynomials in variables  $x_1, \dots, x_m$  of degree  $m$ . This polynomial coefficients depend in a known way [1,6] on elements  $a_{ij} = 1/r_{ij}$  of matrix  $\{a_{ij}\}$  of the reciprocal reactivity ratios. Trajectories  $\mathbf{x}(p)$  completely describe the evolution of the instantaneous and average copolymer composition

$$X_i(p) = \pi_i(\mathbf{x}(p)), \quad \langle X_i \rangle = [x_i^0 - (1-p)x_i(p)] p^{-1} \quad (5)$$

and, consequently, partial composition distributions (3).

To characterize the microstructure of the chains of a copolymer it is necessary to specify the fractions in them of all possible sequences  $\{U_k\}$  consisting of  $k$  units. The Nuclear Magnetic Resonance technique available currently permits finding the values of the fractions of these  $k$ -ad up to  $k=5$ . When calculating them theoretically one should make use of the fact that the sequence distribution in macromolecules formed under any fixed conversion  $p'$  is describable by the Markov chain. Its matrix  $\mathbf{Q}$  of the transition probabilities has elements

$$\nu_{ij} = \frac{a_{ij}x_j}{\sigma_i(\mathbf{x})}, \quad \sigma_i(\mathbf{x}) = \sum_{j=1}^m a_{ij}x_j \quad (6)$$

where the dependence  $\mathbf{x}$  on  $p'$  may be determined from the solution of the set of equations (4). Given stationary vector  $\boldsymbol{\pi}$  of matrix  $\mathbf{Q}$  one may immediately write down an expression for the instantaneous probability  $P\{U_k\}$  of any sequence  $\{U_k\}$  of units in copolymer macromolecules. The subsequent averaging of these probabilities over conversions  $0 < p' < p$  enables the determination of average fractions of any  $k$ -ads. In particular, the fraction of the directed dyads  $\{U_2\}$  composed of units  $\overline{M}_i$  and  $\overline{M}_j$  is found by formula

$$P\{\overline{M}_i \overline{M}_j\} = \frac{1}{p} \int_0^p \pi_i \nu_{ij} dp' \quad (7)$$

Hence it is clear that many statistical characteristics of the chemical structure of copolymerization products along with some of their important service properties are controlled by the dependence of the monomer mixture composition on conversion. This dependence  $\mathbf{x}(p)$  may be found analytically only for binary copolymerization, while for  $m \geq 3$  equations (4) may be solved only numerically. However, the mathematical analysis of these equations invoking the approaches of the theory of dynamical systems provides a possibility to reveal main qualitative peculiarities of the behavior of the trajectories  $\mathbf{x}(p)$  and to perform the classification of copolymerization systems by types of their phase portraits.

### General Qualitative Analysis of Copolymerization Dynamics

It was rigorously proved [6] that the nonlinear system (4) may have at any  $m$  no more than one stationary point (SP)  $\mathbf{x} = \mathbf{x}^*$  inside the  $m$ -simplex. Necessary and sufficient condition for the existence of such a stationary solution of equations (4) is the identity of the signs of the determinants  $D_i (i = 1, \dots, m)$  of all matrices obtained from matrix  $\{a_{ij}\}$  by virtue of the replacement of all elements of its  $i$ -th row by unity. The determinant  $D$  of matrix  $\{a_{ij}\}$  will have therewith the same sign while the quantities  $\omega_i = D_i / D$  at all  $i = 1, \dots, m$  will fall within the interval  $0 < \omega_i < 1$ . Given values of  $\omega_i$  one may determine SP  $\mathbf{x}^*$ , known as ‘‘azeotrop’’ [1,5], from the solution of the linear set of equations

$$x_i^* = \omega_i \sum_{j=1}^m a_{ij} x_j^* \quad (i = 1, \dots, m) \quad \sum_{i=1}^m x_i^* = 1 \quad (8)$$

In parallel with such an internal azeotrop inside the  $m$ -simplex, there can also exist azeotrops located at its boundaries which are the  $n$ -simplexes with  $2 \leq n \leq m - 1$ . Obviously,  $(m - n)$  components of vector  $\mathbf{x}^*$  equal zero for each such boundary  $n$ -azeotrop, so it is an internal azeotrop in the system of the rest  $n$  monomers. Besides, the equations (4) always have  $m$  solutions  $x_i^* = \delta_{is}$  (where  $\delta_{is}$  stands for the Kronecker delta), each corresponding to the homopolymer of monomer  $M_s (s = 1, \dots, m)$ . These solutions to-

gether with all azeotrops located both inside an  $m$ -simplex and on its boundaries constitute a complete set of SPs of the dynamical system (4).

Its qualitative analysis gives the possibility to establish types of these points predetermining the behavior of the trajectories  $\mathbf{x}(p)$  in the vicinity of such SPs as well as to reveal among them the stable ones. This is of practical importance since the trajectories approach only these points when  $p \rightarrow 1$ . Each of them has its own basin of attraction, defined as an area of all initial monomer mixture compositions  $\mathbf{x}^0$ , having started at which the trajectories asymptotically tend to the SP in hand. Consequently, in accordance with the number of these stable points the whole  $m$ -simplex is divided into the same number of their basins. In line with the standard analysis the type of any SP of the dynamical system (4) may be defined by the set of the roots of the characteristic equation

$$\lambda^{m-1} + \alpha_1 \lambda^{m-2} + \dots + \alpha_{m-1} = 0 \quad (9)$$

with coefficients expressed in a known way through the reactivity ratios [1,5,6]. In order for any SP to be stable, all roots of its characteristic equation (9) should have negative real parts. Escaping the calculation of these roots, the Routh-Hurwitz method [10] permits to indicate simple inequalities comprising coefficients  $\alpha_k$  whose fulfillment ensures the stability of an SP. The sufficient condition for an internal azeotrop in the  $m$ -simplex to be unstable is the presence of at least one stable SP in any of its apices [6].

It is possible to carry out the classification of the dynamics of copolymerization systems ranking them according to the topological kinds of their phase portraits. Each of them is specified by the types of all SPs and manifolds (such as separatrices or separatrix surfaces) which separate the basins of attraction of stable SPs. So, for binary copolymerization there are three kinds of phase portraits

$$\text{O} \leftarrow \bullet \quad \text{(I)} \quad \text{O} \leftarrow \bullet \rightarrow \text{O} \quad \text{(II)} \quad \bullet \rightarrow \text{O} \leftarrow \bullet \quad \text{(III)} \quad (10)$$

where open and filled circles denote the attractors and the repellers, respectively. For the realization of the phase portrait of kind III both kinetic parameters,  $a_{12}$  and  $a_{21}$ , should be less than unity. Systems of such a kind are unknown so far.

An exhaustive classification of the phase portraits by their kinds was performed [1,6] for the copolymerization of three monomers. Among 15 such portraits 12 are simple in the sense that all attractors and repellers in them are SPs only. However, in the remaining three systems the boundary of the 3-simplex, i.e., the Gibbs triangle, is the separatrix contour. It contains three apices, each being the saddle point, and three sides that do not contain binary azeotrops. Such a contour attracts or repels trajectories depending on whether the value of the quantity

$$\Lambda = (1 - a_{12})(1 - a_{23})(1 - a_{31}) + (1 - a_{13})(1 - a_{32})(1 - a_{21}) \quad (11)$$

is negative or positive. The sole SP inside the Gibbs triangle in the systems of these three kinds may be only the focus (or node). If at a certain change of the kinetic parameters  $a_{ij}$  this SP remains unstable while the quantity  $\Lambda$  (11) reverses the sign from negative to positive, the “limit cycle birth” bifurcation takes place. It is intriguing enough that this cycle detaches from the separatrix contour rather than originates from the SP under

the change of its stability. Essentially, in this case the very conclusion on the existence of the phase portrait containing the limit cycle may be made directly from the topological considerations without a recourse to the calculation of trajectories.

From the standpoint of the theory of dynamical systems of special interest is the copolymerization of four monomers when neither attractors nor repellers exist on the 4-simplex boundary. This means that all SPs of equations (4) located on the apices, edges and faces of a tetrahedron are saddle points. As for limit cycles on the tetrahedron faces, they represent the saddle periodic motion, situated at the intersection of stable and unstable separatrix surfaces. The surface of the tetrahedron for this four-component system will be in a sense similar to the separatrix contour lying on the sides of the triangle which is the phase space under the description of the terpolymerization dynamics. Just as in this case ( $m = 3$ ) when a certain change of the kinetic parameters leads to the bifurcation of detaching of a stable limiting cycle from the separatrix contour, so under tetrapolymerization the possibility for the "strange attractor" to detach from the surface of a tetrahedron is quite conceivable. Moreover, this bifurcation will necessarily take place provided simple stable manifolds like SPs, limit cycles and invariant tori are absent inside the tetrahedron.

### Theoretical Prediction of Some Properties of Multicomponent Copolymers

These properties may be effectively predicted using experimental data on binary systems only [1,2,5] instead of performing much tedious routine experimentation over entire range of composition of multicomponent systems. Employing these data as a starting information it is often possible to prognosticate in a simple way via mathematical modeling some performance properties of multicomponent copolymers. In particular, this concerns their glass transition temperature  $T_g$  which may be calculated through fractions of the dyads (7) for the products of copolymerization of an arbitrary number  $m$  of monomers at any their conversion  $p$ .

Along with the heat resistance of copolymers characterized by the value of  $T_g$  their transparency is regarded to be one of the most important properties. In order to produce transparent copolymers their synthesis should be conducted so that a reaction system remains homophase throughout the whole process. A necessary condition for such a copolymerization regime is the minimality of the composition inhomogeneity of the products formed. However, in some copolymerization processes this condition may be violated because of the pronounced distinction in the reactivities of monomers involved. Copolymers formed during such processes may turn out to be so polydisperse in composition that the homogeneous state of a reaction system becomes thermodynamically unstable and it undergoes a phase transition. As a result turbid heterophase polymer products with unacceptable physico-mechanical properties are obtained. Essentially, in some copolymerization processes even a minor change of the initial monomer mixture composition  $\mathbf{x}^0$  may dramatically affect the service properties of the products formed under high conversions. This is the case when the properties are compared of the copolymers prepared at values of  $\mathbf{x}^0$  just slightly distinguishing from one another, but located within the basins of attraction of different attractors.

This effect is illustrated in Figure 1. It depicts the phase portrait of the three-component system having three attractors situated in the apices of the Gibbs triangle. On its every side there is a single azeotrop, one being an unstable node while two others are saddle points. These latter are connected with the former by separatrices separating the basins of attraction of three stable SPs of this particular system. Three trajectories depicted in Figure 1 start at points located close to each other, but terminate at different apices of the triangle. Evidently, both the composition distribution and the elements of its covariance matrix (2) (that control the thermodynamic behavior of the terpolymerization products being formed at the three given values of the initial monomer mixture composition) will differ substantially. The reason is that the aforementioned characteristics of the chemical structure of a terpolymer specimen, formed at a given value of vector  $\mathbf{x}^0$ , are the functionals calculated at the trajectory  $\mathbf{x}(p)$ .

In order for the results of modern quantitative theory of copolymerization [1,5-8] to be used for the calculation of the statistical characteristics of multicomponent copolymers ( $m \leq 6$ ) as well as for the prediction of such important properties as the thermostability and the transparency, we developed a user friendly computer program "Copolymerization for Windows" [2,11]. Its potentialities are exemplified in detail for the terpolymerization of Styrene, Methyl methacrylate and Acrylonitrile [2].

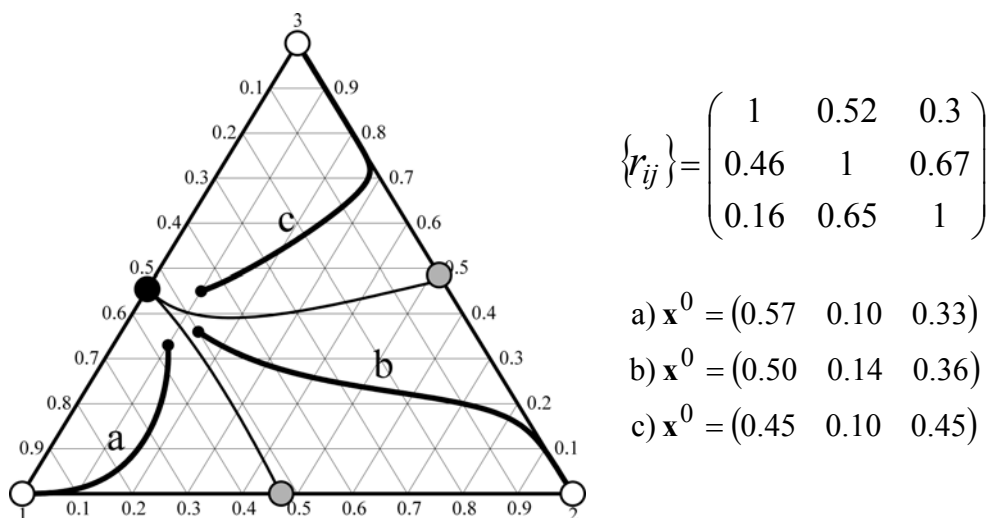


**Figure 1.** Phase portrait of dynamical system (4) describing the terpolymerization with the matrix of reactivity ratios  $\{r_{ij}\}$  for three values of initial composition of monomer mixture. Open, gray and filled circles indicate attractors, saddle points and repeller, respectively.

## References

- [1] S.I. Kuchanov, Modern Aspects of Quantitative Theory of Free-Radical Copolymerization, Adv. Polym. Sci., 1992, 103, 1.

- [2] A. Yakovlev, S. Kuchanov, *Macromol. Symp.*, 2000, 160, 35.
- [3] R.Z. Greenly, *J. Macromol. Sci.*, 1980, A14, 445.
- [4] J.M.G. Cowie, *Macromol. Symp.*, 1994, 78, 15.
- [5] S.I. Kuchanov, *Methods of kinetic calculations in polymer chemistry*, Chimia Publ., Moscow, 1978 (in Russian).
- [6] S.I. Kuchanov, *Vysokomol. Soed.*, 1988, A30, 2312.
- [7] S.I. Kuchanov, S.V. Pugin, M.G. Slin'ko, *Math. Model. Comput. Experiment*, 1993, 1, 197.
- [8] S.I. Kuchanov, *Macromol. Symp.*, 2000, 160, 191.
- [9] S.I. Kuchanov, S.V. Panyukov, *Statistical Thermodynamics of Copolymers and Their Blends*, *Comprehensive Polym. Sci.*, Second Suppl., Ed. G. Allen, Pergamon Press, 1996, 441.
- [10] J.M.T. Thompson, H.B. Stewart, *Nonlinear Dynamics and Chaos*, John Wiley, 1986.
- [11] A.S. Yakovlev, S.I. Kuchanov, *Software Modeling Tool "Copolymerization for Windows"* <http://www.copolymerization.da.ru>.

# **Papers of the Oral Presentations**

# MUTATION – INDUCED CHAOS IN EVOLVING PARASITOID POPULATIONS

I. Gudelj\*, R. E. Beardmore\*\*

\*NERC Centre for Population Biology, Imperial College London, Silwood Park Campus, Ascot, Berkshire SL5 7PY, U.K., \*\*Department of Mathematics, Imperial College London, South Kensington Campus, London SW7 2AZ, U.K.

## Abstract

A numerical bifurcation analysis of a dynamical system modeling parasitoid evolution in a two-host-parasitoid system exhibits chaotic behavior, where we use the mutation rate as the bifurcation parameter. We illustrate this with some numerical experiments and provide a physical interpretation.

## Introduction

One of the current challenges of evolutionary ecology is to identify those ecological mechanisms that lead to host specialization or changes in the host range of parasitoid populations. Parasitoids lay eggs in the bodies of other insects and, in order to reach adulthood, they have to kill their hosts. This inflicts strong selection pressure on the parasitoid population so as to evolve resistance to host defense mechanisms. For that reason, host-parasitoid systems provide a useful paradigm for more general evolutionary problems.

In this paper we consider a parasitoid population exposed to two hosts and we study the evolution of the ability of the parasitoid to parasitize its hosts using a system of *integro-difference equations* or *infinite-dimensional maps*. Over the past century many mathematical models have been employed to study population dynamics of host-parasitoid interactions, as in [1] for example, however, there have been considerably fewer attempts to include evolutionary dynamics in these models.

Here, host-parasitoid dynamics are modeled using a variant of the well-known Nicholson-Bailey model [2], while genetic mutations are included through a dispersal kernel motivated by [3]. The key component of the evolutionary process is the existence of a trade-off, which represents a cost and benefit relationship associated with a change in the evolving trait. Specifically, we assume that an increase in the ability of the parasitoid to parasitize one host, will necessarily carry a cost in the form of a reduced ability to parasitize the other host.

In order to scrutinize the consequences of introducing an evolutionary component into a well-studied dynamical system, we use the mutation rate as our bifurcation parameter. This is simply the variance of the probability distribution that controls genotypic mutations and, surprisingly, altering this parameter leads to a regime in which a chaotic attractor forms. Very high or very low mutation rates lead to much simpler behaviors.

To formulate a mathematical model of our problem we define the following variables:  $P_t(y)$  denotes the density of parasitoids with genotype  $y$  at generation  $t$  and  $H_{it}$  denotes the density of host  $i$  at generation  $t$  (with  $i = 1, 2$ ). The evolving trait

is the probability that a parasitoid parasitizes host one and this is denoted  $y \in \Omega$ , the unit interval, while the probability that a parasitoid parasitizes host two is denoted by  $f(y)$ . Here  $f$  satisfies  $f' < 0$  and so represents a *trade-off function*. Once the host is parasitized, the parasitoid egg will complete its development in host  $i$  with probability  $b_i$  (again, for  $i = 1, 2$ ). The probability that a host escapes parasitism in the current generation is given by  $e^{-p}$  where  $p$  is the parasitoid population size,

$$p = \int_{\Omega} P_t(y) dy,$$

and the fecundity of host  $i$  is denoted by  $a_i$ . This leads to the following discrete dynamical system

$$\begin{aligned} P_{t+1} &= \int_{\Omega} k(y - \eta) (b_1 y H_{1t} + b_2 f(y) H_{2t}) (1 - e^{-p}) \bar{P}_t(\eta) d\eta, \\ H_{1t+1} &= a_1 H_{1t} \left( e^{-p} + (1 - e^{-p}) \int_{\Omega} (1 - y) \bar{P}_t(y) dy \right), \\ H_{2t+1} &= a_2 H_{2t} \left( e^{-p} + (1 - e^{-p}) \int_{\Omega} (1 - f(y)) \bar{P}_t(y) dy \right), \end{aligned} \quad (1)$$

where  $\bar{P}_t(y) = P_t(y) / p$ . The function  $k(y - \eta)$  represents a redistribution kernel as a function of  $\eta$ , and this is normally distributed about  $y$  with mutation rate (standard deviation)  $\sigma$ :

$$k(y) = \frac{1}{\sqrt{2\pi\sigma^2}} e^{-y^2/2\sigma^2}.$$

Hence  $k(y - \eta)$  represents the probability of mutation of parasitoids from parent genotype  $\eta$  to offspring genotype  $y$ . Let us note that in previous work of this type [4,6] mutations are represented by a frequency-independent uniform distribution of genotypes but this permits no control over mutation rates.

## Results and Discussion

In Figure 1 we see the results obtained by iterating the dynamical system (1) as  $\sigma$  is varied. For large values of  $\sigma$ , we find the existence of a globally stable fixed point which, through a Neimark-Sacker bifurcation, sees the creation of an invariant circle in phase-space. As the error-rate is further reduced, the invariant circle becomes a two-dimensional invariant torus which appears to collide with an unstable fixed-point, so forming a chaotic attractor. Finally, for very small error rates, this complex structure disappears to leave an invariant circle.

It is well-known (see [4]) from the many studies of Nicholson-Bailey dynamics that non-evolutionary single-host, single-parasite systems may only exhibit growing

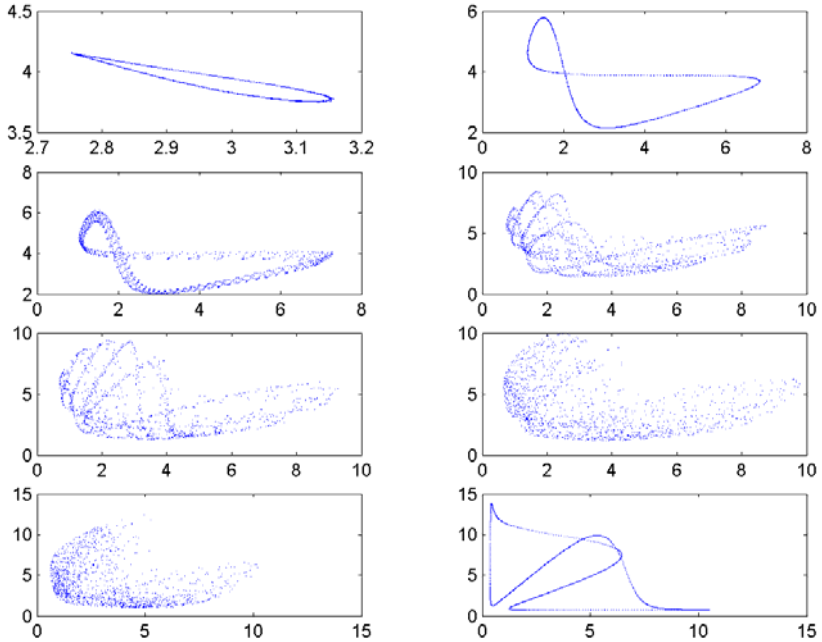


**Figure 1.** Host one (horizontal axis) versus host two (vertical axis). From top left to bottom-right,  $\sigma = 0.14095, 0.088, 0.085, 0.08, 0.076, 0.073, 0.07, 0.06$ .

oscillations of both species due to overexploitation of the host. We have observed that the inclusion of a second host coupled with an evolving parasitoid can stabilize this dynamic and provide a variety of different attractors.

In terms of the genotypic structure of the parasitoids, Figure 2 shows that the genotypic distribution cycles from one form of near-specialism to another, as the relative frequency of the two hosts cycles. (By *specialism* we mean that a parasitoid is only virulent to one of the hosts.) For the simulations in this figure we have used the convex trade-off function  $f(y) = 1 - y^{1/2}$ . This was chosen because it was shown in [5] that the sign-changes of the second derivative of  $f$  govern the number of genotypes present. Although that work covers a continuous-time diffusion model, an asymptotic analysis shows that a similar dependence on the trade-off is present in solutions of (1).

## Conclusions

We have demonstrated that the dynamics of host-parasitoid evolution are extremely sensitive to the manner in which mutations are introduced and it is possible to induce a range of dynamics by tuning the mutation rate alone. The stable behaviour of (1) for high mutation rates is to be anticipated from [4] and the references therein. However, for small mutation rates, a convex trade-off ensures that each host is successfully under- then over-exploited as the convex trade-off leads to specialism in the short term [5]. The oscillations are less pronounced for concave trade-offs because specialization is not favoured in this case and one observes ESS-like behaviour.

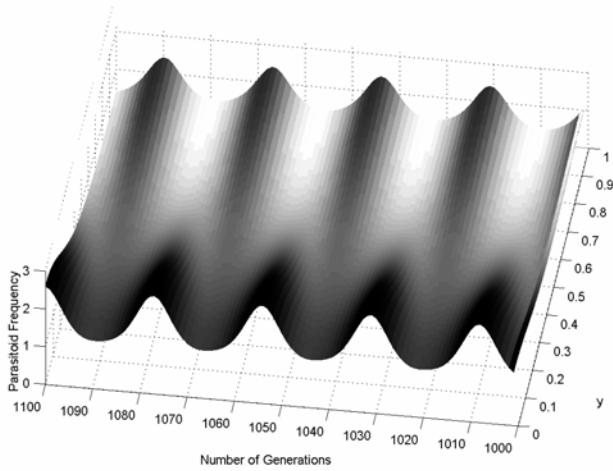


**Figure 2.** Genotypic distribution of Parasitoid ( $y$  denotes genotype).

### References

- [1] M. E. Honeberg and A. R. Ives (eds), Parasitoid Population Biology, Princeton University Press, 2000.
- [2] A. J. Nicholson and V. A. Bailey, Proc. Zool. Soc. Lond., 1935, 3, 551
- [3] M. G. Neubert, M. Kot and M. A. Lewis, Theor. Pop. Biol., 1995, 48, 7.
- [4] A. Sasaki and H. C. J. Godfray, Proc. R. Soc. Lond. B, 1999, 266, 455.
- [5] I. Gudelj, R. Beardmore and C. Coman, submitted to Nonlinearity
- [6] M. E. Honeberg, Oikos, 1997, 80, 342.

## ***Dictyostelium discoideum*: A BIOLOGICAL SYSTEM FOR INVESTIGATION OF NONLINEAR PHENOMENA.**

M. Suchá, P. Vaňková, H. Ševčíková

*Center for Nonlinear Dynamics of Chemical and Biological Systems,  
Institute of Chemical Technology, Prague, Technická 5, 166 28 Prague 6, Czech Republic*

### **Abstract**

*Dictyostelium discoideum* is shown to be an interesting system for investigation of how deterministic nonlinear processes apply in microorganism's reproduction and morphogenesis. Quadratic autocatalysis, as a process characterizing multiplication of cells, is shown to result in propagation of a vegetative front through the lawn of bacteria. Oscillatory and excitable modes of the biochemical production and degradation of cAMP by starving cells are shown to govern the time dependent emergence of aggregation centres, propagation of cAMP waves and break of the cell layer down to aggregation territories.

### **Introduction**

*Dictyostelium discoideum* (*DD*) is a microorganism that represents a transition between uni- and multi-cellular organisms. *DD* spends the vegetative phase of its life as a uni-cellular organism. Each cell behaves independently, eating bacteria in the soil, growing and multiplying. When the bacteria are eaten up, the developmental cycle starts during which the cells behave as a community in order to form an organized, structured, multicellular organism – a fruiting body carrying spores that preserve the *DD*'s life until the food sources are restored [1-3]. Presented paper will discuss some of the life stages of *DD* in more details emphasising the role of nonlinearities of biochemical transformations involved.

### **Results and Discussion**

After adaptation and germination of spores on bacteria, *DD* cells reproduce by cell division giving two daughter cells out of one mother cell. Thus, formally, the exponential phase of growth can be described by quadratic autocatalytic reaction :



where B stands for bacteria and D for *DD* cells. Time dependence of *DD* cells concentration  $c$  is then governed by :

$$dc/dt = k \cdot [B] \cdot c = k_B \cdot c = c \cdot r \cdot \ln 2 \quad (1)$$

where  $k_B$  is a rate constant of the pseudo-first order reaction R1 (assuming B to be in a great excess). Last product of Eq. (1) expresses the increase of cell concentration during the exponential phase in biological terms [4]:  $r$  is the inverse of the generation period  $t_G$  defined as a time during which the number of cells doubles. Since the generation period of *DD* cells  $t_G = 8$  h, one can calculate the kinetic constant  $k_B = 0.87 \text{ h}^{-1}$ .

When *DD* cells are grown on the lawn of bacteria they form a travelling front (cf. Fig. 1) as any other quadratic autocatalysis does [5]. This front, containing vegetative cells in an exponential phase of their growth, is about 0.16 mm wide and propagates into the lawn of bacteria, leaving behind the environment free of bacteria but full of starving cells. The velocity of the vegetative front propagation is  $0.08 \text{ mm h}^{-1}$ .

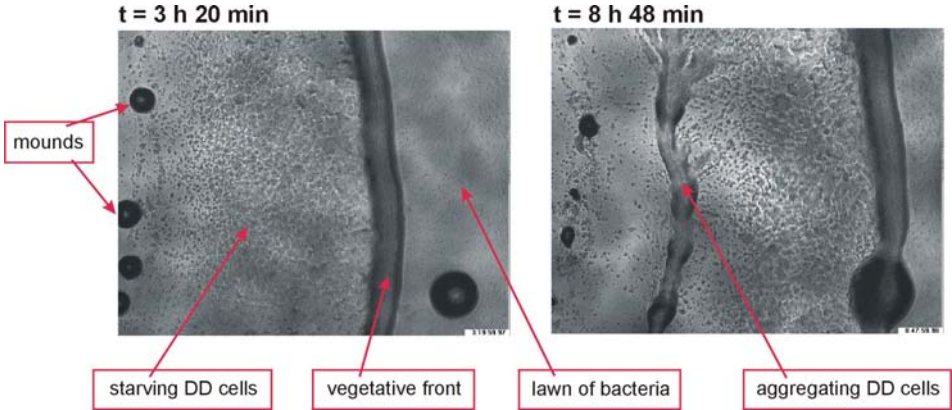


**Figure 1.** The propagation of the vegetative front into the bacterial lawn. The size of the observation area is  $1.8 \times 2.3 \text{ mm}$ . Experiments [6].

During developmental cycle, the biochemical production, release, and degradation of cAMP underlies processes such as propagation of cAMP waves and chemotaxis of cells towards mounds, cell sorting in mounds and slug migration. Dynamics of biochemical transformations is studied in the mathematical model based on Martiel-Goldbeter kinetic scheme [3,7]:

$$d\beta/dt = q\sigma\Phi(\rho_T, \gamma, \alpha) - (k_i - k_e)\beta \quad (4)$$

$$d\gamma/dt = (k_i\beta/h) - k_e\gamma \quad (5)$$

$$d\rho_T/dt = -f_1(\gamma)\rho_T + f_2(\gamma)(1 - \rho_T) \quad (6)$$

Various functions in the Eqs. (4)-(6) are defined as follows:

$$f_1(\gamma) = \frac{k_1 + k_2\gamma}{1 + \gamma}; f_2(\gamma) = \frac{k_1L_1 + k_2L_2c\gamma}{1 + c\gamma}; Y = \frac{\rho_T\gamma}{1 + \gamma}; \Phi(\rho_T, \gamma, \alpha) = \frac{\alpha(\lambda\theta + \varepsilon Y^2)}{1 + \alpha\theta + \varepsilon Y^2(1 + \alpha)}$$

In the kinetic model (4)-(6),  $\beta$  ( $\gamma$ ) are concentrations of intracellular (extracellular) cAMP divided by the dissociation constant of the receptor-cAMP complex and  $\rho_T$  denotes the fraction of cell receptors in the active state to the total number of cell receptor. Other quantities in Eqs. (4)-(6) are parameters derived from kinetic constants, concentrations of (bio)chemical components in excess, and trans-membrane transport parameters; all based on measured properties of cAMP biosynthesis in *DD* cells [7]. The model (4)-(6) enlarged for diffusion flux of cAMP in the extracellular space [8] forms a base of a mathematical description of the formation and propagation of cAMP waves in the *DD* cell population [8-11].

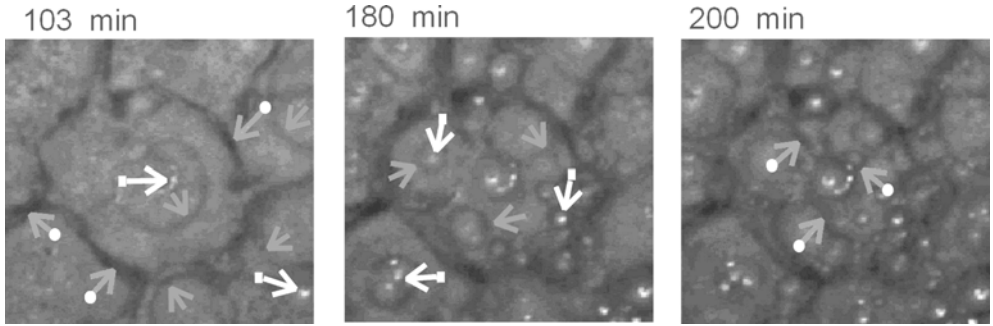


**Figure 2:** Appearance of centers emitting cAMP waves and the break up of the cell layer into aggregation territories. Observation in the dark field. The size of the observed area: 10 x 11 mm.  $\rightarrow$  cAMP waves,  $\circ$  $\rightarrow$  boundaries of aggregation territories,  $\rightarrow$  centers emitting cAMP waves. Experiments [12].

Mathematical analysis of the model (4)-(6) has discovered a variety of solutions, including two different stable stationary states, excitability, oscillations, bistability between two stationary states and bistability between oscillations and excitability [9-11]. These various dynamical modes of the biochemical transformations then display themselves during the developmental stages as shown, e.g. in Fig.2 illustrating the aggregation stage of organism's morphogenesis.

At the beginning of starvation, *DD* cells undergo adaptation during which cAMP production ( $\beta, \gamma$ ) is very low and the system stays in the stationary state. During this period, the cells migrate freely by the process resembling Brownian motion of molecules that leads to the homogenization of the cell layer. As time goes, the internal conditions (i.e. the parameters of the kinetic model (4)-(6)) of cells change and some cells adopt the oscillatory mode. These cells start to periodically produce cAMP that diffuses to the neighbouring cells. If the neighbours are in the excitable stationary state, cAMP waves can form and propagate through the cell layer (Fig. 2,  $t = 103$  min). Head-on collisions of cAMP waves from different centres cause the break of the homogeneous cell layer down to individual aggregation territories (blue arrows in Fig. 2). Further internal changes in cells bring slowly more cells into the oscillatory mode and new wave centres arise in the cell layer (Fig. 2,  $t = 180$  min). The new centres elicit cAMP waves that upon head-on collisions cause further fragmentation of aggregation territories. The fragmentation ensures the limited sizes of fruiting bodies comprising cells from one territory.

## Conclusions

In this paper, we have discussed nonlinear features of complex processes taking place during the vegetative and aggregation stages of *DD*'s life cycle. We assume the approach outlined above can be conveniently used also in understanding and modelling the formation of more complex multicellular forms of *DD* arising in later stages of *DD*'s morphogenesis when transformations of cAMP and propagation of cAMP waves are still in charge [1-3].

## Acknowledgement

This work has been supported by the Research Project of the Ministry of Education of the Czech Republic MSM 223400007.

## References

- [1] P. Devreotes, *Science*, 1989, 245, 1054.
- [2] D. Dormann, B. Vasiev, C.J. Weijer, *Biophys. Chem.*, 1998, 72, 21.
- [3] A. Goldbeter, *Biochemical Oscillations and Cellular Rhythms*, Cambridge University Press, Cambridge, 1996.
- [4] L. Silhankova, „Mikrobiologie (in Czech)“, Victoria Publ., Prague, 1995.
- [5] S.K.Scott, K. Showalter, *J. Phys. Chem.*, 1992, 96, 8702.
- [6] M. Sucha, Diploma Thesis (in Czech), VSCHT Praha, 2003.
- [7] J.-L. Martiel, A. Goldbeter, *Biophys. J.*, 1987, 52, 807.
- [8] J.J. Tyson, K.A. Alexander, V.S. Manoranjan, J.D. Murray, *Physica D*, 1989, 34, 193.
- [9] J. Lindner, H. Sevcikova, M. Marek, *Phys. Rev.*, 2001, 63E, 041904.
- [10] T. Godula, H. Sevcikova, *Proc. of 30<sup>th</sup> Int. Conf. SSCHE, 2003*, CD-ROM, ISBN-80-227-1889-0, B4(1-10).
- [11] T. Godula, J.H. Merkin, H. Sevcikova : Emergence of transient pacemakers in an excitable system. (in preparation).
- [12] P. Vankova, Diploma Thesis (in Czech) , VSCHT Praha, 2004.

# STOICHIOMETRIC APPROACH TO THE MODELING OF THE TERRORISM

Ž. Čupić<sup>1</sup>, S. Anić<sup>2</sup>

<sup>1</sup>*Institute of Chemistry, Technology and Metallurgy, Department of Catalysis and Chemical Engineering, Njegoševa 12, 11000 Belgrade, Serbia and Montenegro,*

<sup>2</sup>*Faculty for Physical Chemistry, University of Belgrade, P.O.Box 137, Studentski trg 16, 11001 Belgrade, Yugoslavia*

## Abstract

Terrorism is considered as the complex non-equilibrium dynamical system and described by the simple model. The model is examined by the Stoichiometric Network Analysis. Stability-instability conditions were determined. Numerical simulation was used to investigate the behavior of the system in the vicinity of the bifurcation point.

## Introduction

The terrorism is one of the phenomena that has a specific network processes. It exists at all kind and order of the human organizations and between them.

The combination of several different approaches is necessary in modeling complex phenomena in order to summarize different aspects of the problem. Therefore, in modeling terrorism, as an extremely important complex dynamical phenomenon, useful insights could be obtained from sociometric investigation, game-theory and multiple agent experiments, but also from the computer simulations based on the models inspired by the collected, previous experiences. [1]

We join to investigators who social interactions like the chemical reaction observe. In this aim it is necessary to make a corresponding model. Therefore, the terrorism can be studied as the nonlinear dynamic system and the network analysis will be used here.

## The Model

Present model is built from the System Dynamics model of Bruce K. Skarin [1]. The original feedbacks are maintained as much as it was possible. The model is simplified and redesigned in terms of population dynamics.

Our model T(1-7) [2] consists of two main populations  $P_1$  and  $P_2$ , three subpopulations, A, B and C, all originating from  $P_1$ , and one subpopulation, D, originating from the  $P_2$ .

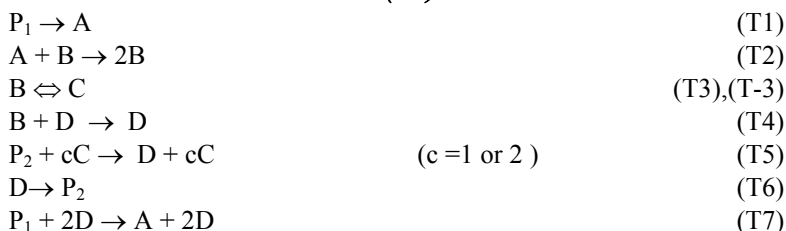
If we accept that army or some special police is antiterrorist group D which fights against terrorists B, the average activity of the terrorist group, B, is described here by the size of the subpopulation C, of the terrorists presently-engaged in terrorist actions. The autocatalytic feedback is involved in recruitment process, because, all of the members of the B are (in average level) active in finding and education of the new-ones. Their efforts are directed, or maybe, most productive, in some subpopulation A

of the population  $P_1$ . This subpopulation consists of angry, unsatisfied, highly motivated members of  $P_1$ . The motivation of the members of  $P_1$  to fight is influenced by the activities of the other population,  $P_2$ .

The population  $P_2$  responds on the terrorist acts and measure of its activities is size of some subpopulation  $D$ , of the members engaged in fight against terror. Their activity is directed mainly to decrease the number of the terrorists, but consequently, it accelerates the motivation process in population  $P_1$ .

The response of the  $P_2$ , against the average intensity of terrorist acts can be proportional or non-proportional. Such different strategies are modeled here with linear and simple quadratic rate law.

#### *MODEL T (1-7)*



Actual values of the population sizes and rate constants need to be determined from the sociometric investigations, or fitted against some monitored time series. Only then, the results of the simulation may be compared with some particular situation. However, the purpose of presented model is only to illustrate the value of the physico-chemical approach in modeling the terror, and more precisely in decision making when the choice between different strategies is necessary.

#### **Stability Analysis**

Stoichiometric Network Analysis [3] was used to perform the stability analysis of the model. In the case of the proportional response, the model has only one stable steady state. If the response is non-proportional (quadratic), then, the steady state can be stable or unstable, depending on the values of the rate constants.

#### **Numerical Simulation**

The computer simulation is performed by the numerical integration of the set of corresponding differential equations. The Gear algorithm with backward integrations was used.

The results are presented for the proportional response ( $c=1$ ), and also for the quadratic response ( $c=2$ ). In the case of the quadratic response, the results are presented for the case of stable steady state and for the unstable steady state.

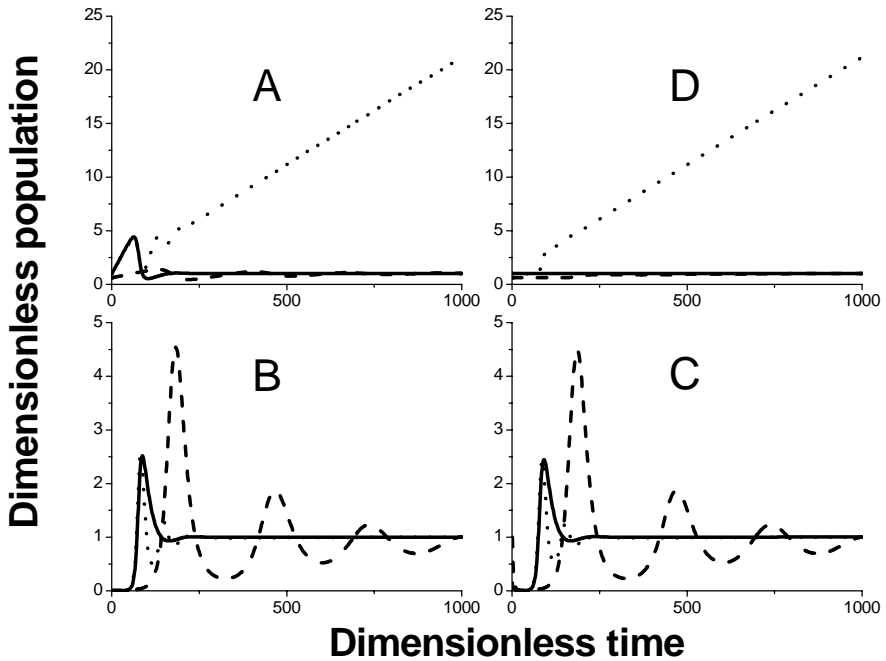


**Figure 1.** Population dynamics of the subpopulations in the model T(1-7), for proportional response (solid), quadratic response with stable steady state (dash) and quadratic response with unstable steady state (dot). Variables are presented in normalized form.

In simulation of the proportional response model, after the initial overshoot, behavior is described by the asymptotical approach to the stable steady state. In real life, such behavior would correspond to constant average activity of the B, and constant level of terrorism.

In the case of the non-proportional response with stable steady state, dumped oscillations are obtained in numerical simulation, leading to constant level of terrorism at the end.

Finally, the simulation of the non-proportional response with unstable steady state resulted in monotonous linear increase of the subpopulations A and D with time. Subpopulations B and C were maintained at constant level after few initial dumped oscillations. This would mean maintaining of the terrorism at some constant level but the price was highly increased engagement of the population  $P_2$  in fight.

Significant attention should be paid also to the fact that the stability depends on the sensitivity of the population  $P_1$  against the activities of D, through the rate constant of the process (T7).

## Conclusion

We can observe terrorism as any stoichiometric chemical process. But, one important question arises: “In the kinetic of the stoichiometric social interactions what corresponds to the temperature or the activation energy or the Arrhenius constant?”

## Acknowledgement

The authors gratefully acknowledge the partial support of the Fund for Science and Technologies and Development of Serbia. Proj. 1448 and 1807.

## References

- [1] B. K. Skarin, Evaluation of an Interactive System Dynamics Model. Understanding the Driving Factors of Terrorism., 26. April 2002. [http://www.humannengineering.com/bruce/\\_private/Understanding\\_the\\_Driving\\_Factors\\_of\\_Terrorism.pdf](http://www.humannengineering.com/bruce/_private/Understanding_the_Driving_Factors_of_Terrorism.pdf) .
- [2] Ž. Čupić, S. Anić, Nauka Tehnika Bezbednost, 2003, 2, 239.
- [3] B.L. Clarke, Cell Biophysics, 1988, 12, 237.

## MODEL OF REACTION-DIFFUSION SYSTEM AS GENERATOR OF OLD HEBREW ALPHABET

A. L. Kawczyński

*Institute of Physical Chemistry, Polish Academy of Sciences,  
Kasprzaka 44/52, 01-224 Warsaw, Poland*

### Abstract

A two-variable model of reaction-diffusion system based on two coupled catalytic (enzymatic) reactions is presented. The model consists of elementary reactions only. Numerical solutions to corresponding reaction-diffusion equations for two-dimensional system (2D continuously feed unstirred reactor) generate stationary patterns which mimicked all Old Hebrew letters (the Siloam inscription). All letters are obtained for the same values of the parameters determining the model. Different sizes of rectangular polygons and various positions of initial excitations are necessary the desired pattern.

### Introduction

One of the most fascinating problems is the generation of shapes (patterns) in biological systems. Alan Turing was the pioneer in explanation of this problem on the most fundamental level. In the paper [1] entitled “*The chemical basis of morphogenesis*” he has shown that a model of one-dimensional (1D) system, in which appropriate chemical reactions and diffusion occur only, had the asymptotic solutions, which were stationary but periodical in space. Now reaction-diffusion systems can be treated as the minimal models of various patterns observed in biology as well as in nature. Real nonlinear reaction-diffusion systems become useful caricatures of many biological systems. For example, running impulses can be easily observed experimentally in a thin layer of the reaction mixture in which the Belousov-Zhabotinsky (B-Z) reaction occurs. Qualitative properties of such waves are similar to the spreading of electrical excitations along axons in neurons as well as to waves in the Purkinje fibers in heart. It is much easier to investigate qualitative properties of such waves in chemical systems than in biological ones.

Asymptotic solutions to excitable reaction-diffusion equations in two dimensional (2D) systems with appropriate initial and boundary conditions can also have the form of stationary but periodical in space distributions of reagents concentrations. Such distributions have been observed in experiments performed in 2D continuously feed unstirred reactors (2D CFUR). Experiments and models of reaction-diffusion systems enrich our knowledge about possibilities of generation of various patterns on the physicochemical level. There arise the quite natural questions. How rich is the variety of patterns generated by reaction-diffusion systems? Shall we construct models, which solutions have desired distributions? The answers to these questions are partially positive.

## Results and Discussion

In order to show the examples illustrating the richness of possible patterns a model of excitable reaction-diffusion system has been elaborated, which asymptotic solutions have the form mimicking all capital letters of the Latin alphabet [2] as well as the Old-Hebrew alphabet [3]. The model consists of two coupled catalytic (enzymatic) reactions. One of them is allosterically inhibited by an excess of its reactant and product. The other one is usual catalytic (enzymatic) reaction, which proceeds in its saturation regime. It is assumed that these reactions occur in an open system, which is 2D CFUR with boundaries impermeable to the reagents. All parameters in the reaction-diffusion equations are the same for the generation of the both alphabets. Only sizes of the reactor and places of initial excitations have to be changed to generate the wanted patterns. All capital Latin letters can be obtained in the reactors with convex areas, whereas some Old-Hebrew letters can be generated in the reactors with convey shapes (rectangular polygons with 6, 8 or 10 apexes). For simplicity all numerical calculations have been performed for 2D CFURs in the form of rectangular polygons. The results of calculations are presented in Fig. 1. The contours of all letters visible on this Fig. have been obtained by separation of the asymptotic solutions into two regions. The regions in which the concentration of the reactant is higher than some selected value are marked in black.

Not all letters have elegant forms. Some of them are similar to scribble, but they are readable, especially when used in sets meaning words. More elegant form of the letters can be obtained, if instead of the rectangular polygons one uses the reactors with smooth boundaries.

It is noteworthy that the reaction-diffusion model is structurally stable, which means that small changes in its parameters do not change the shapes of the asymptotic solutions. Also small changes in sizes of the reactors and positions of initial excitations do not change the qualitative properties of the asymptotic solutions.

All letters have been obtained as the asymptotic solutions of the deterministic problem with well defined inhomogeneities as the initial distributions of reagents. In real systems inhomogeneities can appear due to internal, local fluctuations. Therefore, there is probability greater than zero that the patterns can appear spontaneously in real systems.

It is noteworthy that the model is not exceptional one. The identical patterns can be generated in many reaction-diffusion systems, provided they have the similar qualitative properties to the presented model. Moreover, it is worth to stress that the model contains two variables only, and therefore, it is simple one. One can expect more rich patterns in systems with three, four and more variables.

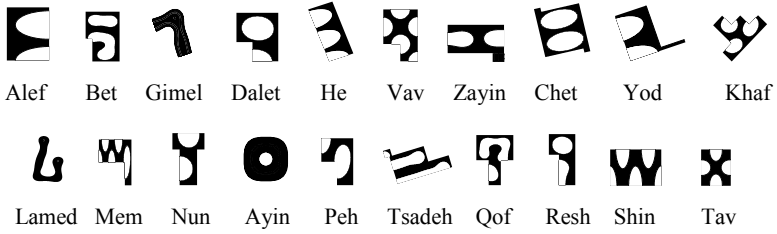


**Figure 1.** The set of asymptotic patterns generated in twenty 2D systems. The patterns have been obtained in convex or concave systems with different sizes and initial conditions. The patterns are little deformed to give the letters with close height and width.

**References:**

[1] A.Turing, Philos. Trans. Roy. Soc. London, 1952, B 237, 37.  
 [2] A.L. Kawczyński and B. Legawiec, Phys. Rev. E, 2001, 64, 056202.  
 [3] A.L. Kawczyński and B. Legawiec, Polish J. Chem., 2004, 78, 733.

## COMPLEX PATTERNS AND CHAOS IN A MODEL OF CATALYTIC CROSS-FLOW REACTOR

T. Trávníčková<sup>1,3</sup>, I. Schreiber<sup>1,3</sup>, M. Kubíček<sup>2,3</sup>

<sup>1</sup>Department of Chemical Engineering and <sup>2</sup>Department of Mathematics,

<sup>3</sup>Center for Nonlinear Dynamics of Chemical and Biological Systems,  
Prague Institute of Chemical Technology, 166 28 Prague 6, Czech Republic,

### Abstract

We study spatiotemporal solutions of reaction-diffusion-convection systems. As an example, we take a catalytic cross-flow tubular reactor with an exothermic chemical reaction of the first order. In this paper, parameter domains are analysed, leading to chaotic or other complex behaviour. The results obtained by continuation for the reaction-diffusion system are related to spatiotemporal patterns obtained directly by numerically solving partial differential equations that describe a bounded system. Waves and complex patterns are investigated in dependence on convection velocity  $v$  and heat transport coefficient  $\alpha_j$ .

### Introduction

Reaction-diffusion and reaction-diffusion-convection systems are able to support waves and complex structures [1]. Origin of nonhomogeneous steady state structures in two-variable reaction-diffusion systems, where the inhibitor diffuses sufficiently faster than the activator, was studied by Turing [2]. More recent work shows that patterns may be induced not only by the interaction of reaction and diffusion, but also by the interaction of reaction and convection. Convective flow is in practice realized, for example, by using a cross-flow reactor. Main advantage of such construction of the reactor is to help maintain reactant concentrations at optimal values that lead to maximal reaction rates.

### Model

The model is the simplest description of a catalytic bed tubular reactor with exothermic reaction of the first order [3, 4]. Concentration and temperature gradients between the fluid and solid phases are assumed absent. The following two equations are dimensionless mass and enthalpy balances in the bed, with conversion  $x$  and dimensionless temperature  $y$  as variables:

$$\frac{\partial x}{\partial \tau} = -v \frac{\partial x}{\partial \xi} - \alpha_x (x - x_w) + Da(1-x)e^{\frac{y}{\gamma+y}},$$

$$Le \frac{\partial y}{\partial \tau} = d \frac{\partial^2 y}{\partial \xi^2} - v \frac{\partial y}{\partial \xi} - \alpha_y (y - y_w) + BDa(1-x)e^{\frac{y}{\gamma+y}},$$

where  $v$  is the flow velocity,  $d$  is the heat diffusion/dispersion coefficient (mass dispersion is neglected),  $\alpha_x$ ,  $\alpha_y$  are mass and heat transfer coefficients, resp.  $Le$  is Lewis number,  $Da$  is Damkohler number and  $B$  is reaction enthalpy.

Danckwerts boundary conditions are used for the system with convective flow,  $\xi = 0$  :

$$x = 0, d \frac{\partial y}{\partial \xi} = \frac{v y}{Le}; \quad \xi = L : \quad \frac{\partial x}{\partial \xi} = 0, \frac{\partial y}{\partial \xi} = 0.$$

Neumann boundary conditions are used for nonflow system,

$$\xi = 0 : \quad \frac{\partial x}{\partial \xi} = 0, \frac{\partial y}{\partial \xi} = 0; \quad \xi = L : \quad \frac{\partial x}{\partial \xi} = 0, \frac{\partial y}{\partial \xi} = 0.$$

### Bifurcations in the Homogeneous System

For determination of parameter domains for particular types of wave solutions it is necessary to construct a bifurcation diagram, for example in the parameter plane  $Da - \alpha_y$  (Fig. 1). This diagram was constructed for  $d=0$  and  $v=0$  and serves as a guideline to the spatially nonhomogeneous system. All solutions were obtained by software tool CONT [5].

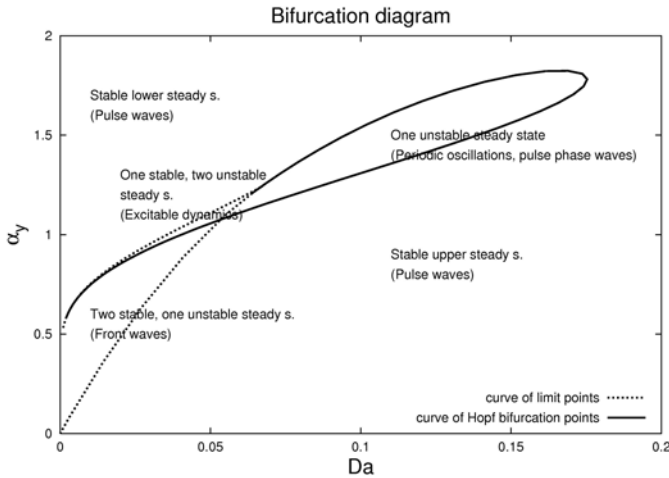


**Figure 1.** Bifurcation diagram  $Da - \alpha_y$ ;  $B = 10$ ,  $\alpha_x = 0.5$ ,  $Le = 1$ ,  $\gamma = 1000$

### Nonflow System

*Spatiotemporal chaos*: The region of occurrence of chaos is located in the bifurcation diagram (Fig. 1) just above the of Hopf bifurcation line, in the excitable and oscillatory regions [6]. Two types of chaotic behaviour occur in the system (see Fig. 2.). In the first case, there are triangle instabilities, which occur first in the chaotic region when  $Da$  is increased. The other case involves undulating instabilities that replace the triangular chaos as  $Da$  is further increased. The degree of chaos was determined by evaluation of Lyapunov exponents and dimension of the system. For example, for  $\alpha_y = 1.0$  and  $Da = 0.039558$  we found 23 positive Lyapunov exponents for chaotic triangular patterns and for  $\alpha_y = 1.15$  and  $Da = 0.064$  14 positive Lyapunov exponents for undulating chaos. Lyapunov fractal dimension of such a system is:

$$D_L = k + \frac{\sum_{i=1}^k \lambda_i}{-\lambda_{k+1}}, \text{ where } \sum_{i=1}^k \lambda_i > 0 \text{ and } \lambda_{k+1} < 0$$

Thus we found for triangular chaos  $D_L = 42.12$  and for undulating chaos  $D_L = 29.16$ .

### Effects of Flow

There are two different effects of convective flow, depending on the stability in the kinetics.

*Stable kinetics:* When the kinetics are stable (pulse and front waves), flow only increases the speed of propagation of the wave through the reactor. This is expected since  $Le = 1$  and there is no differential flow.

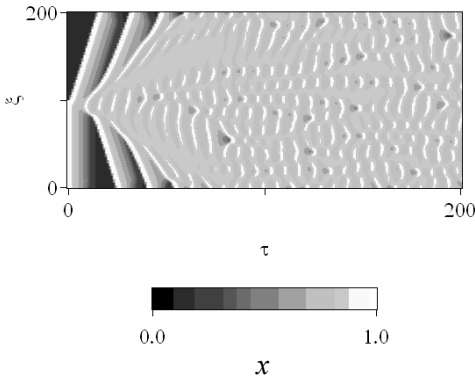


**Figure 2.** Triangular chaos;  
 $Da = 0.039558$ ,  $\alpha_y = 1.0$ ,  $d = 1.0$

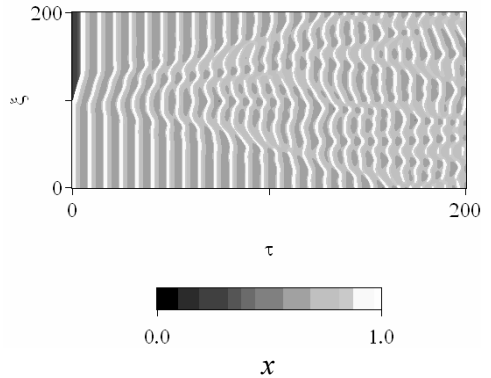
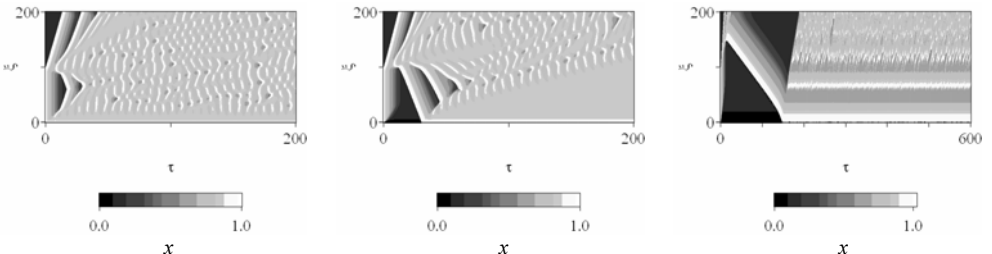


**Figure 3.** Undulating chaos;  
 $Da = 0.064$ ,  $\alpha_y = 1.15$ ,  $d = 1.0$

*Unstable kinetics:* When kinetics are unstable, the results show interesting behaviour for increasing flow rate. There are two marginal values of convection velocity. The first one corresponds to a Hopf bifurcation and its crossing causes appearance of stable interface, between stable steady state with a high conversion and oscillatory regime. The second bifurcation is a Hopf bifurcation again and occurs for high values of convection flow. This bifurcation causes destabilisation of the high conversion steady state. Both bifurcation points are depicted in Fig. 5. (See and compare Figures 4 and 5)



a)  $v = 0.5$

b)  $v = 1.5$

c)  $v = 5.5$

**Figure 4.** Effects of flow on chaotic pattern  $Da = 0.039558$ ,  $\alpha_y = 1.0$ ,  $d = 1.0$

*Zig-zag pattern:* We studied effects of convection also in the region, where front waves occur. Perturbation of the system was due to Danckwerts boundary condition at the beginning of the reactor, which maintains conversion of the reactant equal to zero. In small range of  $\alpha_y$ , this perturbation caused that zig-zag pattern arises. From the entrance point to the reactor the front spreads in the direction of flow, but after a short time it loses its stability and is converted into other front which continues in opposite direction. This effect appears, because the first front spreading from the origin is a transient, which is close to but still out of the region of existence of stably propagating front, see Fig. 6. Accordingly, this transient front is after a short time replaced by counter-propagating stable extinction front.

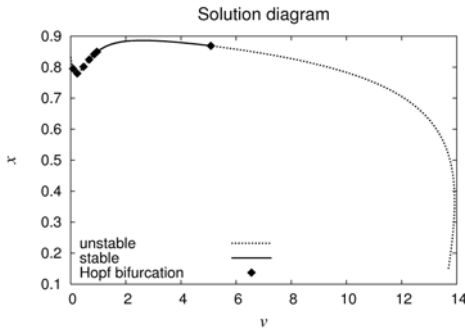


**Figure 5.** Effects of convection on stability of high conversion steady state.

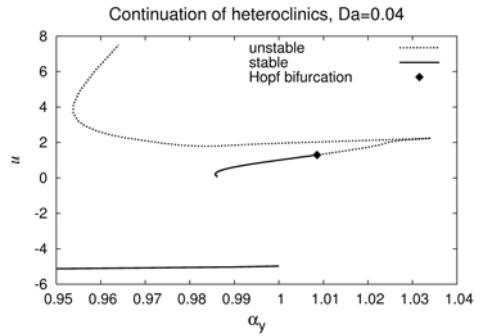


**Figure 6.** Continuation of front waves, transient front appears to the left of the turning point at  $\alpha_y = 0.9825625$ .

Zig-zag pattern and effects of convection on this pattern are shown in Figure 7 ( $Da = 0.04$ ,  $\alpha_y = 0.9825625$ ,  $d = 1.0$ ).

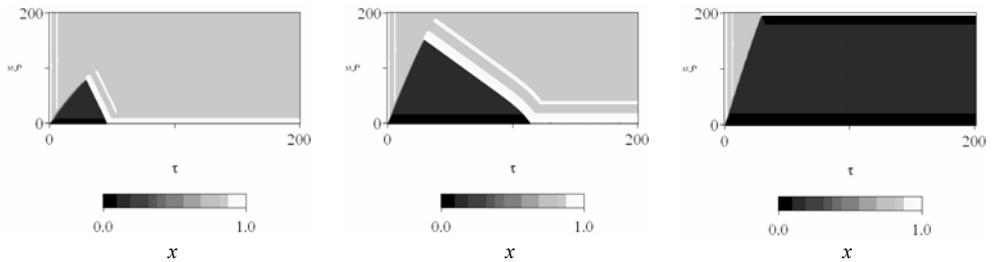


**Figure 7.**  $v=2.5$

$v=5.0$

$v=6.5$

*Continuation of front waves:* Line of front waves plotted in Figure 6 is divided into stable and unstable parts. This solution was obtained by continuation of fronts [7] by using the wave transformation  $\zeta = \xi - u\tau$ , where  $u$  is the wave velocity.

**References:**

- [1] R. Kapral, K. Showalter, Dordrecht: Kluwer Academic Publisher, 1995.
- [2] A. Turing, Phil. Transactions of the Royal Society B, 1952, 237, 37.
- [3] O. Nekhamkina, B. Rubinstein, M. Sheintuch, AIChE J., 2000, 6, 8, 1632.
- [4] M. Sheintuch, O. Nekhamkina, Cat. Today, 2001, 70, 369.
- [5] M. Kohout, I. Schreiber, M. Kubiček, Comp. and. Ch. Eng., 2002, 26, 517.
- [6] J. Merkin, V. Petrov, S. Scott, K. Showalter, Phys. Rev. Lett., 1996, 76, 3.
- [7] M. Kubiček, I. Schreiber, ZAMM 1998, 78, Suppl. 3, 981.

## ELECTRON TRANSFER AT RIGID AND DEFORMABLE INTERFACES: ELECTROVISCOELASTICITY

A.M. Spasić<sup>1</sup>, M.P. Lazarević<sup>2</sup>, M.M. Mitrović<sup>3</sup>, D.N. Krstić<sup>3</sup>

<sup>1</sup>*Institute for Technology of Nuclear and other Mineral Raw Materials, Belgrade,* <sup>2</sup>*Faculty of Mechanical Engineering, University of Belgrade, Belgrade,* <sup>3</sup>*Faculty of Technology & Metallurgy, University of Belgrade, Belgrade, Serbia, Serbia & Montenegro*

### Abstract

Up to now, there are three possible mathematical formalisms discussed related to the theory of electroviscoelasticity. The first is tension tensor model where the normal and tangential forces are considered regardless of their origin (mechanical and/or electrical). The second is Van der Pol derivative model. Finally the third, here presented, model comprise an effort to generalize the previous Van der Pol equation; i.e. the ordinary time derivatives and integrals are now replaced with corresponding fractional-order time derivatives.

### Introduction

A new idea, using deterministic approach, has been applied for the elucidation of the electron and momentum transfer phenomena at, both, rigid and deformable interfaces in finely (micro, nano, atto) dispersed systems. Since the events at the interfaces of finely dispersed systems have to be considered at the molecular, atomic, and/or entities level it is inevitable to introduce the electron transfer beside the classical heat, mass, and momentum transfer commonly used in chemical engineering. Therefore, an entity can be defined as the smallest indivisible element of matter that is related to the particular transfer phenomena. Hence, the entity can be either differential element of mass/demon, ion, phonon as quanta of acoustic energy, infon as quanta of information, photon, and electron [1-5].

### Structure and Dynamics

A number of theories that describe the behavior of liquid-liquid interfaces have been developed and applied to various dispersed systems e.g., Stokes, Reiner-Rivelin, Ericksen, Einstein, Smoluchowski, Kinch, etc. According to the developed model liquid-liquid droplet or droplet-film structure (collective of particles) is considered as a macroscopic system with internal structure determined by the way the molecules (ions) are tuned (structured) into the primary componentns of a cluster configuration [1]. How the tuning/structuring occurs depends on the physical fields involved, both potential (elastic forces) and nonpotential (resistance forces). All these microelements of the primary structure can be considered as electromechanical oscillators assembled into groups, so that excitation by an external physical field may cause oscillations at the resonant/characteristic frequency of the system itself (coupling at the characteristic frequency). If an incident periodic physical field (Fig. 1b), e.g., electromagnetic, is applied to the rigid droplet of Fig. 1a, then the resulting, equivalent electrical circuit can be presented as shown in Fig. 1c.

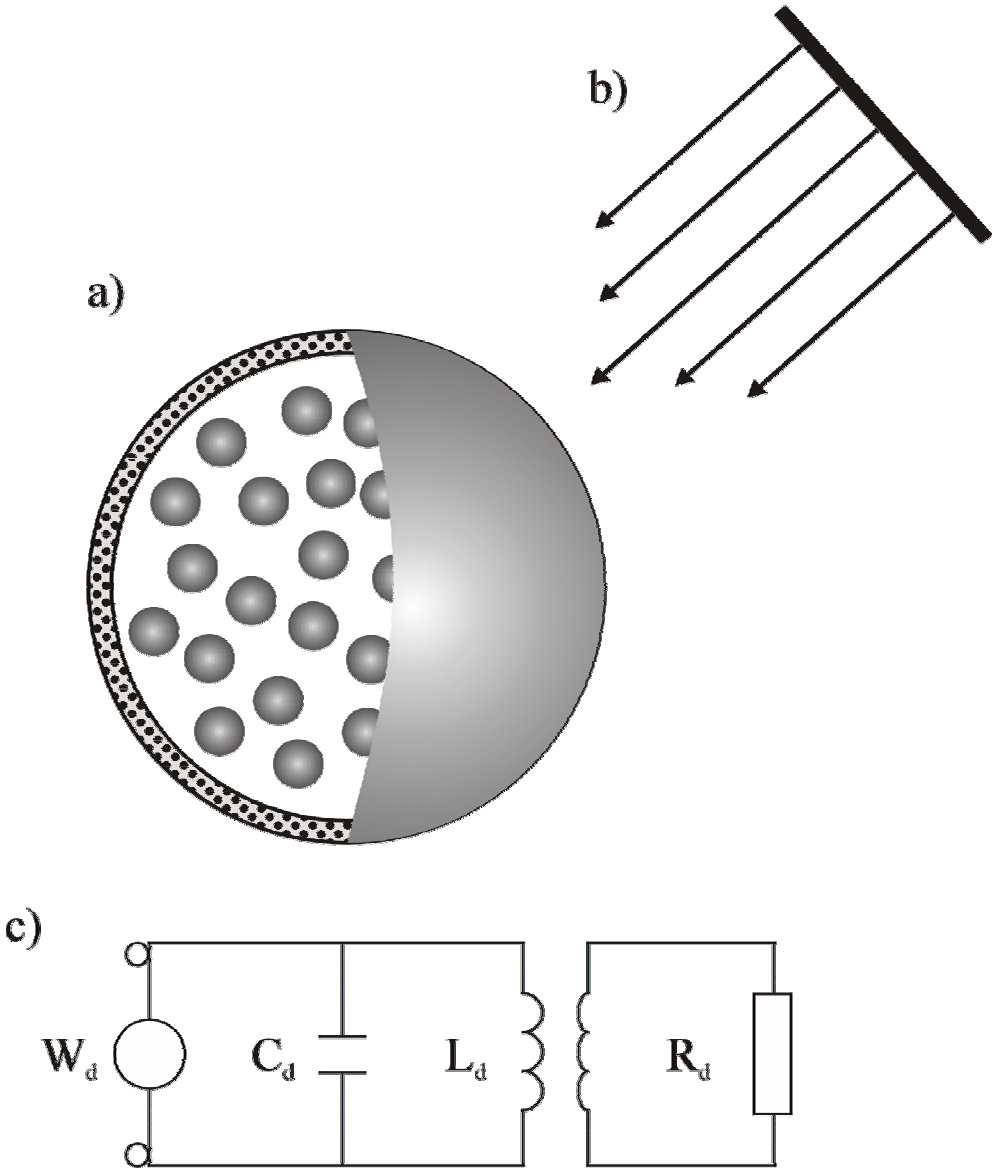


**Figure 1.** a) droplet/double emulsion, b) incident electromagnetic field, c) equivalent antenna output circuit; Courtesy of Marcel Dekker, Inc. New York , New York (2002), [1] Page 854.

The equivalent electrical circuit, rearranged under the influence of an applied physical field, is considered as a parallel resonant circuit coupled with another circuit, such as an antenna output circuit. Electrical analog consists of the passive elements  $R_d, C_d$ , and  $L_d$ , resistive, capacitive and inductive, respectively, and an active element, emitter coupled oscillator  $W_d$ . Now, the electromagnetic oscillation, for all

the noise frequency components, may be presented by the following linear differential equation:

$$C \frac{dU}{dt} + \left( \frac{1}{R} - \alpha \right) U + \frac{1}{L} \int U dt = i(t) = \frac{1}{2\pi} \int_{-\infty}^{+\infty} \exp(i\omega t) A_n(\omega) d\omega \quad (1)$$

where  $i(t)$  is the noise current and  $A_n(\omega)$  is the spectral distribution of the noise current as a function of frequency. Particular solution of (1) may be expressed by:

$$U_n = \frac{i\omega A_n \exp(i\omega t)}{C(\omega_0^2 - \omega^2) + i\left(\frac{1}{R} - \alpha\right)\omega} - \frac{i\omega A_n \exp(-i\omega t)}{C(\omega_0^2 - \omega^2) + i\left(\frac{1}{R} - \alpha\right)\omega} \quad (2)$$

Fractional derivatives provide an excellent instrument for the description of memory and hereditary properties of various materials and processes. This is the main advantage of fractional derivatives compared to the classical integer-order models, in which such effects are in fact neglected. The mathematical modeling and simulation of systems and processes, based on the description of their properties in terms of fractional derivatives, naturally leads to differential equations of fractional order and to necessity to solve such equations. Here, the capacitive and inductive elements, using fractional order  $p \in (0,1)$ , enable formation of the fractional differential equation, i.e. more flexible or general model of liquid-liquid interfaces behaviour. Now, an integral form using Riemann-Liouville definition is given by:

$${}_0D_t^p [U(t)] = \frac{d^p U}{dt^p} = \frac{1}{\Gamma(1-p)} \frac{d}{dt} \int_0^t \frac{U(\tau)}{(t-\tau)^p} d\tau, \quad {}_0D_t^{-p} [U(t)] = \frac{1}{\Gamma(p)} \int_0^t \frac{U(\tau)}{(t-\tau)^{1-p}} d\tau, \quad (3)$$

$0 < p < 1$   $p > 0$

where  $\Gamma(\cdot)$  denotes the Euler's gamma function.

$$\Gamma(z) = \int_0^{\infty} e^{-t} t^{z-1} dt, \quad z = x + iy, \quad \Gamma(z+1) = \Gamma(z) \quad (4)$$

So, in that way one can obtain linear fractional differential equation with zeros initial conditions as follows:

$$C_0 D_t^p [U(t)] + \left( \frac{1}{R} - \alpha \right) U + \frac{1}{L} {}_0D_t^{-p} [U(t)] = i(t) \quad (5)$$

Using Laplace transform of (5) leads to

$$G(s) = \frac{U(s)}{i(s)} = \frac{1}{Cs^p + 1/Ls^{-p} + (1/R - \alpha)} = \frac{s^p}{Cs^{2p} + (1/R - \alpha)s^p + 1/L} \quad (6)$$

or

$$G(s) = s^p G_3(s), \quad G_3(s) = \frac{1}{as^{2p} + bs^p + c}, \quad a = C, \quad b = (1/R - \alpha), \quad c = 1/L \quad (7)$$

The term-by-term inversion, based on the general expansion theorem for the Laplace transform [4] produces

$$G_3(t) = \frac{1}{a} \sum_{k=0}^{\infty} \frac{(-1)^k}{k!} \left(\frac{c}{a}\right)^k t^{2p(k+1)-1} E_{2p-p, 2p+pk}^{(k)}\left(-\frac{b}{a} t^{2p-p}\right), \quad (8)$$

where  $E_{\lambda, \mu}(z)$  is the Mittag-Leffler function in two parameters,

$$E_{\lambda, \mu}^{(k)}(t) = \frac{d^k}{dt^k} E_{\lambda, \mu}(t) = \sum_{j=0}^{\infty} \frac{(j+k)! t^j}{j! \Gamma(\lambda j + \lambda k + \mu)}, \quad k = 0, 1, 2, \dots \quad (9)$$

Inverse Laplace transform of  $G(s)$  is fractional Greens function:

$$G(t) = D^p G_3(t) \quad (10)$$

where the fractional derivatives of  $G_3(t)$ , (10) are evaluated with the help of (3). At last, an explicit representation of the solution is:

$$U(t) = \int_0^t G(t-u) i(u) du \quad (11)$$

## Conclusion

The theory of electroviscoelasticity using fractional approach constitutes a new interdisciplinary approach to colloid and interface science. Hence, 1-more degrees of freedom are in the model, 2-memory storage considerations and hereditary properties are included in the model, and 3-history impact to the present and future is in the game!

## References

- [1] A.M. Spasić Electroviscoelasticity of Liquid-Liquid Interfaces in A.V. Delgado Interfacial Electrokinetics and Electrophoresis, Marcel Dekker, Inc. New York, NY, 2002, 837-868.
- [2] A.M. Spasic, M.D. Babic, M.M. Marinko, N,N, Djokovic, M.M. Mitrovic, D.N. Krstic, 4 ECCE, Granada, Spain, 2003, 1-3.
- [3] M.P. Lazarevic and A.M. Spasic, 4 ECCE, Granada, Spain, 2003, 1-3.
- [4] I. Podlubny, Fractional Differential Equations, Academic Press, San Diego, 1999.
- [5] A.M. Spasic and M.P. Lazarevic, 16th CHISA, Prague, 2004, D.5.1.

## MATHEMATICAL MODELING OF RATE OSCILLATIONS IN $N_2O+CO$ REACTION OVER IR(110)

<sup>1</sup>N.V. Peskov, <sup>2</sup>M.M. Slinko, <sup>3</sup>S.A.C. Carabineiro, <sup>3</sup>B.E. Nieuwenhuys

<sup>1</sup>Moscow State University, Depart. of Comput. Math. & Cybernet., Moscow, Russia, <sup>2</sup>Institute of Chemical Physics, Moscow, Russia, <sup>3</sup>Leiden University, Leiden Institute of Chemistry, Surface Science and Catalysis, Einsteinweg 55, 2333 CC, Leiden, The Netherlands

### Introduction

Oscillatory behaviour is frequently observed in heterogeneous catalytic systems [1]. The first oscillatory systems were CO and H<sub>2</sub> oxidation reactions, where self sustained oscillations of the only reaction product CO<sub>2</sub> or H<sub>2</sub>O has been detected [2,3]. Later oscillations were observed during the NO+H<sub>2</sub> reaction over Pt, Rh and Ir single crystal surfaces, where the concentrations of the 3 N-containing products namely N<sub>2</sub>, N<sub>2</sub>O and NH<sub>3</sub> exhibited oscillatory behaviour [4,5]. It was demonstrated that the activity and the selectivity are strongly dependent on the nature and the structure of the chosen single crystal surface. Moreover, the character of reaction rate oscillations was found to depend strongly on the surface structure. On Pt(100) the rates of N<sub>2</sub>, NH<sub>3</sub> and H<sub>2</sub>O formation oscillate in phase. On Rh(111) and Rh(533) the rate of N<sub>2</sub> formation oscillates roughly in antiphase with the rates of NH<sub>3</sub> and H<sub>2</sub>O formation and, finally, on Ir(110) the rates of NH<sub>3</sub> and H<sub>2</sub>O produced oscillations exactly in counter phase. The analysis of the phase shifts between the products allowed to obtain additional information about the reaction mechanism and helps in the discrimination of the possible mathematical models [6].

Recently, a phase shift between oscillations of N<sub>2</sub> and H<sub>2</sub>O production rates has been detected during N<sub>2</sub>O+H<sub>2</sub> reaction over Ir(110) [7]. It was demonstrated that this phase shift could be simulated if lateral interactions in the adsorbed layer are considered [8]. The change of the reducing component hydrogen to CO in this oscillating system revealed even more interesting and puzzling properties of oscillations. It was discovered that not only the products N<sub>2</sub> and CO<sub>2</sub> oscillate nearly in counter phase, but also the reactants N<sub>2</sub>O and CO produce the counter phase oscillations [9]. To our knowledge this is the first observation of a phase shift between the 2 reactants participating in one reaction. Earlier, antiphase oscillations between reactants have been detected during the oxidation of a CH<sub>4</sub>+NO mixture over Titania-Supported Pd catalysts [10]. However, in this case 2 reactions of methane oxidation CH<sub>4</sub>+O<sub>2</sub> and CH<sub>4</sub>+NO proceed together with the NO decomposition reaction.

The goal of the present study is to develop a mathematical model, which can describe the experimentally observed oscillatory behaviour in the N<sub>2</sub>O+CO reaction and to explain the origin of the phase shift between oscillations in reactant concentrations N<sub>2</sub>O, CO as well as oscillations in the N<sub>2</sub> and CO<sub>2</sub> production rates.

## Results and Discussion

Experiments were performed in a UHV system equipped with facilities for LEED, AES and a differentially pumped quadrupole mass spectrometer. The base pressure was always better than  $2 \times 10^{-10}$  mbar.

The Ir sample was cut from an Ir single crystal by spark erosion to within  $0.5^\circ$  of the desired direction and polished down to a grain size of  $1 \mu\text{m}$ . The crystal was spot-welded to a Ta support and could be heated resistively up to 1400 K. The temperature was measured using a Pt-Pt/Rh thermocouple, which was spotwelded to the back of the crystal. The crystal was cleaned by multiple heating cycles in an oxygen or hydrogen atmosphere,  $\text{Ar}^+$  ion bombardment and flashing in UHV to 1400 K. The  $\text{Ar}^+$  ion sputtering and flashing treatments were repeated at the beginning of each series of experiments and the surface cleanliness and structure were checked by AES and LEED.

During the reaction, the crystal was turned in front of a small opening, which gave access to the quadrupole mass spectrometer (QMS) chamber. Reaction was performed in the flow mode using a turbomolecular pump.

High purity gases (Messer Griesheim, purity: 99.5-99.999%) were used without further purification. The pressure readings of the ion gauge were corrected using relative sensitivities for  $\text{N}_2\text{O}$  and  $\text{CO}$  to  $\text{N}_2$  of 1.0 and 1.05, respectively. Since some species have the same mass ( $\text{CO}$  and  $\text{N}_2$  – mass 28,  $\text{N}_2\text{O}$  and  $\text{CO}_2$  – mass 44), the use of labelled  $\text{CO}$  ( $^{13}\text{CO}$  from Sigma Aldrich) was required to distinguish them. To make reading easier it will be further referred in the text simply as  $\text{CO}$ . The details of experimental procedures are described elsewhere [7, 9].

Oscillatory behaviour has been detected in the temperature range between 373 K to 377 K at a  $\text{N}_2\text{O}$  pressure in the order of  $1 \times 10^{-6}$  mbar and very low  $\text{CO}/\text{N}_2\text{O}$  ratios (close to 0.1). The oscillations were triggered by slowly heating the crystal in the presence of  $\text{N}_2\text{O}$  ( $1 \times 10^{-6}$  mbar) with a very low amount of  $\text{CO}$  added ( $\text{CO}/\text{N}_2\text{O}$  ratio of approximately 0.05), from room temperature to 800 K and then subsequent cooling down to a temperature between 370 K and 390 K. Then the pressure of  $\text{CO}$  was increased stepwise until sustained oscillations in rate started.

Fig. 1 shows the oscillatory behaviour at 375 K for a  $\text{CO}/\text{N}_2\text{O}$  ratio equal to 0.1. The period of oscillations is approximately 60 s. As expected, the rate of  $\text{N}_2$  formation oscillates in counter-phase with that of the reactant  $\text{N}_2\text{O}$  and the  $\text{CO}_2$  pressure oscillates in counter-phase with the pressure of the other reactant  $\text{CO}$ . The most striking result is that the pressure of the reactant  $\text{N}_2\text{O}$  oscillates in an almost counter-phase relationship with the oscillations of the other reactant  $\text{CO}$ . This results in nearly anti-phase oscillations of the  $\text{N}_2$  and  $\text{CO}_2$  production rates.

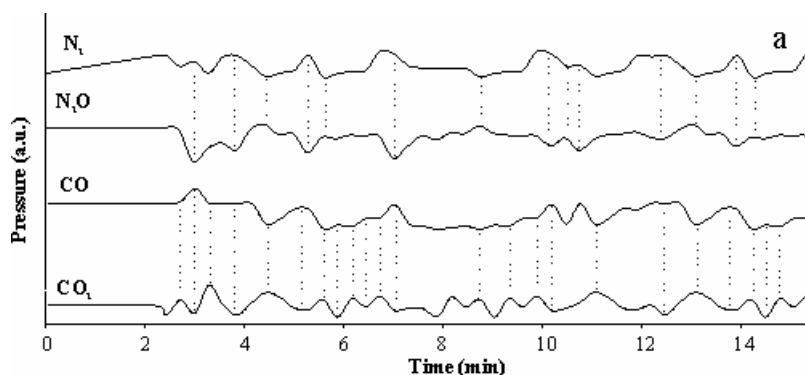
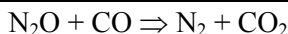
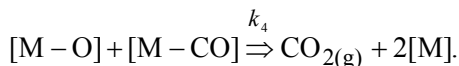
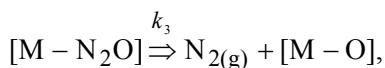
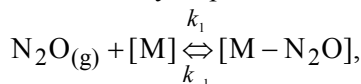


**Figure 1.** Oscillations in the partial pressures of  $N_2O$ ,  $N_2$ ,  $CO$  and  $CO_2$ , on the  $Ir(110)$  surface, at a  $N_2O$  pressure of  $1 \times 10^{-6}$  mbar and 375 K.  $CO/N_2O$  ratio was 0.1.

## Mathematical Modeling

Temperature programmed reaction studies revealed that on  $Ir(110)$  only  $N_2$  and  $N_2O$  were released from the surface in the temperature range from 350 K to 500 K and no  $NO$  desorption was detected [7,9]. Taking these data as a basis the following set of elementary steps was formulated:



The reaction mechanism includes the adsorption/desorption of  $N_2O$ ,  $CO$  and  $N_2O$  dissociation. According to the data of TPD studies [7] the reaction products  $N_2$  and  $CO_2$ , produced at  $T > 400$  K, desorb immediately after their formation on the catalyst surface.

The dynamic behavior of the system can be described by the following system of differential equations, corresponding to mechanism (1):

$$\begin{aligned}
 x' &= k_1 p_{N_2O} (1 - x - y - z) - k_{-1} x - k_3 x, \\
 y' &= k_2 p_{CO} (1 - x - y - z) - k_{-2} y - k_4 y z, \\
 z' &= k_3 x - k_4 y z, \\
 p_1' &= (F/V)(P_{N_2O} - p_{N_2O}) - \sigma(p_{N_2O} k_1 (1 - x - y - z) - k_{-1} x), \\
 p_2' &= (F/V)(P_{CO} - p_{CO}) - \sigma(p_{CO} k_2 (1 - x - y - z) - k_{-2} y);
 \end{aligned} \tag{2}$$

where  $x$  denotes  $N_2O$  coverage,  $y$  – CO coverage,  $z$  – O coverage,  $p_{N_2O}$  ( $P_{N_2O}$ ),  $p_{CO}$  ( $P_{CO}$ ) –  $N_2O$  and CO pressures in the reactor (inlet),  $V$  – the reactor volume,  $F$  – the pumping rate.  $\sigma = (SNRT)/V$ , where  $N_s$  and  $S$  stand for the adsorption capacity and the surface area of the Ir(110) single crystal surface, respectively.

The system (2) describes the variation of reagents coverages on the catalyst surface. The variations of the  $N_2O$  and CO partial pressures in the chamber are described by system (3). To simulate the variation of the  $N_2$  and  $CO_2$  partial pressures the following differential equations must be added:

$$\begin{aligned}
 p_{N_2}' &= -(F/V)p_{N_2} + \sigma k_3 x, \\
 p_{CO_2}' &= -(F/V)p_{CO_2} + \sigma k_4 y z.
 \end{aligned} \tag{4}$$

Table 1 shows the values of parameters, which are known from the experimental data and were used in the simulations.

**Table 1**

F, pumping rate	cm <sup>3</sup> /s	42500
V <sub>k</sub> , volume of the reactor	cm <sup>3</sup>	40000
S, Ir(110) surface area	cm <sup>2</sup>	0.56
N <sub>s</sub> , the adsorption capacity	mol/cm <sup>2</sup>	1.67×10 <sup>-9</sup>

Mathematical analysis demonstrates, that there is no any limit cycle solutions in the system (2), (3) at any values of the constants  $k_i$ , where  $i = \pm 1, \pm 2, 3, 4$ . Earlier it was demonstrated that oscillatory behaviour during  $N_2O+H_2$  reaction could arise due to the lateral interactions [8]. An analysis of the temperature programmed reaction studies presented in ref. 7 demonstrates that oxygen greatly modifies the rates of  $N_2O$  desorption and dissociation. At some range of oxygen coverages due to lateral interactions adsorbed oxygen accelerates the rate of  $N_2O$  dissociation. This kind of lateral interactions was demonstrated to be crucial for the appearance of oscillatory behaviour during the  $N_2O+H_2$  reaction. Therefore, this kind of lateral interactions was also introduced in the present model. The difference between both systems is determined by the fact, that CO could inhibit the  $CO_2$  production rate over Ir(110) [11]. Therefore, this type of lateral interactions was also included in the model. However, this effect was not enough to simulate a very large phase shift between the reactants  $N_2O$  and CO. A special study has been done to reveal the type of lateral interactions that can simulate

the experimental data presented in Fig.1. The rate constants  $k_i$  are supposed to be expressed in the following form:

$$k_i = k_i^0 \exp(-E_i / RT) \times \exp((e_{ix}.x + e_{iy}.y + e_{iz}.z) / RT),$$

where  $e_{ix}, e_{iy}, e_{iz}$  are parameters of the lateral interactions. The values of reaction stages constants were chosen in such a way that they are in agreement with the known literature data and produce the best qualitative similarity of model solutions and experimental data. The obtained values of parameters at  $P_{N_2O} = 10^{-6}$  mbar,  $P_{CO} = 1.3 \times 10^{-7}$  mbar are shown in the Table 2.

**Table 2.**

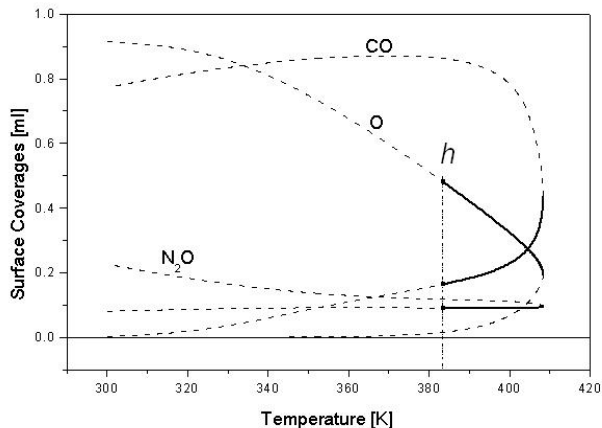
	$k^0$	$E$ [cal/mol]	Value of $k$ at $T = 375$ K
1	$7.638358 \times 10^4$ (s×mbar) <sup>-1</sup>	0	$7.638 \times 10^4$ (s×mbar) <sup>-1</sup>
-1	$1.415794 \times 10^{11}$ s <sup>-1</sup>	25000	$3.729 \times 10^{-4}$ s <sup>-1</sup>
2	$2.20 \times 10^6$ (s×mbar) <sup>-1</sup>	0	$2.200 \times 10^6$ (s×mbar) <sup>-1</sup>
-2	$2.58 \times 10^9$ s <sup>-1</sup>	28000	$1.210 \times 10^{-7}$ s <sup>-1</sup>
3	$1.00 \times 10^{18}$ s <sup>-1</sup>	36000	$1.013 \times 10^{-3}$ s <sup>-1</sup>
4	$3.00 \times 10^6$ s <sup>-1</sup>	12000	$3.013 \times 10^{-1}$ s <sup>-1</sup>

In order to describe the rate oscillations with the observed phase shift between CO and N<sub>2</sub>O oscillations the following lateral interactions in the adsorbed layer were introduced:

**Table 3.**

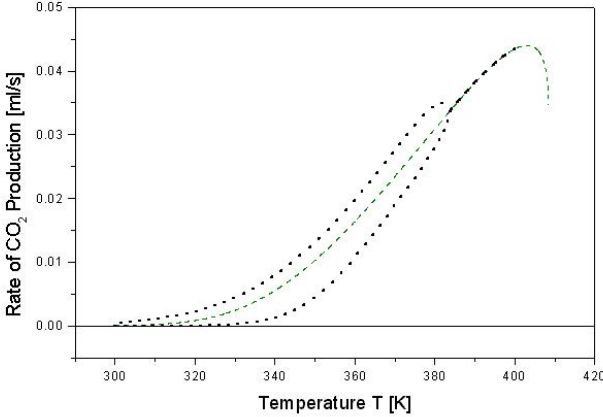
Stage 1	$e_{1,x} = 6$	N <sub>2</sub> O activates N <sub>2</sub> O adsorption
Stage 2	$e_{2,x} = -7$	N <sub>2</sub> O inhibits the adsorption of CO
Stage 3	$e_{3,x} = 1.5$	N <sub>2</sub> O activates N <sub>2</sub> O decomposition
Stage 3	$e_{3,z} = 10$	O activates N <sub>2</sub> O decomposition
Stage 4	$e_{4,y} = -3$	CO inhibits the CO+O reaction.
Stage 4	$e_{4,z} = 1$	O activates the CO+O reaction.

Fig.2 shows the stationary solutions of system (2), (3) in dependence on T with the parameters from tables 1-3.



**Figure 2.** The stationary solutions of (2), (3) versus T. Solid line denotes the stable solution, dashed line – the unstable solution. The black squares at  $T_h = 384$  K mark the Andronov-Hopf bifurcation point.

The stable limit cycle solution arises at  $T_h$  and exists at  $T < T_h$  until colliding with unstable solution  $X_0$  (not shown) and disappearing at  $T \approx 300$  K. The rate of  $\text{CO}_2$  production in the unsteady state together with the amplitude of the rate oscillations is shown in the next Figure.



**Figure 3.** The rate of  $\text{CO}_2$  production versus the temperature. Dotted line indicates the amplitude of rate oscillations.

The period of oscillations depends greatly upon the temperature. At low temperatures the amplitude of oscillations diminishes, the period increases and oscillatory behaviour can be hardly detected.

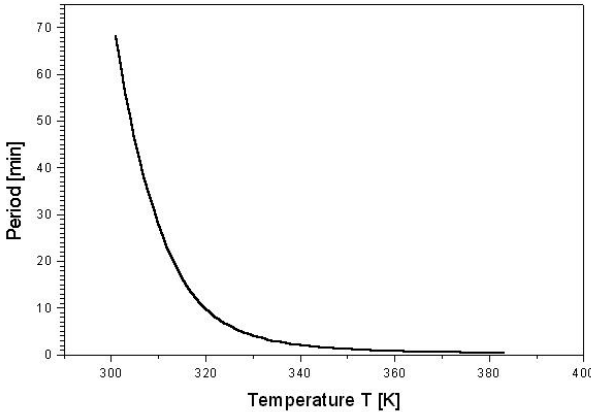


**Figure 4.** The dependence of the period of limit cycle oscillations upon the temperature

The variation of  $N_2$  and  $CO_2$  partial pressures were simulated with model (2) and equations (3). The results of simulations are demonstrated in Fig.5.

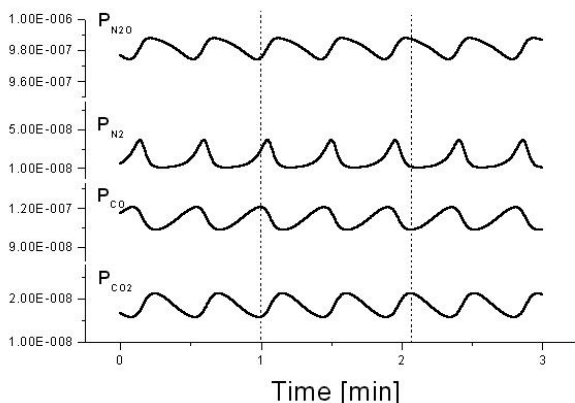


**Fig. 5.** Steady oscillations of  $N_2O$ ,  $N_2$ ,  $CO$ , and  $CO_2$  partial pressures at  $T = 375$  K.

Similar to the experimental data the  $N_2O$  partial pressure oscillates in antiphase with the  $N_2$  partial pressure and the  $CO$  partial pressure oscillates in antiphase with the  $CO_2$  partial pressure. Moreover, the results of the simulation demonstrate that as in the experiments the reactants  $N_2O$  and  $CO$  produce nearly antiphase oscillations. To understand the origin of the phase shift, let us consider the oscillatory behavior of surface coverages shown in Figure 6.

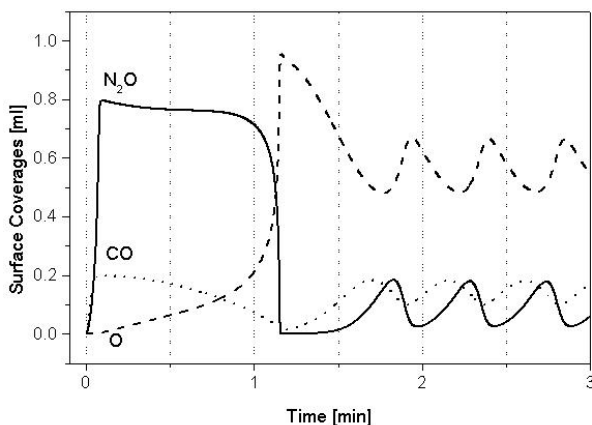


**Fig. 6.** Development of the oscillations of  $N_2O$ ,  $CO$ , and  $O$  surface coverages at 375 K.

The coverage oscillations in the model are caused by the competition between  $N_2O$  and  $CO$  adsorption. After the introduction of the reactant mixture in the reactor adsorption of  $CO$  and  $N_2O$  proceeds. The surface is covered mainly by  $N_2O$ , because its partial pressure is higher and  $N_2O$  inhibits  $CO$  adsorption. The rate of  $N_2O$  decomposition is slow due to a low oxygen coverage. As the  $O$  concentration increases, it accelerates  $N_2O$  decomposition rate until it is completely decomposed and the  $N_2O$  concen-

tration will fall nearly to zero. At this point the concentration of free sites is low, the rate of  $N_2O$  decomposition decreases and the  $N_2O$  concentration starts to increase. At a low  $N_2O$  concentration the CO adsorption is large and the CO coverage also begins to increase leading to a decrease of the O coverage. The CO coverage will continue to increase until the  $N_2O$  will reach such a critical value, that it will inhibit CO adsorption. The phase shift between the  $N_2O$  and O coverages results from the influence of the O coverage on the rate of  $N_2O$  decomposition. The second reason is the inhibition of CO adsorption by  $N_2O$ .

## References

- [1] M. M. Slinko and N. I. Jaeger, *Oscillating Heterogeneous Catalytic Systems, Studies in Surface Science and Catalysis*, vol.86, Elsevier, Amsterdam, 1994.
- [2] P. Hugo, M. Jakubith, *Chem.-Ingr.-Techn.*, 1972, 44, 383.
- [3] V. D. Belyev, M. M. Slinko, V. I. Timoshenko, M. G. Slinko *Kinetika i Kataliz*, 1973, 14, 810.
- [4] P. D. Cobden, N. M. H. Janssen, Y. van Breugel, B. E. Nieuwenhuys, *Faraday Discuss.*, 1996, 105, 57.
- [5] C.A. de Wolf, B.E. Nieuwenhuys, *Catal. Today*, 2001, 70, 287.
- [6] A. G. Makeev, M. M. Slinko, N. M. H. Janssen, P. D. Cobden, B. E. Nieuwenhuys, *J. Chem. Phys.*, 1996, 105, 7210.
- [7] S. A. Carabineiro, B. E. Nieuwenhuys, *Surf. Sci.*, 2001, 495, 1.
- [8] N.V. Peskov, M.M. Slinko, S. A. Carabineiro, B. E. Nieuwenhuys, *Proc. of the Russian-Dutch Workshop "Catalysis for Sustainable Development"*, Novosibirsk, 2002, 167.
- [9] S.A.C. Carabineiro, W.D. van Noort, B.E. Nieuwenhuys *Catalysis Letters*, 2002, 84, 135.
- [10] U. S. Ozkan, M. W. Kumthekar, G. Karakas, *J.Catal.*, 1997, 171, 67.
- [11] J. L. Taylor, D. E. Ibbotson, and W. H. Weinberg, *Surf. Sci.*, 1979, 90, 37.

## SPATIOTEMPORAL PHENOMENA IN THE NO+CO REACTION OVER Pt(100): SIMULATION RESULTS

E.S. Kurkina, N.L. Semendyaeva

*Moscow State University  
Department of Computational Mathematics & Cybernetics  
Leninskie Gory, Moscow, 119992, GSP-2, Russia*

Heterogeneous catalytic reactions exhibit a rich variety of interesting non-linear phenomena, including homogeneous self-sustained oscillations and bistability, propagating waves, pulses and fronts, spiral waves and stationary patterns. Spatiotemporal patterns with typical length scales in the  $\mu\text{m}$  range have been observed under ultra-high vacuum (UHV) isothermal conditions in investigations with the photoemission electron microscope (PEEM).

One of the most studied reactions is the catalytic NO reduction on the Pt(100) single crystal surface. Real time observations of the Pt(100) surface by means of PEEM detected propagating fronts, target patterns, rotating spirals, standing waves, solitary pulses, and chemical turbulence.

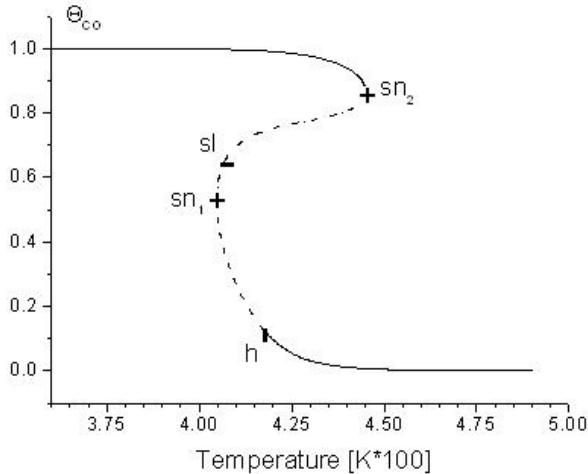


**Figure 1.** Bifurcation diagram for ODE system.  $\Theta_{\text{CO}}$  – concentration of  $\text{CO}_{\text{ads}}$ . Solid (dashed) lines represent the stable (unstable) steady states.  $h$  - supercritical Hopf bifurcation;  $sn_1, sn_2$  - saddle-node bifurcations;  $sl$  - saddle-loop bifurcation.

In this paper the system of consistent mathematical models of NO+CO/Pt(100) is constructed to describe spatiotemporal patterns observed in experiments. The system includes the kinetic Monte Carlo lattice-gas model (kMC), the mean-field differential equation model (ODE) and the reaction-diffusion model

(PDE). The characteristic feature of the models is that they take into account non-ideality of the adsorbed layer, namely lateral interactions play a crucial role in the adequate description of experimental data.

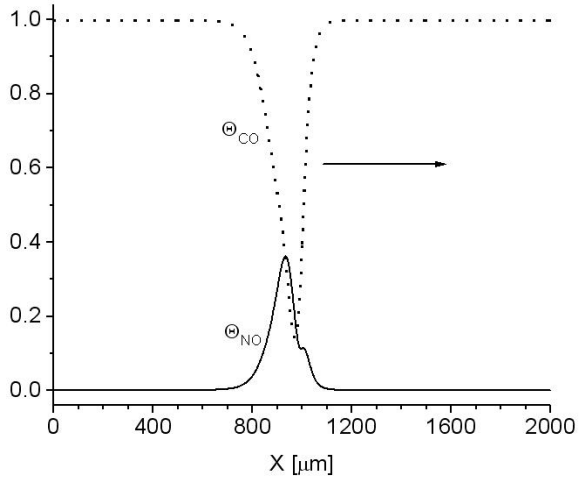


**Figure 2.** Traveling pulse in PDE model.

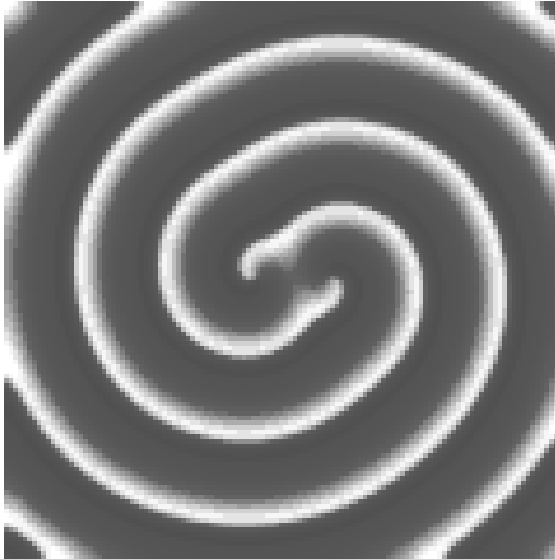


**Figure 3.** Spiral waves in PDE model.

The influence of internal fluctuations on the spatiotemporal formation was studied by means of kMC model. Different types of oscillatory-like behavior of lattice

gas model were revealed: kinetic oscillations, noise-induced oscillations and transitions. Pulses in the excitable medium and fronts in the bistable region were simulated.

The detailed one parameter and two parameters bifurcation analysis of ODE system has been performed (fig.1). The space of external parameters (the temperature  $T$ , the NO and CO partial pressures) was divided on the regions with different dynamic behavior. The boundaries of these regions were constructed with the help of path-following algorithms. The bifurcation analysis revealed the oscillatory domains and the regions of multiple steady states. The regions of excitable dynamics were also determined.

The spatiotemporal phenomena were investigated in the frame of the PDE models. Solitary pulses (fig.2) and spatiotemporal chaos were found in the excitable medium. Fronts were simulated in the region of bistability. Self-sustained oscillations and spiral waves (fig.3) exist in oscillatory region of ODE.

# SISTEMATIZATION OF REACTION MECHANISMS WITH MULTIPLICITY STATIONARY STATES ON THE CHANGING ACTIVITY OF THE CATALYST

N.I. Koltsov, E.S. Patmar

*Department of Physical Chemistry, Chuvash State University,  
Moskovskii prospect 15, 428015 Cheboksary, Russia*

## Abstract

In this communication we lead sistematization of two–three-and four-stages mechanisms of reactions for which deactivation of the catalyst results in multiplicity of stationary states and increase of number internal stationary states.

## Introduction

In works [1-3] it is shown that change of activity of the catalyst results in occurrence of multiplicity of internal stationary states (ISS) (the stationary states described by absence of zero concentration of intermediate substances) in two-stage reactions. In the present message sistematization of mechanisms of two-three-and four-stages reactions for which deactivation of the catalyst results in multiplicity of ISS.

## Results and Discussion

Researches were carried out in isothermal conditions non-gradient a differential reactor in the assumption quasi-stationarity of reactions on the basic substances. The changes in catalyst activity are determined by the presence of the following stages in the reaction mechanism [4]

$$\sum_i a_i X_i = \sum_i a_{-i} X_i + \sum b_i Z_i, \quad (1)$$

where  $X_i$  and  $Z_i$  are intermediate and buffer substances,  $Z_j$  occurring only in the right part of the stages,  $a_i$ ,  $a_{-i}$  and  $b_i$  are stoichiometric numbers ( $a_i = a_{-i} + b_i$ ). To automatize the research of MSS existence under the condition of MSS existence under the condition of catalyst decontamination the process of the analysis of reaction stages schemes is developed by us in general outline. In the first stages of this process the stages with buffer substances are described as linear literal equations with constant coefficients. In these equations the intermediate  $X_i$  substances stand for buffer  $Z_j$  ones in the following form

$$Z_i = \sum_j d_{i,j} X_j, \quad (2)$$

where  $d_{i,j}$  are some rational numbers. The analysis shows that if all the coefficients  $d_{i,j}$  are not negative ( $d_{i,j} \geq 0$ ) then catalyst decontamination does not lead to MSS. But if there is only one negative coefficient  $d_{i,j}$  ( $d_{i,j} < 0$ ), then catalyst

contamination leads to MSS at the definite mechanism structure.

Let us take two models to illustrate the process of the MSS analysis. For buffer stages

$$X_1 = Z_1, X_1 + X_2 = Z_1 + Z_2. \quad (3)$$

equations (2) are written

$$Z_1 = X_1, Z_2 = X_2. \quad (4)$$

As these equations do not contain negative coefficients  $d_{i,j}$ , catalyst decontamination does not lead to MSS owing to the introduction of stages (3) into the reaction mechanism.

For buffer stages

$$3X_1 = 3Z_1, 2X_2 = Z_1 + Z_2 \quad (5)$$

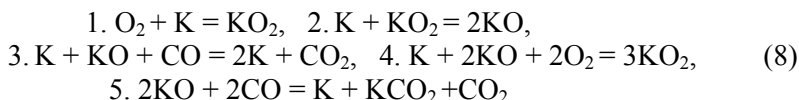
equations (2) have the following form

$$Z_1 = X_1, Z_2 = 2X_2 - X_1. \quad (6)$$

As there are negative  $d_{i,j}$ , in these equations, catalyst decontamination in the form of stages (5) can lead to MSS. Making use of this method we conclude that the presence of one bimolecular buffer stage of form

$$2X_{i_1} = X_{i_2} + Z, X_{i_1} + X_{i_2} = X_{i_3} + Z \quad (7)$$

leads to MSS for the reaction mechanisms having one SS under the conditions of lack of catalysts decontamination. In total it has been found accordingly 1, 5 and 21 two-three-and four-stages mechanisms which addition of one of buffer stages of a kind (7) results in occurrence of two ISS. For an establishment of structure of these mechanisms the criterion of multiplicity [5] which is taking into account stages of deactivation of the catalyst was used. We also investigated mechanisms of reactions for which deactivation of the catalyst results in increase of number ISS twice. For the decision of this task in a general view the simplified method [6] is developed. This method to find number of decisions of systems of the nonlinear algebraic equations describing stationary behaviour of reactions. The analysis has shown that two and more ISS arise in the reactions containing one buffer stages of a kind (1). Introduction of one of buffer stages of a kind (1) can result in growth ISS only at corresponding structure of the basic mechanism. 11 four-stages schemes for which the increase twice numbers ISS is observed at loss of a constancy of activity of the catalyst are established. On fig. 1 kinetic gives dependence with four ISS for reaction of carbon monoxide oxidation proceeding on the mechanism is submitted



( $KCO_2$  - buffer substance). Scheme (8) correspond to one of the established schemes.

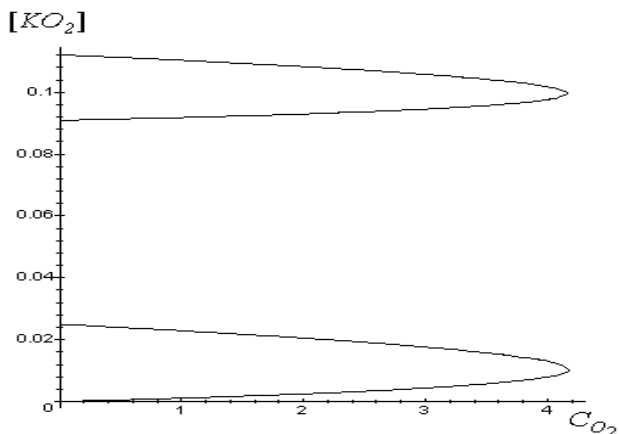


**Figure 1.** Dependence of concentration of substance  $KO_2$  on concentration of oxygen for reaction of carbon monoxide oxidation proceeding under the scheme (8) at:  $k_1 = 0,001$ ;  $k_2 = 1$ ;  $k_{-2} = 0,001$ ;  $k_3 = 2$ ;  $k_4 = 30$ ;  $k_5 = 0,01$ ;  $k_{-5} = 1$  ( $s^{-1}$ )

The received results open new peculiarities of reactions proceed on catalysts of variable activity.

## References

- [1] N.I. Koltsov and V.Kh. Fedotov, Surface Science, 1988, 206, 518.
- [2] N.I. Koltsov and B.V. Alexeev, J. Phys. Chemistry, 1989, 53, 1966.
- [3] E.S. Patmar and N.I. Koltsov, 13-th Russian conf. "The Problems of Catalysts Deactivation". Theses of reports, Novosibirsk, 2000, 259.
- [4] G. Eigenberger, Chem. Eng. Science, 1978, 33, 1263.
- [5] B.V. Alexeev, I.V. Kozhevnikov and N.I. Koltsov, Computer and Chemistry, 1999, 23, 69.
- [6] E.S. Patmar, B.V. Alexeev and N.I. Koltsov, Intern. conf. "Methods of Cybernetics of Chemical-Technological Processes". Theses of reports, Ufa, 1999, 2(1), 58.

## SIMULATIONS OF COMPLEX OSCILLATIONS BASED ON A MODEL OF THE BRAY-LIEBHAFSKY REACTION

Lj. Kolar-Anić<sup>1</sup>, T. Grozdić<sup>2</sup>, V. Vukojević<sup>1</sup>, G. Schmitz<sup>3</sup>, S. Anić<sup>1</sup>

<sup>1</sup>*Faculty of Physical Chemistry, University of Belgrade,  
Studentski trg 12-16, P. O. Box 137, 11001 Beograd*

<sup>2</sup>*Institute for Security, Kraljice Ane b.b, 11000 Beograd*

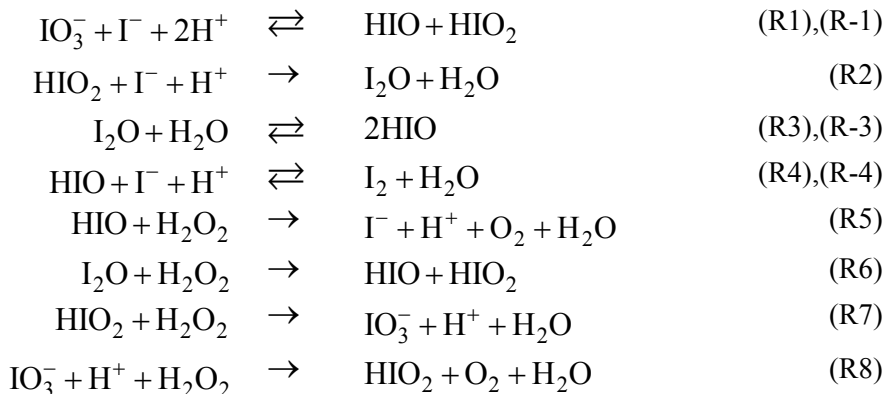
<sup>3</sup>*Faculté des Sciences Appliquées, Université Libre de Bruxelles,  
CP165/63, Av.F.Roosevelt 50, 1050 Bruxelles, Belgium*

### Abstract

A model mechanism of the Bray-Liebhafsky oscillatory reaction without direct autocatalytic and/or autoinhibition steps is utilized to simulate numerically complex oscillations when the reaction is conducted in a well-stirred open reactor.

### Introduction

A model mechanism for the Bray-Liebhafsky reaction consisting of the following reactions:



which is one variant of a model proposed by Schmitz [2], has been found to simulate well a number of experimentally observed phenomena in closed and open reactors [1,3-6]. Our intention here is to see whether complex oscillations, found experimentally in the Continuously-fed well Stirred Tank Reactor (CSTR), can be simulated by the same model and with exactly the same set of rate constants that was optimized for batch conditions.

The analyzed model is based on the liquid phase reactions; the rates of escape of volatile species and gaseous O<sub>2</sub> and I<sub>2</sub> from the system are not considered. There is no direct autocatalytic or autoinhibition step in the form of A + xB → (x ± 1)B, that would obviously induce non-linearity in the model.

## Results

To simulate numerically the dynamics of the BL reaction in the CSTR, the reactions due to the flow of the reactants through the reactor were added. Specific flow rate, as the control parameter, was varied from  $k_f = 1.0 \times 10^{-6}$  to  $k_f = 1.0 \times 10^{-1} \text{ min}^{-1}$ . Simulated time series in an interval from 1000 to 1200 min, which are presented in Fig. 1, show change in dynamic pattern from simple periodic oscillations (a) and (d), to complex periodic oscillations ((b) and (c)). In the last two cases different number of small-amplitude oscillations between the large-amplitude excursions can be noted. The observed dynamics emerges apparently through a stable steady state, characterized by a point attractor in the phase space, which loses stability at  $k_f = 2.99 \times 10^{-4} \text{ min}^{-1}$  (Fig. 2) and, through a supercritical Hopf bifurcation, makes a transition to a periodic limit cycle. By increasing the flow rate the complex oscillations with different numbers of small amplitudes emerge and attracting periodic orbit becomes of saddle type but only with respect to large-amplitude oscillations. In subsequent transitions, the number of small-amplitude oscillations arises and, finally, at  $k_f = 5.1400 \times 10^{-3} \text{ min}^{-1}$ , a new limit cycle due to small regular oscillations appears. This limit cycle loses stability and reverts to a stationary point attractor at  $k_f = 5.1446 \times 10^{-3} \text{ min}^{-1}$  through the subcritical Hopf bifurcation. The stationary point attractor once more loses stability, but in a very narrow region between  $5.1500 \times 10^{-3}$  and  $5.1501 \times 10^{-3} \text{ min}^{-1}$ , after which it appears to be generally stable.

## Discussion

The complex oscillations are found in transient, but also in permanent regime (until 10000 min), as in real experiments. The corresponding phase space diagram, but only for the case given in Fig. 1(c), is presented in Fig. 3. The simulations are very sensitive on the periods between two successive steps and numerical parameters.

In numerical simulations small-amplitude oscillations emerge at the end of the reduction pathway. This is opposite to the experimentally obtained results, where such dynamic behavior is observed at the end of the oxidation pathway. [7] This means that contributions of the existing pathways should be rearranged by adjusting the proposed set of rate constants.

## Conclusion

Complex periodic oscillations and transition dynamics is successfully simulated numerically by an already known variant of the model for the Bray-Liebafsky oscillatory reaction. Discrepancies from real experiments are found in that small-amplitude oscillations emerge at the end of the reduction pathway, whereas they are found experimentally at the end of the oxidation pathway. To achieve a better agreement, rate constants that were not determined experimentally should be adjusted.

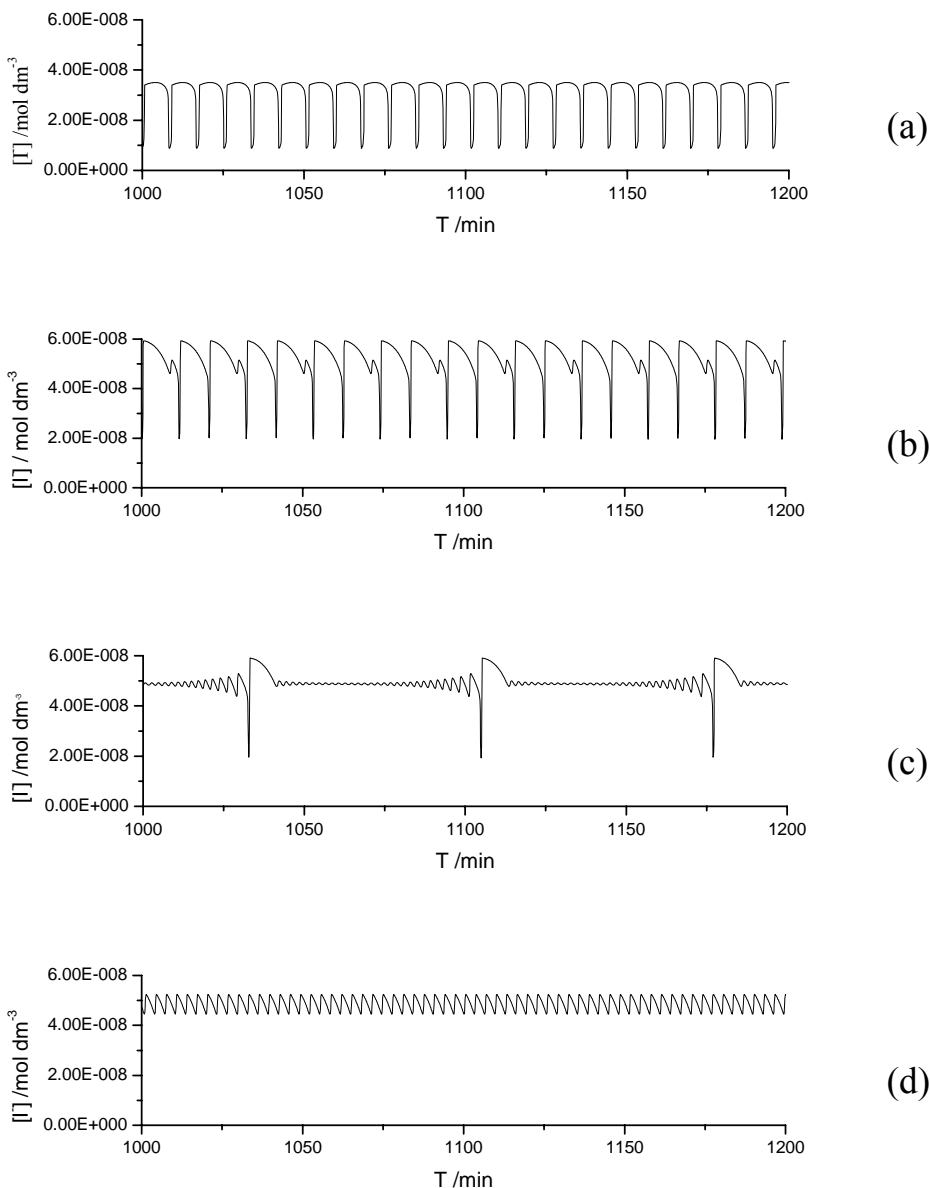


**Figure 1.** Numerical simulations of the iodide-ion concentration oscillations (in  $\text{mol}\cdot\text{dm}^{-3}$ ) (segment from 1000 to 1200 min). (a) and (d) the simple periodic oscillations,  $k_f = 1.00 \times 10^{-3} \text{ min}^{-1}$  and  $k_f = 5.14 \times 10^{-3} \text{ min}^{-1}$ , respectively; (b) and (c) the mixed mode oscillations,  $k_f = 4.90 \times 10^{-3} \text{ min}^{-1}$  and  $k_f = 5.13 \times 10^{-3} \text{ min}^{-1}$ , respectively;  $T = 333 \text{ K}$ .  $[\text{H}_2\text{O}_2]_0 = 1.55 \times 10^{-1} \text{ mol}/\text{dm}^3$ ;  $[\text{KIO}_3]_0 = 4.74 \times 10^{-2} \text{ mol}/\text{dm}^3$ ;  $[\text{H}^+]_0 = 9.58 \times 10^{-2} \text{ mol}/\text{dm}^3$ ; the rate constants and other initial conditions are taken from ref. [3].

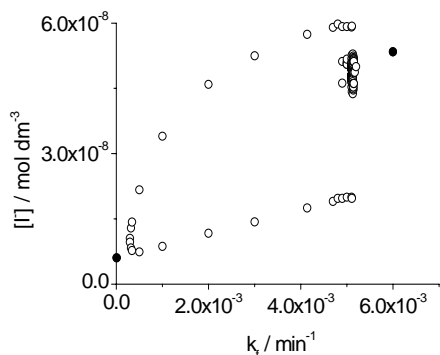


**Figure 2.** Bifurcation diagram with stable steady states (.), and envelop of large- and small-amplitude oscillations (–) where the small-amplitude oscillations are inside the large ones.

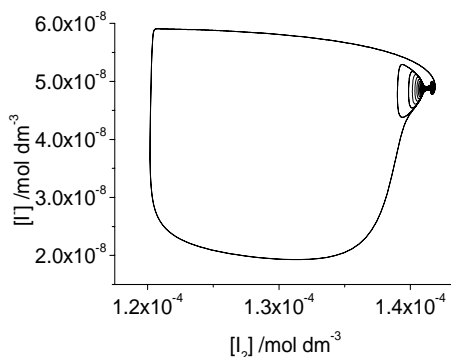


**Figure 3.** Phase space diagram for the case given in Fig. 1(c).

### Acknowledgement

Present investigations are partially supported by the Ministry of Sciences and Environmental Protection of Serbia under the project no.1448.

### References

- [1] Lj. Kolar-Anić, Đ. Mišljenović, S. Anić, G. Nicolis, *React.Kinet.Catal.Lett.*, 1995, 54, 35.
- [2] G. Schmitz, *J.Chim.Phys.*, 1987, 84, 957.
- [3] Lj. Kolar-Anić, Ž. Čupić, S. Anić, G. Schmitz, *J.Chem.Soc.Faraday Trans.*, 1997, 93, 2147.
- [4] K. Kissimonova, I. Valent, L. Adamčiková, P. Ševčík, *Chem.Phys.Lett.*, 2001, 341, 345.
- [5] V. Vukojević, S. Anić, Lj. Kolar-Anić, *Phys.Chem.Chem.Phys.*, 2002, 4, 1276.
- [6] M. Radenković, *Oksidacija joda vodonikperoksidom u uslovima Bray-Liebhaufsky sistema*, Master Degree Thesis, University of Belgrade, 1996.
- [7] V. Vukojević, S. Anić, Lj. Kolar-Anić, *J. Phys. Chem. A*, 2000, 104, 10731.

## DETERMINATION OF ASCORBIC ACID IN PURE AND PHARMACEUTICAL DOSAGE FORM BY USING PULSE PERTURBATION TECHNIQUE

N. Pejić<sup>1</sup>, Lj. Kolar-Anić<sup>2</sup>, V. Vukojević<sup>3</sup>, M. Milošević<sup>2</sup>

<sup>1</sup>*Faculty of Pharmacy, University of Belgrade, Vojvode Stepe 450, Belgrade,* <sup>2</sup>*Faculty of Physical Chemistry, University of Belgrade, Studentski trg 12-16, P.O. Box 137, Belgrade, Yugoslavia*

<sup>3</sup>*Alcohol and Drug Addiction Research Section, Department of Clinical Neuroscience, Karolinska Institutet, S 17176 Stockholm, Sweden*

### Abstract

The analytical method for the determination of ascorbic acid (AA) based on the perturbation of the Bray-Liebhafsky oscillatory (BL) reaction by different amounts of AA is proposed. The method relies on the linear relationship between the maximal change in potential, defined as difference,  $\Delta E_m = E_p - E_s$ , where  $E_p$  is the potential after perturbations while  $E_s$  is the potential of the steady state, and logarithm of the concentration of ascorbic acid. The calibration curve is linearly proportional to the logarithm of ascorbic acid concentration over the range  $2.2 \times 10^{-5} \text{ mol dm}^{-3} \leq [AA] \leq 2.0 \times 10^{-3} \text{ mol dm}^{-3}$ . The detection limits is  $[A] = 2.0 \times 10^{-5} \text{ mol dm}^{-3}$ . The proposed method was verified for ascorbic acid determination in pharmaceutical dosage forms.

### Introduction

Ascorbic acid (AA) is an essential vitamin with recommended daily intake about 70 mg. Continuing interest in the benefits of a well-balanced vitamin intake has resulted in the fortification of many food products with variety of vitamins, including vitamin C. On the other hand, vitamin C degrades quickly and therefore, there is special concern regarding the shelf life of these fortified foods. Consecutively, the analytical determination of them is of a significant importance.

On the other hand, the oscillatory chemical system as non-linear chemical system in the states far from equilibrium may be utilized as matrix for analytical determinations. Application of oscillation reactions to this effect originates from its complexity and its implicitly extreme sensitivity to various perturbations [1-3].

Here, the Bray-Liebhafsky oscillatory reaction [4], as the reaction where hydrogen peroxide decomposes into the water and oxygen in the presence of both  $\text{IO}_3^-$  and  $\text{H}^+$  ions, is used as the matrix for micro-quantitative determination of ascorbic acid. This deceptively simple reaction proceeds through the complex mechanism involving a number of intermediates, such as  $\text{I}^-$ ,  $\text{I}_2$ ,  $\text{HIO}$  and  $\text{HIO}_2$ , etc., which makes it suitable for such analysis.

### Experimental

The BL reaction was conducted in the Continuously fed well Stirred Tank Reactor (CSTR). The chosen dynamic structure for perturbation analysis is non-equilibrium stationary state that was found under the following experimental conditions: the mixed inflow concentration of reactants  $[\text{H}_2\text{SO}_4]_0 = 5.5 \times 10^{-2} \text{ mol dm}^{-3}$ ,  $[\text{KIO}_3]_0 = 5.9 \times 10^{-2} \text{ mol dm}^{-3}$

and  $[\text{H}_2\text{O}_2]_0 = 2.0 \times 10^{-3} \text{ mol dm}^{-3}$ , the specific flow rate  $j_0 = 2.95 \times 10^{-2} \text{ min}^{-1}$  and  $T = 42.9 \text{ }^\circ\text{C}$ .

Temporal evolution of the system was monitored potentiometrically by Pt electrode (Metrohm Model 6.0301.100) *versus* double junction Ag/AgCl electrode (Metrohm Model 6.0726.100) as a reference.

For ascorbic acid determination in pharmaceutical preparations, then tablets were weighed and average value per capsules was calculated. An amount equivalent to the average weight of one tablet (containing 1000 mg AA, according to the factory of declaration) is weighted out and diluted to volume with water in a 250 mL calibrated flask. Perturbations were performed by adding microvolumes, from 10 to 200  $\mu\text{L}$  of the ascorbic acid stock solution and 20 - 450  $\mu\text{l}$  of the samples by micropipettes. We applied manual injections of approximate duration of 0.5 s.

## Results and Discussion

For AA determinations we used a general approach to the microquantitative analysis, which was realized by adding the analyte in matrix system that was found in the stable non-equilibrium stationary state in the vicinity of a bifurcation point. By introducing the analytes in matrix system a delicate balance among the species existing in the matrix system may be disturbed. The species examined under these conditions, such as AA, need not to be essential for the matrix reaction system, but sufficient for reaction with the matrix.

The response of the matrix system after perturbation is followed potentiometrically, and then the applied perturbation is monitored (Fig. 1) A linear response of the potential shift versus the logarithm of the concentration of ascorbic acid (Fig.2) is found in the following range:  $2.2 \times 10^{-5} \text{ moldm}^{-3} \leq [\text{AA}] \leq 2.0 \times 10^{-3} \text{ mol dm}^{-3}$ . The regression equation of the standard series calibration curve,  $\Delta E_m = 62.6 + 11.1 \times \log c_{\text{AA}}$  (Fig. 2), obtained by analyzing the potential response curves that is received after perturbing a stable non-equilibrium stationary state with additions of different concentrations of ascorbic acid. The maximal change in potential, defined as difference,  $\Delta E_m = E_p - E_s$ , where  $E_p$  is the potential after perturbations whereas  $E_s$  is the potential of the steady state (Fig. 1). The response of the matrix system after perturbation is followed potentiometrically, and then the applied perturbation is monitored. A linear response of the potential shift versus the logarithm of the concentration of ascorbic acid (Fig. 1) is found in the following range:  $2.2 \times 10^{-5} \text{ moldm}^{-3} \leq [\text{AA}] \leq 2.0 \times 10^{-3} \text{ mol dm}^{-3}$ .

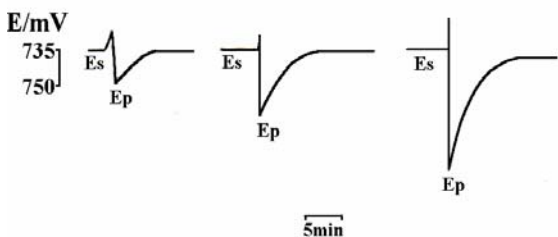


**Figure 1.** Typical response curves obtained after perturbing the stationary state in the BL reaction by addition of different concentrations of AA (on the left to the right):  $6.7 \times 10^{-7} \text{ moldm}^{-3}$ ,  $1.9 \times 10^{-4} \text{ moldm}^{-3}$  and  $5.8 \times 10^{-4} \text{ moldm}^{-3}$

The detection limit defined as the concentration of ascorbic acid, that produce a signal-to-noise ratio of 3, is  $[\text{AA}] = 2.0 \times 10^{-5} \text{ mol dm}^{-3}$ .

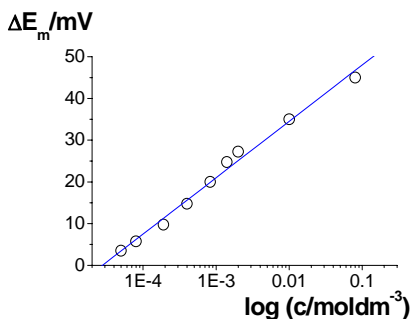


**Figure 2.** A standard series calibration curves for ascorbic acid

The applicability of the method for the assay of the sample was tested with *Vitamin C (Hemofarm, Vršac, Serbia & Montenegro)*, Table 1. The low value of SD and RSD less than 5 % as well as recovery lying in stated range (Ph EUR 97) indicated good application of the method.

**Table 1.** Precision and recovery of ascorbic acid in pharmaceutical dosage form

Sample	Concentration (mol dm <sup>-3</sup> )	Found±SD (mol dm <sup>-3</sup> )	RSD (%)	Recovery (%)
<i>Vitamin C</i>	1.11×10 <sup>-5</sup>	(1.14±0.03) ×10 <sup>-5</sup>	2.8	102.4
	5.10×10 <sup>-5</sup>	(4.84±0.14) ×10 <sup>-5</sup>	2.9	96.9
	1.52×10 <sup>-4</sup>	(1.49±0.71) ×10 <sup>-4</sup>	4.8	98.0

## Conclusion

A new kinetic procedure for determination of ascorbic acid, based on specific features of non-linear chemical systems in states far from thermodynamic equilibrium, is described. The Bray-Liebhafsky oscillatory reaction is used herewith as a matrix for AA determination. The reaction was run under the open conditions in the CSTR. The stationary state, sustained by the flows, was perturbed by additions of microvolumes of AA. The subsequent response of the system was monitored potentiometrically and analyzed. The proposed method for AA determination is simple, fast, accurate and precise - the unknown concentrations of AA can be determined from the standard series calibration curve within the accuracy of ± 5 %, and the detection limit is  $c_{AA} = 2.0 \times 10^{-5} \text{ mol dm}^{-3}$ . The described method was applied for AA determination in pharmaceutical preparations.

## Acknowledgement

Present investigations are partially supported by the Ministry of Sciences and Environmental Protection of Serbia under the project Physical chemistry of Dynamic states and structures of non-equilibrium systems – self-organization, multistability and oscillatory (project no. 1448).

## References

- [1] R. Jimenez-Prieto, M. Silva, D. Perez-Bendito, *Anal. Chim. Acta*, 1996, 321, 53.
- [2] V. Vukojević, N. Pejić, D. Stanisavljev, S. Anić, Lj. Kolar-Anić, *Analyst*, 1999, 124, 147.
- [3] N. Pejić, V. Kuntić, S. Anić, V. Vukojević, Lj. Kolar-Anić, *Micro. Chim. Acta*, 2003, 143, 261.
- [4]. W.C. Bray, *J.Am.Chem.Soc.*, 1921, 43, 1262.

## CONFORMATIONAL SCALING AND SELFORGANIZATION OF ENZYMES

M. B. Plavšić

*Faculty of Technology and Metallurgy, Karnegijeva 4, Belgrade*

### Abstract

Possible influence of quantum entanglement contributing to conformational scaling in highly organized biopolymer systems as protein globule is considered. It can provide fundament for understanding specific, crystal-like density and liquid-like dynamics in globule interior in particular strong and direct coupling of different parts of the molecule and "entropy traps" as well

### Introduction

Recently, a number of papers offered the first look at fine structure of several classes of enzymes that catalyze some of the most complex reactions in biology. For example, in a series of papers D. W. Christiansen et al, J. P. Noel et al. and G. E. Schultz et al presented the structure of terpenoid cyclase enzymes (TCE), and pointed to some key features of enzyme catalysis in general [1]. The conformational structures of enzymes considered are surprisingly similar, although their amino acid sequences are quite different and they make quite different products. Such conformational similarities seem to characterize protein molecules in general. Prokaryotic c-type cytochromes from a variety of organisms in molecule conformation resemble each other and those of eukaryotes even though there are few similarities among their amino acid sequences. Reasons for such conformational scaling are not quite clear.

Conformation is considered at present as one of the most fundamental feature of polymer chains[2] and conformational hierarchy (secondary and tertiary structure) of proteins build the fundamentals of structural biochemistry. But, interpretation of issues presented above varies very much. Some authors take it as a proof that conformational organization is much more important than the chemical structure for function of biomolecules e.g. all cytochromes have the same task in organisms but a variety of constitutions. The other believe that similarity results from conservation during evolutionary change. It could be understood if the tertiary structures are generated only during synthesis, what automatically transfer the problem to the fast growing field of fundamental genetics. But, after the famous Anfinsen experiment, we must keep in mind that generation of tertiary structure is possible (at least in principle) also by folding of protein molecules from denatured state to its native space structure, i.e. by conformational selforganization. Needless to say that it is quite a tough problem from the point of view of molecular mechanics, but it rises a number of challenging issues for polymer science. Here will be presented some new aspects and possible solutions based on organization scaling of polymer systems.

## Formulation of the Problem

All TPE considered bind a substrate in the active site cavity which is mainly non-polar, but has a highly polar patch at the top, and is lined by numerous aromatic residues. The substrate binding in a right starting conformation is followed by channeling the conformations of reactive intermediate [1]. But, how they are "channeled" is not quite clear, in particular a role of aromatic residues. According to Schulz, residues lining the cavity of squalene cyclase are well conserved, but show a gradient with higher conservation at the top and lower at the bottom, indicating occurrence of the first reaction step at the polar top where a general acid B1H protonates squalene at C3 and is finished by deprotonation at C29 of the hopenyl cation, by the general base B2 at the bottom. The aromatic residues "could stabilize the carbocationic intermediates of cyclization by their  $\pi$ -electrons". Also Christianson proposed that Phe<sup>77</sup> and Asn<sup>219</sup> provide a template that channels reactive conformations of farnesyl diphosphate along the exclusive reaction coordinate to pentalene formation, stabilizing intermediates through favorable quadrupole-charge and dipole-charge interactions. That gives a reasonable presentation of the process in the sense of classical organic chemistry, but does not say much about forces driving so stabilized structure down the chain and reasons for conformational similarity of all TPE. Moreover the base B2 mentioned above does not exist at all. The proton is transferred to a solvent molecules probably by concentrated polarization action of Gln<sup>262</sup>:Glu<sup>45</sup>:Glu<sup>93</sup>: Arg<sup>127</sup>. In that sense, focusing the internal and external fields of forces could be the reason for conformational similarity. After the first step of formation of the initial complex, some conformational changes are supposed to occur to allow the right position of the appropriate functional groups at the active site forming preferential transition state. That nonequilibrium state is followed by some bond-breaking and chemical realization of possible (quantum) events. W. Jencks described it as an "ideal mechanism" of enzyme catalyses. The process can be produced by conformational alteration of the substrate so as to increase the stability of the transition state, which may help to mobilize the nonequilibrium state although such couplings have not been indicated by study of structural details. Then, it has been suggested that the oscillation of an enzyme between two conformations differing in their strain would provide an ideal mechanism for catalysis if such oscillations could be induced by some driving force. However, the nature of this driving force has not been identified and according to Jencks, "such oscillations would require a mechanism for the focusing or coordinating of thermal energy in a cooperative manner which has not yet been clearly envisioned". Moreover, this energy should be delivered in such way to support conformational movements and chemical changes been some times of opposite directions. In the oscillating enzyme model this would mean the need of a strong and direct coupling between different parts of the macromolecule, a very unlikely event from classical point of view. As the third, enzyme catalyzes works under very mild process conditions with very low enthalpy contribution to the free energy, or in other terms with "entropy traps" at the active site. What kind of force support such traps for enzyme-substrate complex?

## The Theory

It is well known that in a dissipative system, namely and opens far-from equilibrium system, there arises a dynamic order, a coherent behavior of the ensemble when the values of the system's parameters corresponding to instabilities are exceeded. Such situations typical for open far-from equilibrium systems are often described in terms of macroscopic thermodynamic variables. A dynamic order appears as a result of the increase of fluctuation up to the macroscopic level. But, let us consider effects of the primary fluctuations on the other side of scale of our systems. Generally the criterion for the possibility of emergence of dynamic order, in a dissipative system is the failure to satisfy stability conditions. According to Prigogine theorem, the dependence of the dissipation function  $\sigma$ , on the parameter  $\kappa$  that defines the open- near -to - equilibrium system has a minimum value  $\sigma_0$  in the stationary state  $\kappa = \kappa_0$ . When  $\kappa$  deviates from  $\kappa_0$  the system returns to the state  $\kappa_0$  exponentially, without experiencing oscillations. Let us suppose that it is valid on the other side of the scale. Details of scale properties will be presented later, when necessary. If the system is characterized by many extensive variables the change of its entropy  $S$  with time is expressed by

$$\frac{dS}{dt} = \sum_j X_j J_j \quad (1)$$

where  $X$  and  $J$  are the general forces and general fluxes from Onsager theorem. The entropy change in an open system is made up of the entropy production inside the system  $d_i S$  and the entropy flow  $d_e S$ , and we write  $dS = d_i S + d_e S$ . According to the Second law of thermodynamics

$$\frac{d_i S}{dt} = \int \sigma * dV \geq 0 \quad (2)$$

Now we can write

$$\sigma = \frac{d_i S}{dt} = \sum_j J_j X_j \geq 0 \quad (3)$$

and for system change in time

$$\frac{d\sigma}{dt} = \frac{d_j \sigma}{dt} + \frac{d_x \sigma}{dt} = \sum_j X_j \frac{dJ_j}{dt} + \sum_j J_j \frac{dX_j}{dt} \quad (4)$$

under constant boundary conditions we have

$$\frac{d_x \sigma}{dt} \leq 0 \quad (5)$$

This yields the stability condition for the steady-state under consideration

$$\sum_j \delta J_j \delta X_j \geq 0 \quad (6)$$

where  $\delta J_j$  and  $\delta X_j$  are the deviations of generalized fluxes and forces from their steady-state values.

Let us now define the scale more precisely according to M. Volkenshtein, conformational energy can be represented in terms of structural element interactions as

$E_{con.} = E_{nn} + E_{ne} + T_e + E_{ee}$ , where  $E_{nn}$  represent energy of nucleus to nucleus interaction,  $E_{ne}$  corresponding electron nucleus interaction etc. But according to Einstein paper with Podolsky and Rosen in 1935 and recent experimental evidence particles in general (e.g. atoms, ions, photons etc.) can be quantum entangled (QE). Especially in condensed matter, the existence of QE follows from the first principle of quantum dynamical evolution. For example let  $\Psi_A$  and  $\Psi_B$  the state vectors of two particles (quasi-particles, dressed particles, subsystems etc.) A and B. The two systems (particles) having Hamiltonians  $H_A$  and  $H_B$  interact either directly or indirectly with the interaction Hamiltonian  $V_{AB} \equiv V(q_A, q_B, q_{env})$ , where  $q_X$  is dynamical variable of system X,  $q_{env}$  refers to the additional degrees of freedom, usually called the in environment. For  $t > 0$  the complete evolution operator of the QE system  $U_{AB}(t) = \exp\{-i(H_A + H_B + V_{AB})t/\hbar\}$ , does not factorize in to a product of two individual evolution operators  $U_A$  and  $U_B$ , and

$$\Psi_{AB}(t) = U_{AB}(t)\Psi_{AB}(0) \neq \Psi'_A(t) \otimes \Psi'_B(t) \quad (7)$$

For many particles in the bulk of dense, ordered systems Eq.(7) could be expected valid. But not for dense but conformational specific interior of enzymes.(see Eq.5) So decoherence in enzyme interior produce interaction conformational Hamiltonian  $V_{ent} = CK_K \otimes D_E$ , contributing specifically to fluctuation forces in Eq.6. Here C is the coupling constant, and  $K_K = \sum_i k_i |k_i\rangle_{KK} \langle k_i|$  is conformation observable of the quantum system and  $D_E$  is arbitrary observable of the environment.

## Conclusion

The high conformational similarity of tertiary structures of several classes of enzymes and the fact that peptide in general are able to build the native tertiary structure by self organization in renaturation process, indicate that such a conformational scaling is not a byproduct of evolution dynamic, but essential feature of enzyme structure. It belongs to a global type of structure in terms of scaling concept and can be treated even experimentally according to common dynamical methods for polymers, but it influence dynamics of enzyme catalytic processes as well. Moreover, it seems that scaling supports dynamic order of tertiary structure influencing fluctuations on different levels, starting from very fundamental quantum coherence principles. It can be pronounced, at least in crude through differences in particles decoherence in enzyme interior environment, compared to other highly ordered bulk polymer structures.

## Literature

- [1] K. Wendt, K. Poralla, G. Schulz, Science 277, 1997, 182, C. Starks, K. Back, J. Noel, I. Chappell, ibid. 1815, C. Lesburg, G. Zhai, D. Cane, D. Christianson, ibid 1820.
- [2] P. J. Flory, Statistical Mechanics of Chain Molecules, Wiley, N.Y. 1969.
- [3] P. G. de Gennes, Scaling Concepts in Polymer Physics, Cornell, Ithaca, 1979.

## POLYMERIZATION OF ORGANIZED MONOMERS

D. Stoiljković<sup>1</sup>, B. Pilić<sup>1</sup>, R. Radičević<sup>1</sup>, I. Bakočević<sup>1</sup>, S. Jovanović<sup>2</sup>, D. Panić<sup>3</sup>,  
Lj. Korugić-Karasz<sup>4</sup>

<sup>1</sup>Faculty of Technology, Bulevar Cara Lazara 1, Novi Sad, Serbia, <sup>2</sup>Faculty of Technology and Metallurgy, Belgrade, Serbia, <sup>3</sup>Technical Faculty, Novi Sad, Serbia, <sup>4</sup>Polymer Science and Engineering, University of Massachusetts, Amherst, USA

### Abstract

The selforganization and radical polymerizations of compressed ethene gas and liquid methylmethacrylate and Ziegler-Natta polymerization of adsorbed olefins are presented.

### Introduction

All classical explanations of polymerization [1] propose that polymer chain propagates by addition of **one by one** monomer molecule to the growing chain (1). The same process can be presented as (2) where  $P_n^*$  represents cation, anion or radical of growing chain and M represents individual monomer molecule.



There are some cases (solid, liquid and adsorbed monomer systems), however, with monomer molecules that are organized and exist as the clusters of  $m$  molecules ( $mM$ ). Kargin and Kabanov [2] developed a theory of organized monomer polymerization (TOMP). According to them, each cluster behaves as a single physical and chemical entity and the whole cluster  $mM$  is enchained at once in a single propagation step (3). The fundamental difference between (2) and (3) is that the propagation is random on the molecular level in the first case (2), while it is determined on the molecular level but random on the supra-molecular level in the second case (3). In the first case (2), one by one repeating unit of polymer chain is formed, while in the second case (3) one by one chain segment is formed. Hence, in the second case (3) the both polymerization kinetics and polymer structure ( $M_n$ , MWD, stereoregularity, regioregularity etc.) depend on the organization and arrangement of monomer molecules in those clusters.



Here we present how this concept has been applied to explain radical polymerizations of compressed ethene gas and liquid methylmethacrylate (MMA) and Ziegler-Natta polymerization of olefins adsorbed on the support surface.

## Free Radical Polymerization of Compressed Ethene Gas

It is known that ethene can polymerize by free radical mechanism at the very high pressures. We have explained [3] that the role of pressure is to enable formation of various supra-molecular species (Fig. 1). The basic rule is: by increase of pressure, i.e. by decrease of free volume, such species are formed that need less space for the movement. It was proved that a degree of order, presented by entropy of compressed ethene, has a crucial effect on polymerization mechanism and kinetics as well as on polyethylene structure and properties.

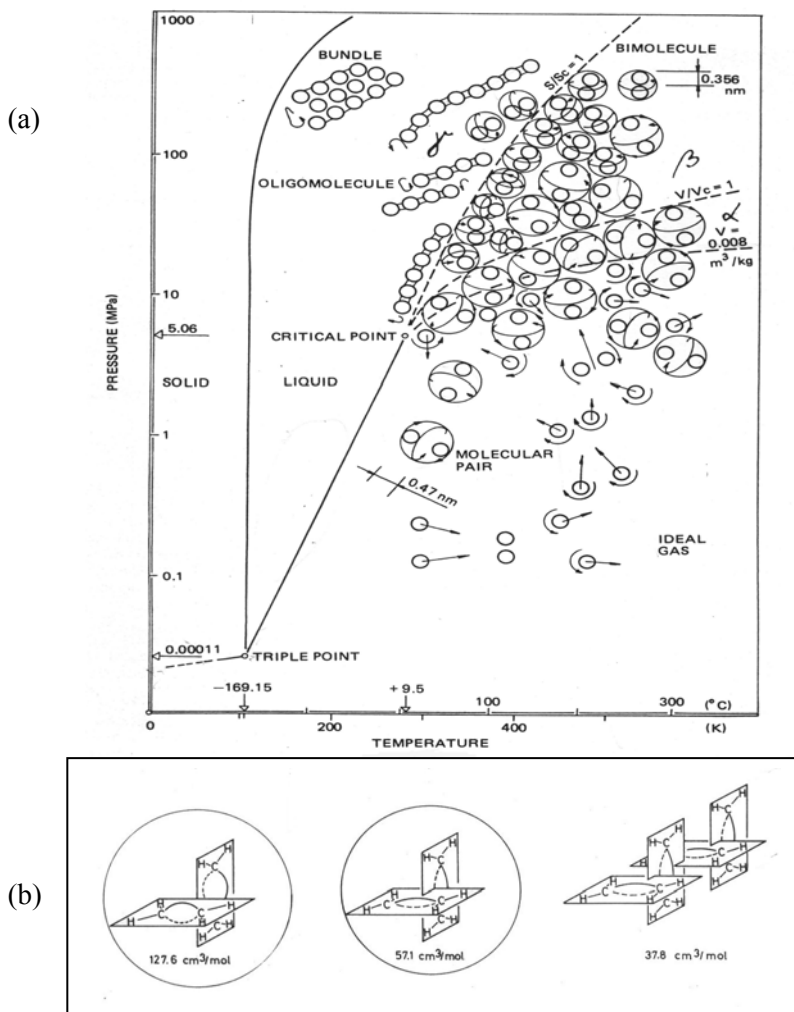


**Figure 1.** Phase state (a) and supramolecular species (b) of compressed ethene gas (molecular pair, bimolecule and oligomolecule, respectively) [3]

## Selforganization and Polymerization of Liquid MMA

Sasuga and Takehisa [4] found that planar molecules of MMA could be properly aligned producing ordered domains in liquid MMA (Fig. 2). We have developed a method [5] to calculate the fractions of molecules in ordered (Fig. 3,  $X_{t,s}$  line) and disordered domains (Fig. 3,  $X_b$  line). According to TOMP, initially the monomer molecules in disordered domains should polymerize followed by polymerization of monomer in ordered domains. We have proved experimentally [5] that the calculated fractions are equal to the experimentally determined fractions of polymerized monomer in ordered and disordered domains (Fig. 3, points).

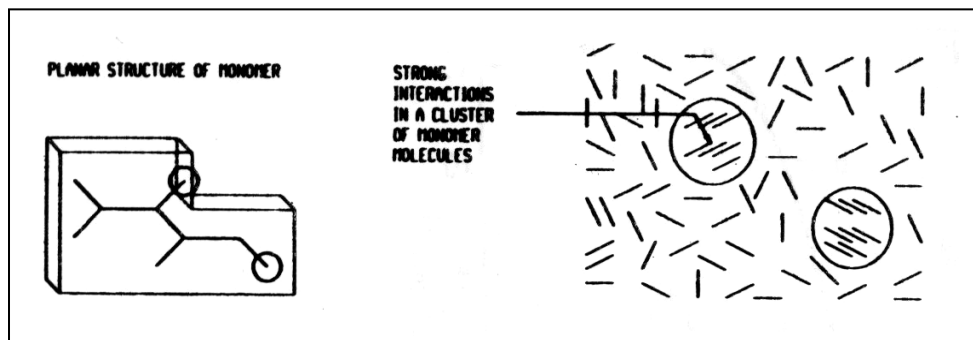


Figure 2. Supramolecular organization of liquid MMA [4]

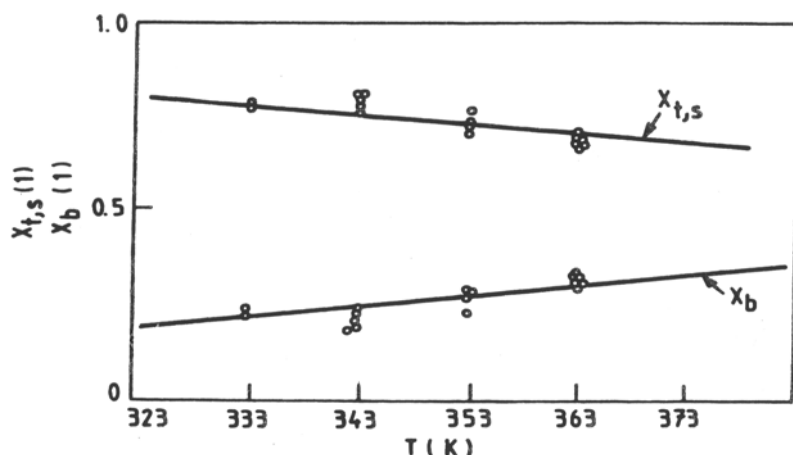
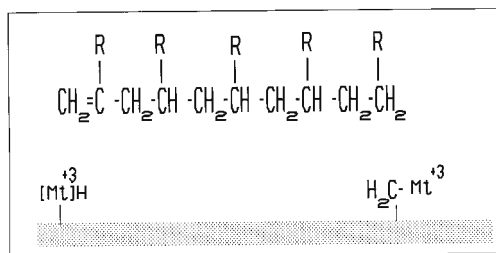
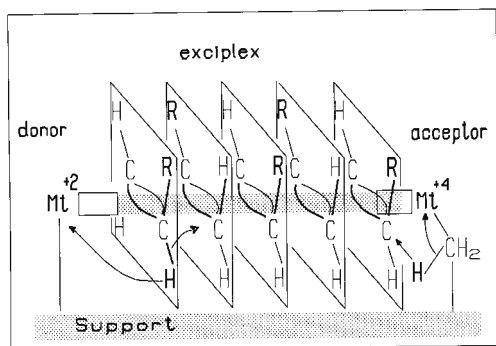


Figure 3. Fractions of ordered ( $X_{t,s}$ ) and disordered ( $X_b$ ) domains of liquid MMA at different temperatures [5]. (Solid lines: predicted by calculation; Points: experimental determination by polymerization)

## Monomer Selforganization and Polymerization by Ziegler-Natta Complexes

Recently a new charge percolation mechanism (CPM) of olefin polymerization by supported transition metal (Mt) complexes has been presented [6]. Different oxidation states of Mt are obtained by activation, i.e.  $Mt^{+(n-1)}$ ,  $Mt^{+(n)}$  to  $Mt^{+(n+1)}$ , producing irregular charge distribution over the support surface. The tendency to equalize the oxidation states by a charge transfer from  $Mt^{+(n-1)}$  (donor) to  $Mt^{+(n+1)}$  (acceptor) cannot be fulfilled since they are immobilized and highly separated on the support. But, monomer molecules are adsorbed on the support producing the clusters with stacked  $\pi$ -bonds making a  $\pi$ -bond bridge between donor and acceptor (Fig. 4). Once a bridge is formed (percolation moment), a charge transfer occurs. Donor and acceptor equalize their oxidation states simultaneously with the polymerization of monomer. Polymer chain is

desorbed from the support making the surface free for the subsequent monomer adsorption. The whole process is repeated by oxidation-reduction of another donor-acceptor ensembles. The theory of active centers ensembles (developed by Kobozev in 1939) has been applied to confirm CPM by experimental data and by computer simulation.



**Figure 4.** Monomer selforganization and charge percolation mechanism of Ziegler-Natta polymerization (upper) and polymer detachment (below)[6]

## Conclusion

Monomer selforganization has a decisive effect on mechanism and kinetics of polymerization as well as on the structure and properties of polymer.

## References:

- [1] P. J. Flory, "Principles of Polymer Chemistry", Cornell Univ. Press, Itacha, 1953.
- [2] V. A. Kargin, V. A. Kabanov, Zh. Vses. Khim. Ob., 1964, 9, 602.
- [3] D. Stoiljkovic, S. Jovanovic, Acta Polymerica, 1988, 39, 670.
- [4] T. Sasuga, M. Takehisa, J. Macromol. Sci., 1978, A12, 1307 and 1321.
- [5] R. Radicevic, Lj. Korugic, D. Stoiljkovic, S. Jovanovic, J. Serb. Chem. Soc., 1995, 60, 347.
- [6] D. Stoiljkovic, B. Pilic, S. Jovanovic, D. Panic, Hem. ind., 2000, 54, 480.

## APPLICATION OF POLYNOMIAL ELIMINATION IN CHEMICAL KINETICS

M. Lazman

*Aspen Technology, Inc, 900, 125 –98<sup>th</sup> Avenue SE  
Calgary, Alberta CANADA T2G OP6*

### Abstract

This paper presents new results on the application of algebraic techniques of polynomial elimination to the analysis and global solution of mass-action-law kinetic models.

### Introduction

Differential equation models of chemical kinetics demonstrate a spectrum of non-linear phenomena, from steady-state multiplicity to self-oscillations and chaos. Polynomial models represent common and important subset of general non-linear kinetic models. At the same time, they allow application of special algebraic techniques. These methods provide a comprehensive solution to problems such as global numerical solution and analysis of common bifurcations. Classic chemical kinetics assumes Mass Action Law (MAL) for the rate  $w$  of reaction step

$$w = k \prod c_i^{\alpha_i}, \quad (1)$$

Where  $c_i$  is concentration of  $i$ th reagent,  $\alpha_i$  is its stoichiometric coefficient,  $k$  is the reaction constant. MAL steady-state model is a system of multivariable polynomial equations. Solution of polynomial systems is the subject of *elimination theory* developed by Bezout, Sylvester, Cayley, Macaulay, Kronecker, and Hurwitz. Recent renaissance of the almost forgotten elimination theory is concerned with Newton polytope approach developed in [1].

We are going to apply both classic and modern elimination theory to the non-linear steady state problem from chemical kinetics. Our model is an algebraic system corresponding to Quasi Steady State Approximation (QSSA) of differential equations of chemical kinetics.

*QSSA system* Material balance in the system where QSSA is applied to concentrations of intermediates can be presented in the form

$$\begin{aligned} \bar{w}(\bar{z}) &= N\bar{W}, \\ \bar{L}(\bar{z}) &= 0, \end{aligned} \quad (2)$$

where  $\bar{z}$  is a vector of intermediate concentrations,  $\bar{w}(\bar{z})$  is a vector of rates of (reversible) elementary reaction steps,  $\bar{L}(\bar{z})$  is a vector of  $B$  linear balances of intermediate concentrations, matrix  $N$  is composed of  $P = S - (J - B)$  vectors of *stoichiometric numbers*  $v_s^p$  ( $s=1, \dots, S; p=1, \dots, P$ ),  $S$  is the number of reactions,  $J$  is the number of intermediates. Each  $v$  column vector is called *reaction path*; vector  $\bar{W}$  is composed of  $P$  rates along the reaction pathway. Linearly independent reaction paths form the *stoichiometric basis*.

*Kinetic polynomial* Polynomial systems allow variable elimination. Our previous studies [2] were concerned with understanding the resultant of system (2) in reaction path rate  $W$  (we studied the case of  $P=1$ ). Resultant (the kinetic polynomial) is a polynomial in terms of  $W$ . Vanishing of resultant is a necessary and sufficient condition of system (2) solvability. Resultant in terms of  $W$  allows the formulation of QSSA conditions in terms of experimentally measurable variable  $W$ . This equation is symmetric in terms of reaction parameters, and it has a thermodynamic interpretation. We have proved that the resultant's constant term always contains multiplier (the cyclic characteristic)

$$C = \prod_{s=1}^S f_s^{v_s} - \prod_{s=1}^S r_s^{v_s}, \quad (3)$$

where  $f_s, r_s$  are reaction weights (i.e. reaction rates at unit intermediate concentrations) of  $s$ th forward and reverse reaction. Equation  $C = 0$  is equivalent to the thermodynamic equilibrium condition for net reaction. Stoichiometric numbers entering formula (3) are relatively prime (i.e. resultant's constant term corresponds to the net reaction equation obtained for minimal integral stoichiometric numbers). Further development of the theory resulted in explicit formulas for all resultant coefficients. This approach permitted computer algebra implementation [3]. Variable elimination proved to be effective in applications ranging from inverse kinetic problem to bifurcation analysis [2-4].

## Results and Discussion

*Multidimensional resultant formulation* Bezout theorem gives the simplest estimate on the number of (complex) zeroes of system (2). Let us define the reaction order  $d_s$  as the maximum of orders of forward and reverse reactions. Index  $\mu$  is assigned to the elementary step with a non-zero stoichiometric number that has the smallest reaction order (the minor reaction). Let  $L_\mu = \prod_{s \neq \mu}^S d_s$ . For the single-path mechanism we have

*Proposition 1.* If  $P=1$ , the number of system (2) complex zeroes is less than or equal to  $L_\mu$ .

In the general case, we have

*Proposition 2.* If  $P > 1$ , the number of system (2) complex zeroes is less than or equal to  $L_\mu$ , where  $\mu$  is defined as

$$\mu = \arg \max_p \min_s d_s : v_s^p \neq 0.$$

Proposition 2 estimate depends on a particular stoichiometric basis. There exists a basis that produces the sharpest estimate.

Variable elimination reduces system (2) solution to solving a single polynomial in one unknown. Other unknowns can be found either by using resultant properties or by iteration of elimination procedure. We could also apply the standard methods as Groebner bases. Implementation of these approaches requires computer algebra. Straightforward application of computer algebra results in a slow, unstable, and unreliable procedure. However, no explicit resultant expression is required to solve system (2) numerically. Multidimensional *resultant matrix* can be built instead. We have proved that for a certain class of systems (the non-degenerate systems, see [3]) this matrix would be non-singular. Non-singular resultant matrix allows us to solve system (2) using exclusively numerical linear algebra. The solution of system (2) is reduced to an algebraic eigenproblem.

*Proposition 3.* Reaction rate can be found as a solution of order  $L_\mu$  eigenproblem. The matrix formulation allows us to locate all roots counted by the Bezout theorem.

*Example* One of possible Macaulay matrices for system

$$f_1 z_1^2 - r_1 z_2^2 = W$$

$$f_2 z_2 - r_2 z_1 = 2W$$

$$z_1 + z_2 = 1,$$

corresponding to the two-stage mechanism of catalytic reaction, is the matrix

$$M(W) = \begin{pmatrix} 0 & r_2 & -f_2 & 2f_1 & 0 & -2r_1 \\ -1 & 1 & 1 & 0 & 0 & 0 \\ 0 & -1 & 0 & 1 & 1 & 0 \\ 0 & 0 & -1 & 0 & 1 & 1 \\ 2W & r_2 & -f_2 & 0 & 0 & 0 \\ 0 & 2W & 0 & r_2 & -f_2 & 0 \end{pmatrix}$$

Reaction rate  $W$  can be found as a solution of order 2 eigenproblem with matrix

$$\frac{\begin{pmatrix} (r_2 + f_2)^2 + 4r_1 r_2 + 2f_2(f_1 + r_1) & 2(f_1 - r_1)(r_2 + f_2) \\ (r_2 + f_2)(f_2 + 2r_1) & 2f_2(f_1 - r_1) \end{pmatrix}}{2(r_1 r_2^2 - f_1 f_2^2)},$$

derived from matrix  $M(W)$ . An eigenvalue is  $\lambda = -1/(2W)$ .

*Cayley trick, circuits and cyclic characteristic* Although the classic Macaulay method allows effective solution of systems (1), the most promising approach is concerned with sparse formulation. Our first result in this direction is the proof of kinetic polynomial thermodynamic property (3) based on A-discriminant theory [1]. The Cayley trick reduces the problem to the analysis of the discriminant of a specific polynomial. Monomials of this polynomial form a *circuit*. Informally, the circuit is a point configuration obtained from the simplex by the addition of a single point. The circuit explains the appearance of the cyclic characteristic (3) in the constant term of the kinetic polynomial. We could say that pure topology governs the connection between thermodynamics and kinetics, encapsulated in property (3).

## Conclusions

We have developed a new method of numerical solution of QSSA equations utilizing multidimensional resultant matrices. We have found the topological interpretation of properties of the kinetic polynomial.

## References

- [1] I.M. Gelfand, M.M. Kapranov, A.V. Zelevinsky, Discriminants, resultants and multidimensional determinants, Birkhauser, Boston, 1994.
- [2] M.Z. Lazman, G.S. Yablonskii, Kinetic polynomial: a new concept of chemical kinetics, Patterns and Dynamics in Reactive Media, Springer-Verlag, 1991, 117-151.
- [3] V.I. Bykov, A.M. Kytmanov, M.Z. Lazman, Elimination methods in polynomial computer algebra, Kluwer Academic Publishers, 1998.
- [4] G.S. Yablonskii, M.Y. Mareels, M.Z. Lazman, The principle of critical simplification in chemical kinetics. Chem. Eng. Sci., 2003, 58, 4833.

## SELFORGANIZATION IN HIGH TEMPERATURE REACTION KINETIC SYSTEMS

T. Turányi, I. Gy. Zsély, J. Zádor

*Department of Physical Chemistry*

*Eötvös University (ELTE)*

*H-1518 Budapest, P.O. Box 32, Hungary*

### Abstract

Models of homogeneous explosions and one-dimensional laminar flames of hydrogen and methane were analysed by a series of mathematical tools. The results indicated that the real dynamical dimension of these systems is 1 to 3, while the number of variables is from 10 to 38. This dimension reduction indicates strong couplings in the model, exhibited in the similarity relations among the sensitivity functions. It has consequences in areas of practical importance, like determination of rate parameters from experimental data or search for a minimal equivalent model.

### Introduction

Selforganization is usually investigated in solution phase chemical or biological systems. In this paper we should like to demonstrate that some high temperature gas-phase chemical kinetic systems are not only highly non-linear, but also may show surprising signs of selforganization.

The systems investigated were the homogeneous explosions and one-dimensional laminar flames of hydrogen and methane. We have investigated both freely propagating and burner stabilized laminar flames. The methane combustion simulations used the Leeds Methane Oxidation Mechanism [1], [2], which contains 37 species and 350 (irreversible) reactions. The hydrogen oxidation calculations were carried out with a subset of the Leeds Mechanism, having 9 species and 46 reaction steps.

The number of variables of the explosion and flame models was equal to the number of reactive species plus one when temperature was also calculated. It has been shown recently, that the real dynamical dimension of high temperature chemical kinetic systems is lower; in the case of the adiabatic explosion of hydrogen it is one instead of ten and in the case of the adiabatic explosion of methane it is three instead of 38. The reason of this huge dimension reduction is the existence of low-dimensional slow manifolds in the variable space of high-temperature chemical kinetic systems.

Lam and Goussis [3] have investigated the presence of different time-scales in a series of single points of the variable space. Roussel and Fraser [4] described the evolution of kinetic systems in connection with slow manifolds. They stated that the existence of very different time scales in chemical kinetic systems causes the trajectory of the solution to move on slow manifolds. The trajectory originally moves on an  $N$  dimensional manifold, but as time advances usually the dynamical dimension of the movement decreases and after some time the trajectory moves close to a two-dimensional surface (curved plate), then close to a one-dimensional curve, and finally arrives to the zero-dimensional equilibrium or stationary point if it exists. Maas and

Pope [5] elaborated algorithms and computer codes for the approximate numerical calculation of slow manifolds. They also studied the existence of manifolds in several combustion models and generated reduced models having few variables only.

We have shown [6], [7] that the presence of low-dimensional manifolds in the composition space of dynamical systems may result in the similarity of local sensitivity functions, which is a sign of several unusual features of such systems. Sensitivity analysis investigates the effect of parameter change on the solution of mathematical models. The local sensitivity coefficient  $s_{i,k} = \partial Y_i / \partial p_k$  shows the effect of the minor change of parameter  $p_k$  on model result  $Y_i$ . In the case of a general model, no relation can be expected among the rows and columns of a local sensitivity matrix. However, the sensitivity functions may exhibit three types of similarity.

### The Similarity of Sensitivity Functions

The local sensitivity functions ( $s_{ik} = \partial Y_i / \partial p_k$ ) of chemical kinetic models may show the following types of similarity:

- (1) *Local similarity*:  $\lambda_{ij}(z) = s_{ik}(z) / s_{jk}(z)$  is equal for any parameter  $k$ , but depends on the results  $Y_i$  and  $Y_j$  investigated,
- (2) *Scaling relation*:  $\lambda_{ij}(z)$  is equal to  $(dY_i(z)/dz) / (dY_j(z)/dz)$ ,
- (3) *Global similarity*:  $\mu_{kl} = s_{ik}(z) / s_{il}(z)$  is constant in a range of the independent variable  $z$  (time or distance).

Scaling relation and global similarity (the latter under the name of self-similarity) have been described [8], but local similarity existing without scaling relation was detected by us.

Similarity of local sensitivity functions was investigated in hydrogen–air explosion and flame models. A series of models were created, consisting of homogeneous explosions and burner-stabilized and freely propagating flames. In all the cases the temperature profiles were either calculated using the assumption of adiabatic conditions, or these profiles were fixed to the previously calculated ones. All calculations were carried out at four different equivalence ratios ( $\varphi = 0.5, 1.0, 2.0, \text{ and } 4.0$ ). Carefully choosing the initial and boundary conditions, the results of all these models could be meaningfully compared. In the cases of the adiabatic explosions of hydrogen–air mixtures, all the three types of similarity were found. In other cases, either similarity existed only for some parameters or no similarity was found for any of the parameters.

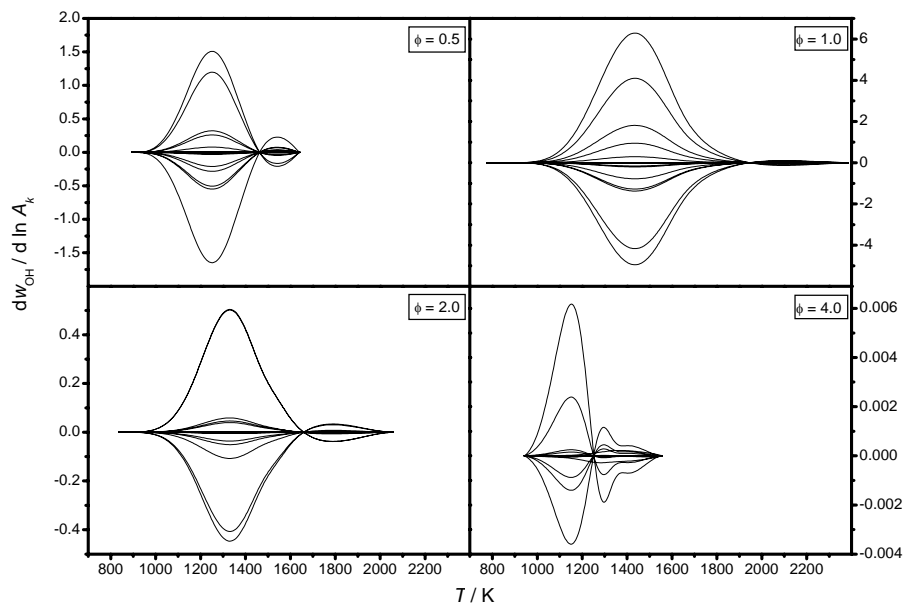


**Figure 1.** Local sensitivity functions of the mass fraction of OH with respect to the natural logarithm of the 46 pre-exponential coefficients of the reaction steps as a function of temperature, calculated for the adiabatic explosion of hydrogen–air mixtures for equivalence ratios  $\phi = 0.5$ , 1.0, 2.0 and 4.0. The sensitivity curves end at the burnt equilibrium temperature.

Adiabatic explosions of methane–air mixtures were also investigated and local similarity was found. The calculations were carried out using three different mechanisms; the similarity relations were similar in all the cases showing that this feature does not depend on the details of the reaction mechanism.

The consequence of the global similarity of the sensitivity functions is that models with different parameter sets can give almost identical simulation results for all variables in a wide range of the independent variable. This statement was illustrated with a series of numerical experiments using modified hydrogen and methane oxidation mechanisms. We have called the attention to the possible problem that using a chemical kinetic model of global similarity, fitted rate coefficients can be determined with large error, while this is not expressed in the deviation of the experimental and fitted model results.

Based on the theory of slow manifolds, an explanation was given to the local similarity and the scaling law. We have shown that scaling relation appears if the trajectory of the simulation is close to a one-dimensional slow manifold. Global similarity appears if the sensitivity functions are locally similar and the sensitivity ODE is pseudohomogeneous.

## Couplings among the reaction steps and the minimal size of the mechanisms

In the case of adiabatic models, heat effect of a reaction step may change the temperature of the reaction mixture, thus affecting the rate of others. This is called the *thermal coupling* among the reaction steps. In the case of models of spatially inhomogeneous systems, a reaction step at one location may produce a reactive species that increases the rate of other reaction steps at another location. This is called the *diffusion coupling* among the reaction steps. We have investigated the thermal and diffusion couplings among the reaction steps of hydrogen combustion models [9].

Reduced mechanisms were created using the principal component analysis of the local sensitivity matrix (PCAS method) and that of the rate sensitivity matrix (PCAF method). Global similarity was found to appear in the results of the PCAS method and its origin was explained. Our calculations indicated that the PCAS and PCAF methods have the same efficiency in mechanism reduction and produce the same results; neither the thermal coupling nor the diffusion have impact on the importance of the reactions at the oxidation of hydrogen. A 31-step minimal reduced mechanism was created that described the combustion of hydrogen at all conditions investigated. The same reactions were important in homogeneous explosions and flames, therefore diffusion coupling did not influence the importance of reactions. The same reactions were important in burner-stabilized and freely propagating flames, although the corresponding sensitivity functions were very different. Rich flames could be modelled by much fewer reaction steps than the stoichiometric and lean ones. Instead of the original 46-step mechanism, the combustion of hydrogen could be described by 15-step to 28-step mechanisms at the various conditions investigated and a 31-step mechanism could replace the original mechanism at all conditions studied.

## References

- [1] K.J. Hughes, T. Turányi, A.R. Clague, M.J. Pilling, *Int. J. Chem. Kinet.* 2001, 33, 513.
- [2] Combustion Simulations at the Leeds University and at the Eötvös University  
<http://www.chem.leeds.ac.uk/Combustion/Combustion.html>  
<http://garfield.chem.elte.hu/Combustion/Combustion.html>
- [3] S. H. Lam, D. A. Goussis, *Proc. Combust. Inst.*, 1988, 22, 931.
- [4] M. R Roussel, S. J., Fraser, *J. Chem. Phys.* 1991, 94, 7106.
- [5] U. Maas, S. B. Pope, *Combust. Flame*, 1992, 88, 239.
- [6] I. Gy. Zsély, J. Zádor, T. Turányi, *J. Phys. Chem. A*, 2003, 107, 2216.
- [7] J. Zádor, I. Gy. Zsély, T. Turányi, *Int. J. Chem. Kinet.*, 2004, 36, 238.
- [8] H. Rabitz and M.D. Smooke, *J. Phys. Chem.*, 1988, 92, 1110.
- [9] I. Gy. Zsély, T. Turányi, *Phys. Chem. Chem. Phys.*, 2003, 5, 3622.

# MASTER EQUATION SIMULATIONS OF BISTABLE AND EXCITABLE DYNAMICS IN A MODEL OF THERMOCHEMICAL SYSTEM

B. Nowakowski, A.L. Kawczyński

*Institute of Physical Chemistry, Polish Academy of Sciences,  
Kasprzaka 44/52, 01-224 Warsaw, Poland*

## Abstract

The effect of fluctuations on the dynamics of a model thermochemical system with three stationary states exhibiting two types of bistability (the coexistence of two stable focuses and the coexistence of stable focus with stable limit cycle separated by saddle point) and excitability is investigated by the master equation approach. This effect is important when the system is close to the supercritical Hopf bifurcation and to the disappearance of the stable limit cycle through the homoclinic orbit. In the last case the distribution of the first passage time from the stable limit cycle to the stable focus exhibits a few peaks. The dependence of this distribution on the number of particles is investigated.

## Introduction

Fluctuations can qualitatively change the dynamics of nonlinear, far-from-equilibrium chemical systems which are close to bifurcations. We study the effect of fluctuations in a model of thermochemical system. The system has three stationary states, two of them may be stable or unstable nodes or focuses and the third one is a saddle point. Changes of a bifurcation parameter cause the following sequence of bifurcations. One of the stable focuses becomes unstable and a stable limit cycle with “radius” growing from zero appears (the supercritical Hopf bifurcation). With increasing of the bifurcation parameter, the “radius” of the stable cycle grows. In some interval of the bifurcation parameter the system has two attractors: the stable limit cycle and the stable focus. At some critical value a homoclinic trajectory appears. The stable limit cycle disappears and the other stationary state remains the sole attractor.

## Model

A well mixed system which exchanges energy with its surroundings is considered [1]. Boundaries of the system are kept at constant temperature  $T_b$ . The system is composed of the reactant  $A$ , the product  $B$  and the catalyst  $C$ . The following reactions occur in the system:



The first reaction is exothermic with the reaction heat  $Q$ . We assume that the second reaction occurs on the walls of the system and it imitates an unspecified mechanism allowing for the supply of the reactant  $A$  and the removal of the product  $B$ . The composition of the system is uniquely determined by the concentration of  $A$ . The system exchanges energy with surroundings by the Newtonian heat flow through the boundaries. The rate constants and the coefficient of heat exchange can be presented in the following form:

$$k_1 = k_1^0 \left( \frac{T}{T_b} \right)^{1/2} \exp \left( - \frac{E_A}{k_B T} \right) \quad (3)$$

$$k_2 = \kappa p_B \quad (4)$$

$$\kappa = \kappa^0 \left( \frac{T}{T_b} \right)^{1/2} \quad (5)$$

where  $E_A$  is the activation energy, and  $p_B$  is a probability of reaction (2). Using dimensionless variables  $\alpha = n_A / n$  and  $\eta = n_C / n$ , (the molar fractions of  $A$  and  $C$ , respectively),  $\theta = T / T_b$  and  $t' = nk_1^0 t$ , the dynamics of the system is described by the following equations:

$$\frac{d\alpha}{dt'} = \sqrt{\theta} [-\alpha\eta \exp(-\varepsilon/\theta) + c_2(1 - \alpha - \eta)] \quad (6)$$

$$\frac{d\theta}{dt'} = \frac{2}{3} \sqrt{\theta} q [\alpha\eta \exp(-\varepsilon/\theta) - c_1(\theta - 1)] \quad (7)$$

where:  $\varepsilon = E_A / k_B T_b$ , and  $c_1, c_2$  are constants. The reaction heat  $q = Q / k_B T_b$  is the bifurcation parameter. In the sequel we assume that  $\varepsilon = 8$ ,  $\eta = 0.1$ ,  $c_1 = 4.747166 \times 10^{-4}$ , and  $c_2 = 6.048452 \times 10^{-4}$ . For these values of the parameters the stationary states have the following coordinates:

$SS_1$  ( $\theta_1 = 1.19273$ ,  $\alpha_1 = 0.748734$ ),  $SP$  ( $\theta_{sp} = 1.33333$ ,  $\alpha_{sp} = 0.638381$ ) and  $SS_3$  ( $\theta_3 = 1.63333$ ,  $\alpha_3 = 0.402924$ ).

For  $q_1 \cong 4.75$  the  $SS_3$  becomes unstable focus and the stable limit cycle with “radius” close to zero appears due to the supercritical Hopf bifurcation. In this range of  $q$  the  $SS_1$  is the stable focus. With increasing  $q$  the “radius” of the limit cycle grows and at  $q_2 \cong 5$  the stable limit cycle touches the separatrices of the saddle point. In consequence, the homoclinic orbit appears coming out and into the saddle point. The stable limit cycle disappears. For  $q \in [q_1, q_2]$  the system has two attractors: the stable focus  $SS_1$  and the stable limit cycle. Therefore, in this range the system is bistable. For  $q > q_2$  the system has one attractor but is excitable.

## Results

In the stochastic description, the state of the system is given by the distribution function  $P(\theta, N_A, t)$  of temperature  $\theta$  and the population  $N_A$  of species A. The dynamics of  $P$  is determined by the master equation [2]. We apply the Monte Carlo method to simulate the stochastic trajectories described by this equation.

In the bistable system, the stochastic trajectory jumps between attractors. The figure 1 shows the time dependence of temperature on time for the case when the stable focus  $SS_1$  coexists with the stable limit cycle around the unstable  $SS_3$ . Close to the bifurcation through homoclinic orbit, the limit cycle is relatively weak, and the residence times are much longer around  $SS_1$  than on the limit cycle.

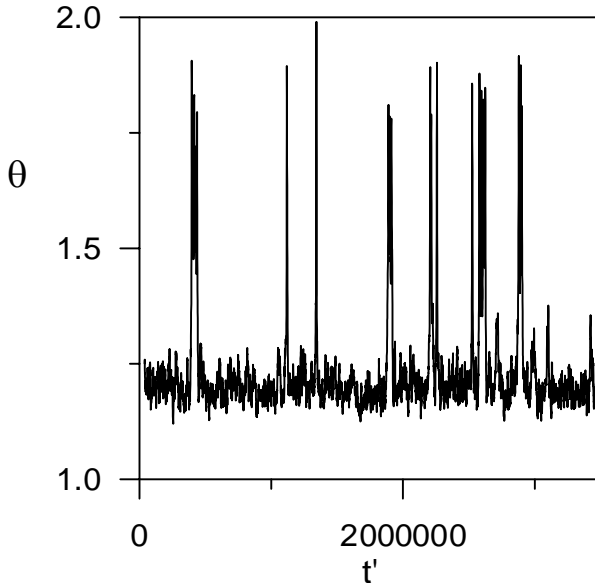


**Figure 1.**

The system escapes from  $SS_1$  when it crosses the separatrix on the boundary between the two basins of attraction. Near the bifurcation, the second separatrix, which surrounds the cycle and subsequently forms the homoclinic orbit, also passes close to the stable focus. In some cases fluctuations can push the system across both of them, and then the trajectory does not enter the basin of attraction of the limit cycle, but instead it makes a single round outside the cycle along the circulating separatrix. Thus, the large impulses observed in the evolution of the system resemble in some sense excitability of the stable focus  $SS_1$ .

From the ensemble of the stochastic trajectories we obtain the probability distribution function  $P(\tau)$  of the first passage times  $\tau$ . The figure 2 shows  $P(\tau)$  for transitions from the stable limit cycle to  $SS_1$ , for three systems containing different number of particles ( $N$ ). We count that the system leaves the limit cycle if it crosses the line  $\theta = 1.3$ , which is lower temperature than the limits of the basin of attraction of the limit cycle.

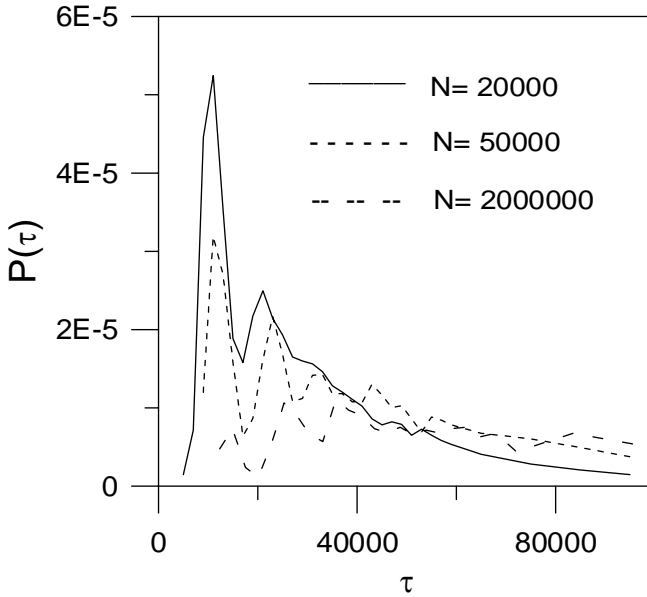


**Figure 2.**

At each round the system has a chance to leave the limit cycle, but if during circulations it does not leave the cycle before passing near the saddle point, then it makes the next round before it can leave the limit cycle. Therefore, the maximum probability of escape time returns periodically, and the probability distribution of  $\tau$  exhibits several peaks separated by approximately equal time intervals. Such form of the distribution function reflects the circulations of the system on the limit cycle. The width of the peaks follows from dephasing of the stochastic trajectory on the limit cycle. The peaks are broader for small systems, because then fluctuations more easily wipe out the phase of the stochastic trajectory. For large systems the highest peak appears for longer time  $\tau$ , because fluctuations become relatively weaker when  $N$  increases.

## References

- [1] A.L. Kawczyński and B. Nowakowski, Phys. Rev. E, 2003, 68, 036218.
- [2] B. Nowakowski and A. Lemarchand, Phys. Rev. E, 2001, 64, 061108.

## **Papers of the Poster Presentations**

# INVESTIGATION OF THE CONTROLLED INITIATION OF cAMP WAVES IN A SLIME MOLD *Dictyostelium discoideum*

P. Vaňková, M. Suchá, H. Ševčíková

*Center for Nonlinear Dynamics of Chemical and Biological Systems, Institute of Chemical Technology, Prague, Technická 5, 166 28 Prague 6, Czech Republic*

## Abstract

The population of synchronised cells of *Dictyostelium discoideum* is investigated as a candidate excitable medium for studies of controlled initiation of cAMP waves during aggregation stage of the organism's morphogenesis. It has been found that cAMP waves are of a short range that can prove as unsuitable for controlled initiation experiments.

## Introduction

The population of starving cells of a slime mold *Dictyostelium discoideum* (*DD*) has been widely used as a model system for studies of nonlinear phenomena in biological systems. *DD* cells are amoeboid cells, that move independently in a population until the adverse living conditions (lack of nutrients) make them to develop a co-operative behaviour. After few (4 – 6) hours of starvation some cells become leading members of the population and start to periodically produce 3',5'-cyclic adenosin monophosphate (cAMP). This substance is excreted to the extracellular space where it diffuses to other cells in the population. These cells respond to the increased concentration of cAMP in their neighborhood by i) the onset of cAMP synthesis and excretion and ii) chemotactic motion against the gradient of cAMP, i.e. towards the leading cells. The process repeats for a several hours period at the end of which the cells gather in mounds containing app.  $10^5$  cells. A morphogenesis of the organism is then triggered leading to the development of fruiting bodies carrying spores that preserve the organism's life until the suitable living conditions are restored [1,2].

In terms of dynamical theories of nonlinear systems, the population of starving *DD* cells represent an excitable medium through which the pulse waves of cAMP propagate. The leading members represent the regions of spontaneous oscillations that serve as a natural source of the waves. Detailed investigation of excitable properties of cAMP waves is often precluded by the fact, that waves arise randomly, both in time and space, that leads in formation of irregular wave patterns. The random character of the cell population behaviour results from the differences in the phases of the vegetative cycle at which cells are stopped at the moment of taking the nutrients away [3,4].

In this paper we present results of the experiment where the cell layer was synchronized by pulsing the cell suspension with the periodic addition of cAMP solution [5]. This method of synchronization has been commonly used when a chemotactic activity of *DD* cells is studied. So far, the synchronized culture was not used for aggregation experiments.

## Experimental

The experiments were performed with AX2 strain of DD obtained from the laboratory of Prof. Peter Folk, Charles University, Prague. The cell culture was cultivated from spores in a liquid HL5 medium in a dark room at 21°C and harvested at the cell density  $2 \div 6 \times 10^6$  cells/ml. After centrifugation and double washing with phosphate buffer the cells were divided in two portions that were treated separately. One half of cells, used as a control sample, was spread over a nutrition-free agar in a Petri dish while the second half was subject to synchronisation. The cell suspension was diluted to  $5 \times 10^6$  cells/ml, placed on a shaker where it was treated with pulses of cAMP solution (10  $\mu$ l; 30  $\mu$ M) added every 6 min for 4 hours. The cell suspension was then centrifuged and double-washed with phosphate buffer and spread on the nutrition-free agar on Petri dishes. Petri dishes with both synchronised and control cells were kept in the dark at 21 °C until the cAMP waves became visible.

The cell layers on Petri dishes were observed both by dark-field photography and in a phase contrast under the microscope. Two CCD cameras connected to two PCs were used to record the development of cell populations. For evaluation the commercial software LUCIA [7] was used. Dark-field photography enable to observe the propagation of cAMP waves and the aggregation process; to observe next developmental stages the microscope has to be used.

## Results and Discussion

Development of both control and synchronised cells is illustrated in Figure 1. In control cells (C-cells) the first waves were usually observed at around 6.5 hours after the beginning of starvation (Fig.1a). The development of synchronised cells (S-cells) started approximately 5 hours later, the time interval the cells spent in the shaken suspension pulsed with cAMP solution. The first waves became visible at 10.5 hours. More wave emitting centres form in S-cells and the waves span over shorter distances than in C-cells (cf. Fig. 1a and b). The aggregation territories emerge at approximately same time in both C and S cells, i.e. at around 11 and 12 hours, resp. The population of C-cells breaks-up to large territories within which the cells form streams along which they crawl to the centre (see Fig. 1b). The aggregation territories in the population of S-cells are small and, very soon, they break down to a large number of mound clusters. No cell streams were observed (see Fig. 1d). The appearance of slugs in S-cells is also delayed when compared to C-cells, though it seemed to catch up with that in C-cells (19 h and 21 h, resp.). At the end of experiment (24 h) fruiting bodies were formed in C-cells only.

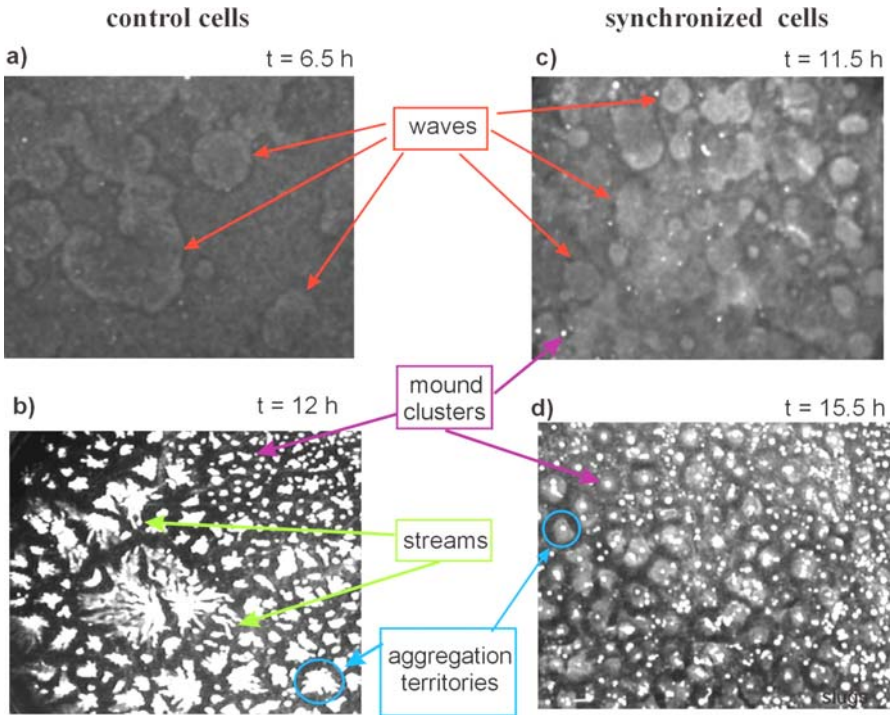


**Figure 1.** Aggregation stage of control and synchronized cells. Panel sizes: 20 x 39 mm.

The most intriguing difference between developmental behaviour of C and S cells rely in the absence of cell streams in the S-cells population. Detail images of the aggregation process as seen under the microscope are shown in Fig. 2. We can see that in both C and S cells the large cluster of cells is first formed within an aggregation territory that later breaks down to many mounds. In C-cells, the aggregation territory ruled by one mound cluster consist of well packed cells in the centre and disintegrates into many thin, long branches or streams at the periphery. In streams, the cells are glued tightly together and piled on top of each other and, thus, the cell structure of the stream is indistinguishable (cf. Fig. 2b). In the population of S-cells, all cells move towards the centre as a crowd and, at the periphery, the individual cells are clearly distinguishable (cf. Fig. 2d). The cells are protracted, with many pseudopods and form short chains. Unlike in C cell population they do not glue together.

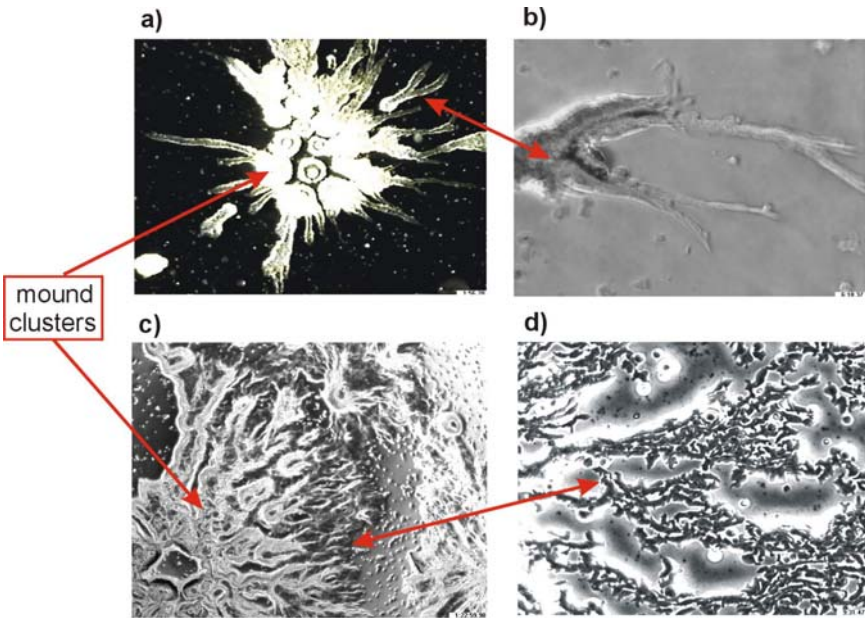


**Figure 2.** Mounds and streams in control [a),b)] and synchronized [c),d)] cells. Sizes of observation areas: a), c) 1.9 x 2.4 mm; b), d) 0.38 x 0.5 mm.

## Conclusions

This paper focuses on comparing the development of control (C) and synchronized (S) populations of cells of slime mold *Dictyostelium discoideum*. It has been found that only short cAMP waves can propagate through S-cells populations. That makes the S-cells unsuitable for detail investigation of cAMP wave propagation. Thus other ways of cell synchronization should be tried.

## Acknowledgement

This work has been supported by the grants No.: 204/04/1421 and 104/03/H141 of GA CR and by the Research Project of the Ministry of Education of the Czech Republic MSM 223400007.

## References

- [1] P. Devreotes, Science, 1989, 245, 1054.
- [2] D. Dormann, B. Vasiev, C.J. Weijer, J. of Biol. Physics, 2002, 28, 765.
- [3] M. Wang, J.R.Aerts, W. Spek, P. Schaap, Dev. Biol., 1988, 125, 410.
- [4] T. Ohmori, Y. Maeda, Cell Differentiation, 1987, 22, 11.
- [5] M. Zhao, T. Jin, C.D. McCaig, J.V. Forrester, P.N. Devreotes, J. Cell Biology, 2002, 157, 921.
- [6] LUCIA – A System for Image Analysis, Laboratory Imaging s.r.o. ([www.lim.cz](http://www.lim.cz)).

## INDUCTION OF OSCILLATORY TRANSMEMBRANE TRANSPORT BY AMMONIUM ION

Č. Radenović<sup>1</sup>, M. Beljanski<sup>2</sup>, A. Ergelj<sup>3</sup>, G.V. Maksimov<sup>4</sup>

<sup>1</sup>The maize Research Institute "Zemun Polje", Belgrade, <sup>2</sup>Faculty of Physical Chemistry, Belgrade,

<sup>3</sup>Institute of General and Physical Chemistry, Belgrade, Serbia and Montenegro, <sup>4</sup>Lomonosov State University, Moscow, Russia

### Abstract

Using different concentrations of  $\text{NH}_4\text{Cl}$  as an stimulant, four types of oscillations of transmembrane bioelectric potential has been observed on algal (*Nittela*) cells as a model system. Characteristics of oscillatons depends on  $\text{NH}_4\text{Cl}$  concentration and generally, physiological state of observed cell i.e., different types of transmembrane transport process that are active during measurements.

### Introduction

Ritmicity and oscillatory behavior are among principal characteristics of life. Oscillations of bioelectric membrane potential have been discovered fifty years ago [1]. Oscillations may be induced both by physical (mechanic, temperature, electric, light) and chemical (action of certain chemicals, change of concentration) factors [2, 4]. Here we describe induction of oscillations of transmembrane bioelectric potential with increasing concentrations of  $\text{NH}_4\text{Cl}$ , using freshwater alga *Nittela* as a model system.

### Results and Discussion

Registration of oscillatory bioelectrical impulses of membrane potential has been performed using microelectrode technique as described previously [3, 4]. Tab I. gives membrane status (membrane resting potential and cyclosis), before  $\text{NH}_4\text{Cl}$  treatment, while Tab II. gives characteristic parameters for different class of oscillations.

On the bases of response to different concentrations of  $\text{NH}_4\text{Cl}$  and oscliiatory period duration, four classes of oscillations may be observed. First class of oscillations (Fig. 1. a, Tab. II.I), is characterized by small number of impulses and short time (~25 min) of oscillations. Second class of oscillations (Fig. 1. b, Tab II.II) is characterized by longer oscillatory period (~40 min), and by changing in impulses intensity. Third class of oscillations (Fig. 1. c, Tab II.III) is characterized by presence of preoscillatory period of local impulses and longer time (~150 min). Fourth class of oscillations (Fig. 1. d, Tab. II.IV) is characterized by preosilatory period and very long time (~5 hour) of oscillations.

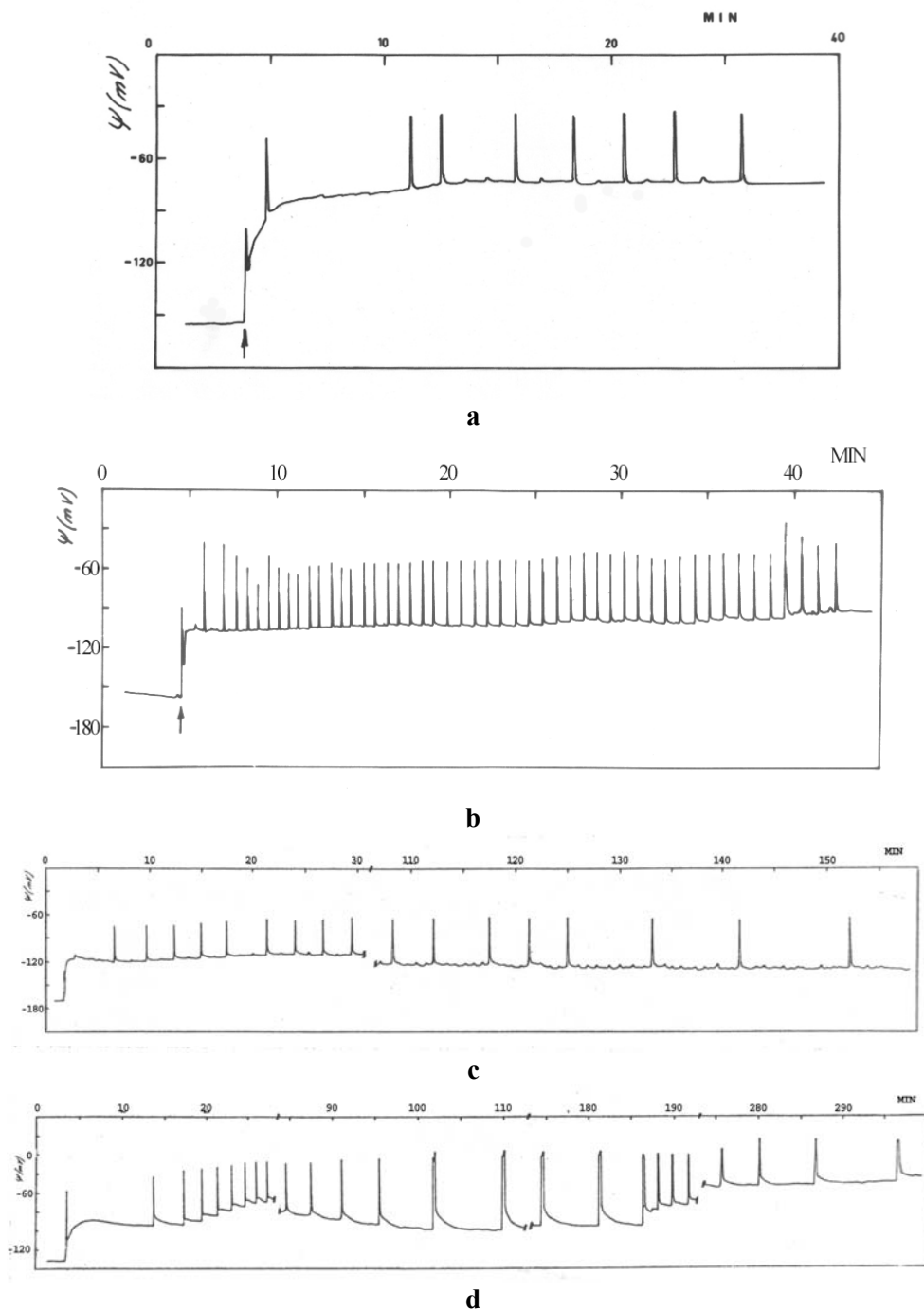


**Fig. 1:** Four class of oscillations induced by different concentrations of  $\text{NH}_4\text{Cl}$ .  
 a) 3.0 mM, b) 7.0 mM, c) 10 mM, d) 10 mM  $\text{NH}_4\text{Cl}$ .

Appearance of oscillations depends on  $\text{NH}_4\text{Cl}$  concentration (being more probable at higher concentrations: 8-10 mM), and individual spike duration is between 2 and 4 sec (sometimes longer: 6-8 sec). It is important to note that it is technically hard to get completely identical oscillations, due inaccuracy of electrode positioning.

Characteristics of oscillations depends on  $\text{NH}_4\text{Cl}$  concentration and generally, physiological state of observed cell i.e., different types of transmembrane transport process that are active during measurements.

**Table I.**

Membrane resting potential ( $\psi_m$ , mV)	Cyclosis ( $\mu\text{/sec}$ )	Standard solution for bioelectric measurements
Average values:		
-90	45	0.1 mM HCl + 1.0mM NaCl
-120	50	
-150	52	

**Table II.**

Oscillations class	Membrane potential oscillation duration (min)	Preoscillatory period duration (min)	Oscillatory period duration (min)	Single oscillation frequency appearance (osc/min)	Oscillations relative amplitude (mV)	$\text{NH}_4\text{Cl}$ conc. (mM)
I	25.60	0.09	25.51	0.35	40.35	3.0
II	38.04	0.00	38.04	1.31	$X_{av}=49.67$	7.0
III	Whole	4.72	151.62	0.31	$X_{av}=44.20$	10.0
	I part					
	II part					
IV	Whole	0.00	295.63	0.21	$X_{av}=99.28$	10.0
	I part					
	II part					
	III part					
	IV part					

### Acknowledgement

Present investigations are partially supported by the Ministry of Sciences and Environmental Protection of Serbia under the project Physical chemistry of Dynamic states and structures of non-equilibrium systems – self-organization, multistability and oscillatory (project no. 1448).

### Literature:

- [1] Radenović Č., Bioelektrične pojave biljnih sistema, Nolit, Beograd, 1974.
- [2] Radenović Č. and Pencić M., Physiol. Plant., 1970, 23, 697.
- [3] Radenović Č. et al., Biofizika, AN SSSR, 1968, 13, 207.
- [4] Radenović Č. et al., 1977, In: Electrical Phenomena at the Biological Membrane, Level (Roux., E. Eds.). Elsevier Sci. Pub Co., Amsterdam, 25.

## MODELLING OF THE HYPOTHALAMIC-PITUITARY-ADRENAL SYSTEM ACTIVITY

S. Jelić<sup>1</sup>, Ž. Čupić<sup>2</sup>, Lj. Kolar-Anić<sup>3</sup>

<sup>1</sup>*Department of Theoretical Physics and Physics of Condensed Matter, The Vinča institute of Nuclear Sciences, Belgrade,* <sup>2</sup>*Institute of Chemistry, Technology and Metallurgy, Department of Catalysis and Chemical Engineering, Njegoševa 12, Belgrade,* <sup>3</sup>*Faculty of Physical Chemistry, Studentski trg 12-16, Beograd, Serbia and Montenegro*

### Abstract

Modelling has proven to be valuable in understanding of the complex biological systems dynamics. We have developed a model of the hypothalamic-pituitary-adrenal system self-regulatory activity to describe empirically observed oscillatory behaviour of this neuroendocrine system.

### Introduction

The hypothalamic-pituitary-adrenal (HPA) system operates as complex feedforward and feedback control system whose main purpose is to regulate wide variety of bodily processes, under basal physiological conditions or during stress, by regulating the level of plasma corticosteroids secreted from adrenal glands (see Fig. 1). The hypothalamic paraventricular nucleus (PVN) is part of the hypothalamus which controls the secretion of corticotrophin-releasing-hormone (CRH) and arginin-vasopressin (AVP) into the pituitary portal circulation, as well as other neuropeptides. CRH and AVP secretion leads to pituitary release of adrenocorticotropin (ACTH) and consequential adrenal gland stimulation, with release of corticosteroids (glucocorticoids, whose main representative in humans is cortisol, and corticosteron in animals, and mineralocorticoids, whose main representative is aldosterone) from appropriate adrenal cortex zones (the zona glomerulosa and zona fasciculata respectively) [1]. The HPA axis activity is restricted by negative glucocorticoid feedback at brain areas known to have mineralocorticoid (MR) and glucocorticoid (GR) receptors and to be involved in the control of the HPA axis: hippocampus, hypothalamus and pituitary [2-4]. Along with their negative feedback effects glucocorticoids can act positively on the CRH gene expression in the brain and placenta [4-6]. This positive feedback is life-sustaining as it keeps the organism responsive to acute stressors under conditions of chronic stress [5].

### Results and Discussion

Since GR is expressed in most peripheral cell types, but not in SCN neurons [7], we shall consider the control influences of the SCN on the secretion of CRH as an external factor. Ultra-short feedback loops by which CRH and ACTH may influence their own production are also neglected here. AVP plays an important role in augmenting the actions of CRH in activating the HPA axis, especially in the chronic stress conditions, but we are not describing AVP secretion because it has less effects on cortisol secretion when it doesn't act in synergy with CRH, and because only some AVP se-

creting neurons in hypothalamus are under the negative feedback effects of cortisol. Since cortisol is not the only physiologically active ligand of MR, we have considered aldosterone influences as well.

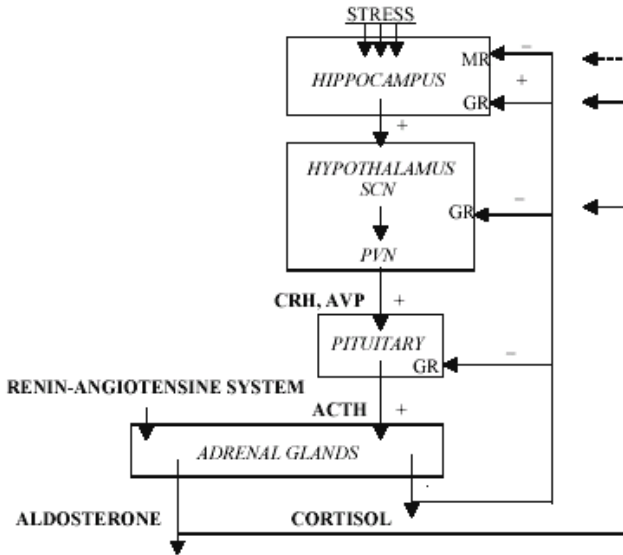
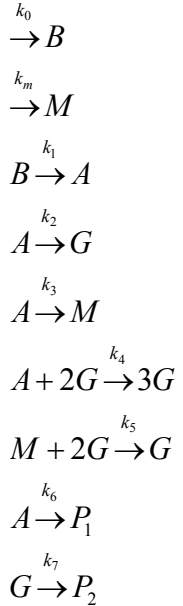


**Figure 1.** The hypothalamic-pituitary-adrenal system feedforward and feedback loops.



**Scheme 1.** Model

Aldosterone occupies some smaller, compared to total, number of the hippocampal MR, thus making them unable to bind cortisol. Aldosterone activation of the hippocampal MR influences GR activation in the hippocampus as well, “pushing” cortisol that way, thus making its positive feedback stronger and negative feedback actions weaker. In the hypothalamus aldosterone makes negative cortisol feedback, exerted through GR, stronger, and in the pituitary aldosterone influences could be neglect in basal conditions. Under these assumptions, the processes taking place could be represented by the simplified model given in Scheme 1.

Here letters B, A, G and M represent CRH, ACTH, cortisol and aldosterone plasma concentrations, while P<sub>1</sub> and P<sub>2</sub> represent the products of ACTH and cortisol elimination, described by the last two equations of this model. The first equation describes basal CRH production from the PVN, the second one describes aldosterone production under the renin-angiotensin system control. The third equation represents ACTH production from the pituitary, stimulated by CRH and the following two are simplified descriptions of the cortisol and aldosterone production from adrenal cortex stimulated by ACTH. The sixth equation describes positive feedback actions of cortisol, acting through hippocampal GR to enhance CRH gene expression and consequentially ACTH and cortisol production. The next one represents cortisol negative feed-

back acting through hippocampal MR (where aldosterone and cortisol “fight for” the same receptors), as well as hypothalamic and pituitary GR. The kinetic equations associated with the model (Scheme 1) are:

$$\begin{aligned}
 dB(t)/dt &= k_0 - k_1 B \\
 dA(t)/dt &= k_1 B - k_2 A - k_3 A - k_4 A G^2 - k_6 A \\
 dG(t)/dt &= k_2 A + k_4 A G^2 - k_5 M G^2 - k_7 G \\
 dM(t)/dt &= k_m + k_3 A - k_5 M G^2
 \end{aligned} \tag{1}$$

If we assume that CRH and aldosterone have much slower dynamics compared to ACTH and cortisol, we can take  $dB/dt = 0$  and  $dM/dt = 0$  ( $\Rightarrow k_3 M G^2 = k_m + k_3 A$ ), and consider the dynamics of the two-dimensional “faster” system

$$\begin{aligned}
 dA(t)/dt &= k_0 - k_2 A - k_3 A - k_4 A G^2 - k_6 A \\
 dG(t)/dt &= k_2 A + k_4 A G^2 - k_m - k_3 A - k_7 G
 \end{aligned} \tag{2}$$

The stability analysis and numerical simulations were performed (Fig.2).

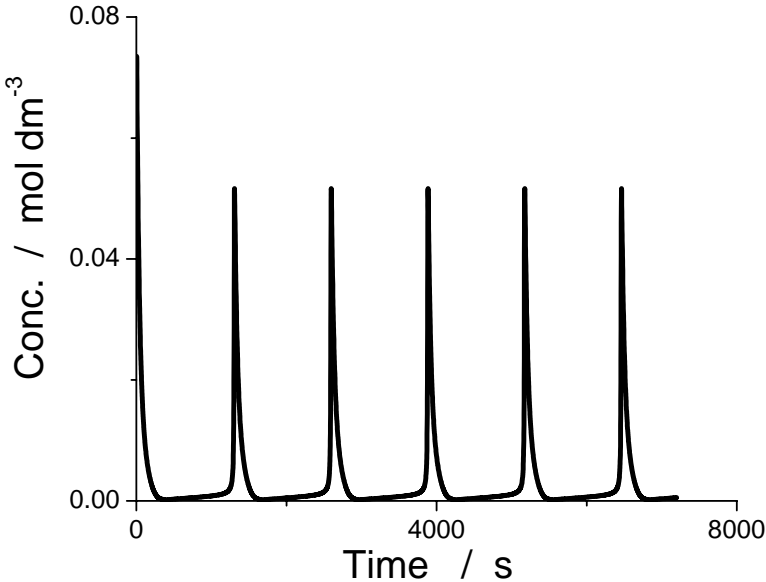


**Figure 2.** Numerical simulation of the cortisol oscillations in time, obtained with backward differentiation formulas - Gear's method, applied on the eq. 2.

$$\begin{aligned}
 A(0) &= 0.04 \text{ mol dm}^{-3}; G(0) = 0.04 \text{ mol dm}^{-3}; k_0 = 2 \cdot 10^{-4} \text{ mol dm}^{-3} \text{ s}^{-1}; k_2 = 3.125 \cdot 10^{-4} \text{ s}^{-1}; \\
 k_3 &= 5 \cdot 10^{-5} \text{ s}^{-1}; k_4 = 2.5 \cdot 10^2 \text{ mol}^{-2} \text{ dm}^6 \text{ s}^{-1}; k_6 = 2.5 \cdot 10^{-3} \text{ s}^{-1}; k_7 = 2.5 \cdot 10^{-2} \text{ s}^{-1}; \\
 k_m &= 5 \cdot 10^{-6} \text{ mol dm}^{-3} \text{ s}^{-1}.
 \end{aligned}$$

## Conclusions

The mathematical model of the HPA axis presented in this report is the first, to our knowledge, that takes into account the positive feedback effects of cortisol exerted at the level of hippocampal GR, where it stimulates CRH gene expression, thus stimulating ACTH and its own production, besides its well-known, classical, negative feedback effects at the level of hippocampal MR, and hypothalamic and pituitary GR, and the influence of aldosterone on these feedforward and feedback pathways.

## Acknowledgement

Present investigations are partially supported by the Ministry of Sciences and Environmental Protection of Serbia under the project no. 1225, 1448, 1807.

## References

- [1] A. Balsalobre, S.A. Brown, L. Marcacci, F. Tronche, C. Kellendonk, H.M. Reichardt, G. Scuty, U. Schibler, *Science*, 2000, 289, 2344.
- [2] B.S. McEwen. *J. Appl. Physiol.*, 2001, 91, 2785.
- [3] C. Kellendonk, P. Gass, O. Kretz, G. Shultz, F. Tronche, *Brain Res. Bulliten*, 2002, 57, 73.
- [4] C. Tsigos, G.P. Chrousos, *J. Psychosom. Res.*, 2002, 53, 865.
- [5] F. Holsboer, *Neuropsychopharmacology*, 2000, 23, 477.
- [6] M.B. Muller, F Holsboer, ME Keck, *Neuropeptides*, 2002, 36, 117.
- [7] P. Gray, S.K. Scott, *Chemical oscillations and Instabilities-Non-linear Chemical Kinetics*, Claredon Press, Oxford, 1990.
- [8] R.H. deRijk, M. Schaaf, E.R. de Kloet, *J. Steroid Biochem. & Mol. Biol.*, 2002, 81, 103.

## CORRELATION OF SECONDARY STRUCTURE TYPES WITH NEARBY AMINO ACIDS

S. Malkov<sup>1</sup>, M. Živković<sup>1</sup>, M. Beljanski<sup>2</sup>, S. Zarić<sup>3</sup>

<sup>1</sup>Faculty of Mathematics, Belgrade, <sup>2</sup>Institute of General and Physical Chemistry, Belgrade, <sup>3</sup>Faculty of Chemistry, Belgrade, Serbia and Montenegro

### Abstract

The statistical correlation is used as a new quantitative description of the relation of the primary and secondary structure.

### Introduction

It is known that protein primary structure determines its overall organization. In other words, the protein is capable of self-organizing in accordance with the information contained in its primary structure. Hardness on protein structure determination makes important the secondary structure prediction, as an intermediate step. Protein secondary structure dependence on its primary structure has been described in [1], using the information measure that amino acid  $R_j$  carries about an element of secondary structure  $S_i$ . Information measure depends on the mutual and single probabilities and it is computed according to

$$I(S_j; R_i) = \log \frac{P(S_j | R_i)}{P(S_j)} \quad (1)$$

where  $R_j$  is amino acid at position  $j$ , and  $S_i$  is a secondary structure type at position  $i$ . This measure is referred to as *directional parameter*.

The information measure about the secondary structure type in position  $j$  contained in a window of the range  $M$  around the position  $j$  is then denoted by  $I(S_j; R_{j-M} \dots R_{j-1} R_j R_{j+1} \dots R_{j+M})$ . That quantity is considered in [2] for fixed  $M=8$ , and it is approximated by

$$I(S_j; R_{j-M} \dots R_{j-1} R_j R_{j+1} \dots R_{j+M}) = \sum_{i=-M}^M I(S_j; R_{j+i}) \quad (2)$$

The idea of secondary structure prediction is to choose the secondary structure type that maximizes this sum. More precisely, secondary structure is predicted in [2] using the relation

$$I(S_j; R_{j-M} \dots R_{j-1} R_j R_{j+1} \dots R_{j+M}) = \underset{k=j-(n_s-1)}{MAX} \left[ \frac{1}{n_s} \sum_{i=k}^{i=k+n_s-1} I(S_j; R_i) - DC_S \right] \quad (3)$$

where parameters  $n_s$  and  $DC_S$  depend on the secondary structure type  $S$ .

Directional parameters (1) are estimated in [2] on the basis of 25, and later in [3] on 68 protein sequences, consisting of about 12000 amino acids. Tables, containing the values of these parameters are given in [3], and their dependence on the distance  $i-j$  for

some particular pairs of amino acids and secondary structure types is qualitatively discussed.

## Results

Here we describe the relation of the protein primary and secondary structure using the statistical correlation. While directional parameter (1) is computed based on three out of four mutual probabilities for chosen amino acid and for fixed secondary structure, the statistical correlation depends on all four of them

$$\rho(S_j, R_i) = \frac{P(S_j R_i) - P(S_j)P(R_i)}{\sqrt{P(S_j)(1 - P(S_j))P(R_i)(1 - P(R_i))}} \quad (4)$$

Correlation values belong to the range from  $-1$  to  $1$ . Positive (negative) values mean that the presence of the amino acid in the position  $i$  "promotes" ("suppresses") the appearance of the given secondary structure type at position  $j$ .

Correlation parameters are computed based on protein secondary structure data, obtained by applying the program DSSP [4] to protein structure data from PDB [5]. In fact, the representative protein subset PDBSELECT [6] with the threshold of 25% is used, containing 1737 sequences with 282329 amino acids. The eight different secondary structure types are considered, as opposed to [3], where only four secondary structure types are dealt with.

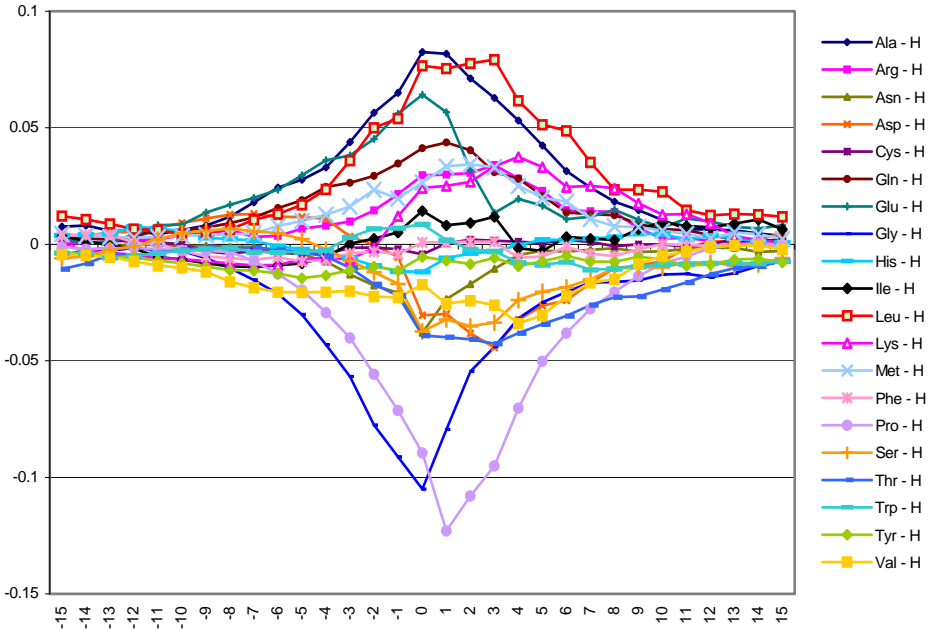


**Figure 1.** Correlation parameters for  $\alpha$ -helix and distances less than 15.

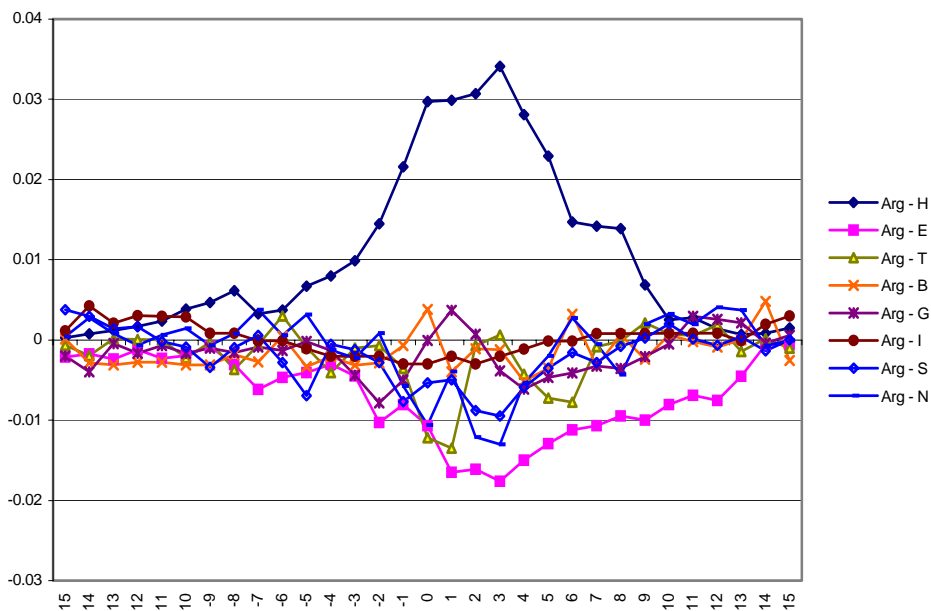


**Figure 2.** Correlation parameters for the Arginine.

The correlations are analyzed in the distance range from 0 to 25 (in both directions), giving 8160 ( $20 \times 8 \times 51$ ) correlation parameters. The  $\alpha$ -helix parameter values for distances less than 15 are shown in Fig. 1. The parameter values for Arginine are shown in Fig. 2, in the same distance range. Remarkable asymmetry of the Arginine correlation with the  $\alpha$ -helix appearance can be observed: the correlation values are higher towards N-, than towards the C-terminal.

Similar diagrams are obtained for other secondary structures and for all amino acids. The general shape of these diagrams is similar to those for directional parameters, computed according to (1) as in [1]. The “noise” outside the central region of these diagrams is less, if correlation parameters are used. It is believed that correlation parameters could be used to improve the secondary structure prediction in GOR algorithms.

## References

- [1] B. Robson, *Biochem. J.*, 1974, 141, 235.
- [2] J. Garnier, *J. Mol. Biol.*, 1978, 120, 97.
- [3] J.-F. Gibrat, *J. Mol. Biol.*, 1987, 198, 425.
- [4] W. Kabsch, *Biopol.*, 1983, 22, 2577.
- [5] H. M. Berman, *Nucleic Acids Res.*, 2000, 28(I), 235.
- [6] U. Hobohm, *Prot. Sci.*, 1994, 3, 522.

# ANALYTIC SOLUTIONS FOR TRAVELING WAVES IN A 3-COMPONENT REACTION-DIFFUSION MODEL

E. P. Zemskov, K. Kassner

*Institut für Theoretische Physik, Otto-von-Guericke-Universität Magdeburg,  
Universitätsplatz 2, 39106 Magdeburg, Germany*

## Abstract

An 1-dimensional 3-component reaction-diffusion system with one activator and two inhibitors is considered. An analytical treatment is possible since the nonlinear activator reaction term is approximated by a piecewise linear function. As a particular case we choose a semisymmetric inhibition and obtain general traveling wave solutions.

## Introduction

Reaction-diffusion equations play an important role in nonlinear dynamics. Due to the nonlinearity of the reaction terms, the theoretical treatment of the problems is complicated. In the approach to be presented in this paper, the nonlinearity is approximated by a piecewise linear function. Piecewise linear approximations of the nonlinear term have been employed in a number of situations [1,2] and have the advantage of enabling the reduction of existence problems for traveling waves to root finding for certain nonlinear algebraic equations.

## Results and Discussion

An 1D three-component activator-inhibitor model with one activator and two inhibitors [3] describing excitable media in terms of reaction-diffusion equations consists of three scalar fields  $u(x,t)$ ,  $v(x,t)$  and  $w(x,t)$  and is described by the system

$$\begin{aligned}\frac{\partial u(x,t)}{\partial t} &= f(u) - v - w + \frac{\partial^2 u(x,t)}{\partial x^2}, \\ \frac{\partial v(x,t)}{\partial t} &= \varepsilon u - \beta v + \frac{\partial^2 v(x,t)}{\partial x^2}, \\ \frac{\partial w(x,t)}{\partial t} &= \varepsilon' u - \beta' w + \frac{\partial^2 w(x,t)}{\partial x^2}, \quad \varepsilon, \beta, \varepsilon', \beta' = \text{const},\end{aligned}$$

where the rate function  $f(u)$  is the activator reaction term which characterizes the nonlinearity of the system. For many reaction-diffusion models (activator-inhibitor systems) the  $f(u)$  term has inverted N-shaped (cubic) or V-shaped (quadratic) profiles on the  $u - f(u)$  diagram. As a basis for the calculation we use here a piecewise linear approximation of the  $f(u)$  term, consisting of two shifted linear pieces:

$$f(u) = -\alpha u - 1 \quad \text{at } u < 0 \quad \text{and}$$

$$f(u) = -\alpha u + 1 \quad \text{at } u > 0, \quad \alpha = \text{const.}$$

The focus of our considerations is a traveling wave solution. Therefore, we introduce the traveling frame coordinate  $\xi = x - ct$ , where  $c$  is the wave velocity, and rewrite the model equations in the form of traveling wave equations

$$\frac{d^2 u(\xi)}{d\xi^2} + c \frac{du(\xi)}{d\xi} + f(u) - v - w = 0$$

$$\frac{d^2 v(\xi)}{d\xi^2} + c \frac{dv(\xi)}{d\xi} + \varepsilon u - \beta v = 0$$

$$\frac{d^2 w(\xi)}{d\xi^2} + c \frac{dw(\xi)}{d\xi} + \varepsilon' u - \beta' w = 0$$

Thanks to the piecewise linear character of the model, the solutions for each piece are expressed as superpositions of six exponentials (the solutions contain cosine and sine terms when  $\lambda_n$  acquire imaginary parts)

$$u(\xi) = \sum_{n=1}^6 A_n e^{\lambda_n \xi} + \text{const.},$$

$$v(\xi) = \sum_{n=1}^6 B_n e^{\lambda_n \xi} + \text{const.},$$

$$w(\xi) = \sum_{n=1}^6 B'_n e^{\lambda_n \xi} + \text{const.}$$

Here  $A_n, B_n$  and  $B'_n$  are constants and  $\lambda_n$  are the eigenvalues. We consider here a particular case of semisymmetric inhibition where  $\beta = \beta'$ . In this case the eigenvalues read

$$\lambda_{1,2} = -c/2 \pm \sqrt{c^2/4 + \gamma_0},$$

$$\lambda_{3,4} = -c/2 \pm \sqrt{c^2/4 + \gamma_1},$$

$$\lambda_{5,6} = -c/2 \pm \sqrt{c^2/4 + \gamma_2},$$

where

$$\gamma_0 = \beta, \gamma_{1,2} = (\alpha + \beta)/2 \pm \sqrt{(\alpha + \beta)^2/4 - \alpha\beta - (\varepsilon + \varepsilon')}.$$

The constants  $A_n$  and  $B'_n$  can be expressed as

$$A_{1,2} = 0, A_{3,4} = \frac{\beta - \gamma_1}{\varepsilon} B_{3,4}, A_{5,6} = \frac{\beta - \gamma_2}{\varepsilon} B_{5,6},$$

$$B'_{1,2} = -B_{1,2}, B'_{3-6} = \frac{\varepsilon'}{\varepsilon} B_{3-6}.$$

These solutions must satisfy appropriate boundary conditions for fronts (heteroclinic) or pulses (homoclinic). Front and pulse solutions consist of two and three pieces, respectively. After the matching procedure [4], we obtain wave solutions and the corresponding velocity equation. The details will be published elsewhere.

## Conclusion

The analytic solutions of the problem of wave propagation in reaction-diffusion systems that we present are much simpler than the standard solutions through numerical calculus. We have considered the model with inverted N type of nullcline which correspond to cubic nonlinearity. However, the piecewise linear approximation can be made for systems with more complicated nonlinear reaction terms leading to a generalization to multistable cases, which may be considered in the context of the above described approach.

Here we have considered an idealized free model. Real systems contain perturbations. Wave propagation in the considered systems can be effectively controlled by application of an external forcing. This forcing can be prescribed a priori, i.e., as a modulation of excitability. If we consider a forcing that is moving with the wave, then the translation invariance of the model equations is violated and the wave solution depends on the phase value, i.e., we have a family of wave solutions with different phases [5].

## Acknowledgements.

The authors acknowledge support by the DFG, grant FOR 301/2-1 (3), in the framework of a research group on "Interface dynamics in pattern forming processes".

## References

- [1] A. S. Mikhailov, Foundations of Synergetics I. Distributed Active Systems, Springer, Berlin, 1994.
- [2] V. S. Zykov, Simulation of Wave Processes in Excitable Media, Manchester University Press, New York, 1987.
- [3] M. Or-Guil, M. Bode, C. P. Schenk, H.-G. Purwins, Phys. Rev. E, 1998, 57, 6432.
- [4] E. P. Zemskov, V. S. Zykov, K. Kassner, S. C. Müller, Nonlinearity, 2000, 13, 2063.
- [5] E. P. Zemskov, K. Kassner, S. C. Müller, Eur. Phys. J B, 2003, 34, 285.

# THE MATHEMATICAL STUDY OF SPONTANEOUS EXCITATIONS IN SPATIALLY 1D AND 2D MEDIA

T. Godula, H. Ševčíková

*Center for Nonlinear Dynamics of Chemical and Biological Systems,  
Institute of Chemical Technology, Prague, Technická 5, 166 28 Prague 6, Czech Republic.*

## Abstract

The paper presented is focused into studies of responses of one- and two-dimensional excitable media to a pulse-like stimulus applied in the refractory tail of a travelling wave of excitation. As a model of an excitable medium the three variable reaction-diffusion model representing the population of starving cells of a slime mould *Dicystelium discoideum* (*DD*) is utilized.

## Introduction

A propagation of excitation along one- or two-dimensional media is essential for living organisms where it provides for various functions, such as travelling of action potentials along neuron fibres, propagation of contractions in heart muscle, communication between cells in cellular populations, etc. In many cases, the most salient feature of excitable media, i.e. one-to-one response to the pulse-like stimulus, is vital for normal functioning of the system. On the other hand, the situations, where the travelling excitation emerge without stimulus, can be pathological and life threatening, as e.g. the fibrillations of heart muscle. Therefore, the investigations of conditions under which the spontaneous excitation can arise in excitable media are of a great interest [1,2].

## Mathematical Model

The modelled system is formed by a layer of starving cells of *DD* through which the population waves of increased concentration of cAMP (cyclic 3',5'-adenosine monophosphate) propagate. The waves mediate the communication between cells, their aggregation in mounds and further morphogenesis of *DD* [3].

The mathematical model is based on the cellular mechanism of biochemical production, excretion and decomposition of cAMP proposed by Martiel and Goldbeter [4] and on the idea of diffusion of extracellular cAMP in the extracellular space [5]:

$$\partial\beta/\partial t = q\sigma\Phi(\rho_T, \gamma, \alpha) - (k_i - k_r)\beta \quad (1)$$

$$\partial\gamma/\partial t = (k_i\beta/h) - k_e\gamma + D_\gamma\nabla^2\gamma \quad (2)$$

$$\partial\rho_T/\partial t = -f_1(\gamma)\rho_T + f_2(\gamma)(1 - \rho_T) \quad (3)$$

where  $\beta$  ( $\gamma$ ) correspond to concentrations of intracellular (extracellular) cAMP and  $\rho_T$  denotes the fraction of cell receptors in the active state to the total number of cell receptors. Functions and quantities used in Eqs. (1-3) are defined in [4,6].

## Results

Fig. 1 illustrates a rich variety of dynamic modes of the reaction kinetics obtained by solving Eqs. (1-3) for  $\partial\beta/\partial z = \partial\gamma/\partial z = \partial\rho_T/\partial z = 0$  and  $\nabla^2 \gamma = 0$  with the continuation software package CONT [8]. Parameters  $\sigma$  and  $k_e$  were chosen as the main continuation parameters since they affect the excitability and refractoriness of the system. Other parameters were kept constant [6,7]. For our simulations the characteristic point [ $k_e = 6.0 \text{ min}^{-1}$ ,  $\sigma = 0.375$ ] lying within the region of excitable dynamics close to the region of coexistence of excitable and oscillatory behaviour ( $B_2$ ) was chosen.

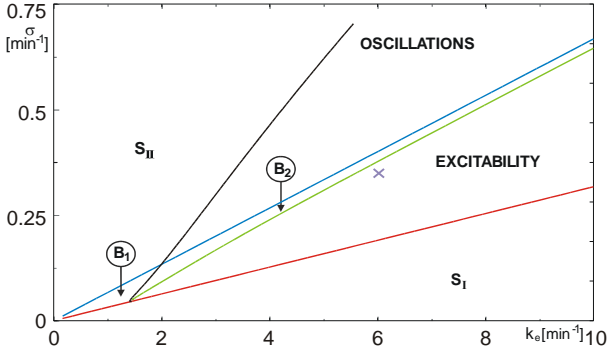


**Figure 1. Bifurcation diagram of the kinetic model described by Eqs. (1–3) in the parametric plane  $\sigma - k_e$ .**  $S_I$  ( $S_{II}$ ) – region of one stable steady state with low (high) values of  $\gamma$  and  $\beta$  and high (low) value of  $\rho_T$ .  $B_1$ ,  $B_2$  – bistable regions; LP1, LP2 – limit points on  $S_I$  and  $S_{II}$  stationary solution branches, resp.; HB – Hopf bifurcation on the  $S_{II}$  branch;  $\times$  – characteristic point for numerical simulations.

## 1D Simulations

In 1D simulations, the travelling wave  $W_0$  was formed in the system resting in its steady state ( $\gamma_{SS}$ ) by increasing the value of  $\gamma$  to the value  $\gamma = (1+100)\gamma_{SS}$  within the spatial interval of the length 1 mm on the left end of the system (see Fig. 2a). When the wave  $W_0$  has passed the centre of the system the pulse-like stimulus was applied in the centre of the system. At suitable values of stimulus parameters (amplitude  $\gamma_p$ , spatial length  $x_p$ , and period  $T_p$  behind the wave  $W_0$ ) a pacemaker emitting spontaneously several travelling waves can emerge. The waves can be emitted either symmetrically or non-symmetrically. A non-symmetrical pacemaker emits  $N$  waves towards the right and  $N+1$  waves towards the left sides of the system. An example of the non-symmetrical pacemaker characterized by excitation number  $NI = 4+5$  is shown in Fig. 2a). A symmetrical pacemaker emits the same number of waves towards both sides of the system.

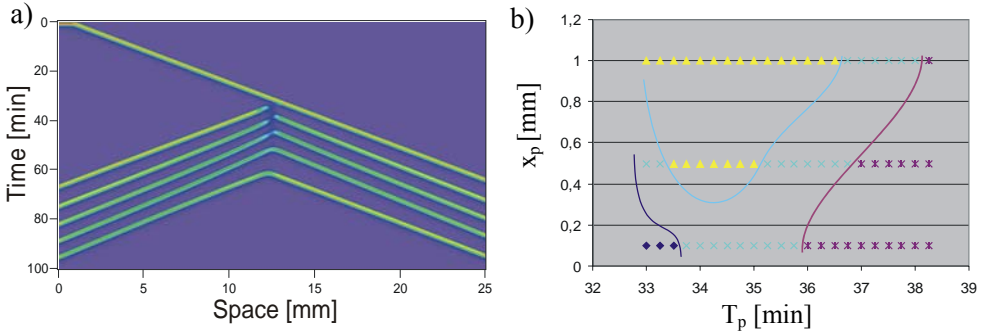


**Fig. 2. Spontaneous excitation of travelling waves in the spatially 1D system.**  
**a)** Time-space plot tracing the maximum of  $\gamma$ ,  $\gamma_P = 100 \gamma_{SS}$ ,  $x_P = 0,5$  mm,  $T_P = 34$  min. **b)** Response dependence on stimulus parameters  $x_P$  and  $T_P$ .  $\blacklozenge$  NI = 0+0;  $\blacktriangle$  Non-symmetrical and  $\times$  Symmetrical emission;  $\blackast$  NI = 1+1

If a stimulus is applied after either short or long period  $T_P$  the system behaves as a “classical” one responding by emergence of either none or one wave pair to a stimulus, respectively. At intermediate values of  $T_P$ , pacemakers emitting several waves emerge. Non-symmetrical pacemakers arise within a coherent region of stimulus parameters embedded within the region of parameters giving rise to symmetrical pacemakers.

Non-symmetrically emitting pacemakers arise only at large amplitudes of stimulus. When  $\gamma_P = 50 \gamma_{SS}$ , only symmetrical pacemakers were observed at the intermediate periods  $T_P$ . Small stimuli ( $\gamma_P = 10 \gamma_{SS}$ ) were able to evoke only “classical” response, i.e. no spontaneous excitations were observed [7].

## 2D Simulations

In 2D system, the wave  $W_0$  had a form of a half circle as shown in Fig. 3a. The stimulus was applied in a square-shaped area of the side  $x_P$  by increasing the value of  $\gamma$  for an increment  $\gamma_P$ . The response of the system to the stimulus of various  $x_P$ ,  $\gamma_P$  and  $x_{hit}$  (i.e. the distance between the wave  $W_0$  and the nearer edge of the perturbed area) was studied.

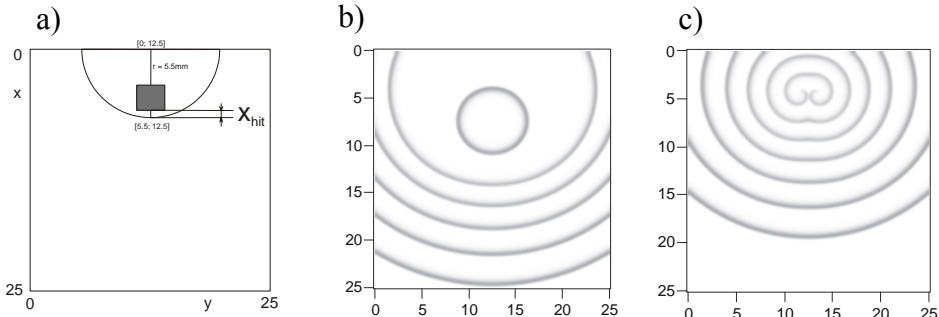


**Fig. 3: Spontaneous excitation of travelling waves in the spatially 2D system,**  $\gamma_P = 100 \gamma_{SS}$ ,  $x_P = 2$  mm. **a)** initial profile of  $\gamma$ , **b)** evolution of 5 circular waves,  $x_{hit} = 1.15$  mm, **c)** evolution of permanent spiral source of waves,  $x_{hit} = 0.5$  mm.

For  $x_{hit}$  larger than 2.0 mm, only one circular wave is formed, i.e. the system responds as a “classical” one. When  $x_{hit}$  is decreased, the temporal pacemakers emitting several waves emerge. The number of emitted waves increases as  $x_{hit}$  further decreases and when  $x_{hit}$  drops below 1.1 mm the pair of spirals is created emitting new waves permanently [7].

## Conclusions

For the chosen set of model parameters only the temporal pacemakers emerge in the 1D system. The type of emission and a number of initiated waves changes in the dependence on stimulus parameters. In the 2D system both temporal and permanent pacemakers can be observed depending on the stimulus parameters.

## Acknowledgement

This work has been supported by the grant No.: 104/03/H141 of GA CR, and by the Research Project of the Ministry of Education of the Czech Republic MSM 223400007.

## References

- [1] Merkin J. H., Poole A. J., Scott S. K.: Chemical wave responses to periodic stimuli in vulnerable excitable media. *J. Chem. Soc., Faraday Trans.*, 1997, 93(9), 1741.
- [2] Starobin J., Zilberter Y. I., Starmer C. F.: Vulnerability in one-dimensional excitable media, *Physica*, 1994, D70, 321.
- [3] P. Devreotes, *Science*, 1989, 245, 1054.
- [4] J.-L. Martiel, A. Goldbeter, *Biophys. J.*, 1987, 52, 807.
- [5] J.J. Tyson, K.A. Alexander, V.S. Manoranjan, J.D. Murray, *Physica D*, 1989, 34, 193.
- [6] J. Lindner, H. Sevcikova, M. Marek, *Phys. Rev.*, 2001, 63E, 041904.
- [7] T. Godula, H. Sevcikova, *Proc. of 31<sup>st</sup> Int. Conf. SSCHE*, 24-28. 5. 2004.

## MODELS OF PRECIPITATION PATTERN FORMATION IN AN ELECTRIC FIELD

I. Lagzi<sup>a</sup>, F. Izsák<sup>b</sup>

<sup>a</sup>Department of Physical Chemistry, Eötvös University (ELTE), H-1518 Budapest, P.O. Box 32, Hungary, <sup>b</sup>Department of Applied Analysis, Eötvös University (ELTE), H-1518 Budapest, P.O. Box 120, Hungary.

### Abstract

We studied the effect of an electric field on the evolution of Liesegang pattern formation. Our aim was to describe quantitatively the changes of the scaling regularities compared with the electric field-free case. We applied a modified deterministic (Ostwald's supersaturation) model to this case and a stochastic model, which also reflects the weak reproducibility of the phenomenon.

### Introduction

Formation of precipitation patterns has been observed in a wide range of coupling chemical reactions with diffusion. A typical example is the Liesegang phenomenon studied by R. E. Liesegang for the first time in 1896 [1,2]. In a usual experimental setup an electrolyte (called outer electrolyte) diffuses into a reaction medium, which contains another electrolyte (called inner electrolyte), the precipitation reaction between them produces a quasiperiodic precipitate distribution.

Liesegang patterns exhibit some regularities, which make connection between the macroscopic quantities of the system:  $X_n$  is the distance of the  $n$ th band measured from the junction point of the two electrolytes,  $t_n$  is the formation time of the  $n$ th band and  $w_n$  is the width of the  $n$ th band.

The *spacing law* [3] can be formalized as

$$\lim_{n \rightarrow \infty} \frac{X_{n+1}}{X_n} = P, \quad (1)$$

where  $P$  is the so-called spacing coefficient, which depends on the initial concentration of the outer and the inner electrolytes (Matalon-Packter law [4-5]).

According to the *time law* [6]

$$X_n = a_0 t_n^{1/2} + c_0,$$

where  $a_0$  and  $c_0$  are constants.

The less precise scaling law is the *width law* [7-9] due to the inaccurate definition of the band thickness in experiments:

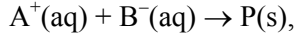
$$w_n \propto X_n^\alpha,$$

where  $\alpha$  has been found equal to *one*.

The aim of this paper is to investigate how a constant electric field modifies the regularities above. Since precipitates in Liesegang experiments are formed by ions, an electric field is expected to have a significant effect on the evolution of patterns.

## Results and Discussion

We studied the effect of an electric field using two models: a deterministic [10] and a stochastic [11,12] one. The models incorporate a simple chemical reaction between two electrolytes



where  $A^+(aq)$  and  $B^-(aq)$  are the ionic species and  $P(s)$  is the precipitate. In both models we applied a most popular description of precipitate formation (ion-product supersaturation theory based on Ostwald's idea [13]) driven by two thresholds:  $K$  is the nucleation product and  $L$  is the solubility product. Precipitation occurs only if the product of the local concentrations of the electrolytes reaches  $K$ . The previously formed precipitate promotes the precipitation process, and the former mentioned product has to reach only a lower threshold  $L$  [14,15].

### *Deterministic (mean-field) model*

In 1D the evolution of the system is described by the following partial differential equations

$$\begin{aligned} \frac{\partial a}{\partial t} &= D_a \frac{\partial^2 a}{\partial x^2} - z_a \varepsilon \frac{\partial a}{\partial x} - \delta(ab, K, L), \\ \frac{\partial b}{\partial t} &= D_b \frac{\partial^2 b}{\partial x^2} - z_b \varepsilon \frac{\partial b}{\partial x} - \delta(ab, K, L), \\ \frac{\partial p}{\partial t} &= \delta(ab, K, L), \end{aligned} \quad (2)$$

where  $a = a(x, t)$  and  $b = b(x, t)$  are the concentrations,  $D_a$  and  $D_b$  are the diffusion coefficients,  $z_a$  and  $z_b$  are the charges of ions  $A^+(aq)$  and  $B^-(aq)$ , respectively.  $\varepsilon$  corresponds to the electric field strength.  $p$  is the amount of the precipitate and  $\delta(ab, K, L)$  describes the precipitation reaction. Equations (2) were solved numerically using "method of lines", which based on spatial discretization (finite difference method on a rectangular grid) and time integration (second order Runge- Kutta method).

### *Stochastic (discrete) model*

In this discrete model we proceed with each of particles in a discretized phase space. We give the number of particles in each "space segment" in every time step. We described the evolution of the system with transition probabilities: we allow a "jump" at most of two segments, and assumed that the precipitate does not diffuse.

The precipitation reaction is supposed to be deterministic. However, the motion is driven by a random walk, which makes the whole system stochastic. We explain the weak reproducibility in the real experiments in this way.

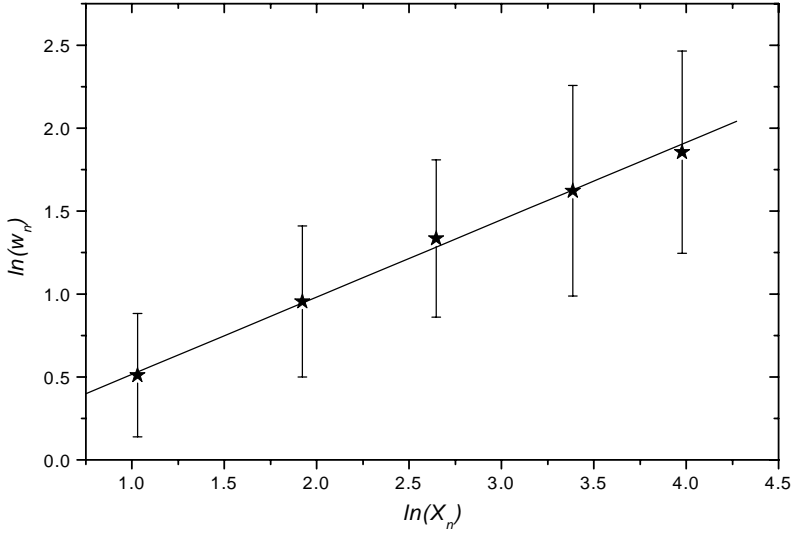


**Figure 1.** Dependence of the width of the bands on their distance measured from the junction point of the two electrolytes in the presence of an electric field (stochastic model). We fitted a linear curve for two steps model in a logarithmic scale.

In the model all segments where band formation occurs “catch” some moving particles. The effect of an electric field (we denote its strength with  $\varepsilon_+$  if it promotes the ion-transport) can be modeled by taking non-symmetric random walk. Started from normally distributed deviations, we used the transition probabilities:

$$p_{-2} = p_2 = 0.0668, \quad p_{-1} = p_1 = 0.2417 \quad \text{and} \quad p_0 = 0.383,$$

where  $p_i = P(\text{step} = i)$  for  $i = -2, -1, 0, 1, 2$ .

The effect of the electric field was incorporated by a modification of the transition probabilities  $p_i^{\varepsilon_+}$  as follows:

$$p_i^{\varepsilon_+} = p_{i-1}^{\varepsilon_+} + p_i(1 - \varepsilon_+) \quad \text{for} \quad i = -1, 0, 1, 2 \quad \text{and} \quad p_{-2}^{\varepsilon_+} = p_{-2}(1 - \varepsilon_+).$$

We modified the transition probabilities similarly, if the electric field retards the diffusion of ions.

## Discussion

*Spacing law:* The simulation results showed that in the presence of an external electric field the  $X_{n+1}$  is still linear proportional to  $X_n$ . At the same time, the spacing coefficient  $P$  in eq. (1) decreases with increasing field strength [10,11].

*Time law:* In both cases were found that in presence of an electric field the position of bands, measured from the junction point of electrolytes can be characterized by the function  $X_n = a(\varepsilon)t^{1/2} + b(\varepsilon)t + c(\varepsilon)$ , where  $a(\varepsilon)$ ,  $b(\varepsilon)$  and  $c(\varepsilon)$  depend on electric field strength. Taking the limit  $\varepsilon_+ \rightarrow 0$  or  $\varepsilon_- \rightarrow 0$ , results in  $a(\varepsilon) \rightarrow a_o$ ,  $b(\varepsilon) \rightarrow 0$  and  $c(\varepsilon) \rightarrow c_o$  [10,11,16,17].

*Width law:* We have proposed an extended form of the width law (Figure 1), which takes into account the effect of a constant electric field. The general form of this scaling law is  $w_n \propto X_n^{\alpha(\varepsilon)}$ , where  $\alpha(\varepsilon)$  is a decreasing function of its argument [11]. We have carried out real experiments to validate our numerical results in AgNO<sub>3</sub>/K<sub>2</sub>Cr<sub>2</sub>O<sub>7</sub>/gelatine system [10,11]. The formation of precipitation bands was monitored by a CCD camera, connected to a computer-controlled imaging system. Our findings are in a good agreement with the results of the numerical simulations described above. All these results show that the stochastic and the deterministic approaches presented here are effective methods to simulate the formation and dynamics of the regular Liesegang patterns even in an external electric field. Our approach based on the supersaturation model is not eligible for the description of the precipitation pattern formation in many situations: e.g. in case of various boundary and initial conditions [2].

## References

- [1] R. E. Liesegang, Naturwiss. Wochenschr., 1896, 11, 353.
- [2] J. Ross and S.C. Müller, J. Phys. Chem. A, 2003, 107, 7997.
- [3] K. Jablczyński, Bull. Soc. Chim. Fr., 1923, 33, 1592.
- [4] R. Matalon, J. Colloid Sci., 1955, 10, 46.
- [5] T. Antal, M. Droz, J. Magnin, Z. Rácz and M. Zrínyi, J. Chem. Phys., 1998, 109, 9479.
- [6] H. W. Morse and G. W. Pierce, Proc. Am. Acad. Arts. Sci., 1903, 38, 625.
- [7] K. M. Pillai, V. K. Vaidyan and M. A. Ittyachan, Colloid Polym. Sci., 1980, 258, 831.
- [8] S. C. Müller, S. Kai and J. Ross, J. Phys. Chem., 1982, 86, 4078.
- [9] M. Droz, J. Magnin and M. Zrínyi, J. Chem. Phys., 1999, 110, 9618.
- [10] I. Lagzi, Phys. Chem. Chem. Phys., 2002, 4, 1268.
- [11] I. Lagzi and F. Izsák, Phys. Chem. Chem. Phys., 2003, 5, 4144.
- [12] F. Izsák and I. Lagzi, Chem. Phys. Lett., 2003, 371, 321.
- [13] W. Ostwald, Kolloid Z., 1925, 36, 380.
- [14] A. Büki, É. Kárpáti-Smidróczki and M. Zrínyi, J. Chem. Phys., 1995, 103, 10387.
- [15] A. Büki, É. Kárpáti-Smidróczki and M. Zrínyi, Physica A, 1995, 220, 357.
- [16] A. H. Sharbaugh III and A. H. Sharbaugh, J. Chem. Educ., 1989, 66, 589.
- [17] R. F. Sultan, Phys. Chem. Chem. Phys., 2002, 4, 1253.

## INFLUENCE OF MICROWAVE HEATING ON THE BRAY-LIEBHAFSKY REACTION DYNAMICS

<sup>1</sup>D. R. Stanisavljev, <sup>2</sup>A. R. Đorđević, <sup>2</sup>V. D. Likar-Smiljanić

<sup>1</sup> Faculty of Physical Chemistry, Studentski trg 12-16, P.O. Box 137, 11001 Belgrade, Serbia and Montenegro, <sup>2</sup> School of Electrical Engineering, University of Belgrade, King Alexander's Boulevard 73, P.O. Box 35-54, 11120 Belgrade, Serbia and Montenegro

### Abstract

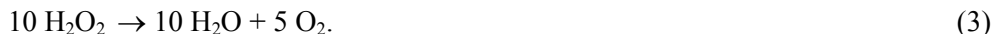
We systematically investigated the dynamics of oscillatory Bray-Liebhafsky reaction under microwave (MW) heating. Here we show that the microwaves can wipe out the oscillatory dynamics by favouring only one reaction pathway. At temperature of 68 °C minimal MW power able to affect reaction dynamics is determined to be about 10W.

### Introduction

Microwave (MW) heating is widely used in chemistry for enhancing reaction yields as well as reaction rates.[1-3] Instead of this common approach in which reaction mixture is analyzed before and after MW irradiation, we designed experimental procedure for continuous monitoring reaction dynamic.[4] It deserves special attention due to the possibility of dangerous MW leaking outside microwave cavity as well as masking of the measuring signal. As a model system for the investigations, Bray-Liebhafsky (BL) oscillatory reaction is chosen.[5;6] This reaction evolves through two alternatively dominating reaction pathways:



The driving force for the whole process is decomposition of hydrogen peroxide represented with the summary process:



This specific reaction is taken for the investigations for two reasons. Oscillatory processes are the very characteristic of living systems [7] and MW effects on the BL oscillatory dynamics would serve as a model system for investigating more complex biochemical systems. On the other side, effects of microwaves on the reaction dynamics may be quite important due to the increasing use of microwave devices and consequently increased levels of environmental MW radiation.

Microwave heating is rather specific. Although quanta of MW radiation are of too small energy to disturb vibration quantum levels (responsible for chemical changes) of reacting molecules, heating of water solutions is effected through two main mechanisms, dipolar polarization and conduction.[1;2]

Dipolar water molecules tend to align with the electric field of the electromagnetic radiation. This movement is not free due to hydrogen bonds among water

molecules. During this process many hydrogen bonds are broken (taking energy from the radiation), as well as newly recreated, evolving heat of formation.[8] It causes efficient transformation of microwave energy to heat, throughout the whole reaction mixture. In an ionic solution, besides the dipolar polarization, conduction effects are another heat producing mechanism. Hydrated ions are forced to oscillate through the solution. Ions are imbedded in the hydrogen bonded water network, which causes a kind of resistance to the electric current and consequently ohmic heating.

Due to the new conditions under which BL reaction can be conducted, systematic investigations of the reaction under different MW irradiation intensities is of high importance. For one chosen temperature, minimal MW power affecting reaction dynamics is determined.

## Results

In order to investigate effects of microwaves, conventional heating (cooling) of the reaction mixture (with the thermostat) and microwave heating (CEM microwave synthesis reactor at 2.45 GHz radiation) is properly balanced to keep constant temperature. The volume of the mixture was 6.05ml in all experiments. MW power is systematically increased in every experiment and reaction is followed electrochemically by recording potential of the platinum electrode versus double-junction Ag/AgCl reference electrode (Metrohm 6.0726.100) with a saturated  $K_2SO_4$  electrolyte bridge. DC signal is additionally filtered from possible masking with 2.45 GHz AC noise.

A set of experiments with 2W, 5W, 10 W and 20W of MW irradiation is performed. To represent the MW effects, only results with no microwaves and with 10W microwave heating (at the reaction mixture temperature of 68 °C) are shown in the Figure. As can be seen, MW heating can prevent oxidation branch (2), with the effect of destroying oscillatory reaction dynamics. Since the temperature of the reaction mixture was the same, results open possibility of nonthermal MW effects.

## Discussion

In discussing results it is essential that the temperature is same in the MW experiments and conventionally conducted experiments. To exclude possible interference of the temperature sensor with the microwaves (and incorrect temperature reading), temperature is measured with fibber-optic sensor. Interference of microwaves with the platinum electrode reading are minimized with good electrical shielding. In our previous work [4] attempt is made to show that electrochemical processes at the electrode surface are too slow to be influenced by the 2.45 GHz radiation.

Because of constant temperature, MW effects could be explained with the changed flow of energy through the system. During MW heating, temperature gradient is systematically increased. It introduces flow of energy as an important reaction parameter which could couple with chemical reactions as well as interphase transport [9] and have important feedback on the reaction dynamics. Since water is the main carrier of energy flow, structuallity of hydrogen bonds network may be of highest importance in microscopic explanation of the effect, in good agreement with previous results in absence of microwaves.[4;10]

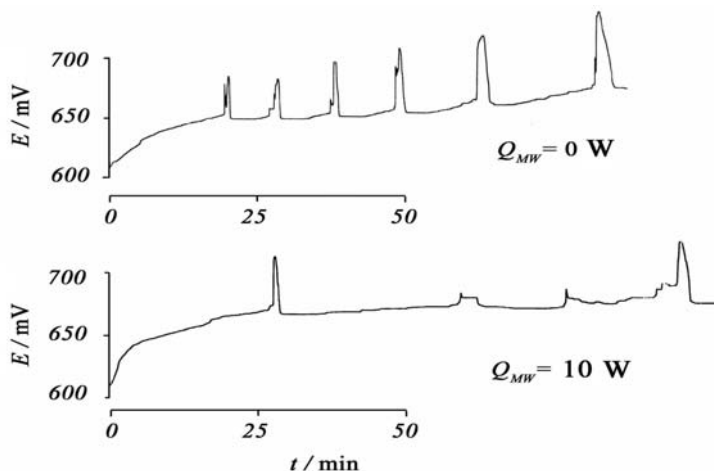


**Figure 1.** The BL reaction dynamic at 68 °C represented with platinum electrode potential versus time. Reaction mixture is heated with different participation of microwaves, starting with no microwaves, and with 10W of microwave power. Initial composition of the reaction mixture in all experiments was the same:  $[KIO_3]_0 = 8.1 \times 10^{-2} \text{ mol/dm}^3$ ,  $[H_2SO_4]_0 = 5.0 \times 10^{-2} \text{ mol/dm}^3$ ,  $[H_2O_2]_0 = 1.6 \times 10^{-2} \text{ mol/dm}^3$ . The temperature of the reaction mixture in both cases was kept constant to within  $68 \pm 1$  °C. Reaction mixture volume is  $V = 6.05 \text{ ml}$ .

## Conclusion

Experiments established new way of controlling BL reaction mechanism (an possibly other complex processes) without direct chemical perturbation. Minimum MW power effecting control is determined to be 10W in the volume of 6.05ml, fortunately not (jet) achieved in environmental MW pollution.

## Acknowledgements

The present investigations, which are included in the project no. 1448, are partially supported by Ministry of Sciences, Technologies and Development of Serbia.

## References

- [1] G. A. Whittaker, D. P. M. Mingos, *J. Microwave Power Electromagn. Energy*, 1994, 29 195.
- [2] D. R. Baghurst, D. P. M. Mingos, in *Microwave-Enhanced Chemistry* Eds.: H. M. Kingston, S. J. Haswell, American Chemical Society Publication, 1997, 523.
- [3] D. R. Baghurst, D. P. M. Mingos, *J. Organomet. Chem.*, 1990, 384 C57.
- [4] R. D. Stanislavljev, R. A. Djordjevic, D. V. Likar-Smiljanic, *ChemPhysChem.*, 2004, 5 140.
- [5] W. C. Bray, *J. Am. Chem. Soc.*, 1921, 43 1262.
- [6] W. C. Bray, H. A. Liebhafsky, *J. Am. Chem. Soc.*, 1931, 53 38.

- [7] A. Goldbeter, *Bio chemical Oscillations and Celular Rhythms*, Cambridge university press, Cambridge, 2002.
- [8] D. Halliday, R. Resnick, J. Walker, in *Fundamentals of Physics*, John Wiley & Sons, New York 1997, 554.
- [9] a) L. Treindl, R. M. Noyes, *J.Phys.Chem.* 1993, 97, 11354. b) J. A. Odutola, C. A. Bohlander, R. M. Noyes, *J.Phys.Chem.* 1982, 86, 818. c) P. Ševčík, L. Adamčíkova, *Chem.Phys.Lett.* 1997, 267, 307. d) P. Ševčík, L. Adamčíkova, *J.Phys.Chem.* 1998, 102, 1288.
- [10]a) D. Stanisavljev, N. Begović, V. Vukojević, *J.Phys.Chem* 1998, 102, 6887. b) D. Stanisavljev, N. Begović, Z. Žujović, D. Vučelić, G. Bačić, *J.Phys.Chem.* 1998, 102 6883.

## THE FRACTAL DIMENSIONS OF ACTIVATED ALUMINA SAMPLES OBTAINED IN THE REACTOR FOR PNEUMATIC TRANSPORT

Lj. S. Rožić, S. Petrović, Ž. Čupić, T. B. Novaković, D. M. Jovanović

*IChTM-Department of Catalysis and Chemical Engineering, Belgrade, Serbia and Montenegro*

### Introduction

Thermal activation of gibbsite was investigated at four different temperatures between 883 K and 943 K in a reactor for pneumatic transport in the dilute two phase flow regime. According to the developed model of two phase flow of gas-small particles ( $d < 10 \mu\text{m}$ ) in the conditions of pneumatic transport, concentration of particles in reactor in all cases is significantly smaller than 5 vol. % [1,2]. This prevents the agglomeration of particles during the dehydration process, which is one of the important factors influencing the product particle size.

The short residence time of the gibbsite particles in a reactor for pneumatic transport prevents crystallization into new phases, as established from XRPD analysis data.

As a consequence of the partial dehydration of the gibbsite, open micro- and mesopores inside the grains of the original gibbsite crystals were formed. Products having a water content smaller than the stoichiometric water content for alumina monohydrate are characterized by a specific surface area greater than  $200 \text{ m}^2/\text{g}$ .

Appropriate modeling of the geometry effects can contribute to the improvement of the performances of activated alumina through rational shape design. Recently, the fractal dimension,  $d_f$  proved to be a useful tool describing the roughness and irregularities of materials on different scales. An approximate version of a generalized BET-formula was developed to yields an easy method for calculating the fractal dimension from adsorption data. The fractal dimensions of activated alumina samples is determined in present paper according to M. Mahne and H. J. M'gel method [3] from a  $\text{N}_2$  adsorption isotherm.

### Experimental

As the starting material, gibbsite,  $\gamma\text{-Al}_2\text{O}_3 \times 3\text{H}_2\text{O}$ , with a granulation 100% particles with  $d < 10 \mu\text{m}$  was used. The characteristics of the gibbsite were as follows: water content of  $2.79 \text{ mol H}_2\text{O}/\text{mol Al}_2\text{O}_3$ , bulk density of  $2.33 \text{ g}/\text{cm}^3$  and  $S_{\text{BET}} 10.01 \text{ m}^2/\text{g}$ . The pore volume, within the range of pore widths from 2 to 50 nm, was  $0.014 \text{ cm}^3/\text{g}$ . The water content of the gibbsite and obtained products were determined by TG analysis.

The specific surface area  $S_{\text{BET}}$  and  $C_{\text{BET}}$  [4], of the gibbsite and products, were calculated from the nitrogen adsorption isotherm determined at 77 K in a high vacuum line.

The X-ray powder diffraction analysis (XRPD) was performed on a Philips PW 1051 diffractometer, using  $\text{CuK}_\alpha$  radiation.

Dehydration experiments were performed in the pilot-scale plant with pneumatic transport of gibbsite particles and its very short residence time, varying between 0.4 s and 0.8 s in the reaction zone at constant temperature. The pilot-scale plant consist of a blower for air supply, electric air preheaters, pneumatic transport reactor with the transport tube diameter 80 mm, mixing chamber for warm and cold air, cyclone and bag filter for product collection. The gibbsite was introduced into reaction section using vibrating feeding device and pneumatic transport line with airflow rate of 1 m<sup>3</sup>/h. Before starting an experiment, the airflow was preheated up to the selected reaction temperature adjusted by temperature inlet controller. Along the reactor, four thermocouples were situated in the center of the reactor, which allows to achieve the desired temperature profile within the zone of aluminum oxide trihydrate decomposition. The cold airflow was used for cooling the outlet mixture of the air and activated gibbsite.

## Results and Discussion

### *Water Content*

The gibbsite used as the starting material contained 34.6 wt. % of water, which corresponds to the theoretical value for Al<sub>2</sub>O<sub>3</sub> · 3H<sub>2</sub>O. Water content in the samples obtained by thermal treatment of gibbsite in the regime of pneumatic transport at temperatures from 883 K to 943 K are given in Table 1

**Table 1.** Water content *m* (mol H<sub>2</sub>O/mol Al<sub>2</sub>O<sub>3</sub>) in products obtained on thermal treatment of gibbsite.

t(s)	m <sub>883 K</sub>	m <sub>903 K</sub>	m <sub>923 K</sub>	m <sub>943 K</sub>
0.00	2.79	2.79	2.79	2.79
0.38	1.99	1.69	1.60	1.24
0.58	1.60	1.51	1.00	1.00
0.65	1.42	1.16	0.92	0.77
0.73	1.24	1.08	0.92	0.77
0.81	1.24	1.16	0.77	0.63

The loss of water content follows the increasing of the residence time, t(s), at all temperatures. This relationship was used to determined optimum condition (residence time and temperature of activation) to obtain the products having desired properties.

The obtained results show that the rate of dehydration of gibbsite obeys the first-order reaction with respect to water content in the solid material [5]. The activation energy of dehydration of gibbsite of 66.5 kJ / mol and frequency factor of  $8.85 \cdot 10^3 \text{ s}^{-1}$ , were calculated from Arrhenius plot. The analysis of results presented in Table 1, shows that the samples obtained after residence time of 0.73s at all measured temperatures, and has water content similar then the stoichiometric water content for alumina monohydrate, which prevent the crystallization of the material into new phases at this condition. These samples are denoted as MPA1, MPA2, MPA3, MPA4 respectively with increase of dehydration temperatures.

### X-ray diffraction

In Fig. 1, the X-ray diffractograms for gibbsite (MPA0) and activated alumina samples (MPA1, MPA2, MPA3, MPA4) are presented. In the X-ray diffractogram of starting sample, a pure crystal gibbsite phase was identified. A decrease in the reflection intensity of gibbsite with increasing temperature, indicate that activated alumina is either microcrystalline or amorphous.

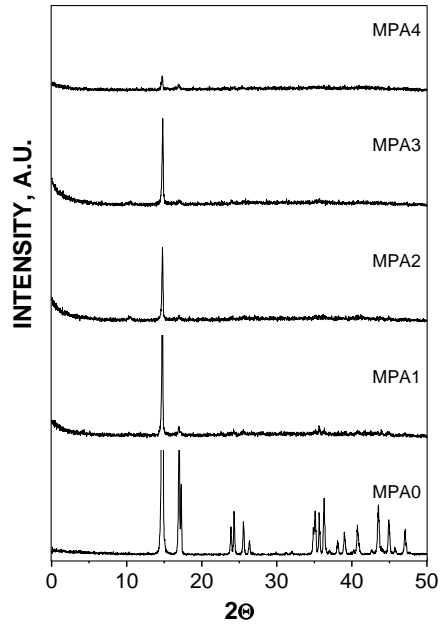


**Figure 1.** XRDP of the gibbsite and activated alumina samples.

### Fractal dimension

From the shape of the adsorption-desorption isotherms for all samples, it was concluded that hysteresis loop corresponds to the H3 type. Such a hysteresis loop can appear in slit-shaped pores. The monolayer volume,  $V_m$  and  $C_{BET}$  were calculated by the BET method from nitrogen adsorption isotherms using data up to  $p/p_0 = 0.3$ .

The M. Mahne and H. J. M'gel metod [3] is based on the approximation of the fractal version of the BET-formula (the Fripiat-Gatineau-Van Damme isotherm):

$$V = v_0 a_0 \frac{c_1}{c} \cdot \sum_{i=1}^{\infty} [i^{\alpha} \cdot (c \cdot P)^i]$$

where,  $V$  is adsorbed volume,  $P$  is measured pressure,  $\alpha = 3 - d_f$ ,  $c_1$  and  $c$  are adhesion and cohesion parameters,  $v_0$  is volume of monomolecular layer covering a unit area and  $a_0$  is area which is not occupied by adsorbate molecules. The approximation of the above isotherm in the logarithmic version is:

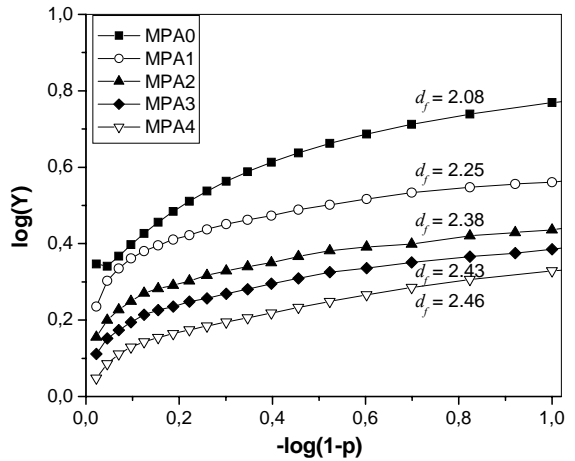


**Figure 2.** Estimation of  $d_f$  according to approximate version of the isotherm [3]. (The ordinate scales are moved up by 0.5 for successive results from MPA4 to MPA0).

$$\log Y = \log \left( \frac{V}{V_m} \frac{1 - p + C_{BET} \cdot p}{C_{BET} \cdot p} \right) = -\alpha \log(1 - p), \text{ where } p = p/p_0.$$

According to above equation, approximative version of the BET isotherm is presented in Fig.2 for all samples.

The starting gibbsite had a fractal dimension of the surfaces  $d_f = 2.08$ , indicating that in the adsorption of molecules its surface behaves like an almost flat surface. Activated alumina samples are characterized by a greater fractal dimension of their surfaces,  $d_f$  values increase with a rise in the temperature of the thermal treatment, indicating that the irregularities of their surfaces are greater.

## Conclusion

It was shown that the activated alumina samples are characterized by the fractal dimension of their surfaces whose value increases from 2.08 to 2.46 with increasing dehydration temperatures. Consequently, in the adsorption of molecules greater than nitrogen, part of activated alumina surfaces is excluded from the adsorption process. Applied method has proved to be of great practical value for the estimation of the fractal dimension.

## Acknowledgement

This work was supported by the Serbian Ministry of Science, Technologies and Development (Project No. MHT. 2.09.0022B and Project No. HE 1807).

## References

- [1] Lj., Rožić, R. Garić-Grulović, Ž. Grbavčić, T. Novaković, *Procesna tehnika* 1997, 3-4, 153.
- [2] Lj. Rožić, R. Garić-Grulović, T. Novaković, Ž. Grbavčić, 4th International Conference on Fundamental and Applied Aspects of Physical Chemistry, Papers, Beograd 1998, 422.
- [3] M. Mahne, H. J. M'gel, *Colloids and Surfaces A: Physicochem. Eng. Aspects*, 2003, 216, 215.
- [4] S. H. Gregg, K. S. Sing, *Adsorption, Surface Area and Porosity*, Academic Press, New York, 1967
- [5] Lj. Rožić, T. Novaković, N. Jovanović, A. Terlecki-Baričević, Ž. Grbavčić, *Journal of the Serbian Chemical Society*, 2001, 4, 273

# EXAMINATION OF THE TEMPERATURE VARIATIONS ON BELOUSOV ZHABOTINSKY OSCILLATORY REACTION

S. Blagojević<sup>1</sup>, S. Anić<sup>2</sup>

<sup>1</sup>Faculty of Pharmacy, University of Belgrade, Vojvode Stepe 450, <sup>2</sup>Faculty of Physical Chemistry, University of Belgrade, Studentski trg 12, Serbia and Montenegro

## Abstract

The influence of temperature and various initial concentration  $\text{Ce}_2(\text{SO}_4)_3$  on characteristic period of evolution in BZ oscillatory reaction was investigated. For equiconcentrations BZ systems and systems with different initial concentration of  $\text{Ce}_2(\text{SO}_4)_3$  activation energy was calculated as a function of reciprocal kinetic parameters  $\tau_1$ ,  $\tau_{2,3}$ ,  $\tau_{\text{end}}$  values and temperature. Calculated values for parameters activation energies indicate that inside investigated temperature and concentration interval, evolution of oscillatory reaction is realised with different mechanism. Also, we have indication that different steady-states in which system are, have different activation energies.

## Introduction

The classical Belousov-Zhabotinsky reaction (BZ) [1] is understood as the oscillatory oxidation of one-electron redox couple (mostly used are  $\text{Ce}^{3+}/\text{Ce}^{4+}$ ,  $\text{Mn}^{2+}/\text{Mn}^{3+}$ , ferriin / feriin,  $\text{Ru}(\text{bipy})_3^{2+}/\text{Ru}(\text{bipy})_3^{3+}$ ) by bromate ions in acid media and in the presence of an organic substrate that can be brominated and oxidized [2-3]. In this paper the examination of the temperature variations on Belousov-Zhabotinsky oscillatory reaction is analyzed on the reaction mixture containing malonic acid, potassium bromate, potassium bromide, sulphuric acid and  $\text{Ce}^{+3}$  as catalyst [4]. The kinetics of different pathways are analyzed by means of the characteristic periods: of the preoscillatory period  $\tau_1$  (the time interval from the beginning of the reaction to the onset of the first oscillation),  $\tau_{2,3}$  (the period between second and third oscillation), and the period  $\tau_{\text{end}}$  (the time elapsed between the start of the reaction and the termination of the oscillatory phase).

In the literature, there are several methods for determination of activation energies. In [5,6] an activation energy of BZ reaction  $E_{\text{os}}$  has been obtained from the relation between the logarithm of reciprocal values of the frequency of the regular oscillations and the reciprocal temperature. Also, in [7] the activation energy of BZ reaction was determined by the preoscillatory period. The method for the determination of activation energies that will be used here, based on temperature dependence of  $\tau_1$ ,  $\tau_{2,3}$  and  $\tau_{\text{end}}$ , has been proposed earlier, but applied on the Bray-Liebhafsky oscillatory reaction [8].

## Experimental

The BZ reaction was realised in the stationary well-stirred reactor with a reaction volume of 51 ml. A glass cell Methrom Ea 876-20 was used as a reactor. Time evolution

of BZ reaction was followed potentiometrically by using bromide ion-selective electrode. The electrode was connected by Ag/AgCl reference electrode by the sulphate bridge.

The measurements were carried out in independent series of experiments performed at different temperatures in intervals from 303 to 332K. The uncertainty in measuring the temperature was  $\pm 0.2$  K. All experiments were carried out under the constant values of the initial concentrations of the following species (in mol/dm<sup>3</sup>):  $[\text{CH}_2(\text{COOH})_2]_0 = 3.20 \times 10^{-2}$ ,  $[\text{H}_2\text{SO}_4]_0 = 1.0$ ,  $[\text{KBrO}_3]_0 = 6.17 \times 10^{-2}$ ,  $[\text{KBr}] = 1.50 \times 10^{-5}$ . The initial concentration  $\text{Ce}_2(\text{SO}_4)_3$  was varied from  $3.75 \times 10^{-3}$  to  $5.0 \times 10^{-3}$  mol/dm<sup>3</sup>.

## Results and Discussion

Well-developed potential-time curves are obtained. The oscillograms with one preoscillatory and oscillatory period are obtained. The form of oscillogram depends on the temperature and the initial concentrations  $\text{Ce}_2(\text{SO}_4)_3$ . Characteristics examples of BZ oscillograms obtained at different temperatures illustrated in Figure 1.

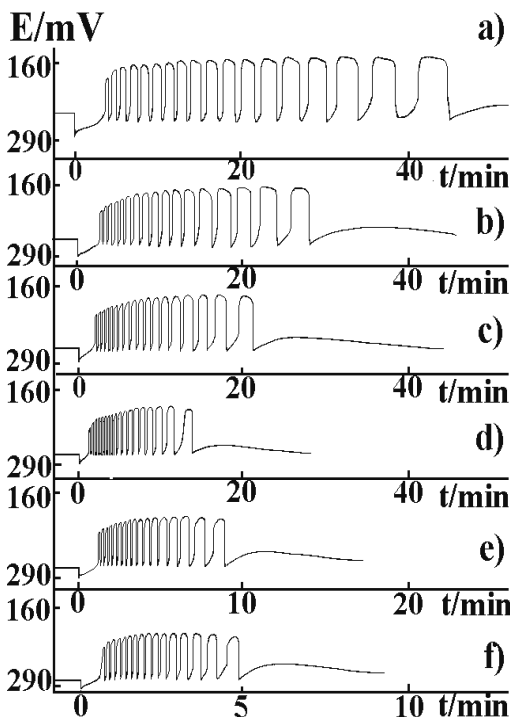


**Figure 1.** The potentiometric traces of the BZ reaction obtained by the Br<sup>-</sup> ion sensitive electrode, in order of increasing temperatures (in K):

a) 303.2, b) 308.2,

c) 313.2,

d) 318.2, e) 323.2,

f) 332.2.

$[\text{Ce}_2(\text{SO}_4)_3]_0 = 5.00 \times 10^{-3}$  mol dm<sup>-3</sup>.

The activation energies (in kJ/mol) calculated by means of the characteristic periods  $\tau_1$ -E( $\tau_1$ ),  $\tau_{2,3}$ -E( $\tau_{2,3}$ ) and period  $\tau_{\text{end}}$ -E( $\tau_{\text{end}}$ ) are obtained from the oscillograms measured at different temperatures. The dependence between the logarithm of the reciprocal kinetic properties and  $1/T$  is in accordance with Arrhenius law (Fig.2).

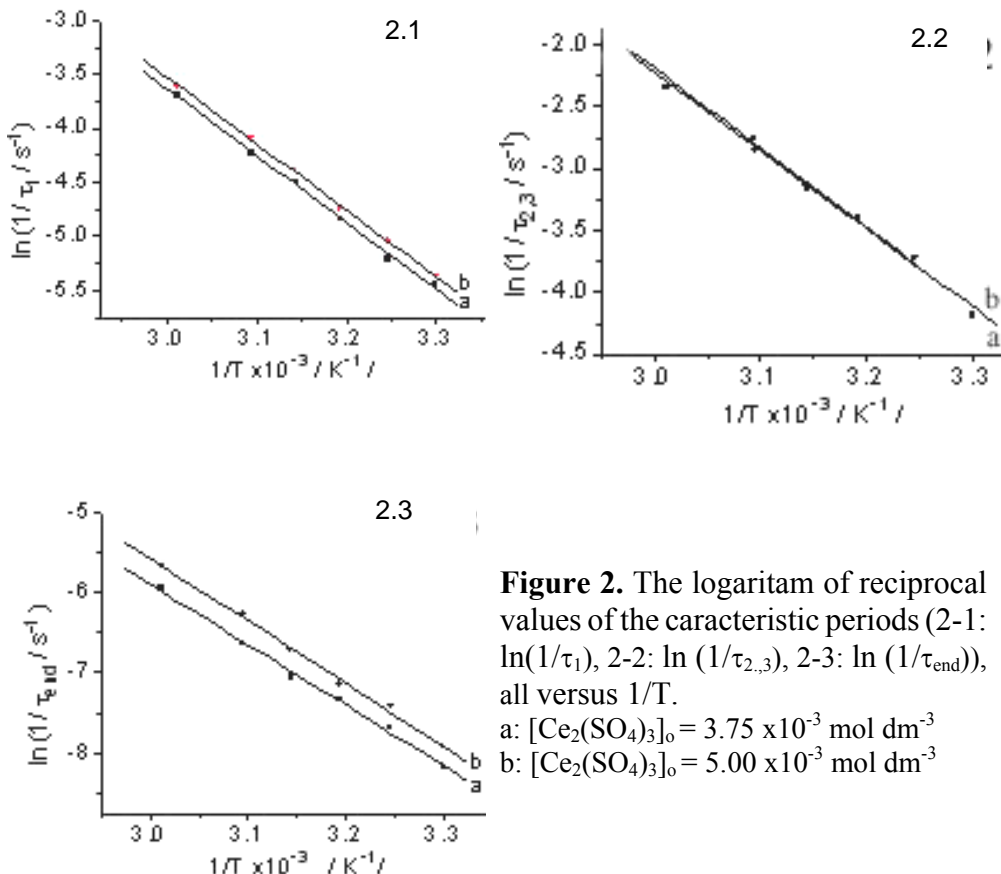


**Figure 2.** The logarithm of reciprocal values of the characteristic periods (2-1:  $\ln(1/\tau_1)$ , 2-2:  $\ln(1/\tau_{2,3})$ , 2-3:  $\ln(1/\tau_{\text{end}})$ ), all versus  $1/T$ .

a:  $[\text{Ce}_2(\text{SO}_4)_3]_0 = 3.75 \times 10^{-3} \text{ mol dm}^{-3}$

b:  $[\text{Ce}_2(\text{SO}_4)_3]_0 = 5.00 \times 10^{-3} \text{ mol dm}^{-3}$

By means of the mentioned parameters, characteristic periods  $\tau_1$ ,  $\tau_{2,3}$  and period  $\tau_{\text{end}}$  obtained from oscillograms at different temperatures (between 303 K and 332 K), the activation energies calculated for two different initial concentrations of  $\text{Ce}_2(\text{SO}_4)_3$  (Table 1).

**Table I** The activation energies calculated by means of the period  $\tau_1$ -E( $\tau_1$ ),  $\tau_{2,3}$ -E( $\tau_{2,3}$ ) and period  $\tau_{\text{end}}$ -E( $\tau_{\text{end}}$ ).

$[\text{Ce}_2(\text{SO}_4)_3]_0$ / $\text{mol dm}^{-3}$ /	E( $\tau_1$ ) / kJ/mol /	E( $\tau_{2,3}$ ) / kJ/mol /	E( $\tau_{\text{end}}$ ) / kJ/mol /
$3.75 \times 10^{-3}$	54	52	63
$5.00 \times 10^{-3}$	51	53	65

## Conclusion

The oscillograms depend on temperature and initial concentrations of  $\text{Ce}_2(\text{SO}_4)_3$ . The kinetic analysis indicate that different reaction steps of the BZ reaction mechanism are determining the values of  $\tau_1$ ,  $\tau_{2,3}$  and  $\tau_{\text{end}}$  and thus they are responsible for the properties of the different dynamic states. We all know that [6], at least two kinetic pathways with different rates for brome malonic acid formation would be present in the BZ reaction. In our case  $\tau_1$  and  $\tau_{2,3}$  are determined by relatively rapid kinetic pathway, whereas  $\tau_{\text{end}}$  is determined by the slower one. The slower kinetic pathway determines the overall reaction rate.

## Acknowledgment

We gratefully acknowledge the partial financial support in grant no. 1448 of the Ministry for Science, Technology and Development of the Republic of Serbia.

## References

- [1] A.M. Zhabotinsky, Ber. Bunsen-Ges. Phys. Chem., 1980, 84, 303.
- [2] P. Shevcik, L. Adamcikova, Collect. Czech. Chem. Commun, 1982, 47, 891.
- [3] Z. Noszticzius, J. Bodiss, J. Am. Chem. Soc., 1979, 101, 3177.
- [4] R. Field, E.Körös, R. Noyes, J. Am. Chem. Soc., 1972, 94, 8649.
- [5] E. Körös, Nature, 1974, 251, 703.
- [6] M. Burger, E.Koros, J. Phys. Chem., 1980, 84, 496.
- [7] O.Z. Didenko, P.E. Strizhak, Chem. Phys. Lett., 2001, 340, 55.
- [8] S. Anić, Lj. Kolar-Anić and E. Körös, React. Kinet. Cat. Lett., 1997, 61, 111.

## NEW DETAILS ABOUT THE INFLUENCE OF ACIDITY AND TEMPERATURE ON THE BELOUSOV-ZHABOTINSKY REACTION

S. Blagojević<sup>1</sup>, N. Pejić<sup>1</sup>

<sup>1</sup>Faculty of Pharmacy, University of Belgrade, Vojvode Stepe 450, <sup>2</sup>Faculty of Physical Chemistry, University of Belgrade, Studentski trg 12, Serbia and Montenegro

### Abstract

The equiconcentration Belousov-Zhabotinsky oscillatory reaction at different initial sulfuric acid concentration from 0.1 to 1.4 mol/dm<sup>3</sup>, and various temperatures from 298 to 342 K was investigated. Two different kinetic oscillatory domains with respect to acidity, one for 0.2-0.4, and another for 0.6-1.4 mol/dm<sup>3</sup>, was found. When the initial concentration of H<sub>2</sub>SO<sub>4</sub> is between 0.6 and 1.4 mol/dm<sup>3</sup>, the activation energies are also determined. They have the values from 57 to 68 kJ/mol depending on acidity.

### Introduction

Belousov-Zhabotinsky (BZ) oscillatory reaction [1] is the metal ion catalyzed oxidation of an easily brominated organic substrate by bromate in an acid medium [1-3]. The BZ reaction is examined in a series of the reaction systems carried out from Belousov solution [4-6] (citric acid, potassium bromate, potassium bromide, cerium ion and sulfuric acid), by combination of different substrates (malonic acid or the other organic substrate) and the metal catalysts (Ce<sup>+4</sup>/Ce<sup>+3</sup>, Mn<sup>+3</sup>/Mn<sup>+2</sup>, Fe<sup>+3</sup>/Fe<sup>+2</sup> etc.).

Here, the influence of acidity and temperature on generation of the oscillograms in the BZ reaction is analyzed on the reaction mixture containing malonic acid, potassium bromate, potassium bromide, sulphuric acid and Ce<sup>+3</sup> as catalyst. The overall stoichiometry can be approximated in general form: [5].

### Experimental

All experiments were carried out in the same manner as earlier [7], under the constant values of the initial concentrations of the following species (in mol/dm<sup>3</sup>): [CH<sub>2</sub>(COOH)<sub>2</sub>]<sub>0</sub> = 3.20 × 10<sup>-2</sup>, [Ce<sub>2</sub>(SO<sub>4</sub>)<sub>3</sub>]<sub>0</sub> = 2.50 × 10<sup>-3</sup>, [KBrO<sub>3</sub>]<sub>0</sub> = 6.17 × 10<sup>-2</sup>, [KBr]<sub>0</sub> = 1.50 × 10<sup>-5</sup>. The initial sulfuric acid concentration was varied from 0.1 to 1.4 mol/dm<sup>3</sup>.

For every given acidity the temperature was varied from 298 K to 342 K. The BZ reaction was realised in a well-stirred closed reactor with a reaction volume of 51 ml. Time evolution of BZ reaction was followed potentiometrically, by using bromide ion-selective electrode connected by Ag/AgCl reference electrode by the sulphate bridge.

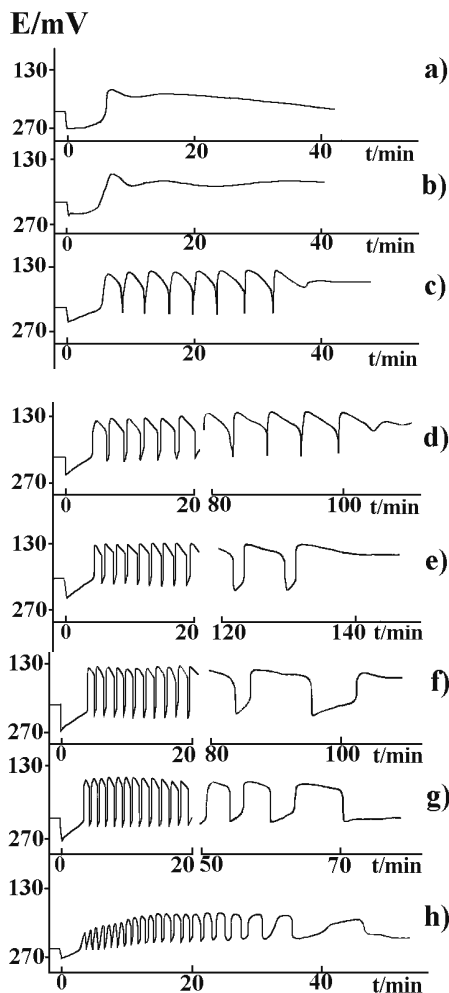


**Figure 1.** The potentiometric traces of the BZ reaction obtained by Br<sup>-</sup>-ion sensitive electrode at 303 K, and following  $[H_2SO_4]_0$  (in mol/dm<sup>3</sup>):  
 a) 0.1, b) 0.2, c) 0.3, d) 0.4, e) 0.6, f) 0.8, g) 1.0 and h) 1.4

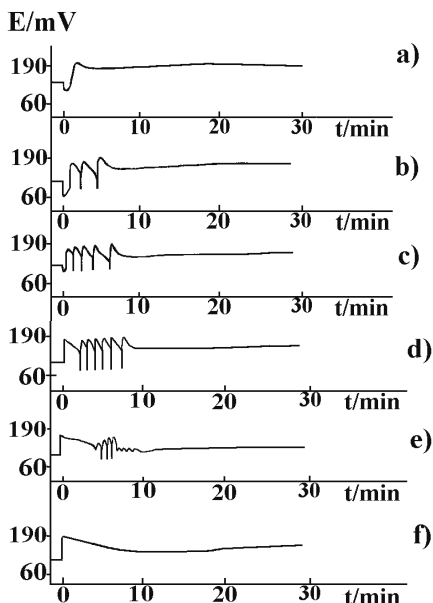


**Figure 2.** The potentiometric traces of the BZ reaction obtained by Br<sup>-</sup>-ion sensitive electrode at  $[H_2SO_4]_0 = 0.1$  mol/dm<sup>3</sup> and temperatures (in K):  
 a) 323, b) 328, c) 333, d) 334, e) 337, f) 342.

## Results and Discussion

Well-developed potential-time curves are obtained. The dependence of the oscillograms on the temperature and acidity is presented in Fig.1 and Fig.2, respectively.

Analysing the oscillograms obtained by changing the initial sulfuric acid concentration from 0.1 to 1.4 mol/dm<sup>3</sup> at constant temperatures, we have found that the system do not exhibit an oscillatory evolution at the lowest concentration of sulfuric

acid ( $0.1 \text{ mol/dm}^3$ ) at any considered temperature in the range from 298 to 342 K (Fig.1).

Moreover, analysing the oscillograms obtained by changing the temperature from 298 to 342 K at constant initial sulphuric acid concentrations, we have found that the system do not exhibit an oscillatory evolution at relatively low ( $\leq 323\text{K}$ ) and relatively high ( $\geq 342\text{K}$ ) temperatures (Fig.2).

The transition from monotonous to oscillatory evolution, found at every considered constant temperature, depends on selected temperature, whereas the same transition found at any considered constant acidity, depends on chosen initial concentration of sulphuric acid.

Two different kinetic oscillatory domains, one for 0.2-0.4, and another for 0.6-1.4  $\text{mol/dm}^3$ , was found (Fig.3). The value for  $\tau_{\text{end}}$  is also the complex function of acidity (Fig.3-1). However, in the region  $0.6 \leq [\text{H}_2\text{SO}_4]_0 \leq 1.4 \text{ mol/dm}^3$ , the curves for  $\tau_{\text{end}}$  (Fig.3-2) decrease monotonously with temperature increasing for any value of the acidity. For these cases the calculated activation energies depend on the acidity (Fig.4). The activation energies was calculated by the method based on the relation  $\ln(1/\tau_{\text{end}}) = f(1/T)$  [7,8].

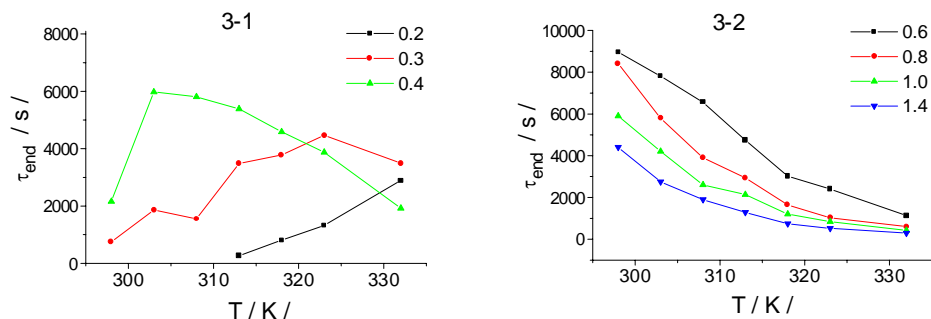


**Figure 3.** Dependence between  $1/\tau_{\text{end}}$  and  $1/T$  for different acidity: from 0.2 to 0.4  $\text{mol/dm}^{-3} \text{H}_2\text{SO}_4$  (3-1), and from 0.6 to 1.4  $\text{mol/dm}^{-3} \text{H}_2\text{SO}_4$  (3-2).

## Conclusion

The evolution of the BZ oscillatory reaction in the acidity-temperature phase-space together with corresponding kinetics is analysed. The obtained results for the activation energies are in agreement with the expected ones.

## Acknowledgment

We gratefully acknowledge the partial financial support in grant no. 1448 of the Ministry for Science, Technology and Development of the Republic Serbia.

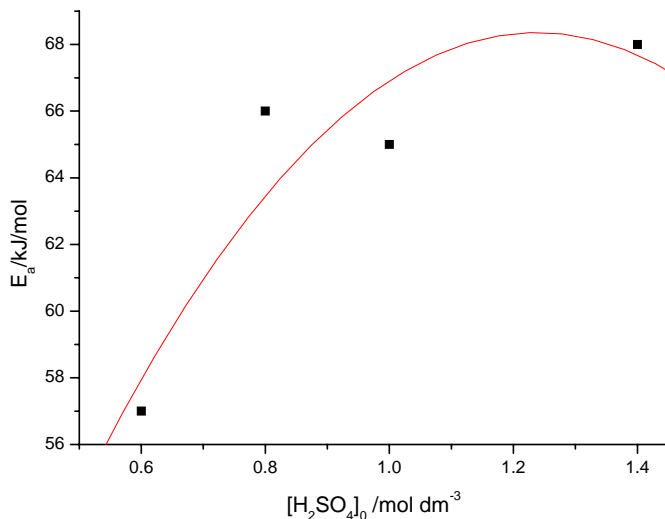


**Fig. 4.** The dependence of activation energies  $E_a$  on the acidity.

## References

- [1] B.P.Belousov, Sb. Ref. Radiats. Med., Medgiz, Moscow, 1958, 1, 145.
- [2] M. Zhabotinsky, Biofizika, 1964, 9, 306.
- [3] C.Herbo, G.Schmitz, M.V. Glabbeke, Can. J. Chem., 1976, 54, 2628.
- [4] J.Wang, F.Hynne, P. Sørensen, International Journal of Bifurcation and Chaos, 1996, 6, 1267.
- [5] E.Körös, Oscillations, Waves and Spirals in chem. systems, World Scientific, London, 1992, 221.
- [6] P.Gray, S.K. Scott, Chemical and Instabilites, Clarendon, Press Oxford, 1990.
- [7] S.Blagojevic, Aktivaciona energija Belousov-Zabotinski oscilatorne reakcije u razlicitim ustaljenim stanjima (Thesis), Univerzitet u Beogradu, Beograd 2001.
- [8] S.Anić, Lj.Kolar-Anić and E.Körös, React. Kinet. Cat. Lett., 1977, 61, 111.

# TEMPERATURE DEPENDANCE OF THE RATE CONSTANT OF THE OVERAL BELOUSOV-ZHABOTINSKY OSCILATORY REACTION

S. Blagojević

Faculty of Pharmacy, University of Belgrade, Vojvode Stepe 450

## Abstract

The decomposition of the malonic acid in the Belousov-Zhabotinsky oscillatory reaction as the pseudo-first order kinetics with respect to itself is analyzed. Particularly, investigated malonic acid decomposition in the presence of bromate, bromide, sulphuric acid and cerium(III)sulphate, a numerous experiments were performed where only the initial concentration of malonic acid ( $[\text{CH}_2(\text{COOH})_2]_0$ ) was varied from  $1.2 \times 10^{-2}$  to  $4.3 \times 10^{-2}$  mol dm<sup>-3</sup>, and temperature from temperature 303 to 318 K.

The obtained rate constants for the malonic acid decomposition have the values between  $9.12 \times 10^{-3}$  min<sup>-1</sup> at 303 K and  $3.54 \times 10^{-2}$  min<sup>-1</sup> at 318 K. The corresponding activation energy has the value of 63 kJ/mol.

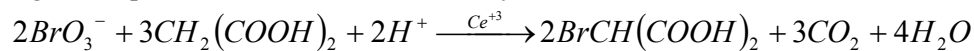
## Introduction

In literature, [1] the reaction mixtures composed of organic substrate, bromat, sulfuric acid and a metallic catalyst are referred as Belousov-Zhabotinsky (BZ) ones. The most studied [2] and by far the best characterized is the malonic acid, bromate, sulfuric acid and cerium (III) reacting system, the system that we analyzed here, too.

The species in the BZ system consisting of malonic acid, bromate, sulfuric acid and cerium (III), can be classify into three distinct groups [3]: a) the reactants ( $\text{BrO}_3^-$  and  $\text{CH}_2(\text{COOH})_2$ ), (b) the recyclic intermediates (e.g.,  $\text{Br}^-$ ,  $\text{BrO}_2$ ,  $\text{HBrO}_2$ ,  $\text{Ce(IV)}$ ) and (c) the final products (e.g.,  $\text{CO}_2$ ,  $\text{CHBr}(\text{COOH})_2$ ).

In the mentioned reaction system the concentration of recyclic intermediates exhibit temporal concentration oscillations, whereas the concentrations of reactans and the final products exhibit the corresponding stepwise evolution.[4]

Since this system can be considered as malonic acid decomposition, as well that the reactions of decomposition are often first order in respect to reactant undergoing decomposition, [5] we decided to analyze the kinetics of the overall reaction



as the pseudo-first order reactions with respect to malonic acid.

## Experimental

The kinetics of the Belousov -Zhabotinsky oscillatory reaction was analyzed in a well stirred closed reactor (magnetic stirrer of 700 rpm) with a reaction volume of 51 ml. The evolution of the reaction was monitored potentiometrically, using a bromide ion-sensitive electrode connected to an Ag/AgCl reference electrode by a sulfate bridge.

The measurements were carried out in independent series of experiments at different temperatures and different malonic acid concentrations. Namely, at every temperature, in the region between 303 and 318 K, independent experiments with different initial concentrations of malonic acid are performed. The initial malonic acid concentration,  $[CH_2(COOH)_2]_0$ , was varied from  $1.2 \times 10^{-2}$  to  $4.3 \times 10^{-2}$  mol dm<sup>-3</sup>. In all cases, experiments were carried out with constant values of the initial concentrations of the following species (in mol dm<sup>-3</sup>): 1.0 H<sub>2</sub>SO<sub>4</sub>;  $6.2 \times 10^{-2}$  KBrO<sub>3</sub>;  $1.5 \times 10^{-5}$  KBr and  $2.5 \times 10^{-3}$  Ce<sub>2</sub>(SO<sub>4</sub>)<sub>3</sub>.

## Results and Discussion

Analysing the potentiometric measurements of the evolution of the Belousov-Zhabotinsky system one can note that the oscillograms are the functions of the temperature and initial concentration of malonic acid. The number of oscillations are the function of the initial concentration of malonic acid only (Table I).

**Table I.** The number of oscillations as a function of the initial concentration of malonic acid.

$[CH_2(COOH)_2]_0$ /10 <sup>-2</sup> mol dm <sup>-3</sup>	T / K /			
	303	308	313	318
1.2	2	2	3	2
1.6	7	7	7	7
2.2	14	14	14	15
3.2	26	26	27	27
4.3	39	40	40	40

However, in all experiments, under the considered conditions, the type of oscillogram is permanent. Hence, we could suppose that the malonic acid concentration at the end of reaction, is approximately constant, independent of the initial malonic acid concentration. With this assumption and the fact that decomposition reactions are often first order with respect to the reactant undergoing decomposition, the kinetic analysis could be done by considering the overall process as pseudo-first order with respect to malonic acid. In other words, if both assumptions are valid, the equation

$$\frac{d(CH_2(COOH)_2)}{dt} = -k[CH_2(COOH)_2]$$

as well as the integrated form of this equation,

$$\tau_{end} = -\frac{2.303}{k} \log[CH_2(COOH)_2]_{end} + \frac{2.303}{k} \log[CH_2(COOH)_2]_0$$

where  $[CH_2(COOH)_2]_0$  and  $[CH_2(COOH)_2]_{end}$  denote the concentrations of malonic acid  $t = 0$  and  $t = \tau_{end}$ , must be satisfied.[4]

In Fig.1 we can see that obtained results obey the last equation very well for all initial malonic acid concentrations less than, or equal to  $3.2 \times 10^{-2} \text{ mol dm}^{-3}$ . Thus, it is shown that the malonic acid decomposition can be analyzed as a pseudo-first order reaction with respect to malonic acid in the concentration range of  $1.2 \times 10^{-2}$  to  $3.2 \times 10^{-2} \text{ mol dm}^{-3}$ . The rate constant is calculated from the straight-lines presented in Fig. 1. The calculated pseudo-first rate constant for the overall proces at different temperatures are given in Table II. The rate constant at 318 K is taken from Ref. [5].

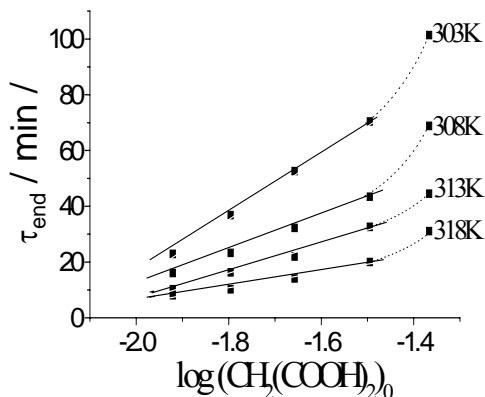


**Figure 1.** The time  $\tau_{\text{end}}$  as a function of  $\log [\text{CH}_2(\text{COOH})_2]_0$  for different temperatures.

The activation energy of BZ oscillatory reaction is calculated by means of the rate constant given in Table II. The dependence between  $\ln k$  and  $1/T$  follows the Arrhenius law (Fig.2). The activation energy of the overall proces is found to be 63 kJ/mol wich is in accordance with the activation energy obtained in literature [3,6].

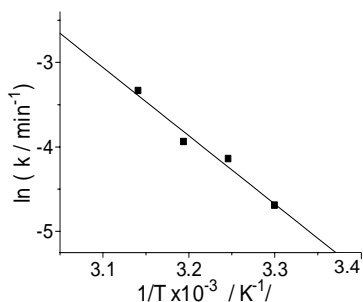


**Figure 2.** The Arrhenius dependence between  $\ln k$  and  $1/T$ .

**Table II.** Value of the pseudo-first rate constant  $k$  for concentration range of hydrogen peroxide from  $1.2 \times 10^{-2}$  to  $3.2 \times 10^{-2} \text{ mol dm}^{-3}$

T/K/	303	308	313	318
K /min <sup>-1</sup> /	$9.12 \times 10^{-3}$	$1.58 \times 10^{-2}$	$1.93 \times 10^{-2}$	$3.54 \times 10^{-2}$

## Conclusion

The decomposition of malonic acid in the presence of bromate, sulfuric acid and Ce(III) Belousov-Zhabotinski oscillatory reaction, is analyzed in temperature range of (303 to 318 K) and variable concentrations of malonic acid. The pseudo-first order kinetics with respect to malonic acid as the species undergoing decomposition with a corresponding rate constants at different temperatures was found. The activation energy of the overall reaction is 63 kJ/mol. It is in agreement with those calculated from temperature dependence of  $\tau_{\text{end}}$  ( $\ln(1/\tau_{\text{end}}) = f(1/T)$ ) for several equiconcentration reaction systems ( $E_a = 65 \pm 3$  kJ/mol).

## Acknowledgment

We gratefully acknowledge the partial financial support in grant no. 1448 of the Ministry for Science and Development of the Republic of Serbia.

## References

- [1] A.M.Zhabotinski, *Biofizika*, 1963, 9, 306.
- [2] R.J.Fild, M.Burger, *Oscillations and Traveling Waves in Chemical system*, Mir, Moscow, 1988, 78.
- [3] E.Körös, *Oscillations, waves and spirals in Chemical systems*, World Scientific, London, 1992, 221.
- [4] S.Blagojević, N.Pejić and S.Anić, *J. Serb.Chem.Soc.*, 2000, 65, 709.
- [5] S.Blagojević, N.Pejić and S.Anić<sup>2</sup>, S.Ribnikar, S.Anić (Eds.), *Physical Chemistry 2000*, Soc.Phys.Chem.Serb., Belgrade, 2000, 223 5<sup>th</sup> International Conference on Fundamental
- [6] G.Nagy, E.Körös and P.Ruoff, *Chem. Phys.Letters*, 1996, 250, 255.

# PERTURBATIONS ON THE OSCILLATIONS OF THE BRIGGS-RAUSCHER REACTION BY FREE-RADICAL SCAVENGERS: AN OVERVIEW

R. Cervellati<sup>1</sup>, S.D. Furrow<sup>2</sup>

<sup>1</sup>Dipartimento di Chimica 'G. Ciamician', Università di Bologna, Via Selmi, 2, I-40126 Bologna, Italy, <sup>2</sup>Penn State University, Berks-Lehigh Valley College, Luerssen Building, PO 7009, Reading, PA 19610-6009, U.S.A.

## Abstract

The oscillatory regime of the Briggs-Rauscher reaction is perturbed by free-radical scavengers. An overview of experimental evidence and mechanistic interpretation is reported.

## Introduction

The most dramatic oscillating reaction in solution is probably that discovered in 1973 by *Briggs and Rauscher* [1] (the BR reaction). When appropriate amounts of hydrogen peroxide, acidic iodate, manganous salt, malonic acid (MA), and starch as indicator are mixed in aqueous solution, the system repeats several times the sequence: colorless → yellow → blue. The main intermediates for which concentrations oscillate in the BR reaction are:  $I^-$ ,  $I_2$ ,  $HOI$ ,  $HOIO$ ,  $IO_2^\bullet$ , and the hydroperoxyl radical  $HOO^\bullet$ .  $IO_2^\bullet$  and  $HOO^\bullet$  radicals were not directly detected in BR mixtures: their presence in the system were proposed in early, nearly identical mechanisms by *Noyes and Furrow* [2] and by *DeKepper and Epstein* [3] in analogy with the experimental findings for the Belousov-Zhabotinsky [4] and the Bray-Liebafsky reactions [5].

A decisive indirect evidence of involvement and important role played by  $HOO^\bullet$  radicals in the onset of oscillations was given by *Cervellati et al.* [6,7] studying the perturbations on the oscillations by addition of free-radical scavengers belonging to the class of polyphenolic antioxidants. The perturbation consists of an immediate cessation of oscillations, an inhibition time followed by a regeneration of oscillations. Since it is well known that polyphenols show strong oxygen free radical scavenging activity [8], inhibitory effects were ascribed to scavenging of  $HOO^\bullet$  radicals by these compounds.

The aim of this work is to give an overview of the experimental and mechanistic investigation of these perturbations, also illustrating the results with a phenolic compound not previously reported, epinephrine (adrenaline).

## Experimental Observations

Oscillations in the BR mixture were followed potentiometrically by recording the potential of a bright-platinum electrode or the potential of a iodide-ion selective electrode, coupled with a reference electrode. As reference electrode we used a double-junction  $Ag/AgCl/Cl^- (KNO_3)$  electrode. Electrodes were connected to a pH multimeter (accuracy  $\pm 1$  mV) controlled by an IBM-compatible PC. A suitable data-

acquisition program was used. All solutions and reaction mixtures were maintained at 25°C by means of a thermostating system (accuracy  $\pm 0.1$  °C).

Solutions used in this study were well-stirred. In the concentration region of the reference solution in Fig. 1, results were not sensitive to exact stirring speed, indicating that interfacial transport of diiodine and dioxygen are not major factors under the conditions here. During the inhibition period, both dioxygen evolution and diiodine production are at very low levels, so potential effects of interfacial transport are diminished.

Typical recordings are shown in Fig. 1: on the left the oscillation behavior of a 30 ml reference mixture to which 1.0 mL of doubly distilled H<sub>2</sub>O was added after the third oscillation is reported; on the right the behavior when 1.0 ml of suitably diluted aqueous solution of adrenaline was added (batch conditions).

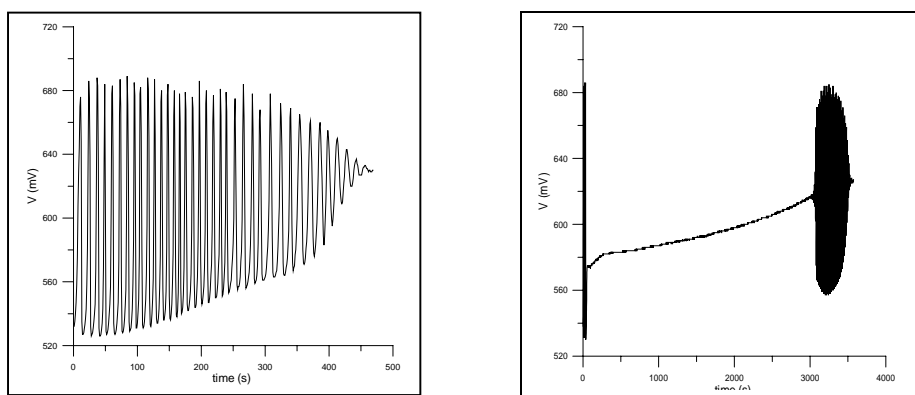


**Figure 1.** Recording of the potential of the bright-platinum electrode vs. time. left) Reference mixture, initial conditions:  $[MA] = 0.05$  M,  $[Mn^{2+}] = 6.67 \times 10^{-3}$  M,  $[IO_3^-] = 6.67 \times 10^{-2}$  M,  $[HClO_4] = 2.66 \times 10^{-2}$  M,  $[H_2O_2] = 1.20$  M; right) Oscillator perturbed by the addition of 1.0 ml adrenaline solution, initial concentration in mixture = 8.98  $\mu$ M.

Similar behaviors were obtained on ten substituted diphenols [7]. The dependence of the inhibition time (i.e. the time elapsed between the cessation and the regeneration of the oscillatory regime) on the concentration of the antioxidant added was found to be linear over a wide range (different for each antioxidant) of concentration [6,7]. The straight line  $t_{inhib}$  vs concentration for adrenaline is shown in Fig. 2.

Below a certain concentration of antioxidant added (different for each antioxidant), the behavior deviates from linearity, and the inhibition times become too low to be detected. At high concentration of antioxidant, the amplitude of the resumed oscillations becomes too low, until up to a given concentration (different for each antioxidant) oscillations do not restart. This means that the reaction reaches its end, not being able to produce radicals anymore.

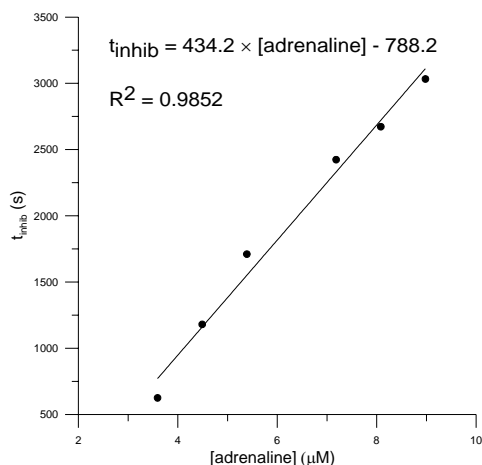


**Figure 2.** Straight line of  $t_{\text{inhib}}$  (s) vs. concentration ( $\mu\text{M}$ ) of adrenaline.

### Mechanistic Interpretation

Recently, *Furrow et al.* [9] reported a 13-step new mechanism (named FCA model) for the BR reaction that takes into account the important role played by  $\text{HOO}\cdot$  radicals in its oscillatory behavior.

To simulate the perturbations by a free-radical scavenger on the oscillations, the following steps were added to the FCA model, where  $\text{Ar}(\text{OH})_2$  indicates a generic substituted diphenol, as adrenaline:



The step IN represents the typical way of subtraction of a radical by an antioxidant: an H atom transfer from a phenolic OH group to the radical. The formed aroxyl radical  $\text{Ar}(\text{OH})\text{O}\cdot$  is quite stable and can react with another radical or with oxygen to give diamagnetic stable compounds. In the simulations  $\text{Ar}(\text{OH})\text{O}\cdot$  was considered an end product. The 1<sup>st</sup> order step DEG represents the possible parallel degradation of the inhibitor to unspecified products. The degradation may be due to oxidation (by acidic iodate) or iodination (by  $\text{I}_2$  or HOI) of  $\text{Ar}(\text{OH})_2$ . The kinetics of these reactions were recently studied in detail [10]: the results showed that for simulation purposes they can be summarized by step DEG.

The kinetic constants of the FCA steps were kept fixed to those reported in [10], while  $k_{\text{IN}}$  and  $k_{\text{DEG}}$  were allowed to vary for the best fit to experimental behaviors. Experimental and simulated behaviors of  $V(\text{Pt})$  and  $[\text{I}^-]$  respectively vs. time for a typical BR mixture perturbed by adrenaline are reported in Fig. 3.

The very good agreement between the experimental and calculated inhibition time can be noted, although both IN and DEG represent overall processes for which individual steps and rate constants have not been determined.

The same agreement was obtained with all the explored concentrations of adrenaline (Table 1), finding the following unique values for the rate constants:  $k_{\text{IN}} = 7.2 \times 10^7 \text{ M}^{-1}\text{s}^{-1}$ ,  $k_{\text{DEG}} = 2.8 \times 10^{-4} \text{ s}^{-1}$ .

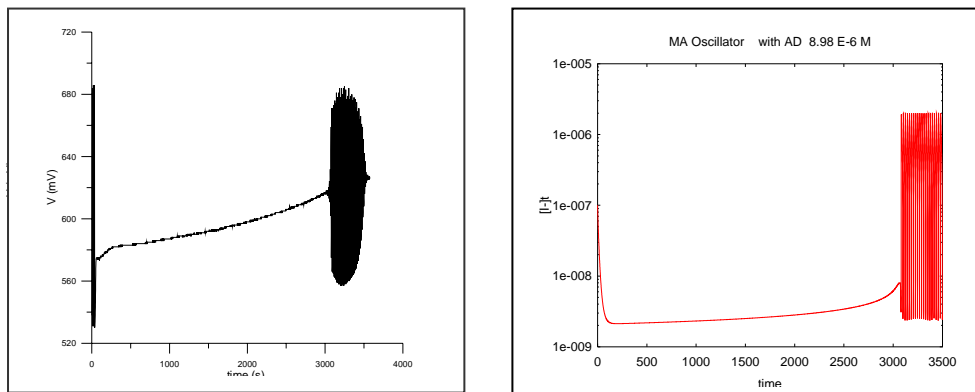


**Figure 3.** left) Experimental behavior of  $V(\text{Pt})$  vs. time right) Simulated behavior of  $[\text{I}^-]$  vs time. Initial conditions see Fig. 1

**Table 1** – Experimental and calculated inhibition times with adrenaline (AD)

AD concn ( $\mu\text{M}$ )	$t_{\text{inhib}}$ (exptl.)	$t_{\text{inhib}}$ (calcd.)
3.59	626	620
4.49	1181	1100
5.34	1711	1650
7.18	2424	2400
8.08	2673	2700
8.98	3033	3040

The obtained values of  $k_{\text{IN}}$  and  $k_{\text{DEG}}$  for the perturbed BR reaction by adrenaline are in line with those obtained for ten substituted diphenols [10], ranging from ca  $10^5$  to  $10^8$   $\text{M}^{-1} \text{s}^{-1}$  and from 0 to  $10^{-5} \text{s}^{-1}$ . Even though it is not permissible to compare rate constants from different-order rate equations,  $k_{\text{INS}}$  are several orders of magnitude higher than  $k_{\text{DEGS}}$ , so we can conclude that in any case the scavenging action by phenolic antioxidants against  $\text{HOO}^\bullet$  radicals is the source of the observed perturbations on the oscillations of the Briggs-Rauscher reaction.

## References

- [1] T.S. Briggs, W.C. Rauscher, *J. Chem. Educ.*, 1973, 50, 496.
- [2] R.M. Noyes, S.D. Furrow, *J. Am. Chem. Soc.*, 1982, 104, 45.
- [3] P. DeKepper, I.R. Epstein, *J. Am. Chem. Soc.*, 1982, 104, 49.
- [4] L. Györgyi, T. Turányi and R.J. Field, *J. Phys. Chem.*, 1990, 94, 7162.
- [5] K.R. Sharma and R.M. Noyes, *J. Am. Chem. Soc.*, 1976, 98, 4345.
- [6] R. Cervellati, N. Crespi-Perellino, S. D. Furrow, A. Minghetti, *Helv. Chim. Acta*, 2000, 83, 3179.
- [7] R. Cervellati, K. Höner, S.D. Furrow, C. Neddens, S. Costa, *Helv. Chim. Acta*, 2001, 84, 3533.
- [8] C.A. Rice-Evans, N.J: Miller, G. Paganga, *Free Radic. Biol. Med.*, 1996, 20, 933.
- [9] S.D. Furrow, R. Cervellati, G. Amadori, *J. Phys. Chem. A*, 2002, 106, 5841.
- [10] R. Cervellati, K. Höner, S.D. Furrow, F. Mazzanti, S. Costa, *Helv. Chim. Acta*, 2004, 87, 133.

## OPTIMIZATION OF PULSE PERTURBATION TECHNIQUE FOR QUANTITATIVE DETERMINATION OF PARACETAMOL IN PHARMACEUTICALS

N. Pejić<sup>1</sup>, M. Milošević<sup>2</sup>, V. Vukojević<sup>3</sup>

<sup>1</sup>Faculty of Pharmacy, University of Belgrade, Vojvode Stepe 450, YU-11000 Belgrade, <sup>2</sup>Faculty of Physical Chemistry, University of Belgrade, Studentski trg 12-16, P.O. Box 137, YU-11001 Belgrade, Yugoslavia, <sup>3</sup>Alcohol and Drug Addiction Research Section, Department of Clinical Neuroscience, Karolinska Institutet, S 17176 Stockholm, Sweden

### Abstract

A new analytical method for the determination of paracetamol using the perturbation caused by different amount of paracetamol on the Bray-Liebhafsky oscillatory reaction system, being in nonequilibrium stationary state, is proposed and optimized. The method relies on the linear relationship between maximal potential shift obtained after adding paracetamol in matrix, and logarithm concentration of paracetamol. The calibration curve obtained is linearly proportional to the logarithm concentration of paracetamol over the range  $6.7 \times 10^{-7} \text{ mol dm}^{-3} - 6.9 \times 10^{-5} \text{ mol dm}^{-3}$ . The proposed method was validated by determining paracetamol in various pharmaceuticals preparations with average RSD of 3.9 %.

### Introduction

The oscillatory chemical system as a non-linear chemical system in the states far from equilibrium may be used as matrix for analytical determinations. The application of oscillation reactions to this effect originates from its complexity and its implicitly extreme sensitivity to various perturbations [1-3]. The species examined under these conditions need not to be essential for the matrix reaction system, but sufficient for reaction with the matrix system. Here, the Bray-Liebhafsky oscillatory reaction [4], as the reaction where hydrogen peroxide decomposes into the water and oxygen in the presence of both  $\text{IO}_3^-$  and  $\text{H}^+$  ions, is used as the matrix for quantitative determination of paracetamol.

Paracetamol, as one of the most important non-narcotic analgesics without the secondary effects of the salicylates on the gastric mucose, is frequently used analgesic drugs, although it may cause liver damage in some instances. At therapeutic dosage levels the drug is relatively no toxic. Because of its increasing therapeutic use, its assay and quality control are of vital importance.

Numerous methods have been reported for the analysis of paracetamol in pharmaceuticals, such as voltametric, spectrophotometric, electrochemical, fluorimetric and chromatographic methods. Based on our previous experience [2,3,5] we have developed Pulse Perturbation of the Oscillatory reaction system in a stable non-equilibrium stationary state or Stable Steady State (PPOSSS) procedure, for quantitative determination of the paracetamol, and, in particular, demonstrated that the mentioned kinetic method could be successfully applied to quantitative determination of paracetamol in bulk drug and pharmaceuticals.

## Experimental

The Bray-Liebhafsky oscillatory reaction (BL), used as the matrix system, was conducted in Continuously fed well Stirred Tank Reactor. Peristaltic pumps generated the inflows of reactants ( $\text{KIO}_3$ ,  $\text{H}_2\text{SO}_4$  and  $\text{H}_2\text{O}_2$ ) as well as outflow of reaction mixture.

The standard stock solution of paracetamol was prepared in 100 (v/v) methanol. The stock solution was stored in refrigerator, protected from daylight and it appeared to be stable during the period of study. Prior to injection, stock solutions were appropriately diluted with methanol before being used as working solutions. Four pharmaceuticals formulations containing paracetamol, excipient and other active ingredients were bought at Serbian chemist's shops and analysed following the proposed procedure. Perturbations were performed by adding microvolumes, from 10 to 100  $\mu\text{L}$ , of both paracetamol stock solution and samples by micropipettes. We applied manual injections of approximate duration of 0.5 s. Temporal evolution of the BL system monitored potentiometrically by Pt electrode *versus* a double junction Ag/AgCl electrode as the reference.

The chosen dynamics structures, when temperature is the control parameter, for perturbation analysis are non-equilibrium stationary states found under the following experimental conditions:  $[\text{KIO}_3]_0 = 5.9 \times 10^{-2} \text{ mol dm}^{-3}$ ,  $[\text{H}_2\text{SO}_4]_0 = 5.5 \times 10^{-2} \text{ mol dm}^{-3}$ ,  $[\text{H}_2\text{O}_2]_0 = 2.0 \times 10^{-1} \text{ mol dm}^{-3}$ , specific flow rate,  $j_0 = 2,9 \times 10^{-2} \text{ min}^{-1}$  and three different temperatures,  $T = 35.5 \text{ }^\circ\text{C}$ ,  $37.0 \text{ }^\circ\text{C}$  and  $42.9 \text{ }^\circ\text{C}$ . The best conditions for calibration curve are obtained at  $T = 42.9 \text{ }^\circ\text{C}$ , that is in a stable non-equilibrium stationary state in the vicinity of a bifurcation point ( $T_{\text{BP}} = 43.2 \text{ }^\circ\text{C}$ ).

## Results and Discussion

The PPOSSS procedure, used for quantitative determination of paracetamol, is based on potentiometric monitoring of the response of the non-linear reaction system as matrix system to the perturbations by different concentration of analyte.

The maximal change in potential (in mV), defined as the difference  $\Delta E_m = E_p - E_s$  is proportional to the added paracetamol concentration. Where  $E_p$  is the maximal potential value attained after the perturbation is performed and  $E_s$  is the potential corresponding to the stable stationary state before the perturbation is performed (Fig. 1.).

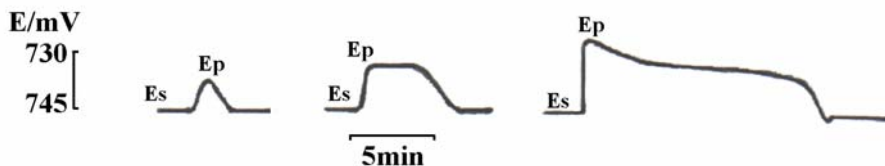


**Figure 1.** Typical response curves obtained after perturbing the stationary state in the BL reaction by addition of different concentrations of paracetamol (on the left to the right):  $6.7 \times 10^{-7} \text{ moldm}^{-3}$ ,  $1.3 \times 10^{-6} \text{ moldm}^{-3}$  and  $1.3 \times 10^{-5} \text{ moldm}^{-3}$

The response of the potential shift *versus* the logarithm of the paracetamol concentrations was linear over the range  $6.7 \times 10^{-7} \text{ mol dm}^{-3} \leq [\text{paracetamol}] \leq 6.9 \times 10^{-5} \text{ mol dm}^{-3}$ . The best linear fit of the experimental points was determined by the least square method. The regression equation of the standard series calibration curves is  $\Delta E_m = -80.6 - 10.7 \log c$  ( $r = 0.996$ ). The detection limit defined as the concentration of paracetamol which produces a signal-to-noise ratio of 3 is  $c = 5.8 \times 10^{-8} \text{ mol dm}^{-3}$ .

In general, for practical purposes of the PPOSSS procedure, the actual mechanism by which the analytes react with the matrix is not necessarily known. However, the composition of the samples that contain different species and possible interference with one another is necessarily known.

Four pharmaceutical formulations that differed in their paracetamol contents, excipients and other active ingredients, were analyzed using the PPOSSS method (Table 1). The average concentrations were calculated from two individual amounts of each sample and determinations were all done in triplicate ( $n = 7$ ). The values of both average recovery determination of paracetamol and a relative standard deviation indicate that reasonable accuracy as well as recovery value is within the state range  $\pm 5\%$  (Ph EUR 97). Thus, the described method can be recommended in the case of high dosage drugs (even in the presence of excipients and other active ingredients).

## Conclusion

The proposed method for the determination of paracetamol is simple, fast, accurate and precise - the unknown concentrations of paracetamol can be determined from the standard series calibration curve within the accuracy of  $\pm 5\%$ , and the detection limit is  $c = 5.8 \times 10^{-8} \text{ mol dm}^{-3}$ . At the same time, the required amount of the sample for a complete analysis may be as small as  $20 \mu\text{L}$ . The method was successfully applied to the determination of paracetamol in analgesic formulations.

Table 1. Precision and recovery of paracetamol in pharmaceutical dosage form

Pharmaceutical formulation	Concentration ( $\text{mol dm}^{-3}$ )	Found $\pm$ SD ( $\text{mol dm}^{-3}$ )	RSD (%)	Recovery (%)
Febricet (tablets)	$5.95 \times 10^{-6}$	$(6.03 \pm 0.19) \times 10^{-6}$	3.3	101.3
	$1.19 \times 10^{-5}$	$(1.21 \pm 0.04) \times 10^{-5}$	3.3	101.9
Paracetamol (syrup)	$5.94 \times 10^{-6}$	$(5.87 \pm 0.22) \times 10^{-6}$	3.9	98.8
	$1.78 \times 10^{-5}$	$(1.77 \pm 0.05) \times 10^{-5}$	3.0	99.4
Efferalgan (syrup)	$3.57 \times 10^{-6}$	$(3.59 \pm 0.16) \times 10^{-6}$	4.5	100.5
	$7.14 \times 10^{-6}$	$(7.24 \pm 0.34) \times 10^{-6}$	4.7	101.4
Fervex (granulated units)	$6.61 \times 10^{-6}$	$(6.88 \pm 0.29) \times 10^{-6}$	4.3	104.1
	$1.49 \times 10^{-5}$	$(1.54 \pm 0.06) \times 10^{-5}$	4.0	103.3

## Acknowledgement

Present investigations are partially supported by the Ministry of Sciences and Environmental Protection of Serbia under the project Physical chemistry of Dynamic states and structures of non-equilibrium systems – self-organization, multistability and oscillatory (project no. 1448).

## References

- [1] R. Jimenez-Prieto, M. Silva, D. Perez-Bendito, *Anal. Chim. Acta*, 1996, 321, 53.
- [2] V. Vukojević, N. Pejić, D. Stanisavljev, S. Anić, Lj. Kolar-Anić, *Analyst*, 1999, 124, 147.
- [3] N. Pejić, V. Kuntić, S. Anić, V. Vukojević, Lj. Kolar-Anić, *Micro. Chim. Acta*, 2003, 143, 261.
- [4] W. C. Bray, *J. Am. Chem. Soc.* 1921, 43, 1262; W. C. Bray, H. A. Liebafsky, *J. Am. Chem. Soc.* 1931, 53, 38.
- [5] Vukojević V, Pejić N, Stanisavljev D, Anić S, Kolar-Anić Lj, *Pharmazie*, 2001, 56, 1.

## WAVE TRAINS IN TWO-VARIABLE CHEMICAL MODEL OF BISTABLE REACTION-DIFFUSION SYSTEM

M. Leda, A.L. Kawczyński

*Institute of Physical Chemistry*

*Polish Academy of Sciences, Warsaw, Poland*

### Abstract

A realistic 1D model of a bistable two-variable chemical system with a stable focus (SF) surrounded by a stable limit cycle (SLC) is investigated. Initial excitations of a subinterval of the system can generate two types of sustained wave sources depending on a value of the bifurcation parameter, which determines the basin of attraction of SF. For a sufficiently small basin of attraction of SF an initial local excitation of a finite system generates a finite sequence of traveling impulses. Each subsequent impulse is wider than the previous one. It is the reason why finite sequences of impulses can be observed in finite systems. In infinite systems, infinite number of impulses is generated. If the basin of attraction of SF is sufficiently large, another type of wave source is induced by an initial excitation. The wave source generates an infinite number of impulses both in finite systems as well as infinite ones. In this case traveling impulses have a local minimum between their front and back.

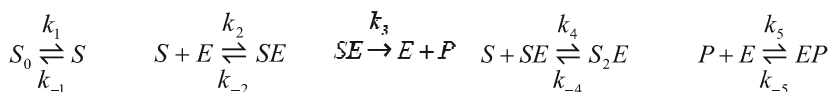
### Introduction

Two kinds of explanations of the creation of target patterns observed in the Belousov-Zhabotinsky reaction are known in literature. One of them is based on the assumption of existence some heterogeneities (pacemakers), where by the definition the system oscillates with higher frequency. The other explanation is based on the assumption that wave sources (leading centers) appear in a homogeneous medium due to fluctuations, which locally excite the system. The known models of leading centers consisted of at least three variables [1,2], whereas the models of pacemakers were based on two-variable systems containing terms with explicit dependence on a space coordinate [2,3,4].

A two-variable model of sources of waves in a one-dimensional (1D) system is presented below. Its dynamics is described by terms, which do not depend explicitly on the space coordinate. The idea of the model is based on the coexistence a stable steady state and a stable limit cycle above the subcritical Hopf bifurcation.

### Results and Discussion

The model describes two coupled catalytic (enzymatic) reactions occurring in open system according to the following scheme:





The assumption that the total concentrations of catalysts (enzymes) are much lower than the concentrations of the reactant  $S$  and the product  $P$  allows us to identify concentrations of the both catalyst as well as their complexes as fast variables and eliminate them in the slow time dynamics.

We consider one-dimensional bounded system of the length  $L'$ . Neglecting the diffusion coefficients of the catalysts and all their complexes allows us to describe local changes of concentrations of  $S$  and  $P$  by two equations:

$$\begin{aligned}
 \frac{\partial s(x,t)}{\partial t} - \frac{\partial^2 s(x,t)}{\partial x^2} &= a_1 - a_2 s - \frac{s}{(1+s+a_3 s^2)(1+p)} \\
 \frac{\partial p(x,t)}{\partial t} - D \frac{\partial^2 p(x,t)}{\partial x^2} &= b \left( \frac{s}{(1+s+a_3 s^2)(1+p)} - b_1 \right)
 \end{aligned}$$

where  $s=S/K_m$ ,  $p=K_5 P$  are dimensionless concentrations of the reactant  $S$  and the product  $P$ ,  $K_m=(k_{-2}+k_3)/k_2$ ,  $K_5=k_5/k_{-5}$ ,  $t=k_3 E_0 / K_m t'$  is the dimensionless time ( $t'$  is real time),  $E_0$  is the total concentration of the enzyme  $E$ ,  $x=[k_3 E_0 / (D_S K_m)]^{1/2} x'$  is the dimensionless spatial coordinate ( $x'$  is the coordinate in a physical one-dimensional space) and  $D=D_P/D_S$ , where  $D_S$  and  $D_P$  are the diffusion coefficients of the reactant and the product, respectively.  $a_1=k_1 S_0 / (k_3 E_0)$ ,  $a_2=k_{-1} K_m / (k_3 E_0)$ ,  $a_3=k_4 / k_{-4} K_m$ ,  $b=K_m K_5$ ,  $b_1=k_7 E_0' / (k_3 E_0)$ ,  $b_2=K'_m K_5$  and  $K'_m=(k_{-6}+k_7)/k_6$ .

For appropriate values of the parameters, nullclines for  $s$  and  $p$  intersect at one point (stationary state)  $(s_0, p_0)$  located on the middle (repelling) branch of the N-shaped nullcline for  $s$ . The stationary state (the stable focus) becomes unstable at the critical value of the bifurcation parameter  $b=b_{cr}$  due to the subcritical Hopf bifurcation. For  $b \in (b_{cr}, b_s)$  the stable focus (SF) coexists with a stable (SLC) and unstable (ULC) limit cycles. The bifurcation parameter  $b$  controls the positions of ULC and SLC. For  $b$  close to  $b_{cr}$ , ULC is very close to SF, whereas SLC is far from SF. With increasing  $b$  ULC comes near to SLC.

We consider the initial-boundary problem with the zero flux boundary conditions:

$$\frac{\partial s}{\partial x}(0,t) = \frac{\partial s}{\partial x}(L,t) = \frac{\partial p}{\partial x}(0,t) = \frac{\partial p}{\partial x}(L,t) = 0$$

and the following initial conditions:  $s(x,0)=s^*$ ,  $p(x,0)=p^*$  for  $x \in [0, l^*]$  and  $s(x,0)=s_0$ ,  $p(x,0)=p_0$  for  $x \in (l^*, L]$ , where  $s^*$  and  $p^*$  belong to the basin of attraction of SLC.

If  $b$  is slightly greater than  $b_{cr}$ , then the initial excitation causes the appearance of a sequence of traveling impulses. The width of each impulse decreases during its spreading and attains asymptotic size sufficiently far from the interval of the initial excitation (see **Fig. 1**). Each next impulse is initially wider than the previous impulse. Because the system is finite, the width of some new generated impulse becomes larger than  $L$ . The back of the impulse is not formed and finally the system oscillates homo-

generously with the period characteristic for SLC. Therefore, in a finite system one can observe the generation of a finite sequence of impulses only.

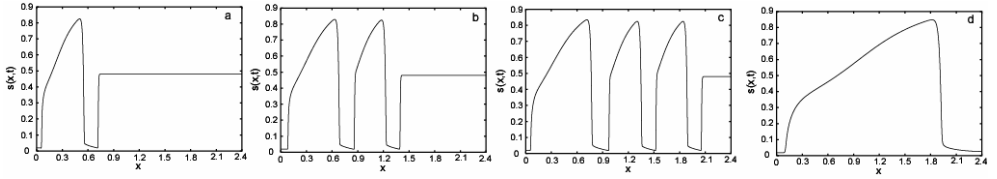


**Figure 1.** Concentrations of the reactant for  $a_1=a_2=0.005$ ,  $a_3=250$ ,  $b_1=0.0026$ ,  $b=0.24$ ,  $s^*=0.01$ ,  $p^*=p_0$ ,  $l^*=0.015$  at the following times: 23000 - (a); 45000 - (b); 66500 - (c); and 1706500 - (d).

For larger values of  $b$  the initial excitation induces the generation of traveling impulses shown in **Fig. 2**. The impulse of  $s(x,t)$  has a small local minimum between the front and the back, whereas the impulse of  $p(x,t)$  has a corresponding small maximum. The back of the impulse is partially positioned inside ULC, where its evolution is governed by the vector field around SF. This part of the trajectory forms a bend, which in further evolution forms a loop. It follows from our numerical calculations that the period of oscillations observed at points, where the traveling impulses have their asymptotic forms, is slightly greater than that for homogeneous oscillations and does not depend on the initial conditions.

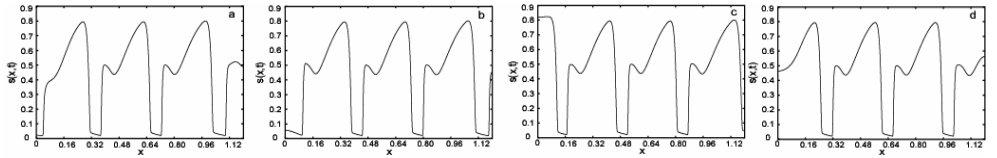


**Figure 2.** Concentrations of the reactant for  $b=0.4$  and  $l^*=0.01$  at the following times: 102000 - (a); 105000 - (b); 108000 - (c) and 114000 - (d). The remaining parameters are the same as in Fig. 1.

For values of  $b$  near  $b_s$ , where ULC is close to SLC, for a sufficiently small width of excitation  $l^*$  only single impulse is generated and then the distributions of the reagents return to their stationary values. However, sequences composed of subsequent numbers of impulses (see **Fig. 3**) appear for greater values of  $l^*$ .

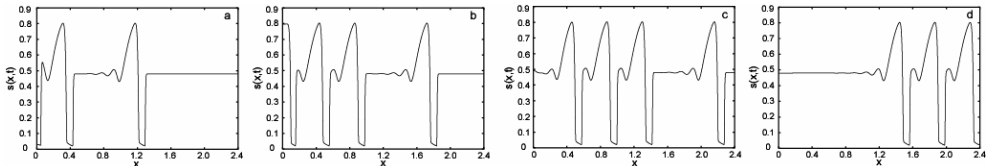


**Figure 3.** Concentrations of the reactant for  $b=0.41$  and  $l^*=0.09$  at the following times: 44000 - (a); 64000 - (b); 80000 - (c) and 116000 - (d). The remaining parameters are the same as in Fig. 1.

## Conclusions

The types of sustained waves sources described above can be observed in all chemical systems in which ULC and SLC surround SF. There are known real chemical systems like the chlorite-iodide oscillator [5] and the peroxidase-oxidase reaction [6], in which the coexistence of the stable stationary state surrounded by SLC has been observed. It should be stressed that the wave sources described in this work have different properties from the target patterns observed in experiments (B-Z reaction, and the others) as well as in the models known so far. In particular, they have nearly the same frequency of impulses generation as the frequency of stable limit cycle oscillations.

## References

- [1] A. N. Zaikin, A. L. Kawczyński, *J. Non-Equilib. Thermodyn.*, 1977, 2, 39.
- [2] A. L. Kawczyński, *Pol. J. Chem.*, 198660, 223.
- [3] P. Ortoleva, J. Ross, *J.Chem. Phys.*, 1974, 60, 5090.
- [4] J. J. Tyson, P. C. Fife, *J.Chem. Phys.*, 1980, 73, 2224.
- [5] C. E. Dateo, M. Orban, P. De Kepper, I. R. Epstein, *J. Am. Chem. Soc.*, 1982, 104, 504.
- [6] B. D. Aguda, L. H. Frisch, L. F. Olsen, *J. Am.Chem. Soc.*, 1990, 112, 6652.

## PREDICTION OF PROPERTIES IN MICROEMULSION: MOLECULAR THEORY

S.N. Blagojević, M. Ilić

Institute of General and Physical Chemistry, POB 551, Belgrade, SCG

### Abstract

Microstructural features including the droplet radius, the thickness of the surfactant layer at the interface, the number of molecules of various species in a droplet, the size and composition dispersions of the droplets, and the distribution of the surfactant, oil and water molecules in microemulsion system are calculated.

### Introduction

In quaternary systems of water/surfactant/co-surfactant/oil in the oil rich region, a thermodynamically stable emulsion, a so-called "microemulsion" is formed. Based on a small droplet size of the inner phase, the mixture is optically isotropic, transparent, but strongly light scattering. The first known system consisted of water/K-oleate/hexanol/benzene. On addition of increasing amount of a short-chain alcohol (co-surfactant) to a milky emulsion of benzene and aqueous K-oleate, a stable, transparent solution is formed. Microemulsions have been defined as a mixture of water and oil in similar portions which are spontaneously transformed into transparent and stable solutions by the presence of large amounts of surfactants and co-surfactants. Normally the co-surfactants are a short-chain alcohol with 4 to 8 carbon atoms. The distinction between microemulsions, micellar and inverse micellar emulsion is difficult, determination of properties with the aid of conductivity measurements, rheological properties, x-ray diffraction, ultracentrifugation, and dynamic light scattering. A rich variety of theories have been used to explain microemulsion phase behavior. The influence of variables such as salinity, temperature and solvent type can be described qualitatively in terms of binary phase diagrams of the components of the microemulsion. In contrast, quantitative theories are required in order to calculate phase diagrams and the size of microemulsion droplets. Lattice model [1] [2], have been developed in which each molecule is treated as a difunctional "dumbbell" oriented so that hydrophilic and hydrophobic ends form separate regions on the lattice. A Flory-Huggins solution model [3] may be used to reproduce a wide variety of types of microemulsions phase diagrams by regressing interaction parameters, which depend upon surfactant concentration. Another quite different approach is based on the tessellation of space by Veronoi cells to describe the onset of percolation [4]. For systems composed of bicontinuous structures, this model is very useful for treating critical fluctuations. These models do not however account explicitly for the presence of the interface and its consequence [5].

## Results and Discussion

Calculations were carried out for a system consisting of the anionic surfactant sodium laureth sulfate, decyl glycoside (co-surfactant), oil phase (Santalum Album, Vetiveria Zizanoides, essential oils from Sandal and Vetiver wood) and water containing 0.2M NaCl and citrate buffer (pH 5.5). In all calculations we assumed the coexistence of an excess dispersed phase. This means that the droplet microemulsion phase is part of a two-phase system and that the amount of dispersed phase present in the droplet is a maximum achievable.

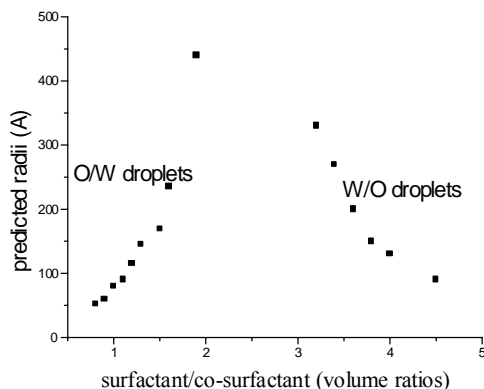


**Figure 1.** Predicted radii of microemulsion droplets as a function of the volume ratios

The number of surfactant molecules in the interfacial layer ( $N_{il}$ ), thicknesses of the interfacial layers ( $F_t$ ) and volume fractions ( $V_f$ ) of oil and water for different surfactant/co-surfactant volume ratios (from 1 to 6) are summarized in table 1.

**Table 1.** Properties of microemulsion

	$N_{il}$	$F_t$ (Å)	$V_{f, oil}$	$V_{f, water}$
1	580	12.8	0.04	0.96
2	45600	12.1	0.28	0.72
3	23400	11.9	0.85	0.15
4	3480	11.7	0.95	0.05
5	980	11.5	0.96	0.04
6	780	11.1	0.98	0.02

As a the most important properties of microemulsion, oil-water interfacial tension (dyne/cm) at the flat surfaces between microemulsion phases and excess dispersed phases as a function of the surfactant/co/surfactant volume ratios are described in figure 2.

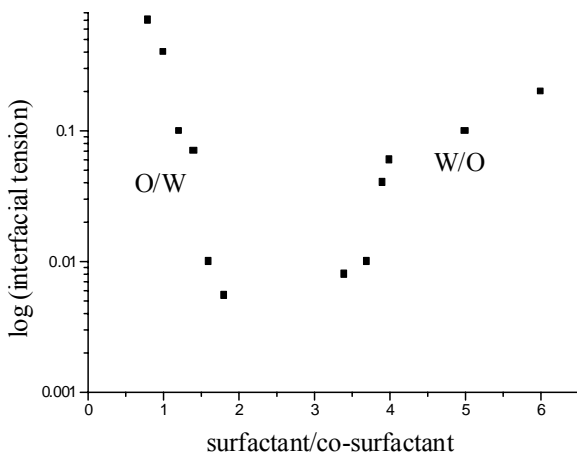


**Figure 2.** Oil-water interfacial tensions as a function of surfactant/co-surfactant volume ratio

In developing a molecular treatment for microemulsion it must be take into account the chain packing, which depends on the curvature of the aggregates, the self-association of surfactant and co-surfactant in oil, the penetration of the interfacial layer region of the microemulsion by the oil molecules, their effects on chain packing and interfacial energies, and the hard core interaction among the droplets.

## Conclusion

In this paper, a predictive molecular thermodynamic approach is developed to calculate the structural and compositional characteristic of microemulsions. Illustrative numerical results are provided for one anionic surfactant /co-surfactant /oil phase/ water system. The model allows the identification from two-phase to a three-phase system, and calculation of the interfacial tension between the microemulsion and the coexisting phase.

## Acknowledgment

We gratefully acknowledge for the financial support in grant no. 1448 of the Ministry for Science, Tehnology and Development of the Republic of Serbia.

## References:

- [1] K.Dawson, M.Lipkin, B.Widom, J.Chem.Phys., 1988, 88, 5149.
- [2] D.Peck, R.Schechter, K.Johnston, J.Phys.Chem., 1991, 95, 9541.
- [3] W.Rossen, R.Brown et all, Soc.Pet.Eng. J., 1982, 945.
- [4] Y.Talmon, S.Prager, J.Chem.Phys., 1978, 69, 2984.
- [5] T.Klein, J.Prausnitz, J.Phys.Chem., 1990, 94, 8811.

## PREDICTION OF PROPERTIES IN MICROEMULSION: THE LATTICE FLUID SELF-CONSISTENT FIELD THEORY

S. N. Blagojević, N. Potkonjak

*Institute of General and Physical Chemistry, POB 551, Belgrade, SCG*

### Abstract

A lattice fluid self-consistent field theory is used to calculate both the composition and interfacial tension ( $\gamma$ ) and bending moment ( $c$ ) of spherical interfaces between oil and water.

### Introduction

A microemulsion is transparent thermodynamically stable mixture of oil, water and one or more amphiphiles which are adsorbed on the interface. Two fundamental interfacial properties, the interfacial tension and bending moment, must be known in order to predict the droplet size, stability and phase behavior of microemulsion. Equilibrium is attained when a balance is struck between the interfacial energy and the energy due to dispersion of the micelle [1]. There have been few attempts to calculate the interfacial tension and bending moment with molecular theories based on statistical mechanics, as a function of the molecular architecture of the oil and surfactants [2,3]. A unified classical and molecular thermodynamic theory of microemulsion has been proposed [4], for dilute polymer solution and it was used to determine the segment distribution function of surfactant tails on a spherical interface. This distribution function was calculated from the diffusion equation for a single chain, neglecting interaction between chains and solvent. From the distribution function, the interfacial tension and bending moment were determined in order to calculate the droplet size and phase behavior. The self-consistent theory (SCF) developed by Scheutjens and Fleer [5,6] is a powerful theory for describing an interface, because it provides a detailed representation of interfacial composition. Once the equilibrium distributions of components are known in each layer of interface, the free energy of the system may be calculated. The theory was first used to treat the adsorption of homopolymers in solution onto flat surfaces and the interaction strength between these surfaces. In the above SCF theories, the lattice is incompressible and the density is constant in each layer of the interface and the bulk. Compressibility has been included by combining the SCF theory with the lattice fluid theory for homopolymers in contact with a vacuum. There are number of practical application for this type of molecular model. For example, solubilization in water swollen reverse micelles depends upon the partition coefficient of the solute between the bulk water core and interface. This partition coefficient may be calculated by integrating the interfacial bonding moment over the micelle radius [7]. The lattice fluid SCF theory offers a means to determine the bending moment at the molecular level. In the case of liquid crystals, the bending moment, interfacial tension and interfacial interaction strength are required to determine the morphology [8].

## Results and Discussion

We use as a basis the thermodynamics of a Gibbs dividing surface. The surface excess free energy ( $F^S$ ) is calculated by subtracting the free energy of the system without the interface from the free energy of the system with the interface.

$$dF^S = \gamma dS + Sc d(2/R) + \sum \mu_i dn_i^S + S^S dT$$

where  $\mu_i$  is a chemical potential of component  $i$  at constant  $R$  (radius of droplet core),  $S$  and  $S^S$  is the surface excess entropy,  $n_i^S$  is the excess number of molecules of type  $i$  in the interface,  $\gamma$  is interfacial tension and  $c$  is the bending moment of the interface. An important advantage of the lattice fluid SCF theory, compared with earlier theories of microemulsions is the ability to calculate composition throughout the interface. In SCF theory the distribution function of polymer conformation is taken into account explicitly. The statistical weight of each conformation can be calculated by performing a step-weighted walk in the lattice. When the lattice is spherical the number of sites in each layer  $z$  is a function of the distance from the center of the sphere as follows:

$$L(z) = 4/3 \pi [(z + R/\delta)^3 - (z-1+R/\delta)^3]$$

where  $R$  is radius of the droplet core and  $\delta$  is a thickness of a lattice layer. For calculated case four components are in the lattice: surfactant tail, solvent, oil and holes. Calculations were carried out for a system consisting of the anionic surfactant MIPA-laureth sulfate, laureth-4 (co-surfactant), oil phase (glicine-soja oil) and water containing citrate buffer (pH 5.5).

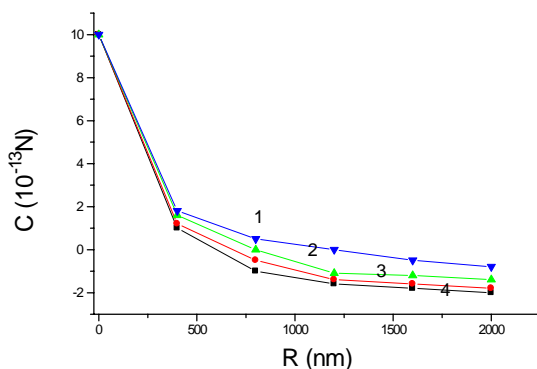


**Figure 1.** Bending moment as a function of radius at different surfactant/co-surfactant mass ratio (1-1, 2-1.5, 3-3, 4-3.5)

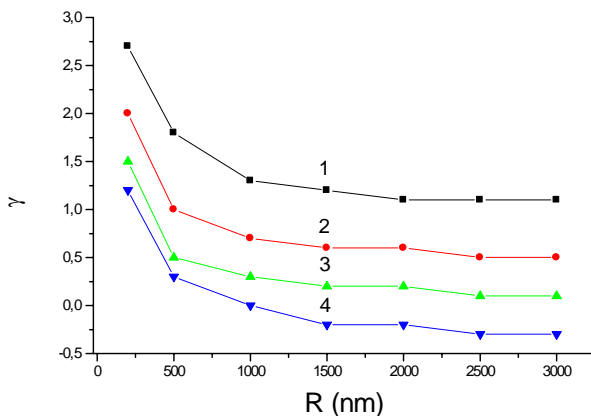


**Figure 2.** Interfacial tension as a function of radius at different surfactant/co-surfactant mass ratio (1-1, 2-1.5, 3-3, 4-3.5)

## Conclusion

The lattice fluid SCF theory offers a means to calculate fundamental interfacial properties of microemulsions. For investigated system the prediction of interfacial thickness is in an agreement with experimental results. For very small droplet radii, the bending moment of the interface is large and positive, indicating that the interface is highly stressed. The interfacial tension is sensitive to the droplet radius. As the droplet radius approaches the natural radius, the bending moment decreases to zero and the interfacial tension becomes less sensitive to the radius.

## Acknowledgment

We gratefully acknowledge for the financial support in grant no. 1448 of the Ministry for Science, Tehnology and Development of the Republic of Serbia.

## References

- [1] E.Ruckenstein, J.Chi, J.Chem.Soc., Faraday Trans., 1975, 71, 1690.
- [2] C.Huh, Soc.Pet.Eng.J., 1983, 829.
- [3] J.Eriksson, S.Ljunggren, J.Colloid Interface Sci., 1991, 145, 224.
- [4] D.Peck, S.Schechter, J.Phys.Chem., 1991, 95, 9541.
- [5] J.Schutjens, J.Fleer, J.Phys.Chem., 1979, 83, 1619.
- [6] J.Schutjens, J.Fleer, J.Phys.Chem., 1980, 84, 178.
- [7] E.Leodidis, A.Bommarius, J.Phys.Chem., 1991, 95, 5913.
- [8] M.Bourrel, R.Schechter, Microemulsions and Related Systems, Marcel Dekker, New York, 1988.

## PREDICTION OF PROPERTIES IN MICROEMULSION: STATISTICAL MECHANICS OF MICROEMULSION

S. N. Blagojević

*Institute of General and Physical Chemistry, POB 551, Belgrade, SCG*

### Abstract

We discuss the statistical mechanics of the droplet microemulsion within the context of the model of configurational partition function.

### Introduction

Microemulsions are thermodynamically stable mixtures of oil, water and surfactants. The stability of such mixtures is the result of a microstructure in which microdomains of oil and water, with characteristic dimensions of ten to hundreds of angstroms, are separated by monolayer films of surfactants. Such systems are found to adopt a variety of geometrical structures for the microdomains, including ordered lammellar phases containing alternating layers of oil and water, phases containing droplets of one fluid dispersed in a continuum of the other and bicontinuous spongelike structures. Such structures may occur either as single phases or in large parts of the phase diagram in two or three-phase coexistence regions. One very successful approach to understanding the behavior of microemulsion has been to describe such systems as ensembles of interfacial surfaces with conformation controlled by a simple interfacial bending free energy of the form proposed by Canham [1] and Helfrich [2]. In this model, the elasticity of the interfacial films is characterized by three elastic parameters: a mean rigidity, a Gaussian (or saddle-splay) rigidity and a spontaneous curvature. In statistical mechanics the Gibbs free energy ( $G$ ) is related to the configurational partition function  $Z$  in the pressure ensemble by:

$$G = -kT \ln Z (T,P)$$

$$Z (T,P) = \sum_V \sum_E \Omega (E,V,N) \exp [-\beta(E+PV)]$$

where  $\Omega (E,V,N)$  is the number of configurations available to a system of  $N$  molecules whose configurational (potential) energy and volume are  $E$  and  $V$ . The summation extends over all values of  $E$  and  $V$ . In the ensemble of systems under consideration, the temperature  $T$  ( $\beta=1/kT$ ) and pressure are fixed. The Gibbs potential and the associated pressure ensemble are the most convenient of the potential ensembles to utilize in the study of fluid phase equilibria. The properties derived from the pressure ensemble in the thermodynamic limit are identical with those of the more commonly used canonical and grand canonical ensemble [3].

## Results and Discussion

The fundamental problem is to determine  $\Omega$ . Solution of the problem is very difficult even when a lattice is used to enumerate configurations. In the lattice formulation, the problem is to determine the number of configurations available to a system of  $N$  molecules each of which occupies  $r$  sites (a  $r$ -mer) and  $N_0$  vacant lattice sites (holes). Approximate value of  $\Omega$  for a multicomponent mixture of  $r$ -mers in a lattice, can be calculated in a mean field approximation:

- the total number of lattice sites for a binary mixture of  $N$   $r$ -mers and  $N_0$  empty sites is  $N_r = N_0 + rN$
- the coordination number of the lattice is  $z$ . Each interior mer of a linear chain is surrounded by  $z-2$  nearest nonbonded neighbors and two bonded neighbors, mers at the chain ends have  $z-1$  nearest nonbonded neighbors and one bonded neighbor. Thus, each  $r$ -mer is surrounded by  $qz$  nearest nonbonded neighbors where  $qz = r(z-2) + 2$
- The total number of nearest neighbor pairs in the system is  $(z/2) N_r$ . Only  $(z/2)N_q$  are nonbonded pairs where  $N_q = N_0 + qN$ .
- An  $r$ -mer is characterized by a symmetry number  $\sigma$ . For example, for a linear  $r$ -mer it is equal to two if the chain ends are indistinguishable and to unity if the chain ends are distinguishable.
- An  $r$ -mer is also characterized by a flexibility parameter  $\delta$ . It is equal to the number of ways in which the  $r$ -mer can be arranged on the lattice after one of its mers has been fixed on a lattice site. It is a measure of the  $r$ -mer internal degrees of freedom.

The number of configurations available to a system of  $N$   $r$ -mers and  $N_0$  empty sites is

$$\Omega = (\delta/\sigma)^N \{N_r!/(N_0!N_r!)\} (N_q!/N_r!)^{z/2}$$

Using Sterlings approximation ( $n! \approx (n/e)^n$ ) for a large  $z$  ( $z \rightarrow \infty$ ),  $\Omega$  can be expressed:

$$\lim \Omega = (1/f_0)^{N_0} (\omega/f)^N \quad \{\omega = \delta r/\sigma e^{r-1}, f_0 = N_0/N_r, f = rN/N_r\}$$

This approximation is known as the "Flory approximation". With two more assumptions: that the flexibility parameter  $\delta$  is independent of temperature and pressure and that close packed volume of molecule is independent of temperature and pressure. The energy of lattice depends only on nearest neighbor interaction, so the attractive lattice energy can be written as

$$E = - (z/2) N_r \sum_i \sum_j p(i,j) \varepsilon_{ij}$$

where  $\varepsilon_{ij}$  is the pair interaction energy between components  $i$  and  $j$  and  $p(i,j)$  is the pair (joint) probability of an  $(i,j)$  pair in the system. In this case it is "holes" and "mers". Since  $E$  and  $\Omega$  are functions of a single parameter, the number of holes in the lattice, the double sum over  $E$  and  $V$  required in the evaluation of the partition function can be replaced by a single sum over  $N_0$ :

$$Z(T,P) = \sum_{N_0} \Omega \exp [-\beta(E + PV)]$$

In statistical mechanics the standard procedure is to approximate to above sum by its maximum term, the maximum term is overwhelmingly larger than any other for macroscopic system. This is equivalent to equating the free energy to the logarithm of the generic term in the partition function and then finding minimum value of the free energy:

$$G = E + PV - kT \ln \Omega$$

For a purposes of calculation it is most convenient to work in a grand-canonical ensemble in which an interface of a variable area  $A$  fluctuates about a reference plane of fixed area  $A_p$ . The average value of  $A$  is controlled in this ensemble by a chemical potential conjugate to  $A$ , where the value of chemical potential is equal to that in the coexisting microemulsion phase. The macroscopic interfacial tension measured by a spinning drop or surface scattering experiment is given by the change of  $\Omega$  of the interface per unit change in the projected area  $A_p$  of the interface at the fixed value of chemical potential. The derivate  $\partial\Omega/\partial A_p$  is equivalent to the corresponding derivate of the total Helmholtz free energy of a system comprised of the interface with coexisting microemulsion phase.

Calculations of surface tension (mN/m) (20C) were done for water/oil/surfactants (W/O/S) system as follows for Na-lauril-ether-sulphate (0.1%) and olive oil (55%):

	Water	Water/surfactant	W/O/S
Calculated	71.5	34.2	38.3
Measured	72.8	33.1	38.5

## Conclusion

We have analysed the effects of approximation in determining  $\Omega$  in microemulsion system. The surface tension was calculated and these calculations are very close to measured values by tensidometry.

## Acknowledgment

We gratefully acknowledge for the financial support in grant no. 1448 of the Ministry for Science, Tehnology and Development of the Republic of Serbia.

## References

- [1] P.Canham, J.Theor.Biol., 1970, 26, 61.
- [2] W.Helfrich, Z.Naturforsch., 1973, 28c, 693.
- [3] M.Lewis, J.Siegert, Phys.Rev., 1956, 101, 1227.

## HPTCu REACTION SYSTEM IN TWO MASS-COUPLED REACTION CELLS

O. Pešek, L. Schreiberová, I. Schreiber

*Institute of Chemical Technology Prague, Department of Chemical Engineering and Center for Nonlinear Dynamics of Chemical and Biological Systems, Technická 5, 166 28 Praha 6, Czech Republic*

### Abstract

Oscillating reactions with an autocatalytic effect involving protons are called pH-oscillators. Here we focus on the reaction between hydrogen peroxide and thiosulfate catalyzed by  $\text{Cu}^{2+}$  in the solution of  $\text{H}_2\text{SO}_4$  (HPTCu). In a single continuous-flow stirred tank reactor, this reaction provides nonlinear dynamical behavior including different types of steady states, spontaneous oscillations, bistability between steady states or between a steady state and oscillations, and hysteretic loops. In addition, there exist conditions under which the system is excitable. When two reaction cells are coupled by diffusion-like mass transfer dynamical behavior becomes very complex. We present results of numerical simulations of dynamics in two coupled flow-through stirred reactors (CSTR).

### Introduction

Following earlier studies in single-CSTR arrangement [1,2] we examined all nonlinear features experimentally by varying the flow rate and inflow concentration of the reactants. Also, we applied perturbations at a particular dynamical mode and studied the system's response to single-pulse or periodic pulsed perturbations [3]. The observed phenomena were compared with the mechanism of the system taken from [1]. Even though this mechanism was found to account for many of the observed dynamical phenomena, some features are inconsistent with experiments and further refinements are needed.

In future experimental work we will focus on two mass-coupled CSTRs. As a preliminary study here we use the original mechanism to predict dynamics in a coupled system with a focus on transfer of signals from one reactor to the other when both CSTRs are oscillating. Nonidentical coupled reactors provide complex multiple steady states including isolas, and also compound oscillations with amplitudes depending on the coupling strength.

### Dynamical Behavior of the Reaction

The mechanism is quite involved [1] and bifurcations leading to complex dynamics can be expected when external constraints are varied. These constraints are the inflow reactant concentrations, the flow rate, temperature in the reactor as well as the intensity of stirring. Variation of the system's dynamics as the constraints are varied was experimentally examined by Orbán and Epstein [2]. They found that pH of the system corresponds to one of the following four states:

- Steady state I (SSI) – pH ~ 7-9
- Steady state II (SSII) – pH ~ 5
- Steady state III (SSIII) – pH ~ 3,5
- Oscillations

The steady states may coexist and the system will operate at one of the alternative attractors depending on its history and, in addition, there is a parameter region, where the system is excitable with respect to pulsed addition of certain chemical species.

### Model

To simulate dynamics of two coupled CSTRs with mutual mass transfer, we use the mass balance equations with diffusion-like coupling terms. By using an assumption of ideal mixing and mechanism elaborated by Kurin-Csörgei et al. [1], we obtain the following equations:

$$\frac{dc_{i1}}{dt} = k_{01}(c_{i01} - c_{i1}) + \sum_{i1} r_j + ka(c_{i2} - c_{i1})$$

$$\frac{dc_{i2}}{dt} = k_{02}(c_{i02} - c_{i2}) + \sum_{i2} r_j + ka(c_{i1} - c_{i2})$$

where

$c_{i1}$ ;  $c_{i2}$ ...the concentration of species  $i$  in the first (second) reactor,

$c_{i01}$ ;  $c_{i02}$ ...the concentration of species  $i$  in the inlet to first (second) reactor,

$\sum_{i1} r_j$ ;  $\sum_{i2} r_j$  ...overall reaction rates for species  $i$  in the first (second) reactor,

$k_{01}$ ;  $k_{02}$ ...reciprocal residence time (=flow rate) in the first (second) reactor,

$k$ ...mass transfer coefficient

$a$ ... *specific area*

### Results

We focused on the region of oscillation and studied how the oscillations in the first reactor can affect the oscillations in the other reactor. We calculated the time series for various values of parameters corresponding to selected dynamics. As expected, we found that the connection causes synchronous oscillations in both reactors in most of the parameter region of oscillations. But there are narrow sub-regions, where the behavior becomes more complex. These results show oscillatory dynamics for gradually increasing values of the reciprocal residence time  $k_0$ . For weak coupling the oscillatory amplitudes in both reactors differ substantially. As the coupling strength is increased, the frequency of oscillations in the first reactor is decreased until oscillations disappear. Finally, for large enough coupling the oscillations become fully synchronized.

The calculated results are summarized in the form of diagrams where the dependence of a firing number on the coupling strength  $ka$  is shown for three different flow rates  $k_0$  (Figs. 1-3). The firing number  $v_0$  is defined as a ratio of the number of oscillations in the first reactor to the number of oscillations in the second reactor. Such plots are called devil's staircase.

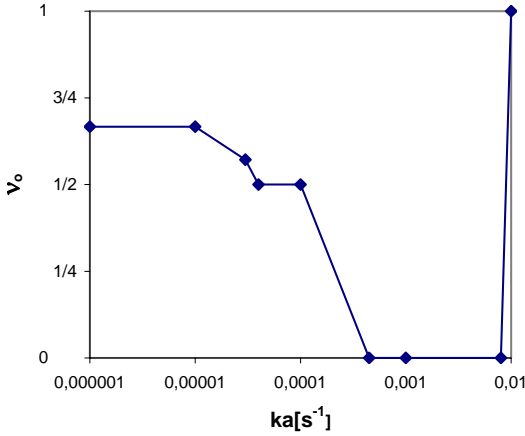


**Figure 1.** – Devil's staircase diagram;  $[H_2O_2]_{01} = [H_2O_2]_{02} = 0.1$  M;  $[S_2O_3^{2-}]_{01} = 0.005$  M,  $[S_2O_3^{2-}]_{02} = 0.008$  M;  $[Cu^{2+}]_{01} = [Cu^{2+}]_{02} = 2.5 \times 10^{-5}$  M;  $[H_2SO_4]_{01} = [H_2SO_4]_{02} = 0.001$  M;  $k_0 = 0.0014$  s<sup>-1</sup>

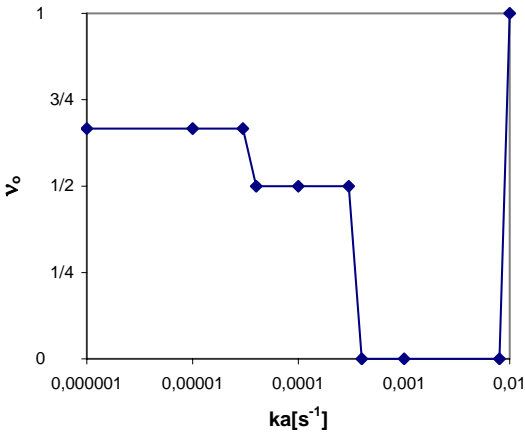


**Figure 2.** – Devil's staircase diagram;  $[H_2O_2]_{01} = [H_2O_2]_{02} = 0.1$  M;  $[S_2O_3^{2-}]_{01} = 0.005$  M,  $[S_2O_3^{2-}]_{02} = 0.008$  M;  $[Cu^{2+}]_{01} = [Cu^{2+}]_{02} = 2.5 \times 10^{-5}$  M;  $[H_2SO_4]_{01} = [H_2SO_4]_{02} = 0.001$  M;  $k_0 = 0.0015$  s<sup>-1</sup>

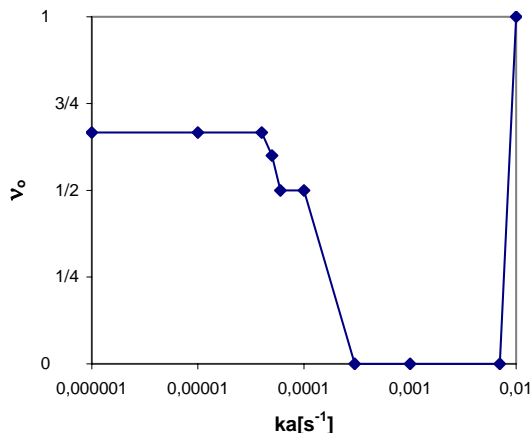


**Figure 3.** – Devil's staircase diagram;  $[\text{H}_2\text{O}_2]_{01} = [\text{H}_2\text{O}_2]_{02} = 0.1 \text{ M}$ ;  $[\text{S}_2\text{O}_3^{2-}]_{01} = 0.005 \text{ M}$ ,  $[\text{S}_2\text{O}_3^{2-}]_{02} = 0.008 \text{ M}$ ;  $[\text{Cu}^{2+}]_{01} = [\text{Cu}^{2+}]_{02} = 2.5 \times 10^{-5} \text{ M}$ ;  $[\text{H}_2\text{SO}_4]_{01} = [\text{H}_2\text{SO}_4]_{02} = 0.001 \text{ M}$ ;  $k_0 = 0.0016 \text{ s}^{-1}$

## Discussion and Conclusions

Due to its complex mechanism, the  $\text{H}_2\text{O}_2\text{-S}_2\text{O}_3^{2-}\text{-H}_2\text{SO}_4\text{-Cu}^{2+}$  system displays a rich variety of dynamical regimes including multiple steady states and periodic oscillations in a single CSTR. By coupling two nonidentical reactors, this system provides more complex behavior than a single reactor. With the knowledge of the behavior of the system in a single reactor, the set of parameters corresponding to autonomous oscillations was chosen and we observed how the strength of mutual coupling changes the patterns of spontaneous oscillations. We found conditions, where the oscillations are not only fully synchronized, but they stabilize in a compound dynamical regime characterized by certain ratio of frequencies. In the future work we intend to compare this numerical study to experiments in a mass-coupled cell system, which represents a simplified model of biochemical and biological pH sensitive systems.

## Acknowledgement

This work was supported by a project MSM223400007 from Ministry of Education of the Czech Republic and by a grant GA203/03/0488 from the Czech Science Foundation.

## References

- [1] Kurin-Csörgei K., Orbán M., Rábai G. and Epstein I.R., *J. Chem. Soc., Faraday Trans.*, 1996, 92, 2851.
- [2] Orbán M., Epstein I. R., *J. Am. Chem. Soc.*, 1985, 107, 2302.
- [3] Pešek O., Master Thesis, Prague Institute of Chemical Technology, 2002.

# ACTIVATION ENERGIES OF HYDROGEN PEROXIDE DECOMPOSITION IN THE PRESENCE OF OXYIODINE SPECIES

N. Begović<sup>1</sup>, Z. Marković<sup>2</sup>

<sup>1</sup>*Institute of General and Physical Chemistry, Studenski trg 12-16, 11000 Beograd*

<sup>2</sup>*Faculty of Science, Department of Chemistry, Radoja Domanovica 12, 34000 Kragujevac*

## Abstracts

Using the Density Functional Theory (DFT) method and LanL2DZ basis set, we analyzed the activation energies and rate constants of hydrogen peroxide decomposition in the presence of HOI, IOI and HOIO, in the gaseous phase.

## Introduction

*Ab initio* study of hydrogen peroxide decomposition in gaseous phase is given in ref [1]. For these calculations the CASPT2//CASSCF method is used. The corresponding analysis of hydrogen peroxide decomposition in the presence of HOI, IOI and HOIO can not be found in literature. For mentioned reactions only enthalpies and Gibbs free energies are already calculated. [2,3] The aim of present paper is to evaluate the activation energies of hydrogen peroxide decomposition in reactions involving different oxy-iodine species (HOI, IOI and HOIO). These reactions are the essential for understanding the course of Bray-Liebafsky reaction system.

## Results and Discussion

The bond lengths, vibrational frequencies and energies for the oxy-iodine and hydrogen-oxy-iodine species are investigated using density functional theory at the level of Gill96 exchange and Perdew-Wang91 correlation functional (G96PW91). The double-zeta valence basis sets augmented with p and d, diffuse and polarization functions are used for oxygen. The double-zeta valence basis set combined with the relativistic effective core potential of Wadt and Hay and augmented with uncontracted diffuse s and p functions (exponents 0.0569 and 0.0330, respectively), and d and f polarization functions (exponents 0.292 and 0.441, respectively) are used for iodine. The 6-311++G(3df,3pd) basis set are used for hydrogen. Geometries for transition state are identified by maximisation of energy with respect to all geometrical parameters. Vibrational frequencies are calculated for all obtained structures in order to show whether structures are real minima, maximum (hessian has only one imaginary frequency) or higher order saddle point on the respective potential energy surface. In addition we performed intrinsic reaction coordinate (IRC) calculations to additionally prove that the founded structure is real transition state (Figure 1).

All quantum chemical calculations are performed by means of the Gaussian 98 program package, Revision A.7, Gaussian, Inc., Pittsburgh PA, 1998, under Windows 2000 operating system.

With aim to test the method that we intend to use for further calculations, we first analyzed the activation energies for hydrogen peroxide decomposition in gaseous phase calculated by Ab initio CASPT2//CASSCF method [1]. The results obtained by the DFT method and LanL2DZ basis set of 204.5 kJ/mol (Table 1., reaction R1) are in a good accordance with the published ones, 201.1 kJ/mol.

**Table I.** Calculated activation energies for gaseous reactions at 298 K.

	Reactions	$\Delta E_a$ (kJ mol <sup>-1</sup> )
R1	HOOH $\rightarrow$ HOH + O	204.5
R2	HOI + HOOH $\rightarrow$ HOH + HOIO	103.4
R3	IOI + HOOH $\rightarrow$ HOH + IOIO	126.5
R4	HOIO + HOOH $\rightarrow$ HOH + HIO <sub>3</sub>	96.8

The activation energies of the hydrogen peroxide decomposition in gaseous phase in the presence of HOI, IOI and HOIO, and the one without any iodine species, are obtained and listed in Table I. It has been found that the reactions R2, R3 and R4 are thermodynamically possible in the considered system because they have  $\Delta_r G < 0$  [2,3]. The obtained activation energies are significantly lower than the activation energy of hydrogen peroxide decomposition, alone (reaction R1). Therefore, the presence of oxy-iodine species catalyzes the decomposition of hydrogen peroxide in accordance with experimental data.

The structures of transition complex for reactions R1-R4 are presented in Figure 1. The structures of transition complex for reactions R2-R4 are similar. The characteristic of transition structure in all of three reactions are the same breaking and forming bonds. In reaction R1 we have only breaking of one O-O bond while in reaction R2-R4 we have additional forming of one I-O bond. The different bond length for breaking and forming bonds in transition complex cause the difference of activation energy for reaction R2-R4.

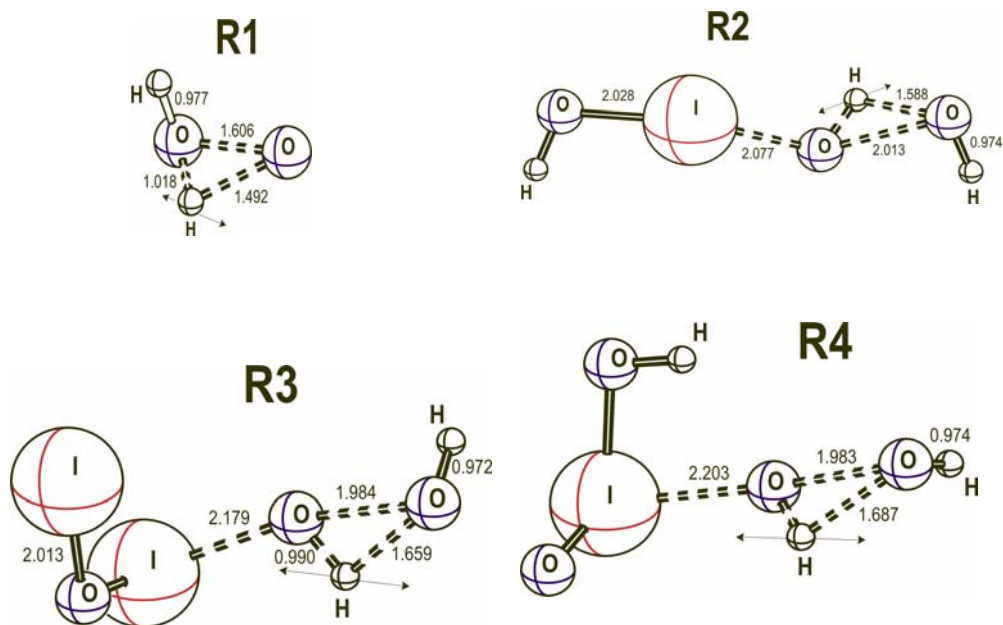


**Figure 1.** The molecular structure in transition state for considered reactions. Bond lengths are in  $10^{-10}$  m, the arrows indicate the vibration direction. The dashed lines correspond to breaking and forming bonds, the once which are the most changed during course of reactions.

In Figure 2, the profile of the minimum energy path for reaction R1 from IRC calculations is given as an example.

## Conclusion

The results for hydrogen peroxide decomposition in gaseous phase obtained by the DFT method and LanL2DZ basis set are in a good accordance with the published ones [1] obtained by Ab initio CASPT2//CASSCF.

Analyzing the calculated activation energies, we can conclude that all three considered reactions are possible. Their activation energies are lower than the activation energy of hydrogen peroxide decomposition, alone.

The obtained results for hydrogen peroxide decomposition in gaseous phase can be used as the starting point for the analysis of the same reactions in solution. [4]

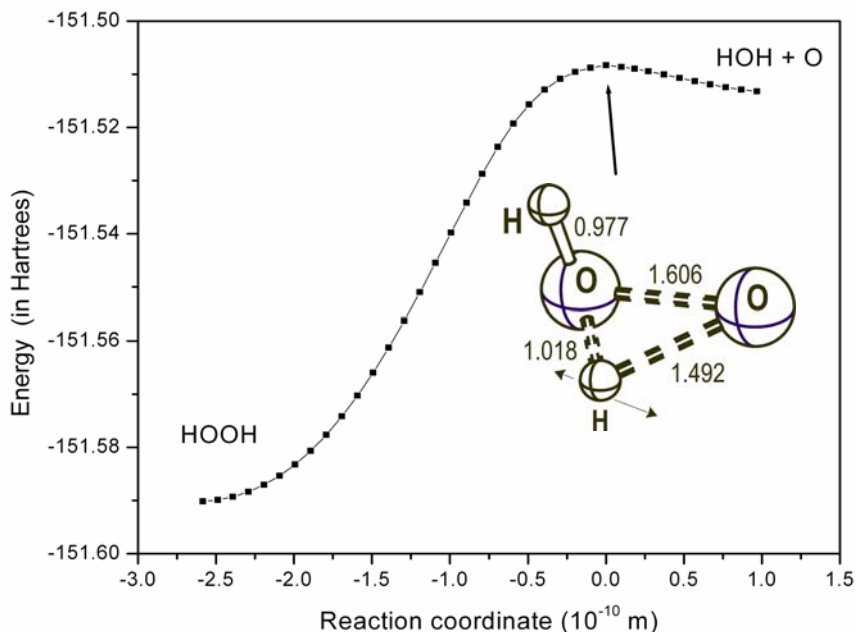


**Figure 2.** Minimum energy path for reaction R1 from IRC calculations. The molecule structure which corresponds to transition state is shown.

### Acknowledgements

The present investigations, which are included in the project no. 1448, are partially supported by Ministry of Sciences, Technologies and Development of Serbia.

### Reference

- [1] R. Sayos, C. Oliva, M. Gonzalez, *J. Chem. Phys.*, 2001, 115, 8828.
- [2] N. Begović, Z. Marković, S. Anić, Lj. Kolar-Anić, *Environ.Chem.Lett.*, 2004, 2, 65.
- [3] N. Begović, Z. Marković, S. Anić, Lj. Kolar-Anić, Gibbs free energies and enthalpies for gaseous reactions of oxy-iodine species  $HI_xO_y$ , in S. Anić (Ed.), *Physical Chemistry 2004*, SPCS, Belgrade 2004, in press.
- [4] N. Begović *et al*, paper in preparation.

# **Author Index**

Allen, P.M.	3	Marković, Z.	215
Anić, S.	85, 115, 178	Milošević, M.	119, 194
Armstrong, G.R.	20	Mitrović, M.M.	97
Bakočević, I.	126	Nieuwenhuys, B.E.	101
Beardmore, R.E.	77	Noszticzius, Z.	49
Begović, N.	215	Novaković, T.B.	174
Beljanski, M.	149, 156	Nowakowski, B.	138
Blagojević, S.	178, 182, 186	Panić, D.	126
Blagojević, S.N.	202, 205, 208	Patmar, E.S.	112
Carabineiro, S.A.C.	101	Pejić, N.	119, 182, 194
Cervellati, R.	190	Pelle, K.	49
Čupić, Ž.	85, 152, 174	Pešek, O.	211
Đorđević, A.R.	170	Peskov, N.V.	101
Elokhin, V.I.	35	Petrov, L.A.	41
Ergelj, A.	149	Petrović, S.	174
Furrow, S.D.	190	Pilić, B.	126
Gáspár, V.	20, 28	Plavšić, M. B.	122
Godula, T.	162	Potkonjak, N.	205
Grozdić, T.	115	Radenović, Č.	149
Gudelj, I.	77	Radičević, R.	126
Ilić, M.	202	Rožić, Lj.S.	174
Izsák, F.	166	Schmitz, G.	58, 115
Jelić, S.	152	Schreiber, I.	92, 211
Jovanović, S.	126	Schreiberová, L.	211
Jovanović, D.M.	174	Scott, S.K.	20
Kassner, K.	159	Semendyaeva, N.L.	109
Kawczyński, A.L.	89, 138, 198	Ševčíková, H.	81, 145, 162
Kazsu, Z.	28	Slinko, M.M.	101
Kiss, I.Z.	28	Spasić, A.M.	97
Kolar-Anić, Lj.	115, 119, 152	Stanisavljev, D. R.	170
Koleva, M.K.	41	Stoiljković, D.	126
Koltsov, N.I.	112	Suchá, M.	81, 145
Korugić-Karasz, Lj.	126	Taba, G.	49
Krstić, D.N.	97	Taylor, A.F.	20
Kubiček, M.	92	Trávníčková, T.	92
Kuchanov, S.I.	66	Turányi, T.	134
Kurkina, E.S.	109	Vaňková, P.	81, 145
Lagzi, I.	166	Vukojević, V.	115, 119, 194
Lazarević, M.P.	97	Wittmann, M.	49
Lazman, M.	130	Zádor, J.	134
Leda, M.	198	Zarić, S.	156
Likar-Smiljanić, V.D.	170	Zemskov, E.P.	159
Maksimov, G.V.	149	Živković, M.	156
Malkov, S.	156	Zsély, I. Gy.	134

## **Participating Institutions**

Alcohol and Drug Addiction Research Section, Department of Clinical Neuroscience, Karolinska Institutet, S 17176 Stockholm, Sweden	119, 194
Aspen Technology, Inc, 900, 125 –98 <sup>th</sup> Avenue SE Calgary, Alberta, Canada	130
Boreskov Institute of Catalysis SB RAS, Prosp. Akad. Lavrentieva, 5, 630090, Novosibirsk, Russia	35
Center for Complex and Nonlinear Systems and the Department of Chemical Physics, Budapest University of Technology and Economics, H-1521 Budapest, Hungary	49
Complex Systems Management Centre, Cranfield University, Bedford, MK43 OAL, England	3
Department of Applied Analysis, Eötvös University (ELTE), H-1518 Budapest, P.O. Box 120, Hungary.	166
Department of Chemistry, University of Debrecen, 4010 Debrecen, Hungary	20
Department of Mathematics, Imperial College London, South Kensington Campus, London SW7 2AZ, U.K.	77
Department of Physical Chemistry, Chuvash State University, Moskovskii prospect 15, 428015 Cheboksary, Russia	112
Department of Physical Chemistry, Eötvös University (ELTE), H-1518 Budapest, P.O. Box 32, Hungary	134, 166
Dept. Chemical Engineering, University of Virginia, Charlottesville, VA, USA	28
Dipartimento di Chimica ‘G. Ciamician’, Università di Bologna, Via Selmi, 2, I-40126 Bologna, Italy,	190
Faculté des Sciences Appliquées, Université Libre de Bruxelles, CP165/63, Av.F.Roosevelt 50, 1050 Bruxelles, Belgium	58, 115
Faculty of Pharmacy, University of Belgrade, Vojvode Stepe 450,	119, 178, 182, 186, 194,
Faculty for Physical Chemistry, University of Belgrade, P.O.Box 137, Studentski trg 16, 11001 Belgrade, Yugoslavia	85
Faculty of Chemistry, Belgrade, Serbia and Montenegro	156
Faculty of Mathematics, Belgrade,	156
Faculty of Mechanical Engineering, University of Belgrade, Belgrade,	97
Faculty of Physical Chemistry, Studentski trg 12-16, P.O. Box 137, 11001 Belgrade, Serbia and Montenegro,	115, 119, 149, 152, 170, 178, 182, 194,
Faculty of Technology & Metallurgy, University of Belgrade, Belgrade, Serbia and Montenegro	97, 122, 126,
Faculty of Technology, Bulevar Cara Lazara 1, Novi Sad, Serbia,	126,
Holding Institute of General and Physical Chemistry, Belgrade, Serbia and Montenegro	149, 156, 202, 205, 208,
Institut of Physical Chemistry, University of Debrecen, Debrecen, Hungary,	28
Institut für Theoretische Physik, Otto-von-Guericke-Universität Magdeburg, Universitätsplatz 2, 39106 Magdeburg, Germany	159

Institute for Security, Kraljice Ane b.b, 11000 Beograd, Serbia and Montenegro	115
Institute for Technology of Nuclear and other Mineral Raw Materials, Belgrade,	97
Institute of Catalysis, BAS, 1113 Sofia, Bulgaria	41
Institute of Chemical Physics, Moscow, Russia,	101
Institute of Chemical Technology Prague, Department of Chemical Engineering and Center for Nonlinear Dynamics of Chemical and Biological Systems, Technická 5, 166 28 Praha 6, Czech Republic	211
Institute of Chemical Technology, Center for Nonlinear Dynamics of Chemical and Biological Systems, Prague, Technicka 5, 166 28 Prague 6, Czech Republic	81
Institute of Chemical Technology, Center for Nonlinear Dynamics of Chemical and Biological Systems, Prague, Technicka 5, 166 28 Prague 6, Czech Republic	145, 162
Institute of Chemistry, Technology and Metallurgy, Department of Catalysis and Chemical Engineering, Njegoševa 12, 11000 Belgrade, Serbia and Montenegro,	85, 152, 174,
Institute of Nuclear Sciences Vinča, Department of Theoretical Physics and Physics of Condensed Matter, Belgrade, Serbia and Montenegro	152
Institute of Physical Chemistry, Polish Academy of Sciences, Kasprzaka 44/52, 01-224 Warsaw, Poland	89, 138, 198
Keldysh Institute of Applied Mathematics, Russian Academy of Sciences, Miusskaya Square 4, 125047 Moscow, Russia	66
Leiden University, Leiden Institute of Chemistry, Surface Science and Catalysis, Einsteinweg 55, 2333 CC, Leiden, The Netherlands	101
Lomonosov State University, Moscow, Russia	149
Moscow State University, Department of Computational Mathematics & Cybernetics, Leninskie Gory, Moscow, 119992, GSP-2, Russia	101, 109
NERC Centre for Population Biology, Imperial College London, Silwood Park Campus, Ascot, Berkshire SL5 7PY, U.K.,	77
Penn State University, Berks-Lehigh Valley College, Luerssen Building, PO 7009, Reading, PA 19610-6009, U.S.A.	190
Polymer Science and Engineering, University of Massachusetts, Amherst, USA	126
Prague Institute of Chemical Technology, Center for Nonlinear Dynamics of Chemical and Biological Systems, 166 28 Prague 6, Czech Republic,	92
Prague Institute of Chemical Technology, Department of Chemical Engineering 166 28 Prague 6, Czech Republic,	92
Prague Institute of Chemical Technology, Department of Mathematics, 166 28 Prague 6, Czech Republic,	92
School of Chemistry, University of Leeds, Leeds LS2 9JT, UK	20
School of Electrical Engineering, University of Belgrade, King Alexander's Boulevard 73, P.O. Box 35-54, 11120 Belgrade, Serbia and Montenegro	170
Technical Faculty, Novi Sad, Serbia and Montenegro,	126
The maize Research Institute "Zemun Polje", Belgrade, Serbia and Montenegro,	149